



Final Project Report

Fire Safe implementation of visible mass timber in tall buildings – compartment fire testing

Daniel Brandon, Johan Sjöström, Alastair Temple, Emil Hallberg and Fredrik Kahl

RISE Report 2021:40

Fire Safe implementation of visible mass timber in tall buildings – compartment fire testing

Daniel Brandon, Johan Sjöström, Alastair Temple, Emil Hallberg and Fredrik Kahl

Abstract

Five real scale fire tests of compartments constructed of cross-laminated timber (CLT) and glued laminated timber, compliant with product standards specified in current US model building code, were performed. Four of the tested compartments were designed to result in a representative and severe fire scenario in a residential fire compartment, using a probabilistic approach. The other tested compartment had additional openings and a greater opening factor, which was aimed to be representative of buildings designed for business occupancy. The interior of the compartments had surface areas of exposed mass timber that varied from approximately the area of the floor plan to approximately two times the area of the floor plan. The tests included measurements to study the internal compartment exposure, the temperature development at gypsum protected surfaces, the temperature development in the structural timber, oxygen concentrations at locations of interest and exposure to exterior surfaces of the wall and façade above the openings. The fire in the compartment with a greater opening factor had two layers of fire-rated gypsum board protection on the back wall and all other surfaces of CLT and glued laminated timber exposed. Despite having the highest peak combustion rate, this compartment fire had the least severe internal and external fire exposure. The fire decayed relatively quickly after flashover and continued to decay until the test was stopped at 4 hours after ignition. This fire resulted in less structural damage than the fires in compartments with fewer and smaller openings.

The compartments with fewer and smaller openings had similar temperatures for approximately the first 10 minutes after flashover. The compartment with only the ceiling (including the glued laminated timber beam) exposed started to decay after 22 minutes of post-flashover fire and continued to decay until the end of the test at 4 hours after ignition. The other three tests had, in addition to the ceiling, significant areas of exposed wall and column surfaces. To accommodate for the extended fire duration that was expected in these configurations an extra layer of gypsum board protection was applied to the protected surfaces. The additional exposed surface areas of walls led to an increase of the fully developed fire duration by 6 - 9 minutes. One of the compartments included corners where two exposed walls intersect. Significantly increased damage was observed in the lower part of these wall corners, and an overall higher radiative exposure in the test with such corners. After more than three hours of decay, surface flaming developed on the walls in that test. The fires in the tests without such corners exhibited continual decay for the full 4-hour test duration. Post-test analysis showed that the structural damage was lower in exposed ceilings than at the bottom of the exposed walls for all tests.

After the tests, remaining smoldering and hot spots were reduced using relatively small amounts of water mist. Overnight measurements to study the thermal wave going through the loadbearing structure indicated no post-test reduction of structural capacity.

Key words: Mass Timber, CLT, Fire, Compartment fire, Glued laminated timber

RISE Research Institutes of Sweden AB, 2021

RISE Report 2021:40

ISBN: 978-91-89385-26-9

Content

Abstract	2
Content	3
Preface	5
1 Introduction	6
2 Background	7
3 Aim and objectives of this study	8
4 Experimental setup	9
4.1 Material properties	15
4.2 Intersections and important details	17
4.3 Measurements	23
4.3.1 Compartment interior measurements.....	23
4.3.2 Material temperature measurements.....	25
4.3.3 Façade and other exterior measurements.....	26
4.3.4 Mass measurements	29
4.3.5 Oxygen measurements & case study measurements.....	30
5 Pass/fail criteria – ICC TWB	32
6 Test results	34
6.1 Events	34
6.2 Video frames	35
6.3 Weather conditions.....	40
6.4 Interior plate thermometers	41
6.5 Thermocouple trees	45
6.6 Incident radiant heat flux (interior)	49
6.7 Internal CLT and gypsum interface temperatures	54
6.8 Gypsum board protection	56
6.9 Post-test temperature measurements	60
6.10 Mass loss of combustibles.....	62
6.11 Heat release rates.....	62
6.12 Char depths.....	63
6.13 Façade exposure	71
6.14 Potential exposure to other buildings.....	74
6.15 Intersections	76
6.16 Performance of different façade details.....	82
6.17 Smoldering inside the compartment at the end of the test	85
7 Discussion	88
7.1 Assessment against previous ICC performance criterion.....	88
7.2 Compartment temperatures	89

7.3	Façade exposure and potential exposure to other buildings	91
7.4	Progression of the thermal wave in CLT after the test	91
7.5	Intersections and detailing	93
7.6	Radiative interaction at bottom of wall corners	95
7.7	Difference with previous test series.....	98
7.8	Variables	100
8	Full list of project reports.....	101
9	Conclusions.....	102
	References	105
	Annex A – Instrumentation locations.....	108
	Annex B – Façade drawings.....	117
	Annex C – Statistical compartment design	119
	Annex D – Fuel load	123
	Annex E –Mass loss measurements and heat release rate calculations ...	126
	Annex F – Maximum Flame Extensions.....	130
	Annex G – Beam Post-test Cross Sections.....	135
	Annex H – Interior thermocouple trees	137
	Annex I – Thermocouples at opening	145
	Annex J – Internal CLT and gypsum interface temperatures.....	151
	Annex K – Oxygen concentration	178
	Annex L – Extinguishing smoldering timber with small quantities of water	180
	Annex M - Photos	188

Preface

This report provides results of a research project on fire-safe implementation of visible wood in tall timber buildings. The main funder of the project is the **US Forest Service (USFS), US Department of Agriculture** (*USFS Grant Number 2019-DG-11083150-022*), the project owner is the **American Wood Council (AWC)**, and **Research Institutes of Sweden (RISE)** is the contractor for this research project.

Other project partners and funders of this project are: **Katerra** providing ANSI/APA PRG 320 (2018)-compliant CLT, **KLH** providing ANSI/APA PRG 320 (2018)-compliant CLT; **Henkel** providing the required ANSI/APA PRG 320 (2018)-compliant adhesive and additional funding, **Boise Cascade** providing ANSI A 190.1-2017 compliant glued laminated timber; **USG**, providing Type X gypsum boards; **Rothoblaas**, providing mass timber screws, sealants, tapes, resilient profiles and equipment for lifting anchors mass timber members; the **Softwood Export Council** providing shipment costs of US products to the test site in Sweden; **Brandforsk** providing **additional** funding for the inclusion of façade extension measurements. The façade measurements are out of the scope of this report. Technical in-kind contributions were provided by **NIST** for recording of videos in severe fire conditions.

A Steering Group was assembled for this project, comprising of:

Kevin Naranjo (USDA)

Kuma Sumathipala, Jason Smart, Kenneth Bland (AWC)

Sean DeCrane (Building & Life Safety Technologies, UL)

Gordian Stapf, Christian Lehringer, Daniel Current, Chris Whelan (Henkel)

Hans-Erik Blomgren (Katerra)

Sebastian Popp, Johannes Habenbacher (KLH)

Kyle Flondor, Ajith Rao, Young-Geun You (USG)

Susan Jones (Atelier Jones)

Rodney McPhee (Canadian Wood Council)

Dan Cheney (Boise Cascade)

Hannes Blaas, Andres Reyes, Paola Brugnara (Rothoblaas)

All steering group members provided in-kind technical contributions in this project.

1 Introduction

The implementation of mass timber materials such as CLT and glued laminated timber as structural materials for tall buildings has been increasingly popular. Mass timber has been cited for its low carbon footprint and architectural desirability. Because mass timber is combustible, the design of such buildings involves new fire safety challenges. A key fire safety objective identified in previous research was the ability of fires to continuously decay after a flashover fire occurred. Fire delamination, failure of fire protection (Su et al. 2018a) and charring behind fire protective layers (Su et al. 2018b) were identified as the main phenomena that reduced the likelihood that a fire would exhibit continual decay in compartments of CLT. Recent developments of technologies and increased performance requirements of CLT in USA and Canada (Janssen 2017, Brandon and Dagenais 2018) reduces the risk of fire delamination of mass timber members, which reduces the challenge to ensure that fires decay. This research project has been performed to study the design limits for compartments to ensure the fire will decay without exhibiting any significant re-growth.

This research project includes topics given in Table 1. Some of these topics are included in other project reports and not discussed in detail in this report.

Table 1: Full list of project topics and location of reporting.

Topic	Report
Survey of design parameters in real buildings.	This report
<i>A priori</i> predictive modeling of fire development and decay in compartments with exposed mass timber	Predictive modeling report (Brandon et al. 2021a)
5 real scale compartment fire tests (Main objective) <ul style="list-style-type: none"> - Measurements of the interior temperature and exposure - Mass loss and heat release rate measurements and calculations - Measurements of the exposure to opposing external surfaces - Measurements of fire exposures to facades - Continued temperature measurements in the structure after tests - Case studies for extinguishing with less water 	This report
Assessment of fire tests against previous performance criteria	This report
Data analysis and discussions	This report
Conclusions	This report
Improved predictive modeling	Predictive modeling report (Brandon et al. 2021a)
Repairing of fire-damaged CLT (case study)	Post-fire repair report (Brandon et al. 2021b)
Comparisons of façade exposure to standard façade fire tests	Façade exposure report (Sjöström et al. 2021)

A summary report has previously been issued (Brandon et al., 2020), however this report presents more data and includes more discussions than the summary. The additional data presented in this report are:

- Temperatures at thermocouple trees
- Incident radiant heat flux within the compartment
- Façade exposure
- Exposure at locations in front of openings
- Mass loss of the structure and floor
- Char depths in glued laminated timber members
- Oxygen concentrations
- Detailed descriptions of smoldering and hot spots after the fire
- Post-test temperature measurements
- Data from case studies to extinguish with small quantities of water (Annex L)

All information of the summary report is also included in this report and some sections are the same.

Besides the summary report and the final project report (this report), there are also reports on predictive modeling¹, comparisons of façade fire exposure to façade fire tests², and a case study of repairing fire damaged CLT³ (due May 2021).

2 Background

New US building regulations for the 2021 International Building Code (2021 IBC) have recently been approved, which allow the construction of tall buildings with mass timber structures. The 2021 IBC includes three new construction types dedicated for mass timber structures, namely IV-A, IV-B and IV-C. Buildings of type IV-A can be up to 18 stories and have the most strict fire safety requirements, including required protection of all mass timber surfaces, using noncombustible fire protection providing no less than 2/3 of the required fire resistance rating of the mass timber itself (2 hrs. of protection for IV-A). Buildings of type IV-B can be built up to 12 stories and can have limited portions of the ceiling (up to 20%) or limited portions of walls (up to 40% of the floor area) exposed. Buildings of type IV-C can have all mass timber surfaces exposed, but have stricter limitations of building height, depending on the type of occupancy. It should be noted that other fire safety requirements hold for all building types, such as the presence of NFPA 13 compliant sprinklers, as summarized by Breneman et al. (2019).

The limitations for buildings of type IV-B were based on two compartment fire tests performed by Zelinka et al. (2018), in which relatively small surface areas of timber were exposed. Both fires continuously decayed after a period of flashover for at least three

¹ Brandon, Temple & Sjöström, Predictive method for fires in CLT and glulam structures – Disseminated predictions versus real scale compartment fire tests, RISE Report 2021:63, ISBN: 978-97-89385-53-5.

² Sjöström, Brandon, Temple, Hallberg & Kahl, Exposure from mass timber compartment fires to facades, RISE Report 2021:39, ISBN: 978-91-89385-24-5

³ Brandon, Sjöström & Kahl, Rehabilitation of fire exposed CLT, RISE Report 2021:67, ISBN: 978-91-89385-57-3.

hours, and were continuously decaying at 4 hours after ignition, which has been a primary acceptance criterion for the ICC TWB Ad hoc committee.

There has, however, been a change of requirements in the CLT product standard (ANSI/APA PRG320, 2018), requiring the face bond adhesive of CLT to withstand a 4-hour-long full-scale compartment fire test without the occurrence of delamination and to pass a bench scale test. As previous research (McGregor 2014, Medina Hevia, 2015, Su et al. 2018, Brandon et al. 2018, Hadden et al. 2017, Emberley, 2017) demonstrated the significant effect that CLT delamination can have on compartment fire dynamics, this change in the ANSI/APA PRG320 (2018) can significantly change the outcome of fires in compartments made of CLT.

The tests by Zelinka et al. (2018) were initiated before the 2018 version of ANSI/APA PRG 320 was published and the tested CLT was not compliant with the new product standard, compromising the potential fire performance of the structure. In addition, the tests by Zelinka et al. involved the highest heat release rates of any indoor CLT compartment fire test to date and the ability of a laboratory to accommodate increased surface areas of timber in an indoor fire test at this scale is restricted because of limited capacities of laboratories' exhausts and calorimeters.

An early study of fires in compartments made of ANSI/APA PRG320 (2018)-compliant CLT, was performed at NRC-CNRC in Canada (Su et al. 2018b). This study showed an improved potential for compartment fires of CLT structures to decay. However, due to charring behind two layers of 1/2 inch gypsum plaster boards and some details in the design, some of these fires did not fully decay.

3 Aim and objectives of this study

This study aims to assess possible changes to US code-prescribed limits of visible mass timber surface areas, for products that comply with current US product standards.

The specific objectives are, therefore, to:

- Perform a series of compartment fire tests in structures constructed of PRG 320-2018 compliant CLT with varying amounts of exposed mass timber areas.
- Provide background for possible changes to code-prescribed limits of exposed mass timber surfaces consistent with the fire performance criterion⁴ used for changes to the International Building Code.
- Identify additional measures necessary (if any) to ensure the fire performance criteria established by the International Code Council (ICC) Ad-Hoc Committee on Tall Wood Buildings (TWB) and additional criteria discussed in Section 5 are met.

In addition, secondary objectives are defined:

- Design and test intersections between exposed mass timber members that are practical, affordable, and sufficient for the compartment fire duration.

⁴ ICC TWB Ad Hoc committee used a fire performance criterion where a compartment fire should exhibit continual decay with no significant fire re-growth following the fully-developed phase.

- Develop and test a method of restoring exposed CLT members after a fire. *Note: this objective is discussed in a separate report.*
- Allow for comparisons of the fire exposure measured on the front façade above ventilation openings of compartments that are fire tested. The exposure of four of these tests is expected to be statistically severe (with respect to quantity of external combustion and duration), based on a survey of recently built residential buildings. *Note: this objective is part of the project add-on funded by Brandforsk (as noted in the Preface) and is discussed by Sjöström et al. (2021).*
- Map the influence of increasing the surface area of exposed mass timber on the façade exposure. *Note: this objective is part of the project add-on funded by Brandforsk (as noted in the Preface) and is discussed by Sjöström et al. (2021).*

4 Experimental setup

Five compartment fire experiments were performed for this study. The compartments had internal dimensions of 23.0 ft x 22.5 ft x 9.0 ft (7.0 m x 6.85 m x 2.73 m). Four of these compartments (Tests 1, 2, 3 and 5) had two ventilation openings (Figure 1) of 7.4 ft x 5.8 ft (2.25 m x 1.78 m, width x height) resulting in an opening factor⁵ of 0.112 ft^{1/2} (0.062 m^{1/2}). The compartment dimensions and the opening factor were based on a probabilistic analysis and surveys of data of tall residential buildings, as discussed in Annex C. The remaining compartment test (Test 4) had six larger openings, resulting in an opening factor of 0.25 m^{1/2} (0.453 ft^{1/2}), which is approximately equal to the midrange of opening factors for office compartments found in the survey of Annex C.



Figure 1: Fully developed fire of Test 1

⁵ Definition of opening factor: $O = A_0 \sqrt{H_0} / A_t$, where $A_0 = \sum A_i$ is the sum of all opening areas, A_t is the total enclosing area (incl. openings), $H_0 = \sum (A_i h_i) / A_0$, and h_i is the height of each opening

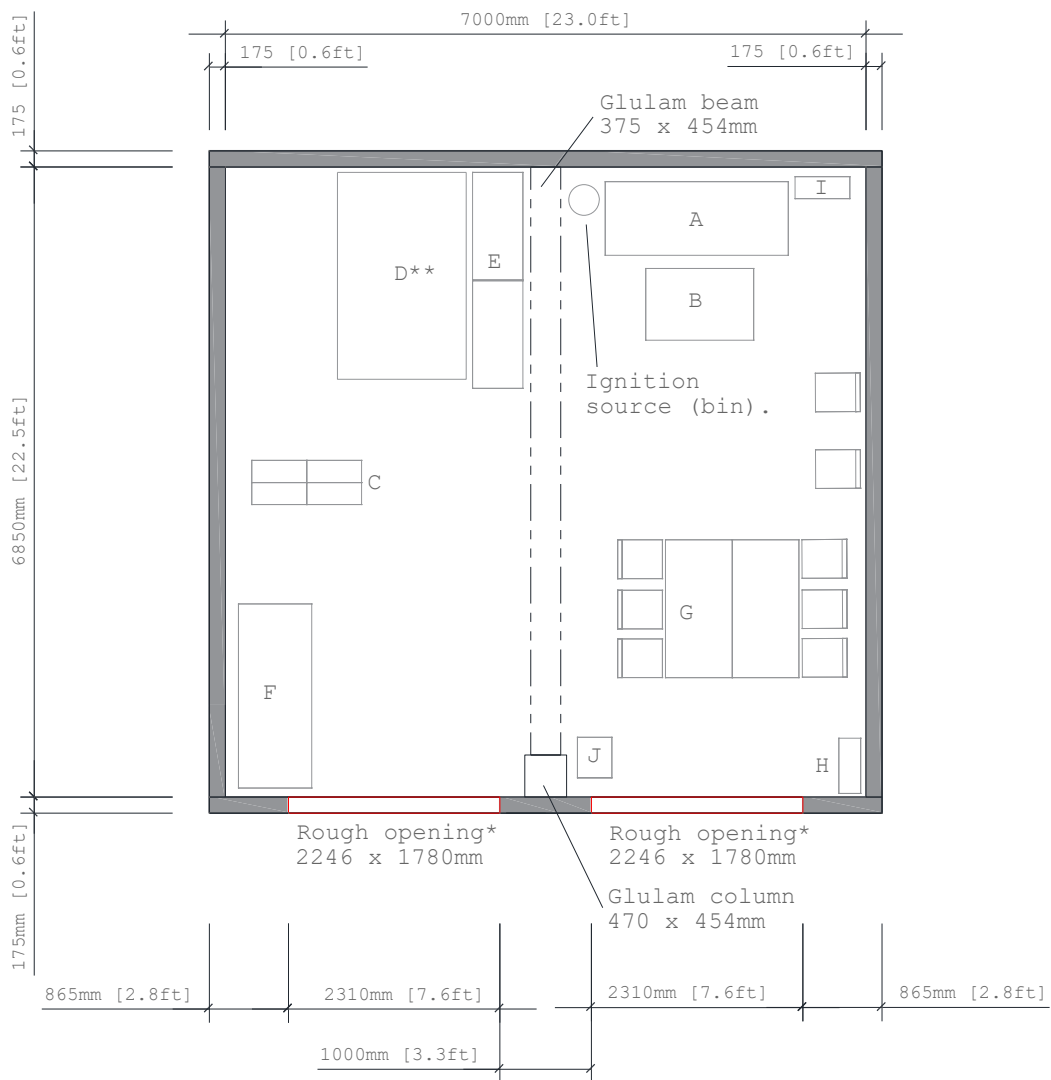
The compartments were constructed of ANSI/APA PRG 320, 2018 compliant 6.9 inch (175 mm) thick 5-ply CLT (each ply was 1.38 inches, 35 mm thick) and ANSI A 190.1-2017 compliant glued laminated timber. It is important to note that in contrast with most previous studies, the tested CLT lay-up with the specific enhanced polyurethane adhesive fulfills the requirements specified in Annex B of the 2018 version of ANSI/APA PRG 320. In this study, varying mass timber surfaces were protected with Type X gypsum boards. All CLT, glued laminated timber and gypsum boards used during the tests complied with current US regulations and standards.

The floor plan of Tests 1, 2, 3 and 5 is shown in Figure 2. The Floor plan of Test 4 is shown in Figure 3. Drawings of all walls with openings are shown in Annex B.

The dimensions of the compartment, size of the openings and fuel load density were determined from a probabilistic analysis aiming to test a severe fire scenario that is based on the designs of real buildings, which is summarized in Annex B. The combination of the compartment dimensions, fuel load density and opening factor results in the 85th percentile of expected total char damage for fire scenarios in residential buildings where sprinklers are not activated, flashover takes place and fire service interference is absent. Details of this analysis are indicated in Annex C. The target fuel load density resulting from the probabilistic study is 560 MJ/m² (52 MJ/ft²).

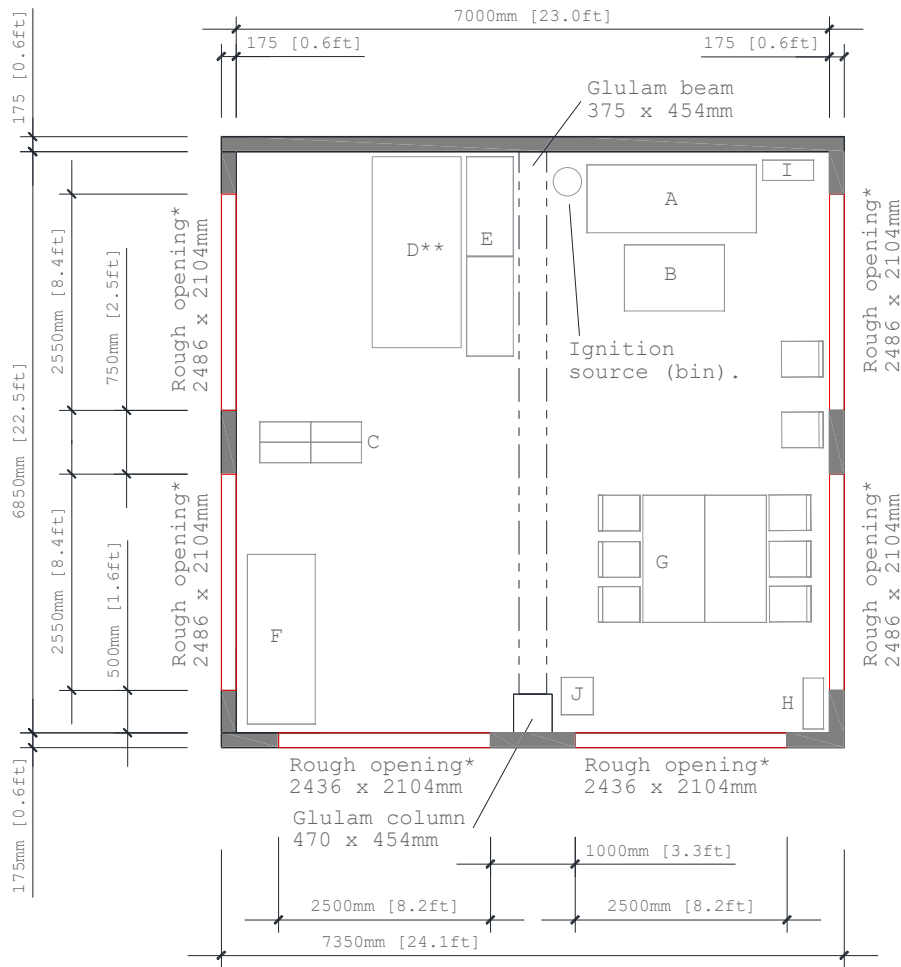
The fuel used was a combination of typical apartment furniture, particle board sheets on the floor to represent a wood floor covering, and additional wood cribs⁶ representing fuel in storage spaces. The calculation of the moveable fuel load is provided in Annex D, in which the fuel items denoted with the letters A to J in Figure 2 and Figure 3 are specified. The total mass of the moveable fuel on the floor was measured using load cells under the floor for every test and was 2881 ± 22 lb (1307 ± 10 kg) in total. The ignited item was a metallic bin filled with 1.4 lbs (635 g) of crumbled A4 print paper.

⁶ The wood cribs consisted of Norway spruce with a 45 mm x 45 mm cross section, a density (based on a random sample) of 435 kg/m³, and an average moisture content of 13.0 %. The total weight of the wood cribs was checked for every test.



*The sides of the opening are gypsum board protected. The opening dimensions after gypsum board installation are given
 **Combustible D is a sofa bed, implemented as a bed in Test 1, 2, 3 and 5 to correspond to residential occupancy and as a sofa in Test 4 to correspond to mercantile occupancy. The fuel load is the same.

Figure 2: Floor plan of Test 1, 2, 3 and 5



**The sides of the opening are gypsum board protected. The opening dimensions after gypsum board installation are given
 **Combustible D is a sofa bed, implemented as a bed in Test 1, 2, 3 and 5 to correspond to residential occupancy and as a sofa in Test 4 to correspond to mercantile occupancy. The fuel load is the same.*

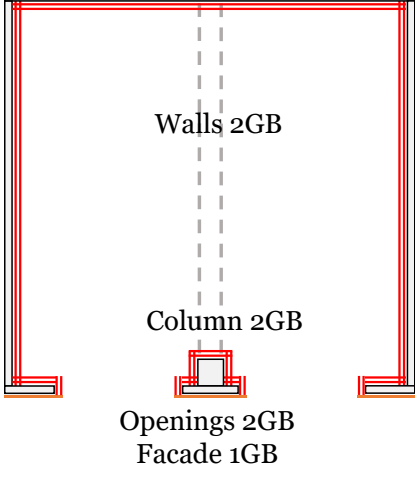
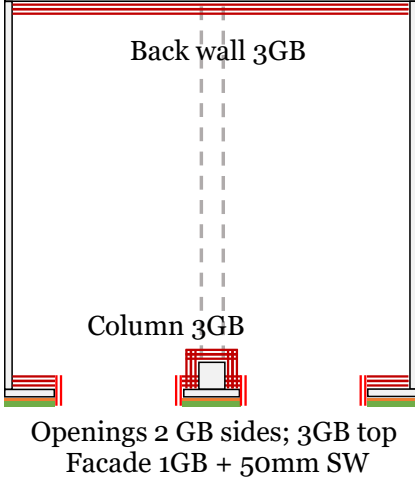
Figure 3: Floor plan of Test 4

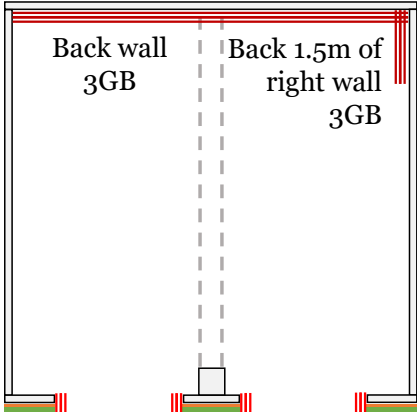
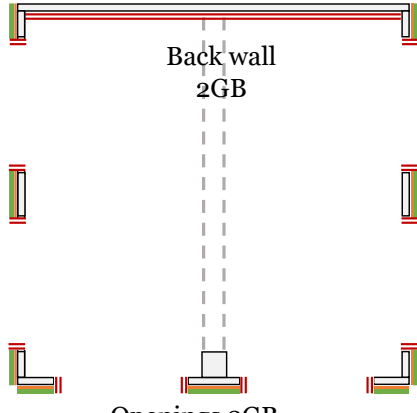
The locations and the number of layers of gypsum board protection along with the percentages of exposed surface areas are provided in Table 2. The CLT ceiling and the glued laminated timber beam were exposed in all tests. The table includes the number of 5/8 inch thick (15.9 mm) Type X gypsum board layers (GB) that were implemented on interior surfaces. Schematic floor plans (not to scale) indicate the locations of the protected surfaces. In addition, the drawings also indicate the fire protection that was implemented on the sides and top of the opening and on the fire exposed façades. All gypsum board layers were attached with gypsum screws at a maximum relative distance of 10.8 inch (274 mm) in both horizontal and vertical direction. Edge distances of 2.5 inch (64 mm) were implemented for screws at the edge of the gypsum boards. The lengths of the gypsum screws were 1.6 inch (41 mm) long for the base layer, 2.2 inch (55 mm) long for the second layer and 2.8 inch (72 mm) long for the third layer. Specialized equipment was used to prevent the screw heads from punching through the paper surface of the gypsum boards and prevent premature damage of the boards. The gypsum board layers were staggered with an offset of at least 12 inches (300 mm) between joints of two

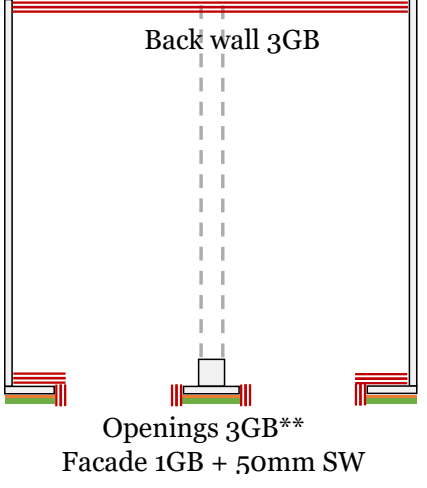
subsequent layers. On the exposed surface all screw heads and joints between gypsum boards were finished with regular joint compound.

Of the small opening tests (tests 1, 2, 3 and 5 - representative of dwellings), Test 1 had the least surface area of exposed wood followed by Test 2. Test 3 and 5 had the same exposed wood surface area, but in Test 5 no corners with two exposed walls were present. For Test 4 (large opening – representative of business occupancy) all internal walls except for the back wall were exposed.

Table 2: Test matrix (GB indicates gypsum boards; SW indicates stone wool)

Test name Window Opening size	Gypsum Board (GB) Protected interior surfaces*	Exposed wood surfaces	Floor plan (schematic)***
Test 1 Two window openings 86 ft ² (8.0 m ²) of exterior wall open	- All walls and - Column protected by 2 layers of GB	100% of ceiling, 100% of beam exposed [†] No exposed wood surfaces in walls (53.8 m ² /579 ft ²)	 <p>Walls 2GB Column 2GB Openings 2GB Facade 1GB</p>
Test 2 Two window openings 86 ft ² (8.0 m ²) of exterior wall open	-Back wall and -Front wall protected by 3 layers of GB	100% of ceiling, 100% of beam, 100% of left wall, 100% of right wall exposed No exposed wood wall surfaces meeting in a corner (91.2 m ² /981 ft ²)	 <p>Back wall 3GB Column 3GB Openings 2 GB sides; 3GB top Facade 1GB + 50mm SW</p>

Test name Window Opening size	Gypsum Board (GB) Protected interior surfaces*	Exposed wood surfaces	Floor plan (schematic)***
Test 3* Two window openings 86 ft ² (8.0 m ²) of exterior wall open	-Back wall and -Back 5 ft (1.5 m) length of right wall protected by 3 layers of GB	100% ceiling 100% beam, 100% of left wall, 78% of right wall, 100% of front wall, and 100% of column exposed. Two exposed wood wall surfaces meeting in a corner (front left and front right) (96.2 m ² /1035 ft ²)	
Test 4* Six Window openings 336 ft ² (31.2 m ²) of exterior wall open	Back wall protected by 2 layers of GB	100% ceiling, 100% of beam, 100% of left wall, 100% of right wall, 100% of front wall, 100% of column exposed. Two exposed wood wall surfaces meeting in a corner (front left and right) (77.9 m ² /838 ft ²)	

Test name Window Opening size	Gypsum Board (GB) Protected interior surfaces*	Exposed wood surfaces	Floor plan (schematic)***
Test 5* Two window openings 86 ft ² (8.0 m ²) of exterior wall open	-Back wall and -2.3 ft (0.7 m) on left and right-side edges of the front wall protected by 3 layers of GB	100% ceiling, 100% beam, 100% of left wall, 100% of right wall, 60% of front wall, 100% of column exposed. No exposed wood wall surfaces meeting in a corner (97.2 m ² /1046 ft ²)	

†In Test 1, a strip of 50 mm high 2-layer thick gypsum board was implemented on the top right side of the beam. This was not done on the left side of the beam to allow studying the effect of an expected radiative feedback loop in the top corners. In contrast with expectations, this location did not show increased charring or smoldering, and the strip was not implemented in any other test.

*To be able to weigh the floor separately from the structure, the floor was not directly attached to the walls of the fire test compartment. The small gap, between the floors and the walls was filled with stone wool insulation for all tests. In Test 2, some of the stone wool fell out of place and resulted in fire spread downward from the compartment floor in this (artificially created) gap. Therefore, for subsequent tests, a 10 cm (4") strip of gypsum board was applied to the bottom of all exposed walls to cover the wall/floor gap in Test 3, 4 and 5.

** In Test 3 and 5, three layers of gypsum boards were applied on the side of the ventilation openings instead of two layers. The extra layer made the openings slightly narrower than the openings of Test 1 and 2. To compensate for this, the height of the ventilation opening was increased so that the opening factor for Tests 1, 2, 3 and 5 was the same.

***Protection on the façade and façade details at the opening have been changed iteratively. Section 6.16 gives an overview of details and pictures after the tests.

4.1 Material properties

The structural material and the gypsum boards used, all compliant with relevant USA standards, were factory made in regular industry production lines and shipped to the test site in Sweden. The structure of the test compartments was made of ANSI/APA PRG 320-2018 compliant CLT supplied by Katerra and KLH and ANSI A 190.1-2017 compliant glued laminated timber supplied by Boise Cascade. The CLT of Katerra (Test 1-3) and KLH (Test 4 & 5⁷) have the same lay-up and adhesive. The CLT was 175 mm thick and made of 5 plies of 35 mm thick each and had a density of 39.3 ± 0.6 lb/ft³ (470 ± 10

⁷ In Test 5 the (exposed) left wall was made of CLT by Katerra.

kg/m³). Thermogravimetric analysis (TGA) was performed of both CLT products (Figure 4), which gave similar results in oxygen poor and oxygen rich environments, indicating similar mass loss and, indirectly, similar potential release of heat at elevated temperatures during different stages of the fire. The average moisture content of 13.0% with a standard deviation of 1.0%, measured using electrical resistance meters the day before tests at measurements at a depth of 20 to 30 mm at approximately 100 random locations in total. The adhesive used was *HB X Purbond* supplied by Henkel, which is compliant with the requirements of ANSI/APA PRG 320-2018, which includes mandatory compartment fire testing to demonstrate adhesive performance in fire. No edge gluing was implemented, i.e. lamellas in the same layer were not glued to each other.

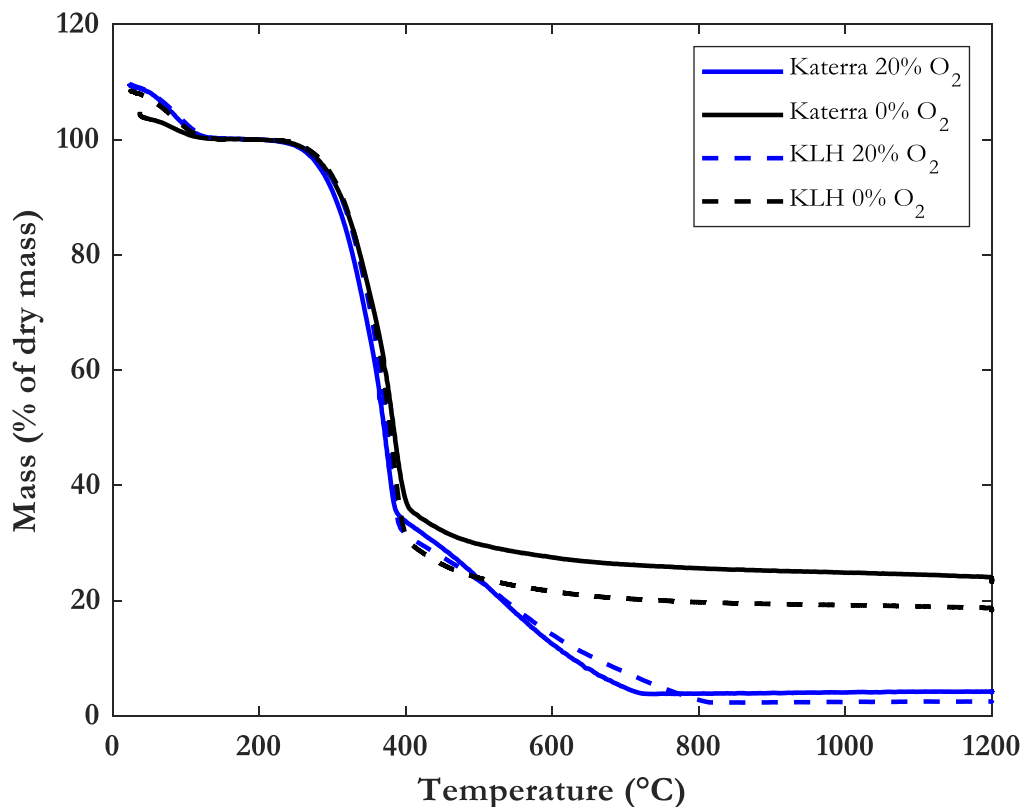


Figure 4: Thermogravimetric analysis results of CLT samples in ambient and nitrogen environment. Heating rate of 20°C/min.

The glued laminated timber was made of Douglas Fir and a phenolic adhesive. The density of the glued laminated timber was 36.2 ± 0.6 lb/ft³ (580 ± 10 kg/m³) and the moisture content was 13.4 % with a standard deviation of 0.8 % determined in a similar way.

Type X gypsum boards complying with ASTM C1396 with a thickness of 5/8" (15.9 mm) were used. The density of the gypsum boards was 42.0 lb/ft³ (673 kg/m³). TGA results of a material sample are shown in Figure 5.

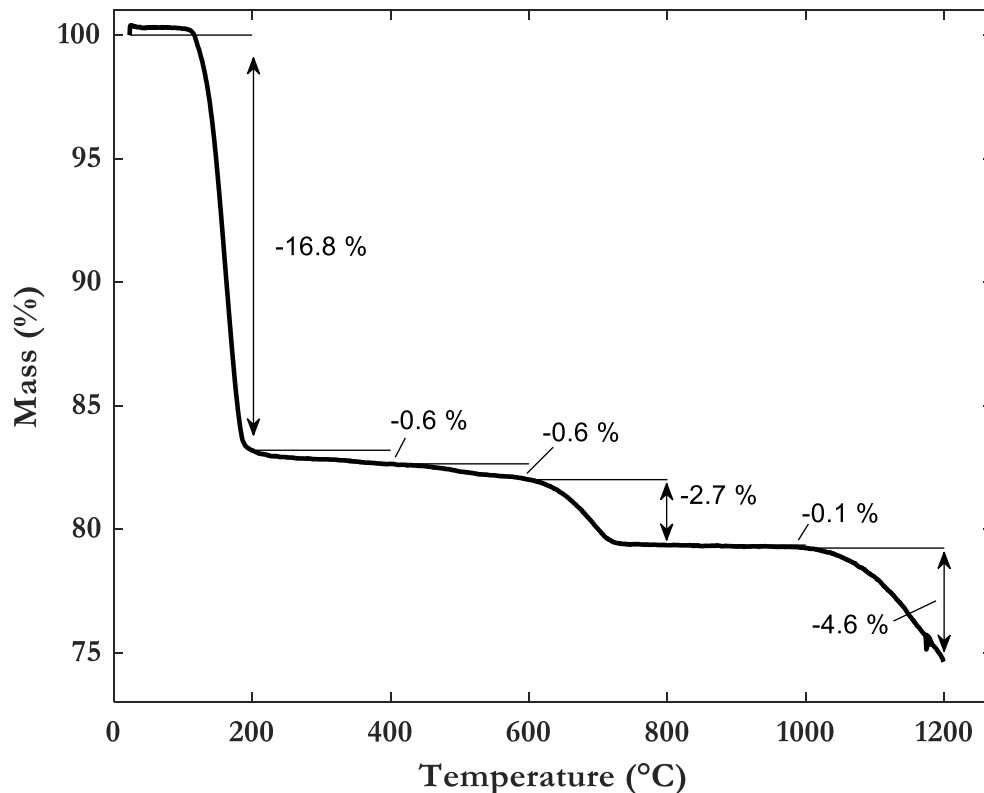


Figure 5: Thermogravimetric analysis results of the used type-X gypsum board. Heating rate of 20°C/min in an N₂ atmosphere. Mass losses at consecutive temperature intervals of 200 °C are indicated.

4.2 Intersections and important details

One of the secondary objectives of this study was to “*Design and test intersections between exposed mass timber members that are practical, affordable and sufficient for the entire fire duration of compartment fires*” (Section 1.2).

For intersections of mass timber building elements with other building elements, where both are required to be fire resistance rated, the IBC 2021 requires the use of sealants in accordance with ASTM C920 and ASTM D3498. Instead of complying with IBC 2021, it was aimed to study the performance of alternative solutions that potentially increase practicability and possibly lower costs. To this end several types of commercially available sealants were applied between mass timber elements during this study.

Sealants were applied between mass timber elements to reduce the risk of fire spread through mass timber intersections, by eliminating the flow of hot gasses between mass timber elements at intersections. It is expected that sealing materials do not need a high temperature resistance if the sealant is used in locations not directly exposed to high temperatures. The tested sealants were primarily those generally used to improve effective gas seal, water proofing or acoustic performance. Test results should indicate if these are suitable to prevent fire spread through intersections. Table 2 gives an overview

of the materials used to seal the intersections, including information of their temperature resistance, if available.

Table 3: Materials used at intersections of CLT members.

Product	Common functions	Detailed description
Construction tape	Water proofing Improving effective gas seal	Tape comprising of a polyethylene film, with reinforcing Polyethylene grid and acrylate adhesive. Width: 60 mm (2.36 inch); Thickness: 0.25 mm (0.01 inch); Temperature resistance: -40/80 °C.
Expanding tape	Improving sound insulation Improving effective gas seal	Elastic expanding tape developed to fill irregular gaps, sound proofing up to 58 dB. Width: 20 mm (0.8 inch); Max expansion (thickness): 20 mm (0.8 inch). Temperature resistance: -30/90 °C.
Resilient profile	Sound proofing Improving water tightness	Resilient profile of polyurethane. Width: 140 mm (0.46 ft); Thickness: 0.24 inch (6 mm); Thermal conductivity: 0.2 W/mK. Maximum processing temperature: >200 °C.
Construction sealing	Improving effective gas seal Improving sound insulation	Expanded EPDM (synthetic rubber). Width: 46 mm (0.15 ft); Thickness: 3 mm (0.12 inch); Temperature resistance: -35/100 °C.
Fire Sealing	Fire sealing Acoustic insulation	1-component silicon elastomer adhesive. Up to 90 minutes fire-rated.
Intumescent paint	Fire sealing	Intumescent paint for protecting indoor steel profiles with up to 90 min fire resistance. One-layer application

Figure 6 shows details of the CLT intersection and indicates which sealing material was used in each test. Spline board joints with Ø0.24 x 3.1 inch (Ø6 x 80 mm) washer-head screws with 10 inches (250 mm) spacing were used to connect CLT panels in the ceiling. Four different variants were used to seal the spline board joint, using either construction tape or expanding tape. It was expected that a slight offset of height between two CLT members may cause a channel of air along the spline board in the details of Test 1 and 3. For that reason, tape that sealed the end of this potential channel (at the ends of the spline board) was implemented in those tests. This was not done for the other tests, because the implemented tape was expected not to allow hot gasses in any potential channel under the spline board.

Lap joints were used to connect wall elements that were in the same plane. The members were connected using Ø0.32 x 4.7 inch (Ø8 x 120 mm) countersunk head screws with 10 inches (250 mm) spacing. In Tests 3, 4 and 5 no sealing materials were implemented for lap joints in gypsum protected walls. For exposed walls two variants have been implemented using either construction tape or expanding tape as shown in Figure 6 C.

Butt-joints between CLT walls and ceiling panels were implemented using Ø0.32 x 11.8 inch (Ø8 x 300 mm) washer-head screws. Three variants to seal the joints were

implemented using resilient profile and/or construction tape. The resilient profile was positioned centrally on top of the walls. Since the CLT wall is 35 mm wider than the resilient profile, a small void was formed between the construction tape and the resilient profile on the external side in Tests 2, 4 and 5. Although it was not expected that high temperatures would be reached in this void, a small amount of fire sealing adhesive was used every two meters, to limit flow of gasses in the longitudinal direction of the void in case it would manage to pass the resilient profile. For locations at which the walls were protected by gypsum boards, a small amount of fire sealing adhesive was used to avoid gasses flowing into the void between the resilient profile and the gypsum boards. Fire sealing adhesive was used to fill up some visible voids between the resilient profile and the CLT in a few locations of the left and right walls of the Test 2 and Test 3 compartments.

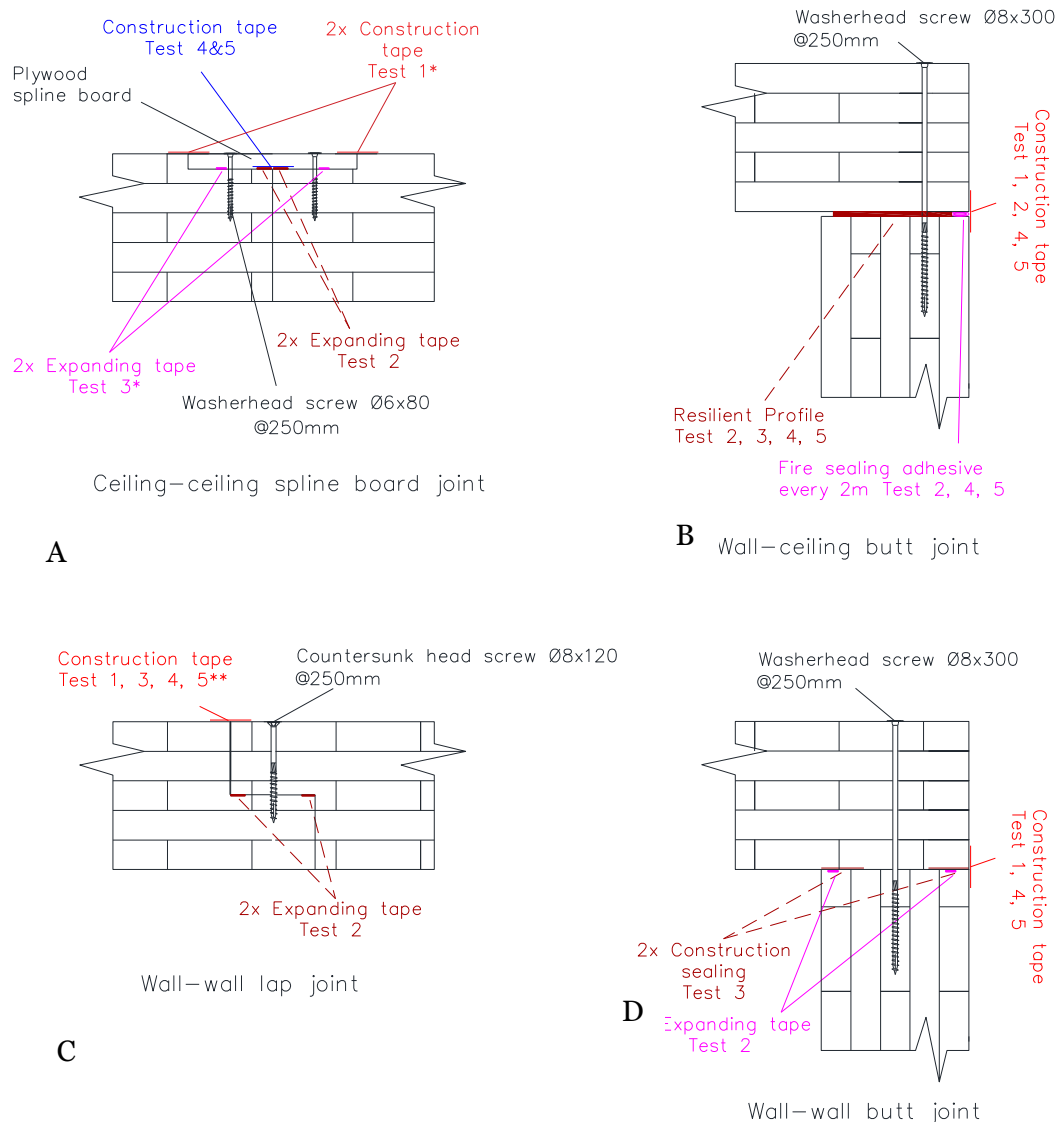


Figure 6: Variants of sealed CLT intersections and their sealing details (different colors represent different sealing types and/or locations)

* Construction tape was used to close potential voids between the spline board and the CLT at the end of the spline board, for Tests 1 and 3.

** Construction tape was not used for lap joints between gypsum protected walls in Test 3, 4 and 5.

CLT wall corner joints were connected also using Ø0.32 x 11.8 inch (Ø8 x 300 mm) washer-head screws. Three variants to seal the joints were implemented, using construction sealing, construction tape, or expanding tape (Figure 6 D). The construction sealing was stapled to the end of the walls before assembly.

All configurations of CLT joints of Figure 6 were at least in one test implemented without any gypsum board protection, with the exception of the wall-ceiling joint of Test 1 and the wall-wall butt joint of Test 2. Those two configurations were subjected to less severe exposure because of the gypsum board protection. Therefore, the detail of these specific tests including gypsum boards is shown in Figure 7. In Test 1, no fire sealant was implemented between gypsum and abutting CLT members in corners. Before all subsequent tests, a small amount of fire sealing adhesive was used only in locations where a gap between gypsum and abutting CLT was visible.

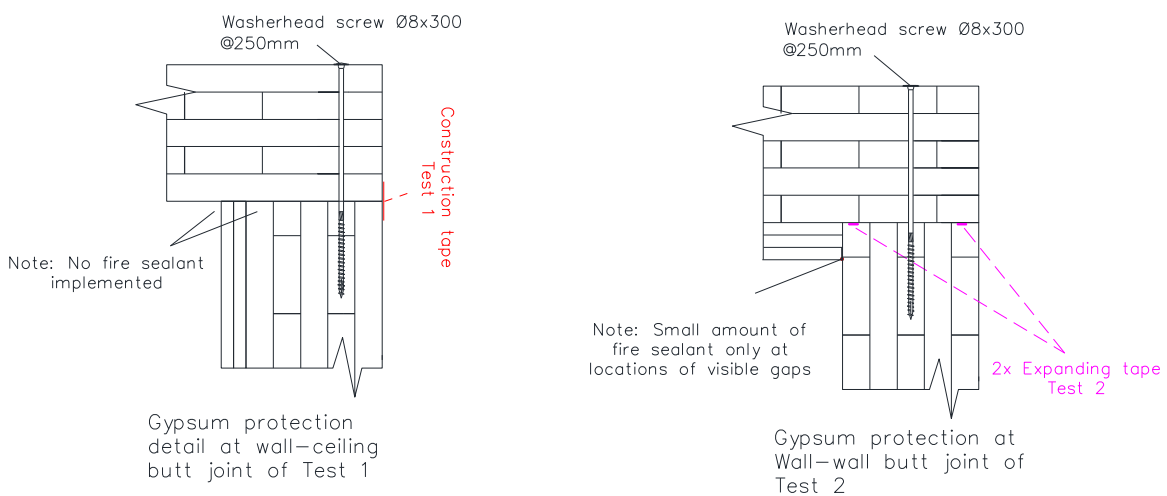


Figure 7: Variants of CLT intersections that only were implemented together with gypsum board protection.

The top of the beam was connected using two rows of 8 x 300 mm washer-head screws @ 200 mm. In Test 1, there was no sealant implemented, in this connection. In Test 2, 3, 4 and 5 there were two strips of resilient profile implemented (see Table 3), as can be seen in Figure 6 and Figure 8. In Test 3, the sealant method was varied along the length. At approximately half the length, two strips of resilient profile were used, and the other half had two double strips of construction sealant (with approximately the same total thickness). The interface between the front wall and the column had no sealants in any of the tests.

The glued laminated timber beam and column were connected using an embedded aluminum connector, as shown in Figure 9. A slot was milled in the column, in which the connector was embedded. To allow geometrical tolerances, there was a small gap with a width of 3 mm ± 2 mm after assembly. Fire sealant was applied on the end of the beam before assembly was implemented for Test 1 and 2 (Figure 10). In Test 3, 4 and 5 the end of the beam was painted using intumescent paint, which aimed to close the gap at the beam-end, if elevated temperatures are reached. It should be noted that in Test 1 and 2 the column was protected by 2 layers and 3 layers of gypsum boards, respectively. In Tests 3-5 the column and beam were fully exposed.

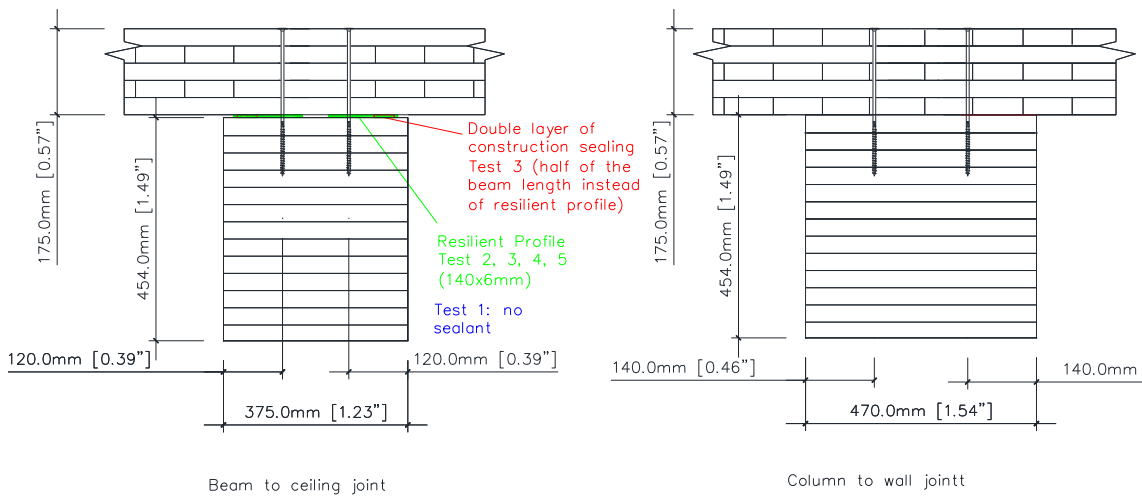


Figure 8: Connection between beam and ceiling (left) and column and ceiling (right)

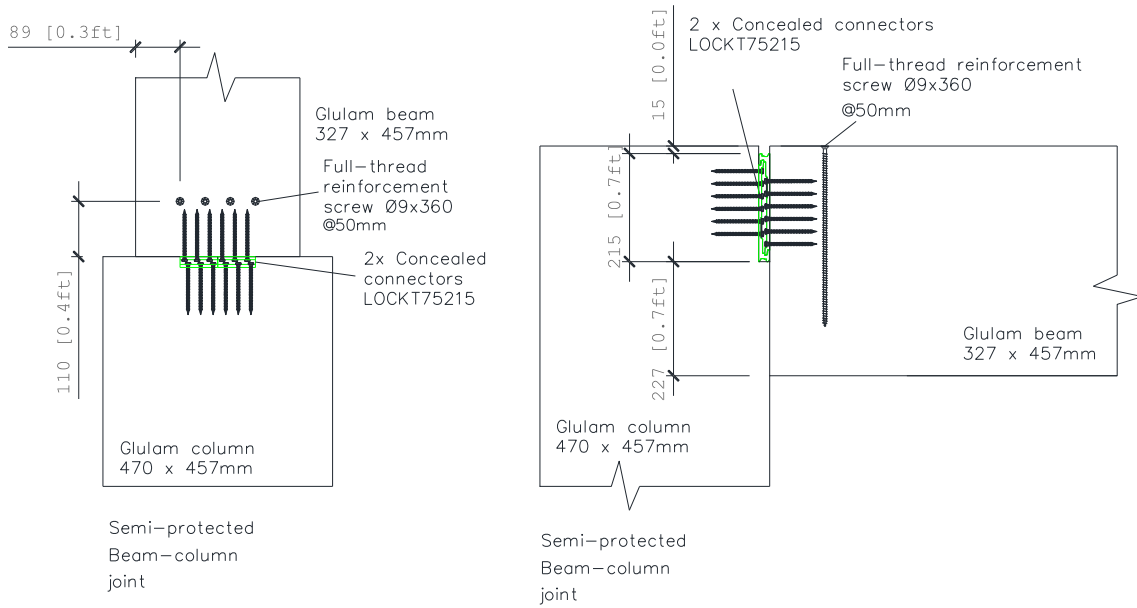


Figure 9: Column beam connection detail



Figure 10: Fire sealant applied on the beam for Test 1 and 2 (left) intumescent paint applied on the beam for Test 3, 4 and 5 (right)

The hole where the beam goes through the backwall was cut on site, which was done with a jig saw. The gap size varied significantly and was up to an inch at some locations and was, therefore, not representative for factory-made cuts. For this reason, no effort was made to use representative sealing methods. In Test 1 the gap was filled with ceramic insulation. As this appeared not to be enough to avoid some combustion through this detail, construction tape (see Table 3) was added on the unexposed side in all other tests.

The detail on the top and the sides of the openings has been changed iteratively to improve its performance. After the results of Test 1 it was clear that the detail should account for an increased exposure from the fire plume, by avoiding the direct inflow of hot gasses through the gypsum board joints in the (predictable) direction of the flow of hot gasses (Figure 11). The details implemented in subsequent tests aimed to limit this. Figure 11 shows the details used at the top of the opening. In addition, after assembly of the CLT structure, fire sealant was applied to seal the lap joints at the front side in the CLT above the opening in Test 2 and 3. In Test 4 and 5, construction tape was used to seal these lap joints instead. This was implemented to limit potential smouldering which was seen in Test 1.

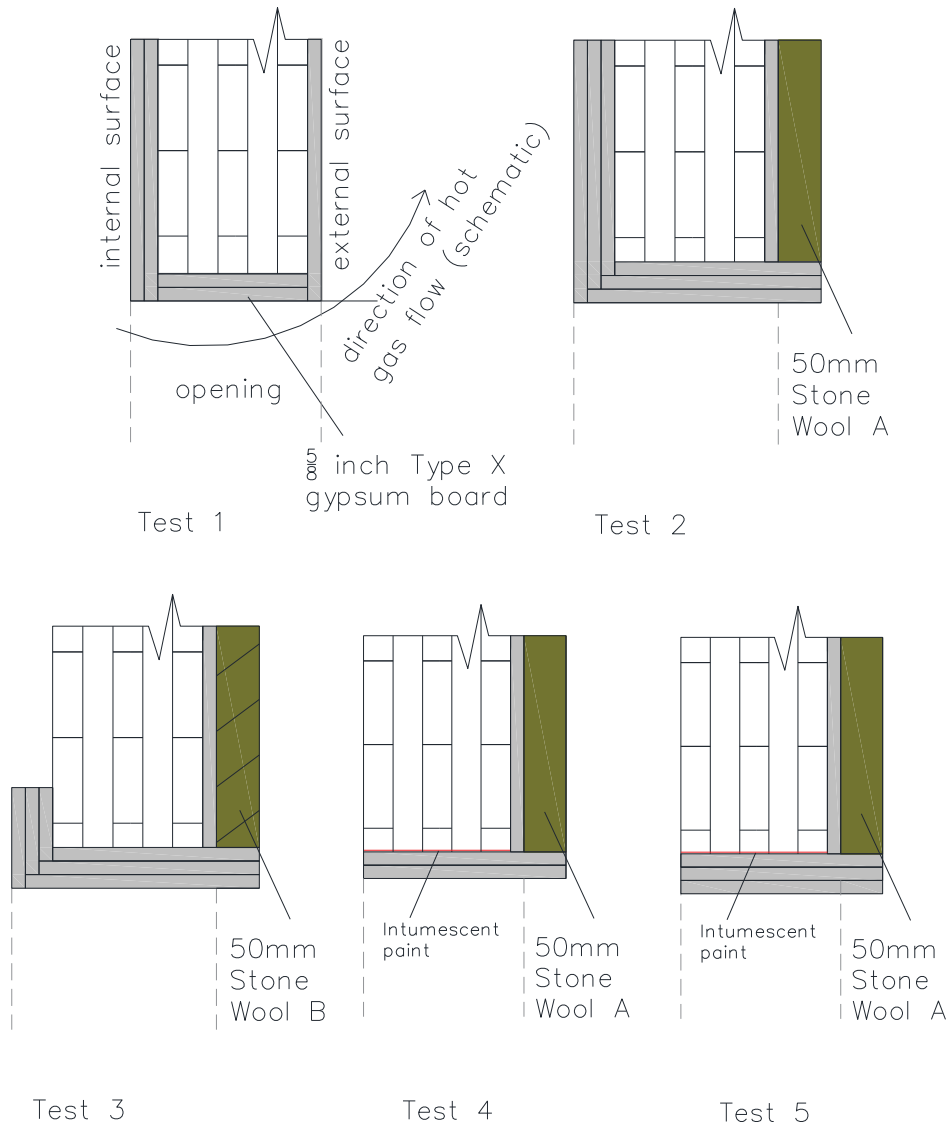


Figure 11: Detail at the top of the openings for each test.

4.3 Measurements

Measurements have been made to map the interior fire exposure, the heating of the structure and the fire exposure to exterior surfaces, among other things. Most measurements have been repeated for all tests. However, because some design parameters were only decided upon during the test series (such as the location and area of exposed surfaces), a number of datalogger channels were dedicated to small case studies of local effects. This Section gives an overview of measurements that were similar in all tests first. In addition, a sub-section with the case-study measurements is included.

4.3.1 Compartment interior measurements

The exposure inside the compartments has been recorded using plate thermometers, positioned about 4 inches (100 mm) in front of surfaces, and thermocouples in

thermocouple trees. The interior plate thermometers are constructed in accordance with EN 1363-1 (2020)

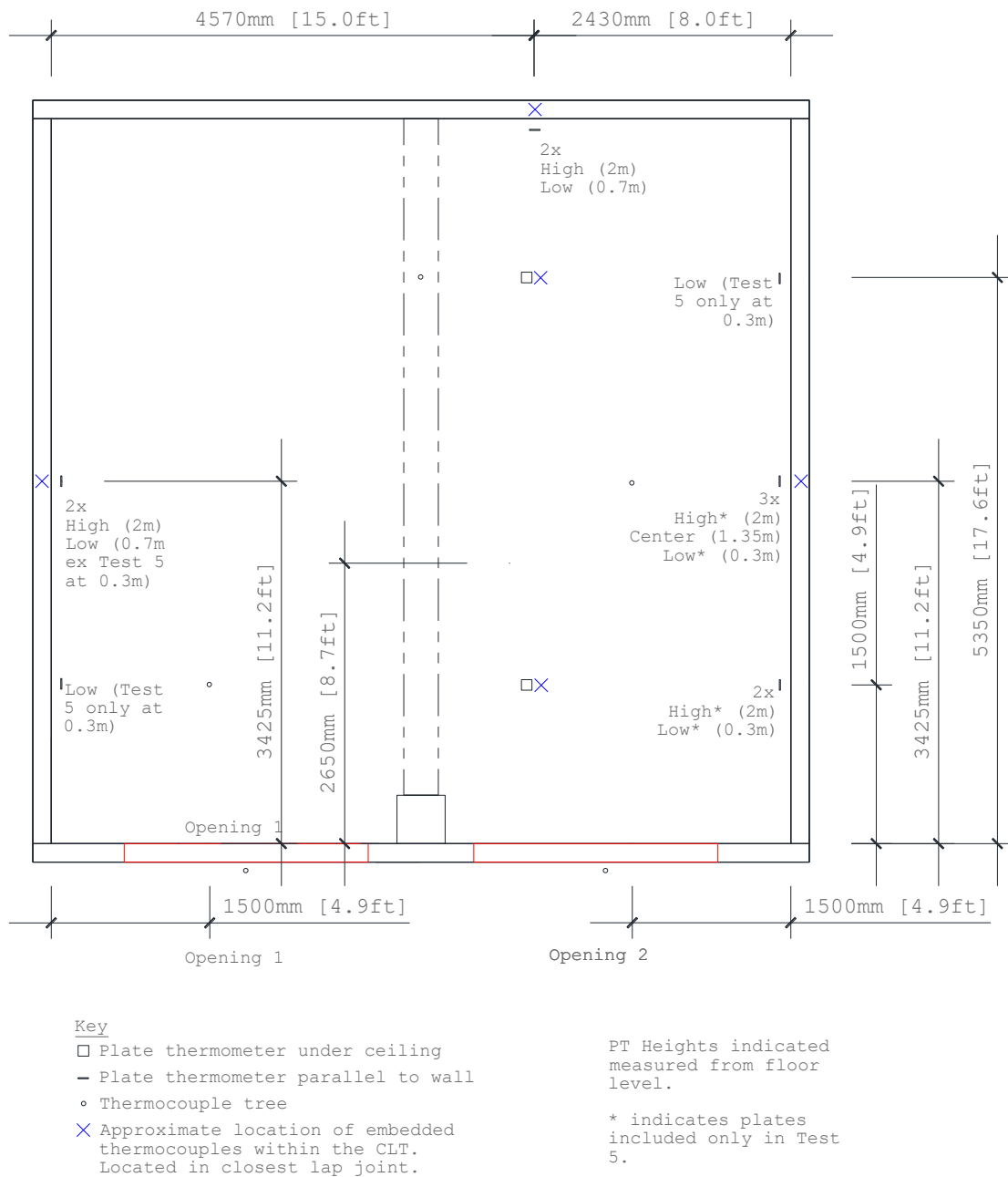


Figure 12: Locations of plate thermometers. See Annex A for full list of coordinates.

The interior thermocouple trees have thermocouples at 0.2, 0.8, 1.2, 1.8 and 2.4 m from the floor and were positioned in three locations as indicated in Figure 12. Two additional thermocouple trees were positioned in the center of the openings (one for opening) as indicated in the figure. The thermocouples used were Inconel sheathed type-K thermocouples with a diameter of 1.0 mm, rated for temperatures up to 1200 °C.

4.3.2 Material temperature measurements

Temperature measurements inside the walls and ceiling were made at several locations indicated in Figure 13. At each location thermocouples were installed at 5 depths of the CLT and, if protected, behind every layer of gypsum board. The direction of the thermocouples has been proven to be very important for measurements inside thermally insulating materials, such as timber. Installation of the thermocouples parallel to the heat flow can lead to a delay of measured temperature increase (Fahrni et al., 2018), and in fires with a decay phase can misrepresent the peak temperatures by several hundred °C (Brandon and Dagenais, 2018). Therefore, all thermocouples were installed with at least 170 mm of the final length parallel to the expected isotherms (perpendicular to the heat flow). This was done by leading the thermocouple through a groove in a lap joint in the wall (Figure 14) or a spline board joint in the ceiling (Figure 15). At the end of the groove the 1.0 mm thermocouple is inserted in a 1.5 mm, 75 mm deep hole that was drilled using a drill guide to control a drill angle of 90° with the surface.

After Test 1 and 2 the temperature measurements within the CLT and gypsum board intersections continued until the next day to study the potential progression of the heat wave through timber.

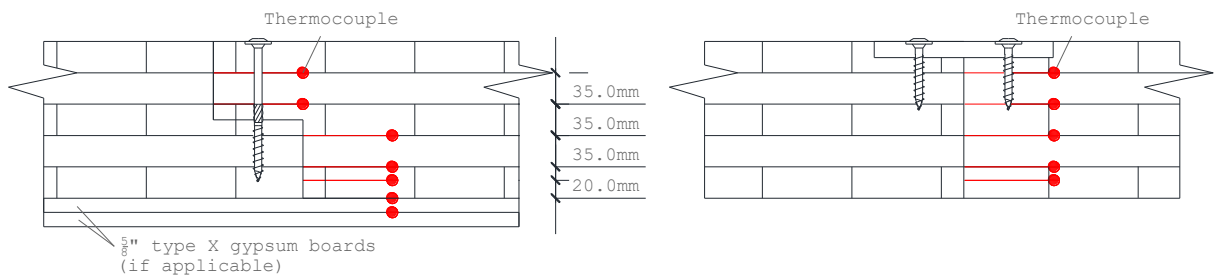


Figure 13: Embedded thermocouples at lap and spline board joint.



Figure 14: Thermocouples installed at lap-joint of a wall. The thermocouple tip is located at a depth of 75 mm from the visible surface.

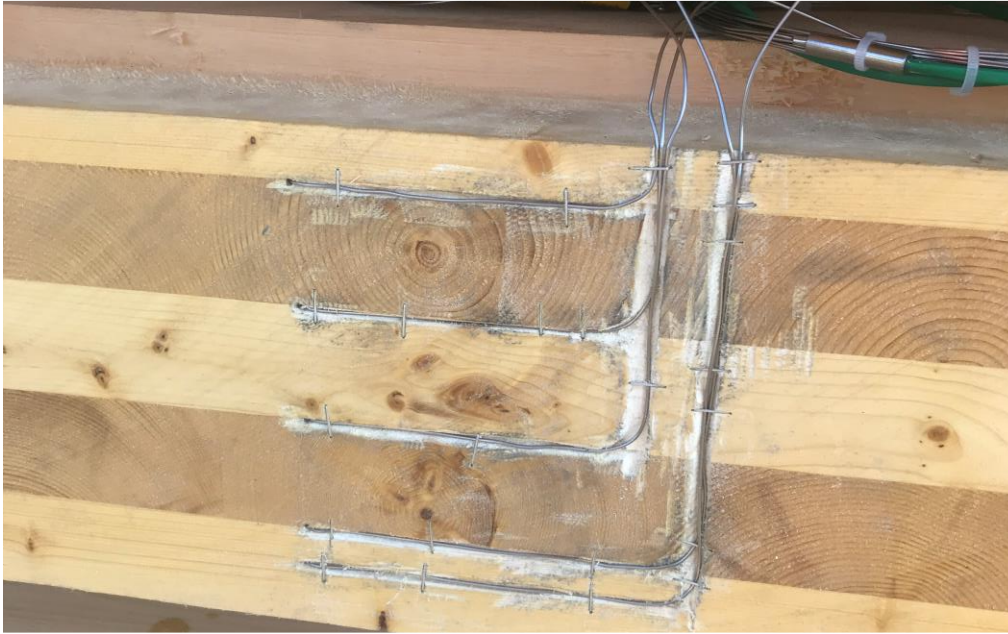


Figure 15: Thermocouples installed at the spline board joint of the ceiling. The thermocouple tip is located at a depth of 75 mm from the visible surface.

4.3.3 Façade and other exterior measurements

Two façade extensions were placed on top of each compartment above the openings. The façades were light weight concrete with nominal density of 575 kg/m^3 . The moisture content of the concrete was checked before Test 1 on a reference sample to be 22 %. For corrections of the mass loss calculation the façades were weighed before and after each test. Blocks of $600 \times 400 \times 50 \text{ mm}$ (width x height x thickness) were supported by a steel frame and could be lifted on and off the compartments for reuse during all tests (Figure 16).



Figure 16: Placement of a façade segment on the construction (left). Facades in place prior to test 1.

The façade structure was instrumented with a number of thermocouples (TC) corresponding to some of the assessment points of test standards (NFPA, CAN/ULC, BS 8414, ISO 13785-2, SP Fire 105 as well as the recently proposed European method), as shown in Figure 17. In addition, four plate thermometers (PT), as used in standard fire resistance furnaces (Wickström, 1994) were embedded flush to the surface of each façade (Figure 18). A full list of instrumentation including their location and number can be found in Annex A.

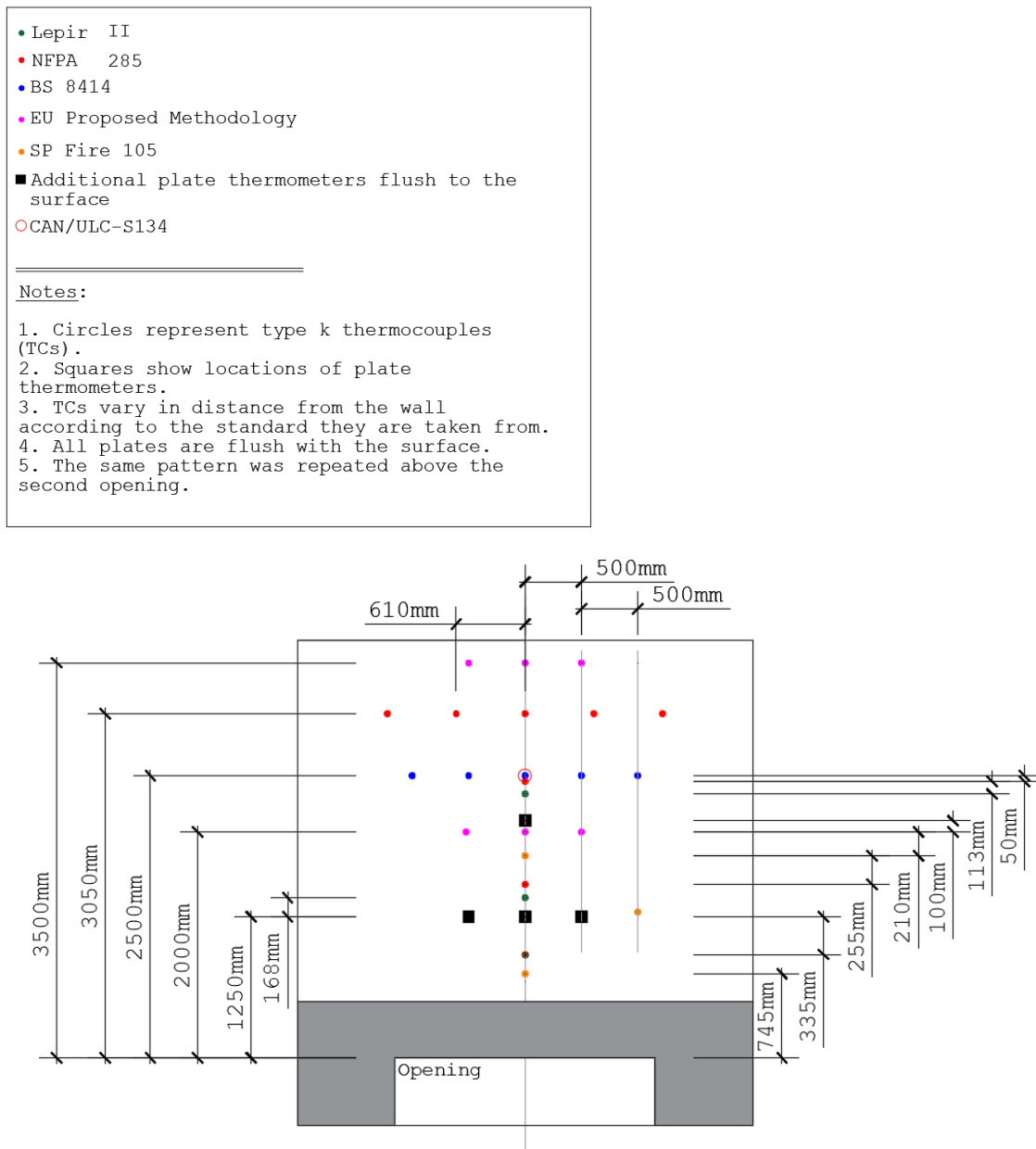


Figure 17: Placement of the PTs and TCs installed in the façade above the opening. The same positions are repeated above the second front opening.



Figure 18: PT 4 embedded flush to the façade surface. Under the PT a 1 mm diameter TC (TC 7) extrudes 5 cm and above a 3 mm diameter TC extrudes 10 cm.

Additionally, special plate thermometers with thicker, lighter insulation and thinner Inconel plate were placed at 4.8 m and 8 m in front of each opening (4 in total) at mid-height of the opening (1.3 m in Tests 1, 2, 3 and 5 and 1.1 m in Test 4) from the floor level. Such plates have previously been used for assessing the irradiance from fire to objects in ambient temperatures (Sjöström et al, 2015). Additionally, at 8 m distance and at a height of 4 m one additional standard PT was installed to exemplify differences in irradiance with height.

At each opening a TC tree with 1 mm shielded Inconel TCs were placed at heights 0.6 m, 1 m, 1.4 m, 1.8 m and 2.2 m from the floor level.

Test 5 had reduced measurements above the façade, as a consequence of wind damage to the façade frames during the days before the test. In Test 5 only PTs 1, 2 and 3 and TCs 5 and 25 were included above the left opening, and none above the right opening (see full list in Annex A for details of their locations).

Cameras were placed at different angles and distances to evaluate the flame height and shape during the tests, recording at 120 fps. The method of determining the flame height digitally, is discussed in the façade exposure report (Sjöström et al. 2018).

4.3.4 Mass measurements

The mass of the floor and the mass of the rest of the structure were measured separately. This was achieved by positioning the floor and walls on separate welded steel frames (Figure 19). The steel frames comprised of 300 mm high (IPE 300) I-beams positioned on top of four 50 kN capacity load cells each (Figure 20). The floor consisted of a 175 mm CLT slab, with 20 mm stone wool and 100 mm light weight concrete on top to avoid any combustion of the CLT floor. Using the mass loss of both frames, the potential heat release rate corresponding to the fuel on the floor and the CLT structure was calculated according to Annex E.

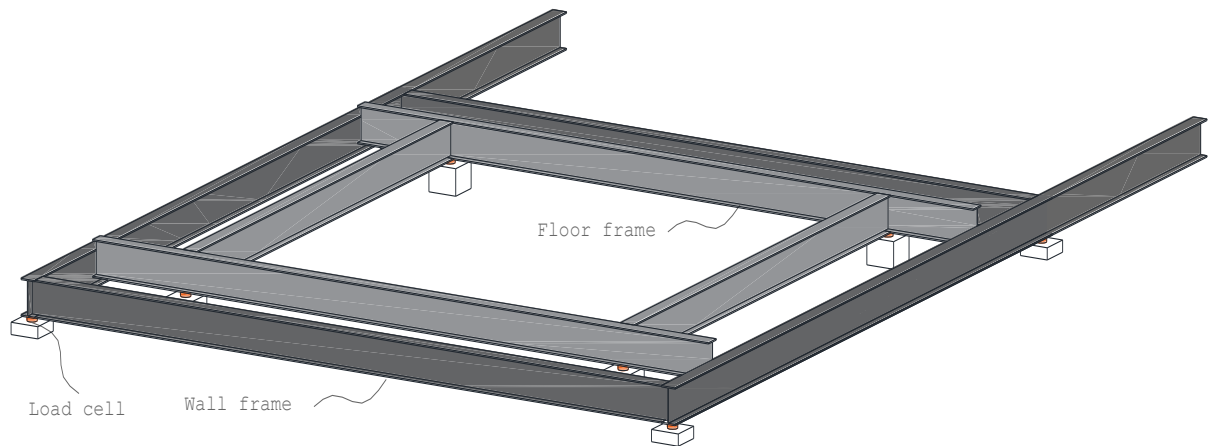


Figure 19: The steel frames for the floor (light grey) and for the walls and ceiling (dark grey)



Figure 20: Load cell underneath one of the steel frames

4.3.5 Oxygen measurements & case study measurements

Oxygen measurements were made using broad band zirconium, Bosch LSU 4.9, lambda sensors. Although lambda sensors are widely used in the automotive industry, their use for fire testing has been introduced relatively recently. Thiry et al. (2013) assessed the use of lambda sensors in fire test and concluded that their lambda sensor measurements were reliable for oxygen concentrations in at least the range of 5-20 % (their test did not go below 5 %). It should be noted that several technical problems have resulted in loss of data and an extensive proof of concept is still ongoing and until it is finished the measurement uncertainties are not fully known. However, for completeness, the measurement results are included in Annex K.

Stainless steel tubes were used to extract small amounts of gasses from the test compartment at the specified locations. Through the tubes, the gasses are led through a chamber where the sensor is installed (Figure 21). In the setup of this study, a gas pump was installed at the end of the system, implementing the required suction. The system should be fully airtight for correct measurements.

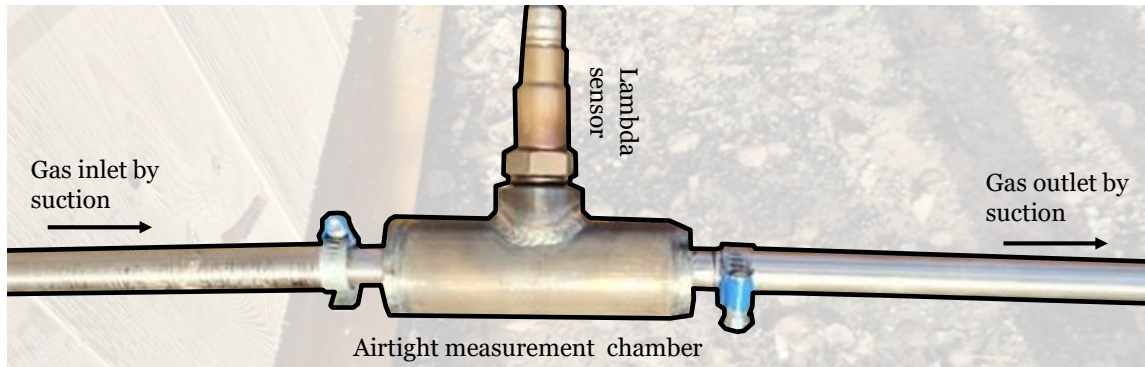
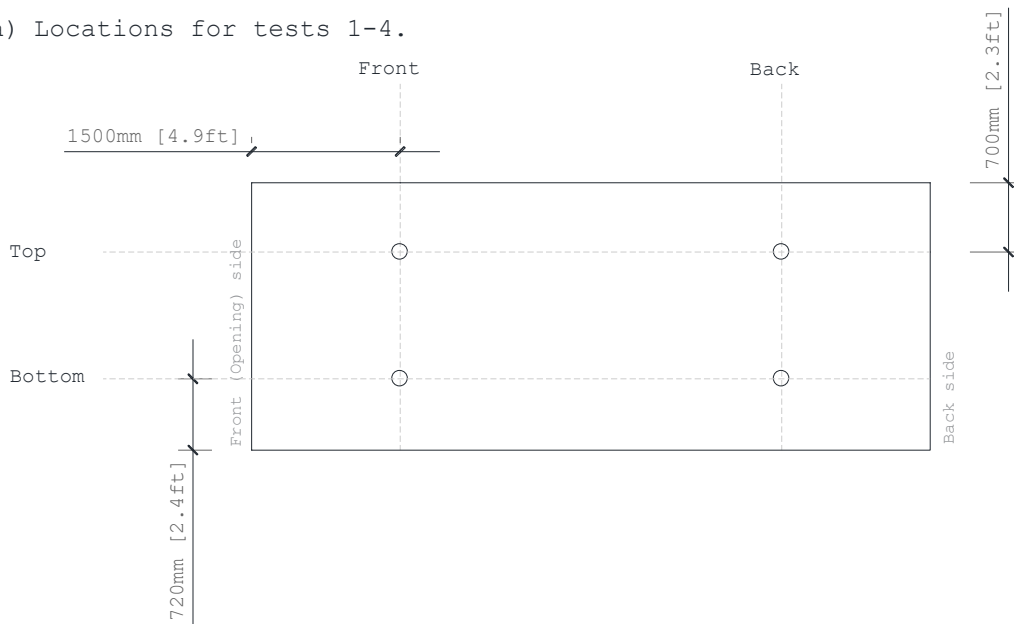


Figure 21: Lambda sensor implemented for oxygen analysis of fire tests (highlighted from background for clarification)

Due to leakage of air into the system, the measurements of Test 1 and 4 were invalid and are not included in this report. Test 2, 3 and 5 included oxygen measurements in different locations indicated in Figure 22.

a) Locations for tests 1-4.



b) Locations for test 5.

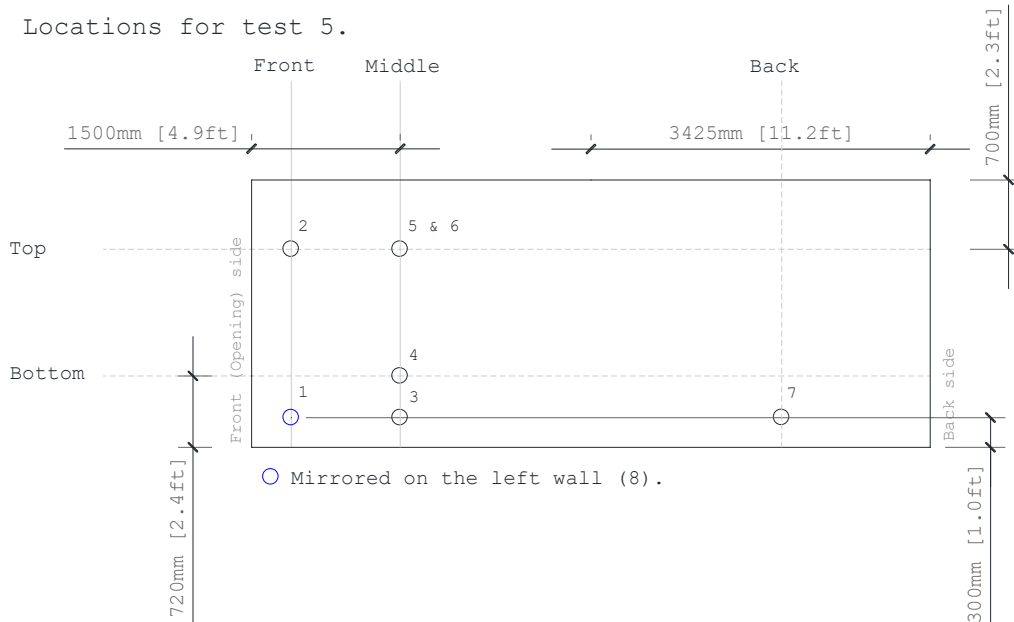


Figure 22: Oxygen measurement locations, at a distance of 200 mm away from the exposed CLT walls. For tests 2 and 3 the measurements were taken on the left wall, for test 5 these were on the right wall.

5 Pass/fail criteria – ICC TWB

The test matrix given previously in Section 4 was decided upon during the execution of the test series. Instead of planning the configurations of exposed surfaces, gypsum board protection and the number of protective layers before the execution of all tests, it was chosen to only plan the configuration of Test 1 and let the project steering group decide on the configuration of each subsequent test based on the test results. This approach was chosen with the aim to find the surface area limits of exposed mass timber and

corresponding requirements for gypsum board protection (amount and location) iteratively. To support this procedure, the project steering group defined pass criteria to reach a common agreement of the desired outcome of the fire tests needed to justify fire safe changes of current code prescribed limits. These criteria are a quantifiable adaption of the criterion (where a compartment fire should exhibit continual decay without significant fire re-growth during the decay phase for 4 hours following fire initiation) used by the International Code Council Ad Hoc Committee on Tall Wood Building (ICC-TWB) to develop the code provisions that are now part of the 2021 International Building Code (IBC 2021). The criterion was used for the assessment of the results by Zelinka et al. (2018) and a comparable criterion is being used in the required CLT compartment fire test of Annex B in the ANSI/APA PRG 320 (2018), where temperatures should be equal to or below 510 °C after 4 hours of compartment fire testing.

The following quantifiable adaptation of the ICC pass criterion was developed by the project Steering Group at the outset of this project and was included in the test plan:

- **At 4 hours after ignition the plate thermometer temperatures should be below 300 °C.** The corresponding incident radiant heat flux is roughly⁸ 6 kW/m², which has previously been identified as one of the extinction criteria of smoldering in timber (Crielaard, 2019). Achieving a complete stop of all smoldering is, however, not an aim of this study. Instead, this study aims at assessing techniques for fire fighters of locating and extinguishing smoldering that is left after the fire.
- **No secondary flashover** (identified by absence of flashover criteria as specified in UL 1715, ASTM E2257, and ISO 9705) **should occur between 3 hours and 4 hours after ignition.** Flashover shall be considered to have occurred when any two of the following conditions have been attained:
 - a. Heat release rate exceeds 0.12 MW/m² of floor area, which is determined from the mass loss rate)
 - b. Average upper layer temperature exceeds 600°C.
 - c. Flames exit one of the openings.

Exception:

In case the criteria above are locally not fulfilled caused by a detailing issue, that could be solved with a change of details, the results will be considered satisfactory (i.e. pass). In that case recommendations for further study of the fire performance of this detail will be made.

⁸ The incident heat flux of roughly 6 kW/m² is based on the assumption that the gas temperature is equal or lower than the plate thermometer temperature, which is generally the case in a decaying fire.

6 Test results

6.1 Events

Significant events that occurred during the tests are listed in Table 4 together with the corresponding time after ignition. The highly variable time to flashover is expected to be to some extent caused by the relatively high variability of the time it took for the ignited bin, to ignite the sofa cushions.

The tests were stopped at the indicated times. In Test 1, 2, 4 and 5 the fires decayed until the test was stopped at 4 hours after ignition. At that time, there were some hot-spots and embers left in the compartment. In Test 4 (large opening) the smoldering almost completely stopped. In Tests, 2, 3 and 5 there were some occasional local flames at the wall surface during the final stages, but they had no significant effect on the global temperatures. In Test 3 increased flaming on the left wall starting at around 3:12 h which led to increased flaming on the right wall as well.

Table 4: Significant events and time after ignition (h:mm)

	Test 1	Test 2	Test 3	Test 4	Test 5
Flashover	0:14 h	0:08 h	0:12 h**	0:17 h	0:04 h*
Start of decay	0:36 h	0:36 h	0:43 h	0:22 h	0:34 h
Duration of the fully developed phase	0:22 h	0:28 h	0:31 h	0:05 h	0:30 h
Fall-off of exposed GB layer	-	0:32 h ~1-2 m ² <i>Above combustible 'A' of Figure 2</i>	-	-	0:36 h ~1 m ² <i>Above combustible 'A' of Figure 2</i>
Fall-off of other GB layers	-	-	-	-	-
Overall temperature increases during the decay phase	-	-	3:05 h and onwards	-	-
Smoldering/flaming through intersections	See Section 6.15	-	See Section 6.15	-	-
Stop of the test	4:00 h	4:00 h	3:31 h***	4:00 h	4:00 h

* The sofa cushions ignited significantly faster than in other tests, leading to a faster fire growth

** The pillow near the ignited bin did not ignite automatically. At approximately 5 minutes after the initial ignition, the fire brigade ignited that specific pillow manually.

*** The test was stopped as it did not pass the criterion set by the project steering group to have continuous decay until 4 hours after ignition, as such, this configuration of mass timber surface exposure (i.e., where two exposed wall surfaces meet at a corner) would not be recommended for high rise buildings, where there

is possibility that an automatic sprinkler system could fail and that fire service intervention may not occur for 4 hours.

Photos taken during the tests are shown in Annex M. Videos of the tests are available online at the web addresses listed below.

Test 1: <https://youtu.be/V4VUF-FbraY>

Test 2: <https://youtu.be/UgtHJwfhaJs>

Test 3: https://youtu.be/_R4EfKnQd2Q

Test 4: <https://youtu.be/jOELM-cv-U8>

Test 5: <https://youtu.be/WUy-NEBLRoE>

More are available through the RISE Fire Research YouTube account, at:

<https://www.youtube.com/channel/UCi7ee3Rvuc1mZw-GsFjROgQ/videos>

6.2 Video frames

Frames of videos with a view into the compartment are shown in this section. Frames of the video at: the moment of flashover; 30 minutes after flashover and every hour after flashover until the end of the tests are shown in Figure 23 to Figure 37.



Figure 23: Test 1 - Video snapshots at flashover (left) and 30 minutes after flashover (right)



Figure 24: Test 1 - Video snapshots at 1 hour (left) and 2 hours (right) after ignition



Figure 25: Test 1 - Video snapshots at 3 hours (left) and 4 hours (right) after ignition



Figure 26: Test 2 - Video snapshots at flashover (left) and 30 min after flashover (right)



Figure 27: Test 2 - Video snapshots at 1 hour (left) and 2 hours (right) after ignition



Figure 28: Test 2 - Video snapshots at 3 hours (left) and 4 hours (right) after ignition



Figure 29: Test 3 - Video snapshots at flashover (left) and 30 minutes after flashover (right)



Figure 30: Test 3 - Video snapshots at 1 hour (left) and 2 hours (right) after ignition



Figure 31: Test 3 - Video snapshots at 3 hours (left) and 3.5 hours (right) after ignition



Figure 32: Test 4 - Video snapshots at flashover (left) and 30 minutes after flashover (right)



Figure 33: Test 4 - Video snapshots at 1 hour (left) and 2 hours (right) after ignition



Figure 34: Test 4 - Video snapshots at 3 hours (left) and 4 hours (right) after ignition



Figure 35: Test 5 - Video snapshots at flashover (left) and 30 minutes after flashover (right)



Figure 36: Test 5 - Video snapshots at 1 hour (left) and 2 hours (right) after ignition



Figure 37: Test 5 - Video snapshots at 3 hours (left) and 4 hours (right) after ignition

6.3 Weather conditions

To avoid laboratory limitations to govern the compartment design it was decided to perform the tests outdoors on a fire test site of Södra Älvsborgs Räddningstjänstförbund, Borås, Sweden. Significant effort was made to protect the compartment against rain by covering the compartment during construction using a thick plastic tarpaulin (Figure 38 and Figure 39) at any time this was possible and by only removing this at times without rain. Also the façade extensions, which were made of light weight concrete were covered to prevent direct rainfall on the concrete parts. The timber materials were covered similarly and the gypsum boards were stored indoors. The tests were conducted in a valley at days where the forecasted wind velocity and the risk of precipitation was low.

Table 5: Weather conditions for each test.

Test	Date	Average Temp. F (°C)	Average Relative Humidity	On site wind velocity mph(m/s)	Wind direction **
1	2020/ 09/16	59°F(15°C)	89%	0.9 (0.4)	North
2	2020/ 09/30	54°F(12°C)	89%	0.9 (0.4)	
3	2020/ 10/09	52°F (11°C)	73%	1.0-3.0 (0.45-1.35)*	
4	2020/ 10/21	52°F (11°C)	98%	2.0 (0.9)	
5	2020/ 11/09	45°F (7°C)	83%	2.0 (0.9)	

* In Test 3 the measurements failed, but based on measurements of the nearest weather station (18.3 km away) the expected average wind velocity to have been up to approximately 50 % higher than other tests.

** In all tests the wind direction was towards the open façade at an angle close to 90°.



Figure 38: Tarpaulin covering the compartment



Figure 39: Interior during construction

6.4 Interior plate thermometers

Measurements using plate thermometers inside the compartment, installed at a distance of 2.8 inch (10 cm) from wall or ceiling surfaces, facing away from the surface, are shown

in this chapter together with the temperature criterion discussed in Chapter 5. Figure 40 to Figure 44 show the plate temperatures for Test 1 to 5, respectively. The plate thermometers were located as indicated in Figure 12 (Section 4.3.1). The front plate thermometer in the ceiling malfunctioned repeatedly and is, therefore, not visible in most of these figures.

Figure 45 shows temperatures of the plate thermometers on the left wall 6.6 ft (2.0 m) from the floor of every test for comparative purposes. To improve the clarity of the figure for comparisons, the curves were time adjusted so that the moment of flashover is at 10 minutes on the x-axis.

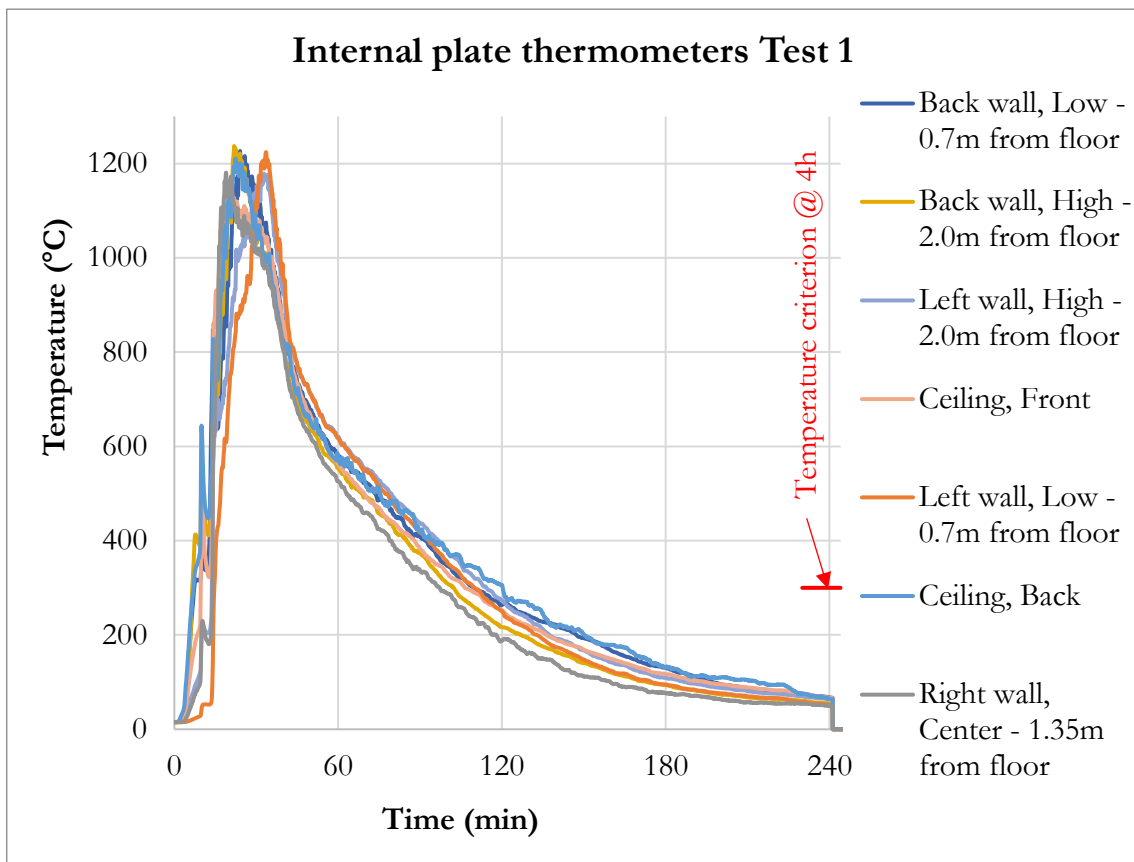


Figure 40: Internal plate thermometer measurements of Test 1

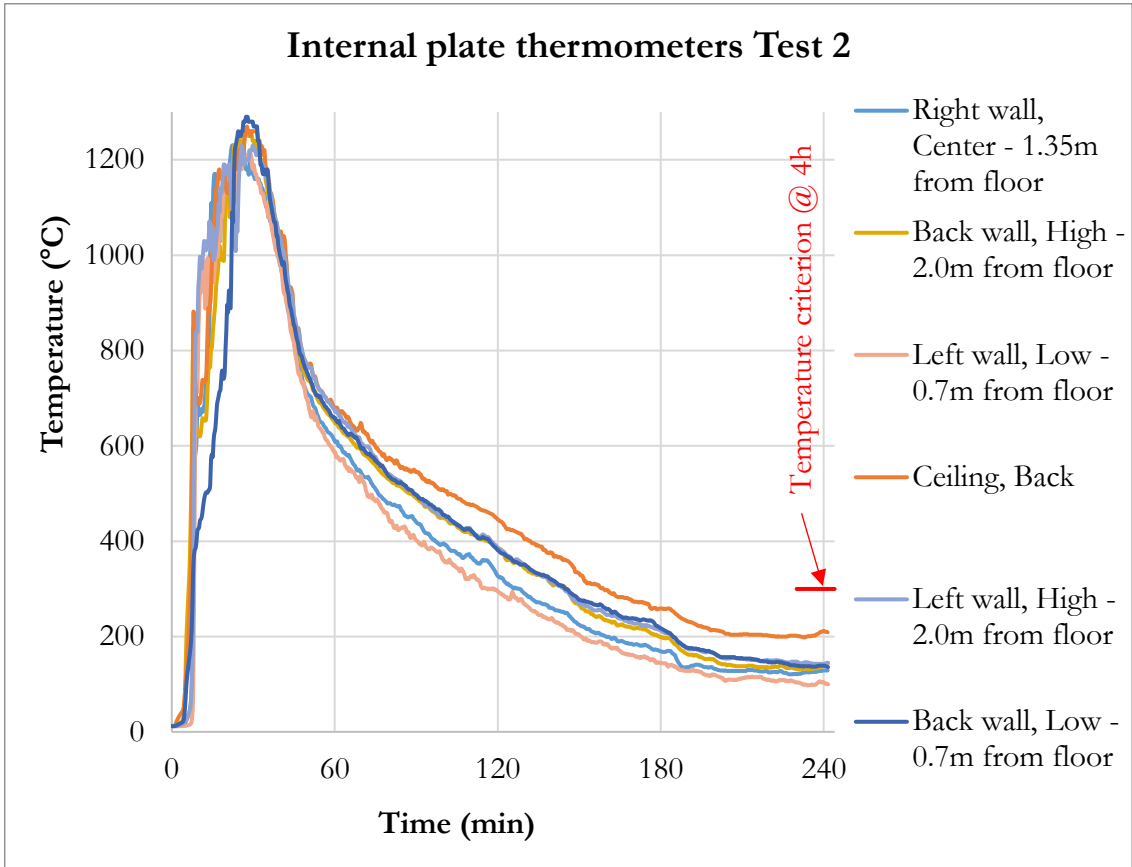


Figure 41: Internal plate thermometer measurements of Test 2

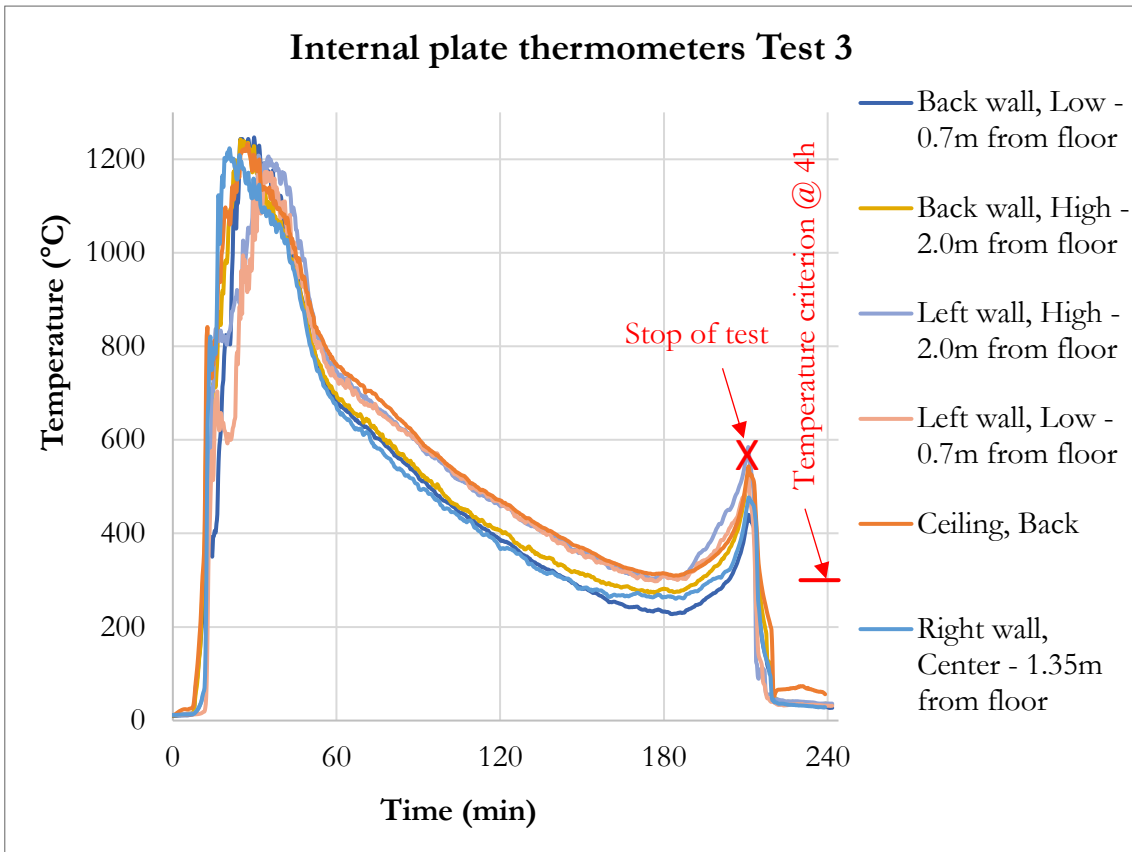


Figure 42: Internal plate thermometer measurements of Test 3

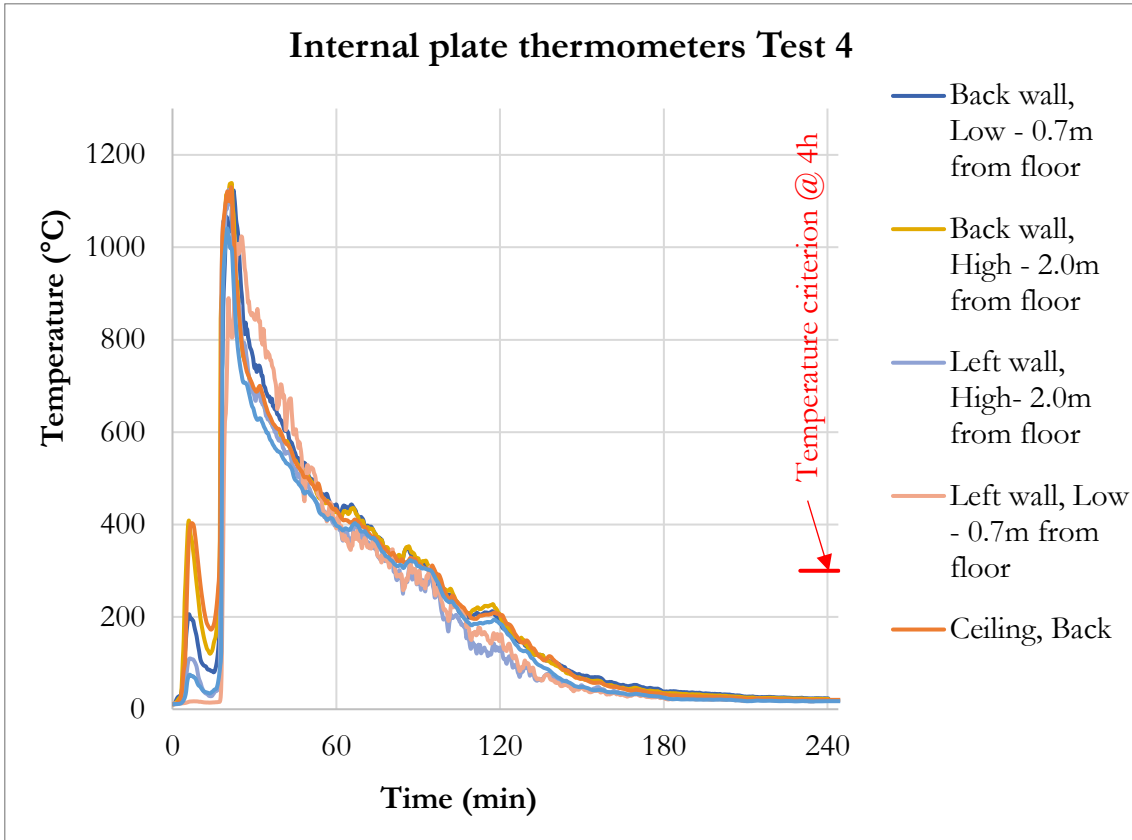


Figure 43: Internal plate thermometer measurements of Test 4

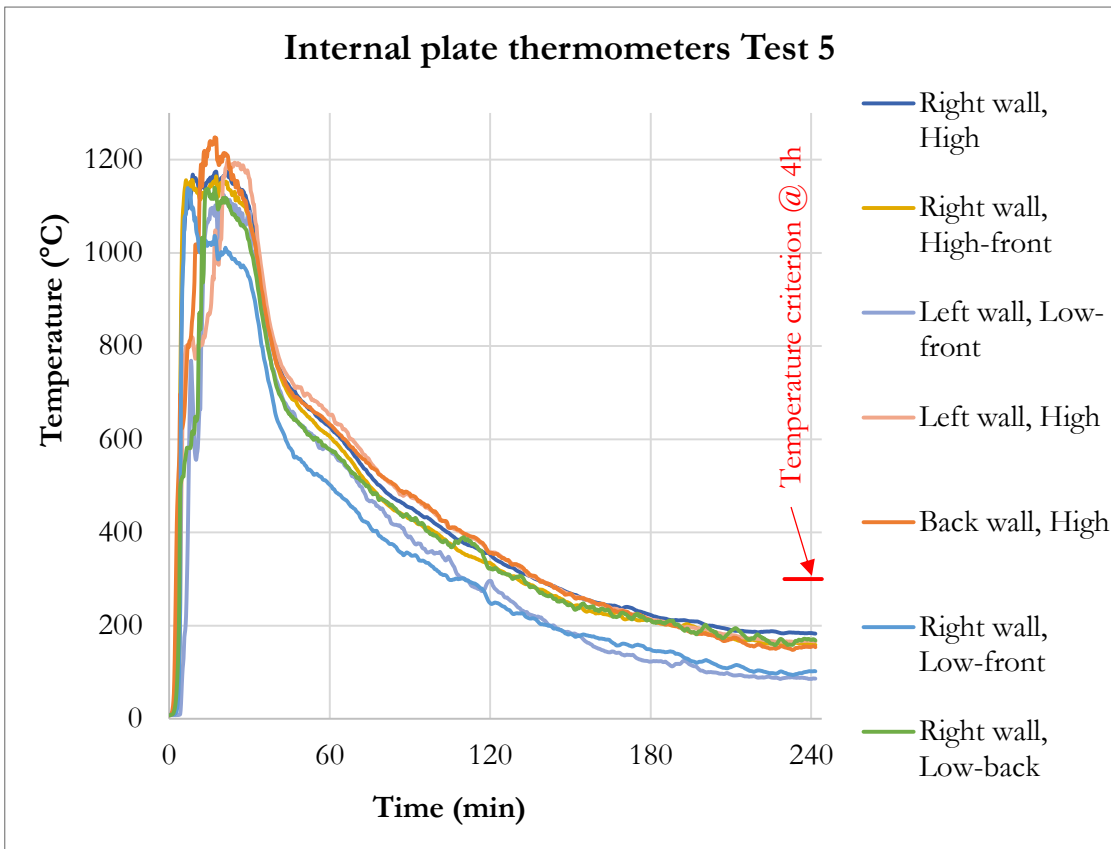


Figure 44: Internal plate thermometer measurements of Test 5

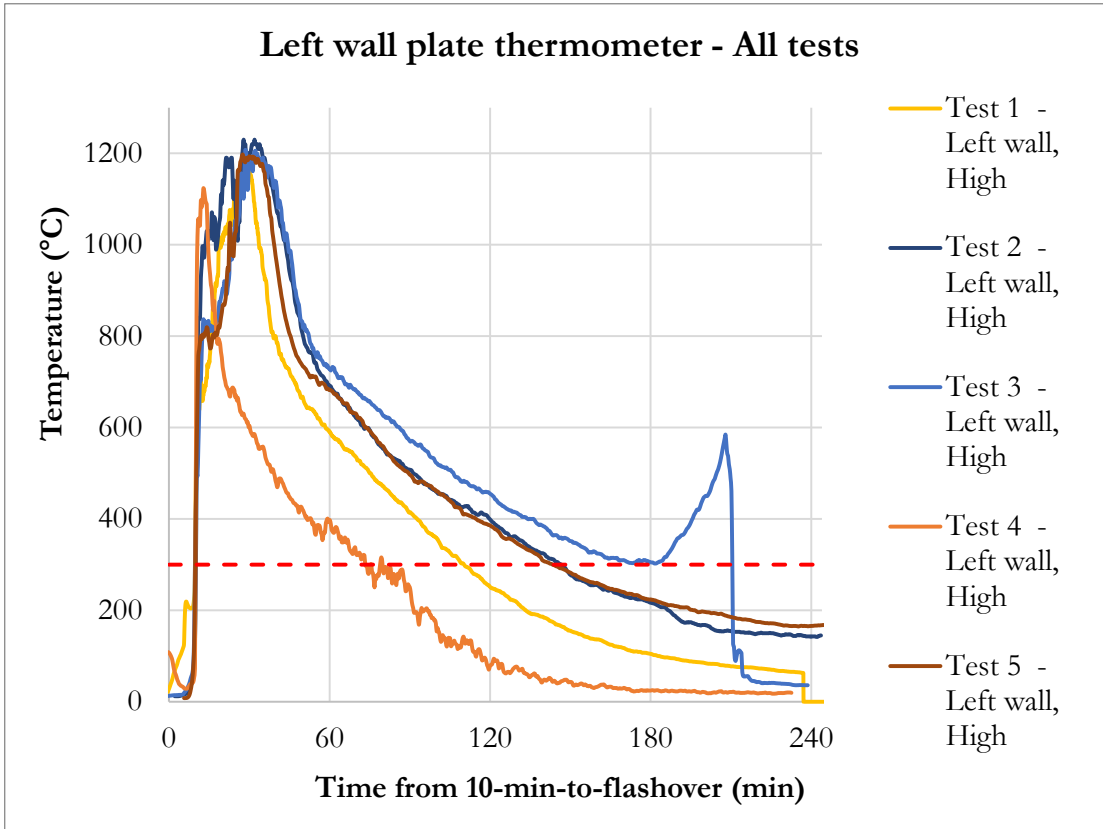


Figure 45: Left wall plate thermometer measurements at 2.0 meters (6.6ft) from the floor of all tests. The red dashed line indicates the 300 °C criterion at 4 hours.

6.5 Thermocouple trees

Annex H shows all interior thermocouple tree measurements and Annex I shows measurements of the thermocouple trees (TCT) located at the openings. In this section only a selection of data to show the most relevant findings is given.

In tests of compartments with the smaller opening factor (Test 1, 2, 3 and 5) temperature measurements indicated an approximately homogeneous temperature profile. The temperature measurements from thermocouples installed at different heights were similar and the temperatures at different locations of the floor plan were similar. TCT 2 fell consistently between 30 and 40 minutes in Test 1, 2 and 3. As an example, the thermocouple tree measurements of Test 2 are shown (Figure 46 to Figure 48).

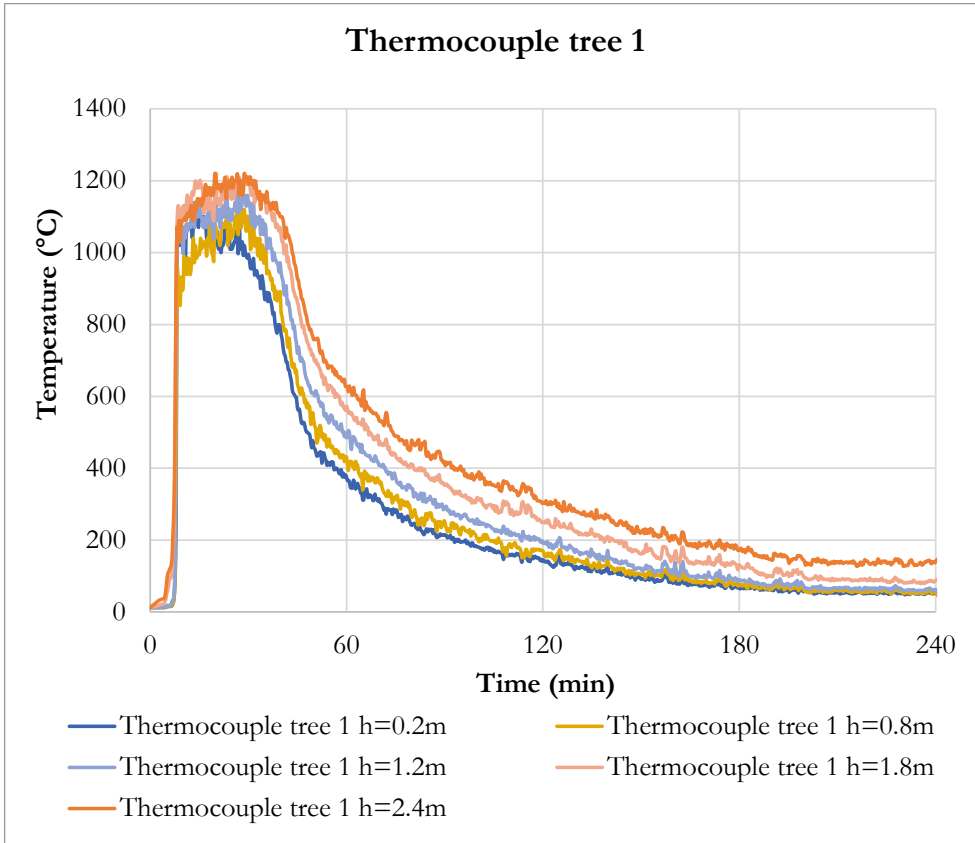


Figure 46: Test 2 - Thermocouple tree 1

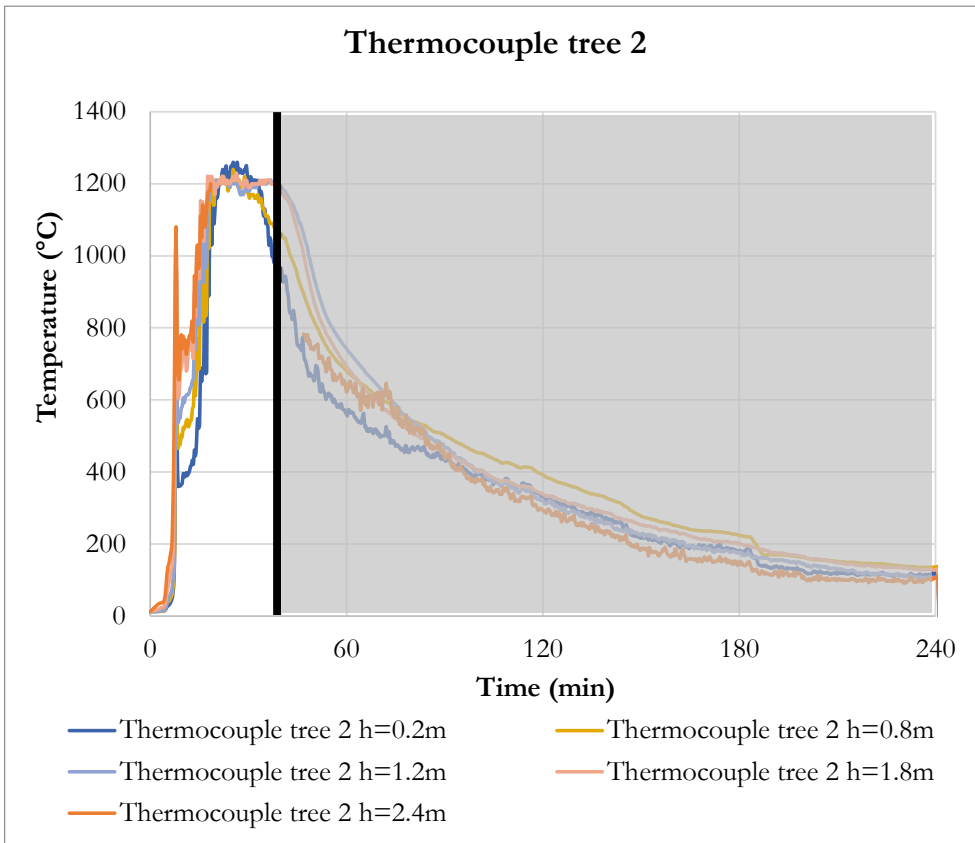


Figure 47: Test 2 - Thermocouple tree 2 (fell down at 40 min)

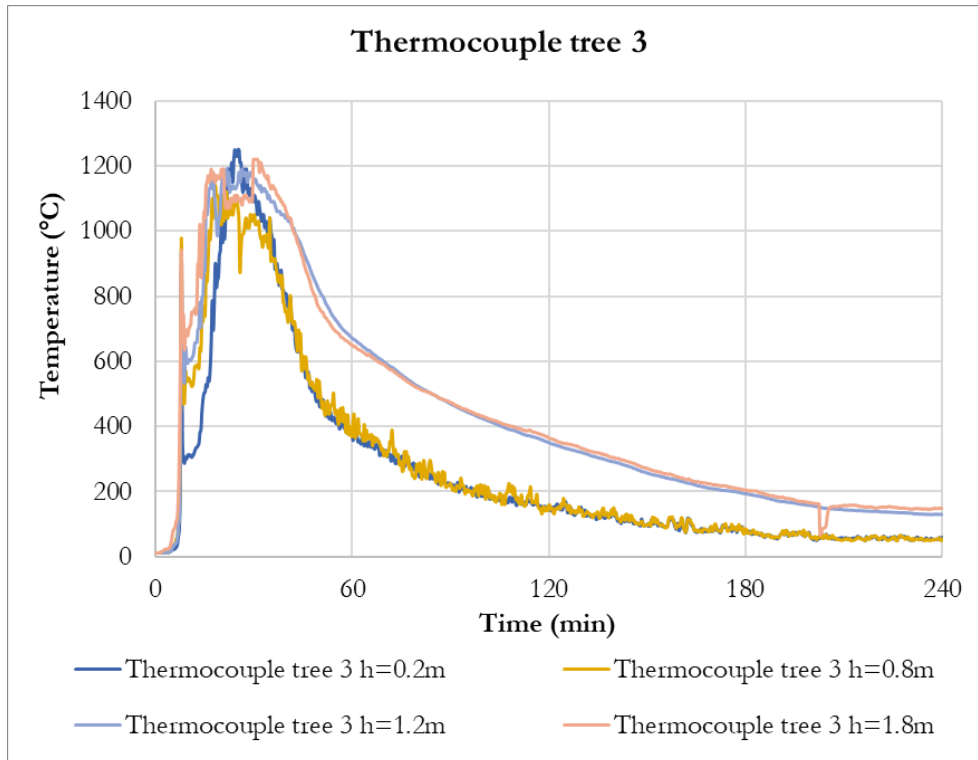


Figure 48: Test 2 - Thermocouple tree 3

A comparison between thermocouple tree temperatures of the small opening tests (1, 2, 3 and 5) is made using Figure 49. It should be noted that the time to flashover is shifted to 10 minutes for each test, to allow a clear comparison of the post-flashover phase. Because TCT 2 fell at a relatively early stage in three of these fires it is not included in this analysis.

The temperatures of Figure 49 follow the same initial curve in the developing phase and the start of the fully developed phase. The temperatures of Test 2, 3 and 5 decayed at approximately the same time after flashover and followed a comparable decline until approximately 3 h. Test 3 started to increase in temperature from that point, while Test 2 and 5 kept decaying. Further discussions regarding the difference between Test 3 and the other tests is provided in Section 0. Test 1 decayed at an earlier stage than the other tests. This matches modeling done for this project as discussed in the project modelling report (Brandon et al. 2021) and it is therefore concluded that this earlier decay is related to the difference of exposed surface areas of mass timber.

The thermocouple trees in Test 4 showed more significant variation over height (e.g. Figure 50). In a short period after flashover the temperatures in the top of the thermocouple trees were highest but dropped quickly after that. At TCT 2 and TCT 3, temperatures from the base up to 1.2 m high showed a slower decrease (see Annex H).

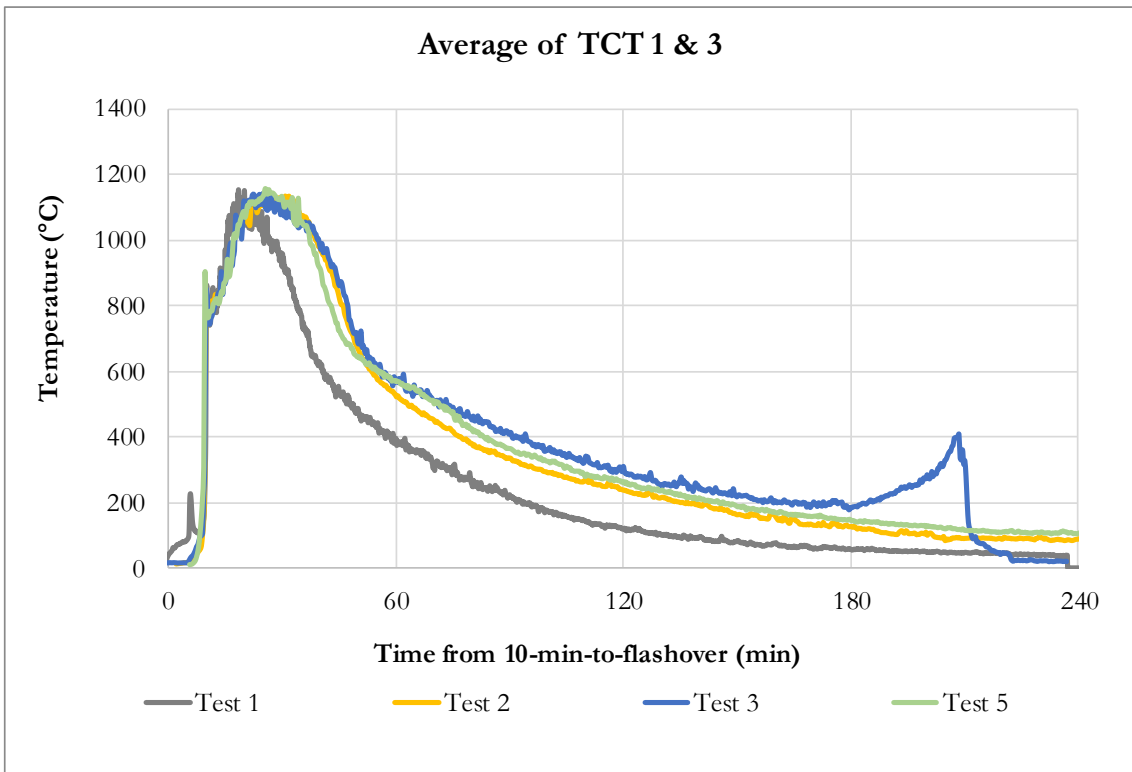


Figure 49: Average temperatures of TCT 1 and 3 in Test 1, 2, 3 and 5.

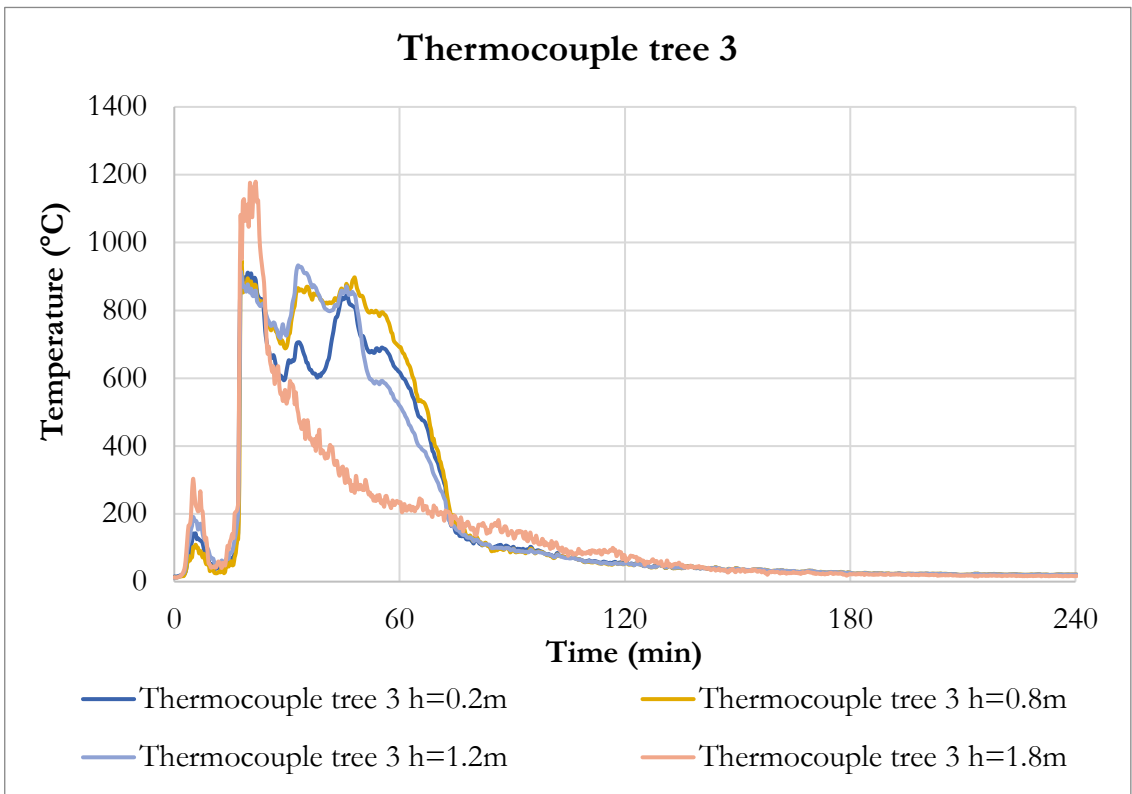


Figure 50: Test 4 - Temperatures of TCT 13

6.6 Incident radiant heat flux (interior)

The incident radiant heat flux, or irradiance can be calculated from plate thermometer measurements, if there is knowledge of the gas environment (known gas temperature and convective heat transfer coefficient). It can be determined by (Häggkvist et al, 2013):

$$\dot{q}_{inc}'' = \sigma T_{PT}^4 + \frac{(h_c + K)(T_{PT} - T_g) + C \frac{\partial T_{PT}}{\partial t}}{\varepsilon} \quad \text{Eq.1}$$

Where:

- \dot{q}_{inc}'' is the incident radiant heat flux
- σ is the Stefan-Boltzmann constant
- h_c is the convection coefficient
- T_{PT} is the temperature measured by a plate thermometer
- T_g is the gas temperature
- K is the heat loss correction according to Häggkvist et al (2013)
- $C \frac{\partial T_{PT}}{\partial t}$ is the heat storage correction associated with the lumped specific heat of the plate and the insulation according to Häggkvist et al (2013)
- t is the time
- ε is the emissivity

For fire conditions, it is recognized that the exact gas temperature is not easily measured as it requires complete elimination of radiative impact on the measurement device. However, because the calculated heat flux in this case is highly insensitive to variations of the gas temperature inside a compartment fire, it is considered reasonable in this case to approximate the gas temperature by measuring with thin thermocouples (1 mm, type K, Inconel sheathed). The response time of the plate thermometers, which is in general 1 to 2 minutes, is significantly shorter than the time scale of interest. Therefore, the term $C \frac{\partial T_{PT}}{\partial t}$ is neglected. Brandon and Dagenais (2018) showed with an experimental study in comparable fire conditions that (a) the calculated incident radiant thermometer measurements by a plate thermometer in combination with a thermocouple and (b) the incident radiant heat flux to a water cooled heat flux gauge (corrected using measured temperatures of the sensor) were similar. They also showed that the calculations of the incident radiant heat flux using plate thermometer measurements were insensitive to variations of the convective coefficient. The reason for the insensitivity is the vast ratio between the two terms of Eq. 1 for compartment fire temperatures:

$$\sigma T_{PT}^4 \gg \frac{(h_c + K)(T_{PT} - T_g)}{\varepsilon} \quad \text{Eq. 2}$$

To confirm this lack of sensitivity to both the heat transfer coefficient and the chosen representative gas temperature, a small sensitivity study was conducted utilizing the internal PT at 6'7" (2.0 m) from the floor at the center of the right wall in Test 5, which also had a TC provided adjacent to it. The plate was painted with special paint to achieve an emissivity of 0.92. Three different gas temperatures were considered, a low set of

temperatures from TC Tree 1 at 1.2 m, a hot set of temperatures from TC Tree 3 at 1.8 m and the temperatures from adjacent thermocouple, see Figure 51. Two variations of the $h_c + K$ term have also been used, an upper bound of 30 W/m²K (i.e. $h_c = 25$ W/m²K as recommend by Eurocode 1 Part 1-2, and $K = 8$ (Hägglkvist et al, 2013)) and a lower bound of 5 W/m²K (i.e. $h_c = 0$). The matrix of cases considered can be seen in Table 6.

Table 6: Incident radiant heat flux sensitivity study matrix

Sensitivity Case	Gas Temperature	$h_c + K$ (W/m ² K)
1	TC tree 3 h=1.8m (high temperatures)	30
2	TC tree 1 h=1.2m (low temperatures)	30
3	TC tree 3 h=1.8m (high temperatures)	5
4	TC Right Wall Centre Hi	30

The results of the sensitivity study show very little influence in the results due to either the chosen gas temperature or the $h_c + K$ term (Figure 52). The maximum variation was 8 kW/m² (between cases 1 and 2) or 3% of the peak incident radiant heat flux.

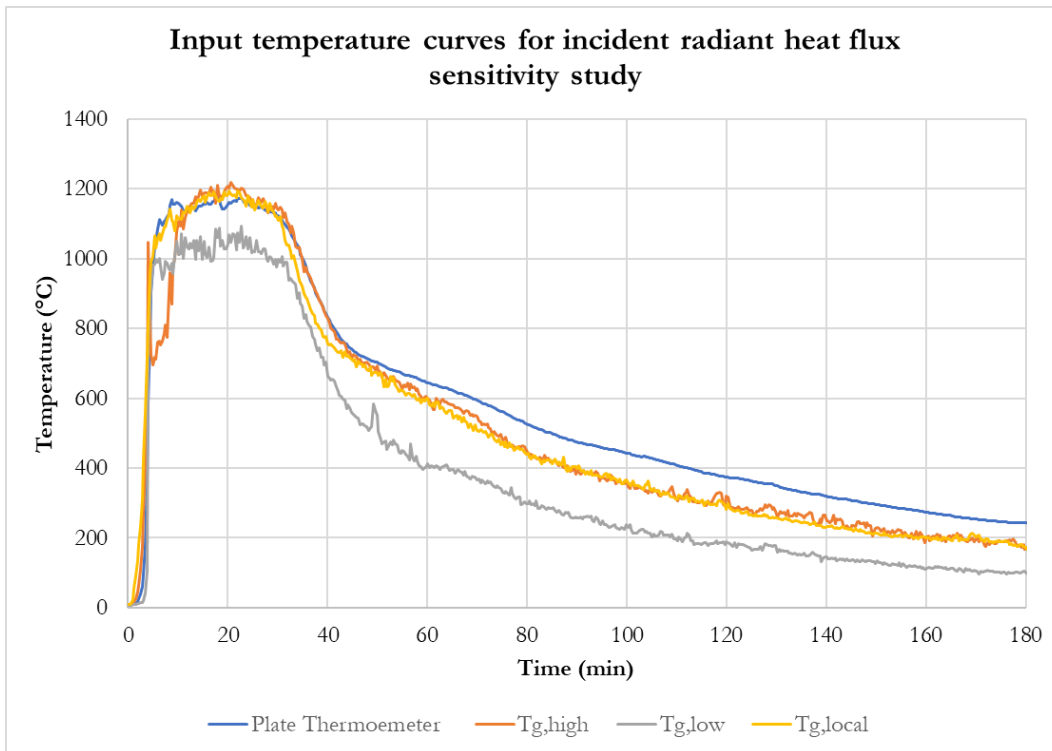


Figure 51: Input temperature time histories for incident radiant heat flux sensitivity study.

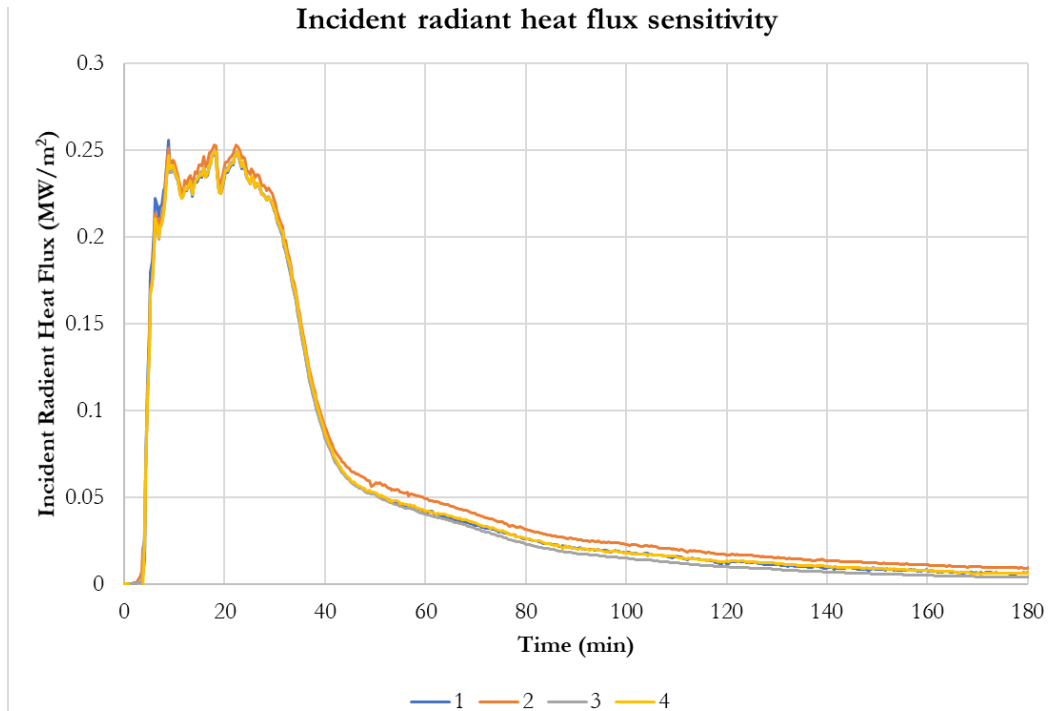


Figure 52: Incident radiant heat flux sensitivity study results

The incident radiant heat fluxes were calculated at each internal plate thermometer location (Figure 53 - Figure 57) using the mean thermocouple temperature from the thermocouple trees within the compartment for each test and $h_c + K = 30 \text{ W/m}^2\text{K}$. The error due to this assumption is expected to be within $\pm 1.5 \%$ during the fire peak, and within $\pm 7.5 \%$ during the decay phase (averaged over the 1st hour of decay). Due to the large ventilation in Test 4 with less homogenous conditions than the other tests, the gas temperatures varies to a greater degree and the error in the calculated incident radiant heat fluxes will therefore be greater.

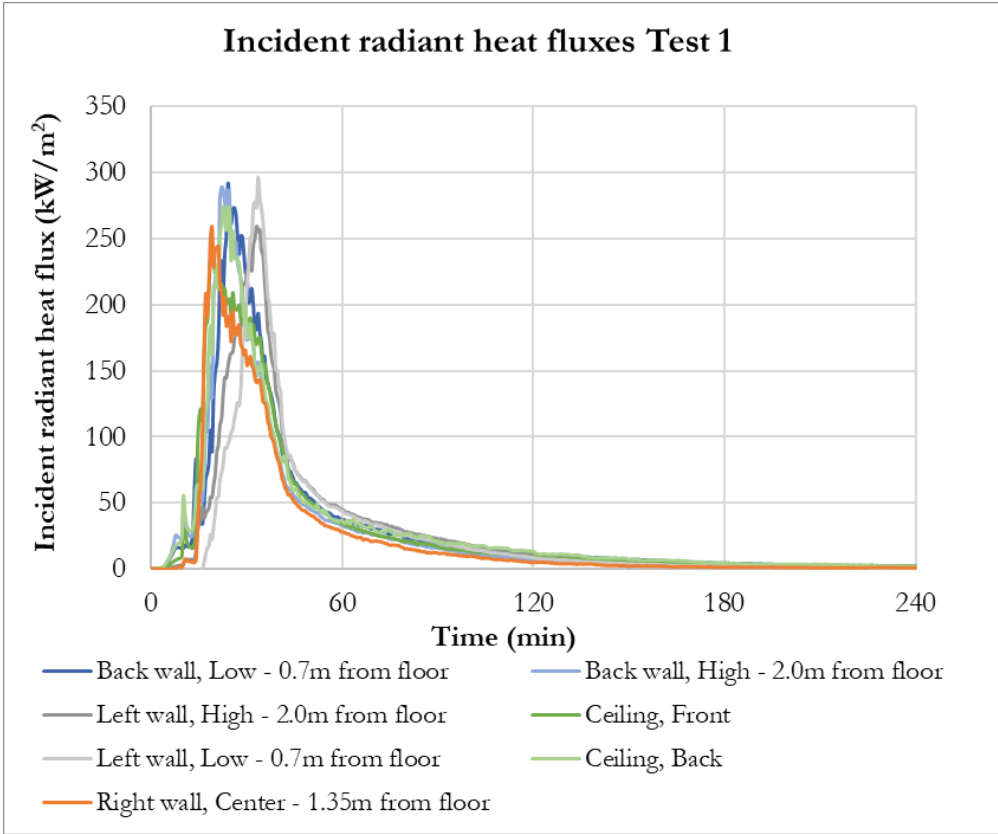


Figure 53: Calculated incident radiant heat fluxes inside the compartment for Test 1

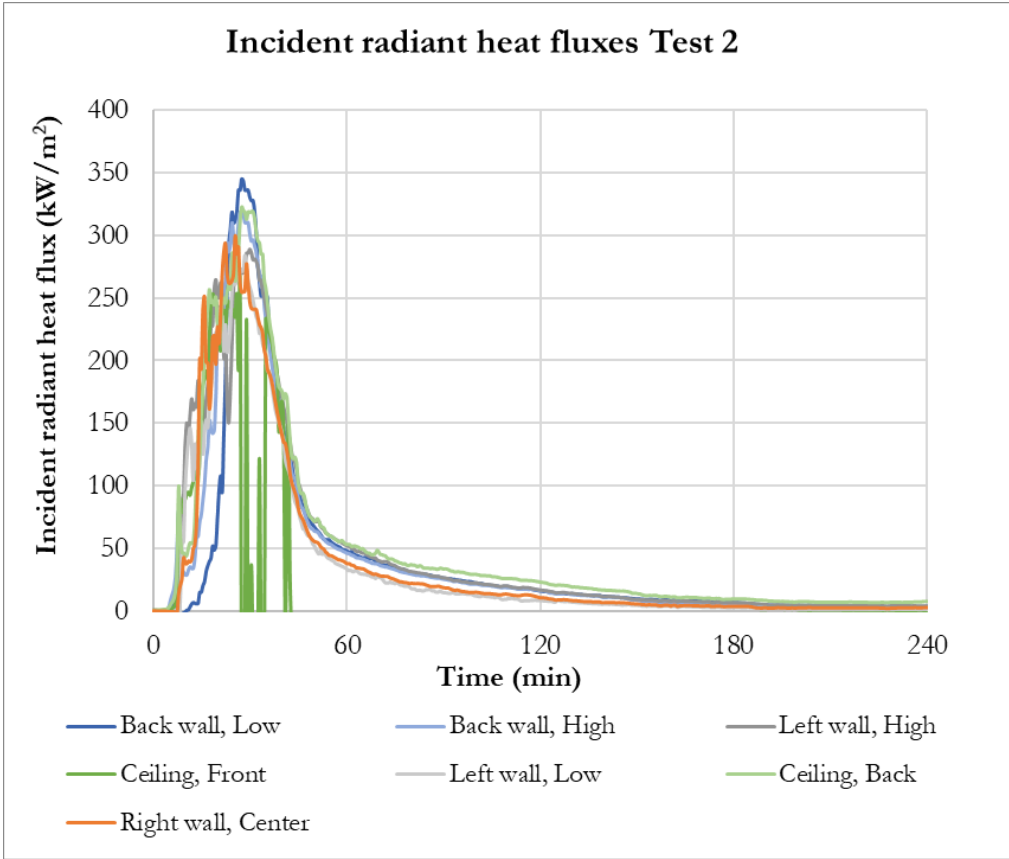


Figure 54: Calculated incident radiant heat fluxes inside the compartment for Test 2

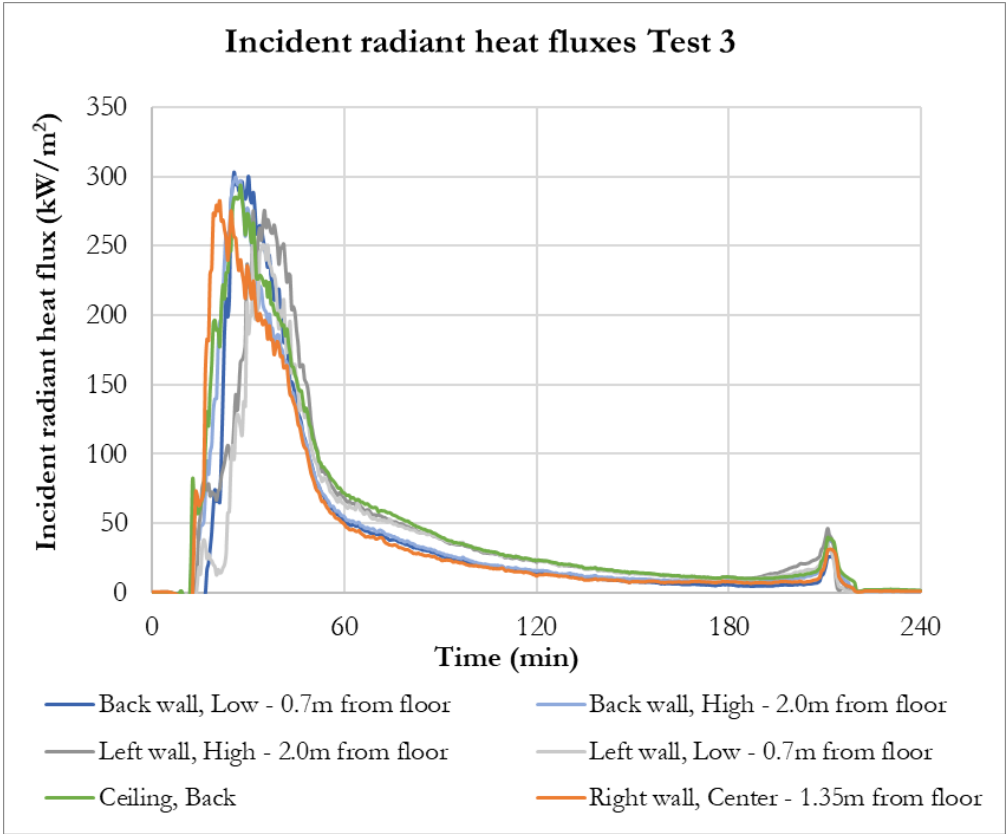


Figure 55: Calculated incident radiant heat fluxes inside the compartment for Test 3

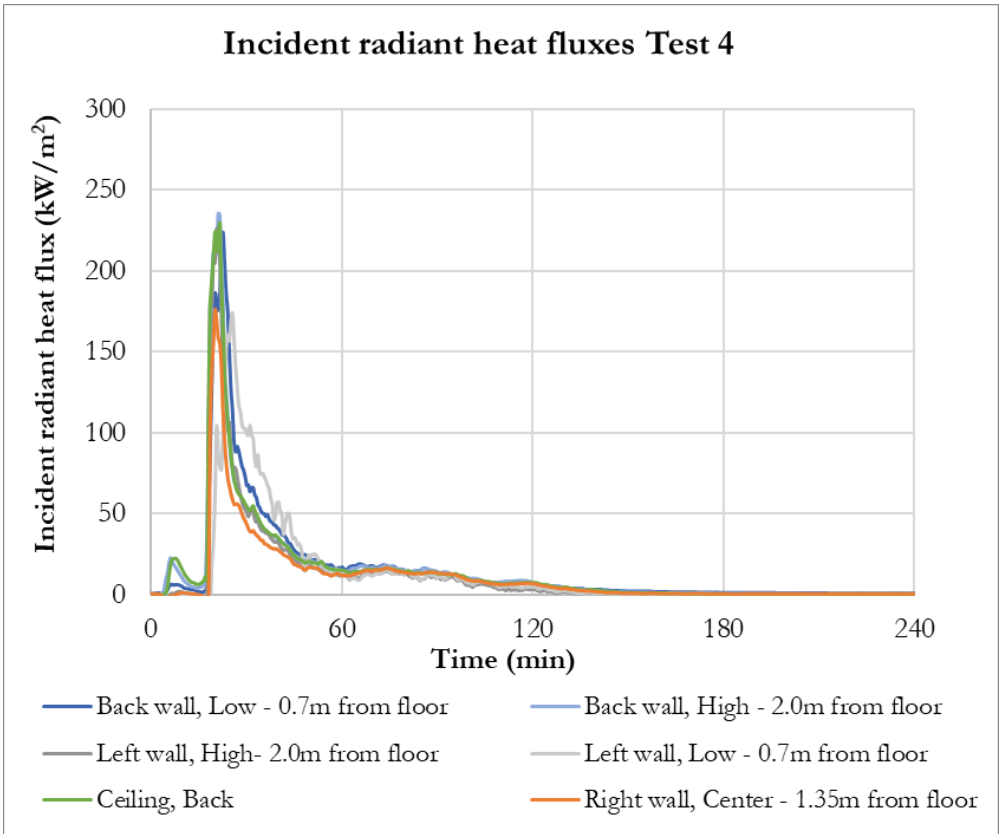


Figure 56: Calculated incident radiant heat fluxes inside the compartment for Test 4

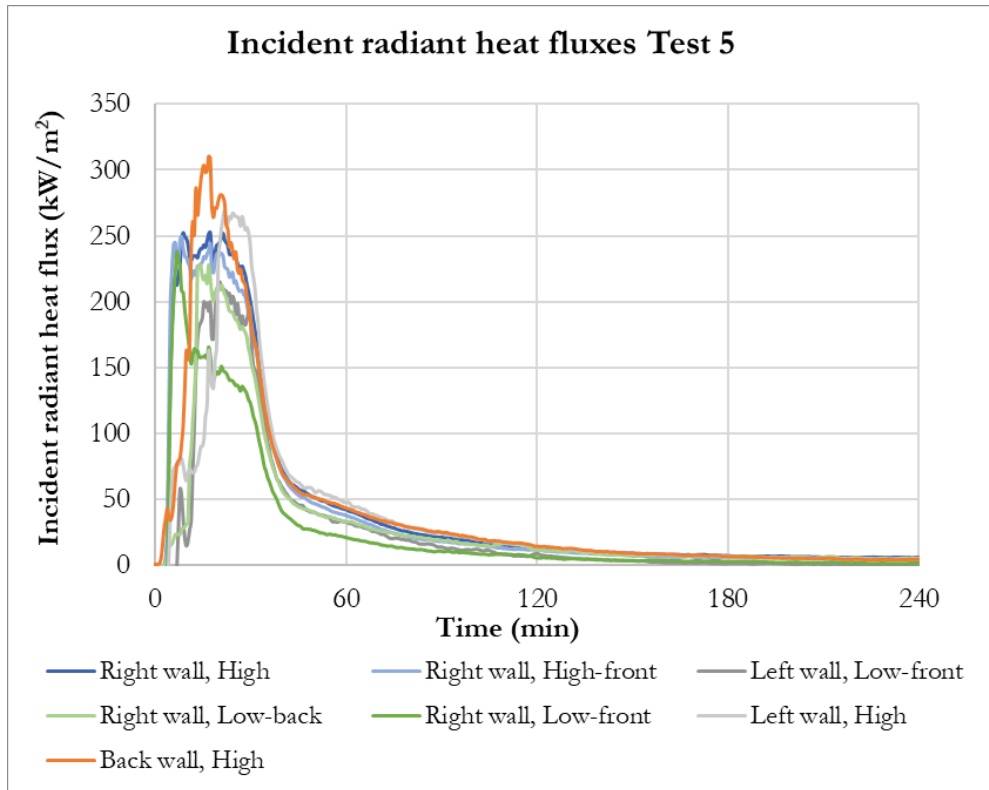


Figure 57: Calculated incident radiant heat fluxes inside the compartment for Test 5

6.7 Internal CLT and gypsum interface temperatures

Annex J shows all CLT through depth temperature measurements and temperatures behind each layer of gypsum. In this section only a selection of data to show the most relevant findings is given. Discussion of the performance of the gypsum protection can be found in the Section 6.8 and focus here will be given to the unprotected CLT and post fire conditions.

For all tests other than Test 3, where increased flaming of the CLT occurred after 3 hours of the test, temperatures had peaked in exposed CLT sections for temperatures within the first 100 mm of CLT (i.e. areas where charring occurred) by the end of the test and were either dropping or had plateaued. At deeper depths where the peak temperatures are below 100 °C the peak was reached shortly after the end of the fire, e.g. the temperatures high on the left wall as shown in Figure 58 and Figure 59. In Test 3, the through depth temperatures continued to grow for the full duration of the test until it was terminated, as illustrated in Figure 60.

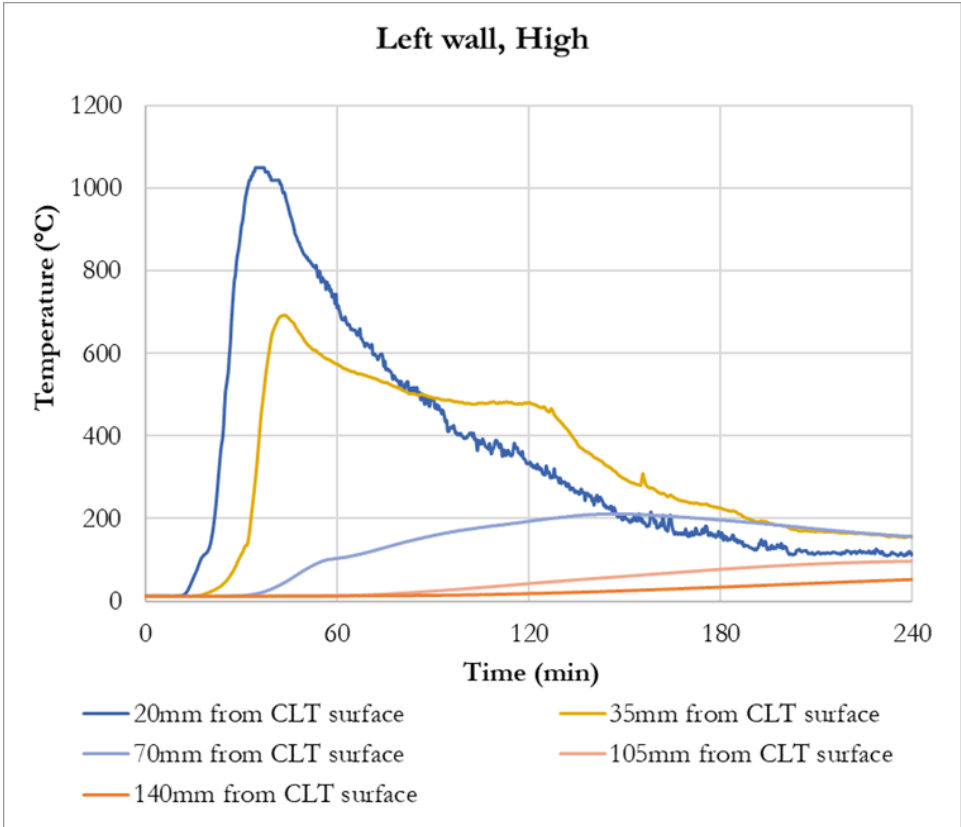


Figure 58: Test 2, through CLT temperatures high on the left wall, showing peak of 70 mm measurements prior to the end of the test.

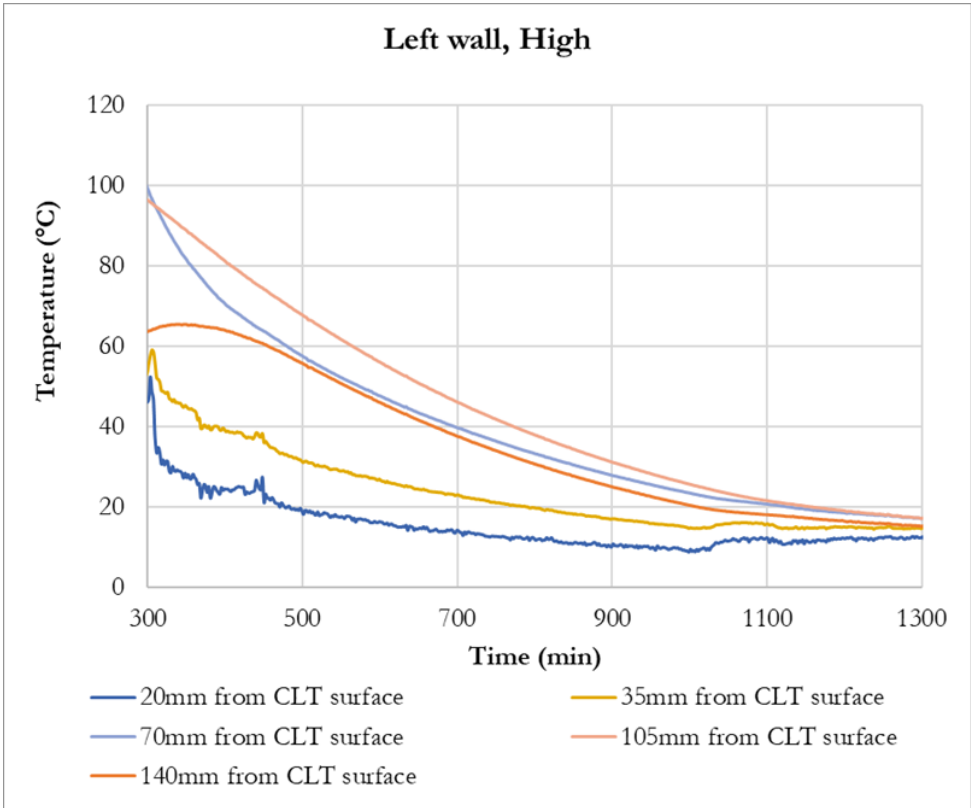


Figure 59: Test 2, through CLT temperatures high on the left wall, showing peak of 105 mm and 140 mm measurements shortly after the end of the test.

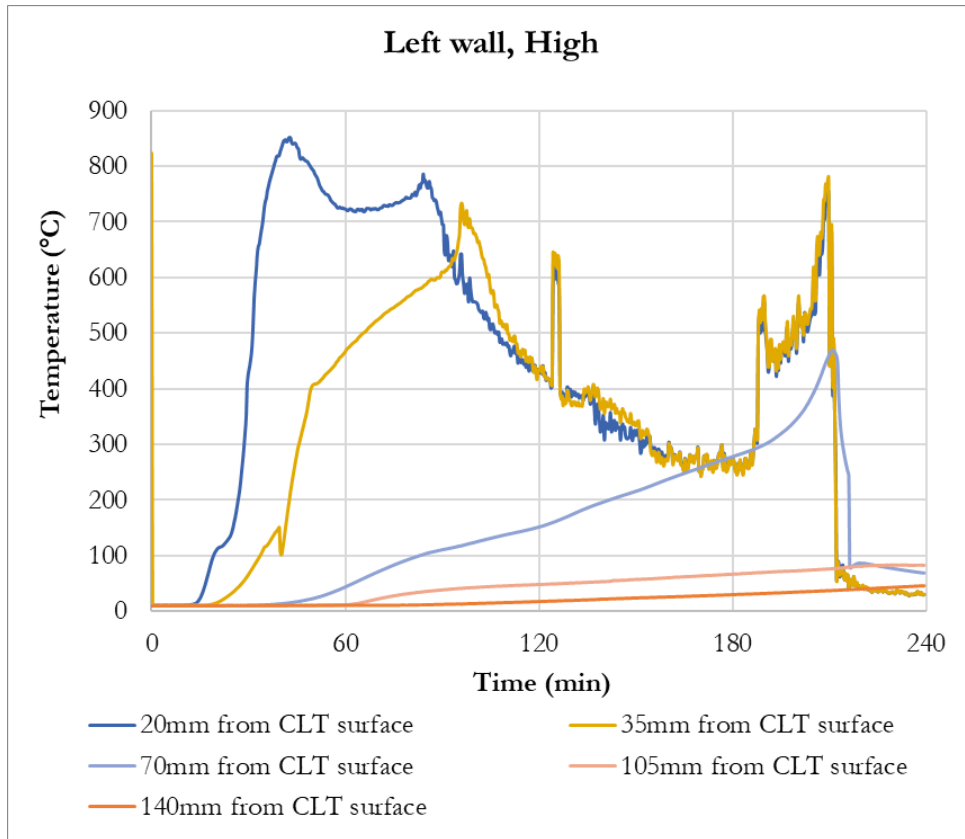


Figure 60: Though depth CLT temperatures high on the left wall for Test 3. Internal temperatures continuing to increase prior to fire extinguishment.

6.8 Gypsum board protection

Temperatures were measured behind every layer of gypsum board at various locations. These temperatures are shown in Annex J. In this section an assessment of the involvement of protected CLT in the compartment fires is made. That assessment is made by temperatures measured at the interface between the CLT surface and the base layer of gypsum board protection. In Tests 2, 3, 4 and 5, all measured temperatures at the protected CLT or glulam surfaces were lower than 200 °C for the whole test duration, indicating no material decomposition and, therefore, no contribution to the heat release in the locations where temperatures were measured. In Test 1 the protected CLT or glulam surface temperatures were measured in seven locations of which one location, at the back wall 700 mm from the floor, had temperatures above 300 °C (but below 350 °C), indicating local charring at this location (Buchanan and Abu, 2017). In three other locations the temperatures exceeded 200 °C (but not 250 °C), indicating some local and minor material decomposition and contribution to the fuel load at the CLT surface. There was no gypsum board fall-off observed in Test 1 and the exposed layer of gypsum was still fully visible (see Figure 61).



Figure 61: Interior at the end of Test 1

Figure 62 and Figure 63 show photos of CLT surfaces after removal of the gypsum after Test 1 (2 gypsum board layers). Local charring was seen, especially in locations near the intersection of walls and the exposed ceiling and in some lap joints between two wall panels. Figure 64 shows the top of the back wall after removal of the ceiling. The right picture shows the location of the most significant charring that took place in a lap joint where the ceiling meets the wall. As indicated before in Figure 7, there was no fire sealant applied at the interface between the gypsum boards and the ceiling of Test 1. In all other tests a fire sealant adhesive was used in this location only at locations where a gap was visible between the outer boards and the ceiling. The location of the local maximum char depths on gypsum protected surface after Test 1 was determined and indicated in the char diagram of Section 6.12. Figure 65 and Figure 66 show the CLT surface after removal of the gypsum boards for Tests 2 to 5. It should be noted that the gypsum boards in Test 2 and 3 were removed by the local fire brigade with water mist, which left stains and some damage of wood grains. Water mist was used to assess its potential as an alternative technique for extinguishing smoldering behind the gypsum boards using less water than conventional methods, as discussed in Annex L.



Figure 62: **Test 1**, Back wall (left) and right wall (right) after removal of the 2 gypsum board layers.



Figure 63: **Test 1**, Front wall (left) and left wall (right) after removal of the 2 gypsum board layers.



Figure 64: **Test 1**, Top of back wall after removal of ceiling.



Figure 65: Protected walls of **Test 2** (left) and **Test 3** (right) of left wall after removal of the 3 gypsum board layers.



Figure 66: Protected walls of Test 4 (left, 2 GB layers) and Test 5 (right, 3 GB layers) after removal of gypsum boards.

6.9 Post-test temperature measurements

The CLT temperatures were logged overnight for both Tests 1 and 2, to allow studying the effect of heat dissipation through the structure after the fire. Annex J includes the temperatures that were measured throughout the CLT walls and the ceiling in at least 16 hours after stopping the fire test. For Test 2 all temperatures continued to cool throughout the compartment. To provide an overview, Figure 68 shows the measurements in the walls in an uncharred position of the walls, 105 mm deep for exposed surfaces and 35 mm deep for protected surfaces. In Test 1 this cooling was measured in all but one location. Locally at the back wall, 700 mm above the floor, behind the gypsum protection in Test 1 at approximately the temperatures behind the gypsum increased, as can be seen in Figure 67. This indicates that there was localized smoldering behind the gypsum boards in Test 1. This location was identified using a thermal camera and temperatures dropped rapidly when the gypsum boards were removed at this location around 450 minutes after ignition.

Test 1 post fire, 35mm depth

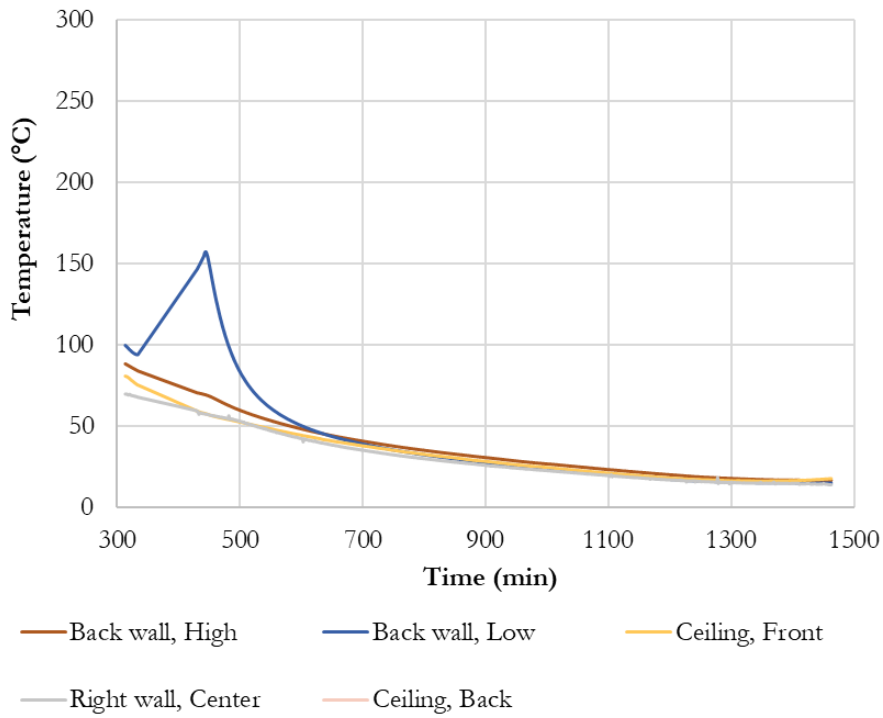


Figure 67: Post-test CLT temperatures for Test 1 at 35mm depth in the CLT. The temperatures low on the back wall in a lap-joint started to increase but rapidly but cooled after removal of the gypsum protection.

Test 2 post fire temperatures (uncharred)

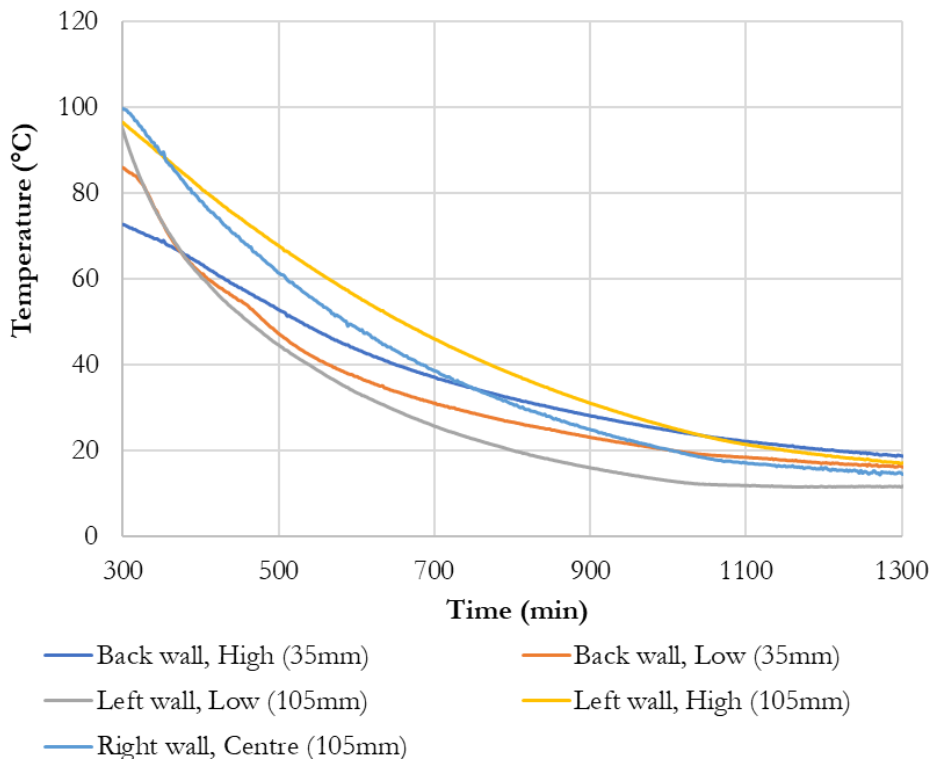


Figure 68: Post-test CLT temperatures for Test 2 at 35mm depth in protected CLT and 105 in exposed CLT.

6.10 Mass loss of combustibles

The mass of the floor and the mass of the rest of the structure were determined separately. As discussed in Annex E, the mass loss of combustibles is used to calculate the potential heat release rate (i.e. the heat release rate that occurs if all combustible volatiles combust). Figure 69 shows the mass loss of the combustibles calculated in accordance with Annex E.

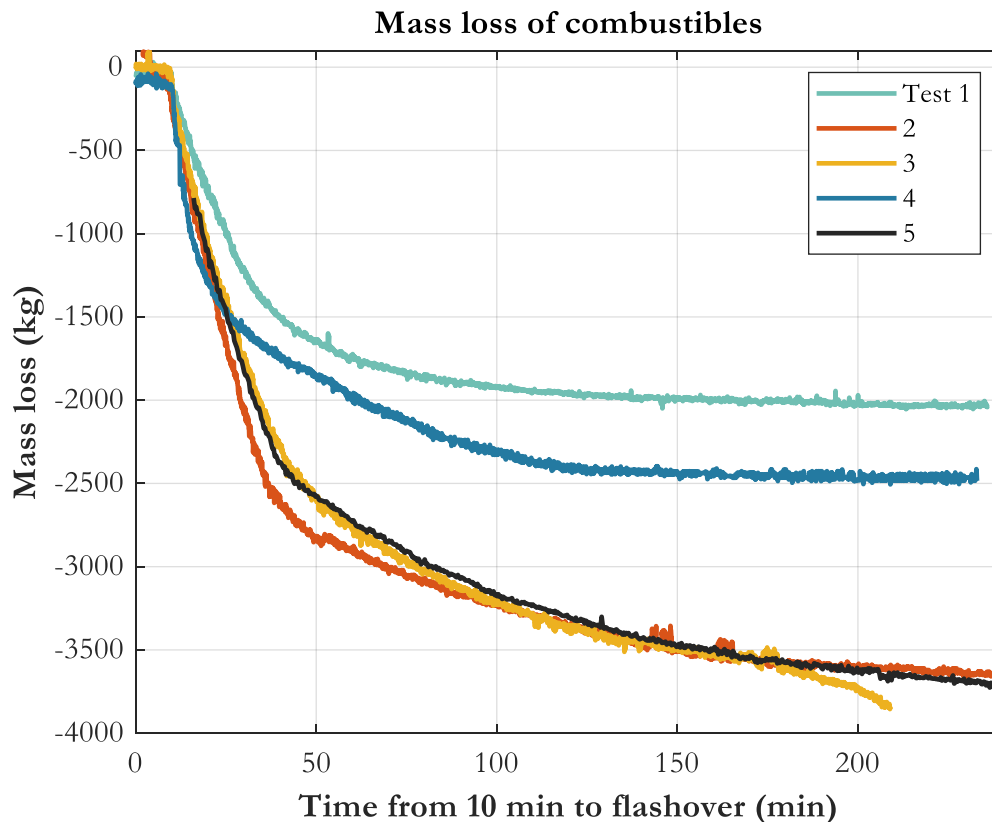


Figure 69: Total mass loss of combustibles.

6.11 Heat release rates

Heat release rates were determined from load cell measurements of the floor and the structure separately, assuming that all released combustible mass combusts. The method used is summarized in Annex E and includes corrections for the mass loss of the lightweight concrete floor structure (by drying out), the façade extension, and the gypsum boards. The movement of firefighters in the compartment at the beginning of the fire and in some instances at other times during the fire was identified using video recordings and the mass change caused by it was disregarded for the calculation of the heat release rates.

Heat release rates of all tests are shown in Figure 70. It should be noted that the first 9 minutes of Test 5 were lost due to a technical issue with the load cells. To increase the clarity of the figure, the heat release rate curves were time adjusted so that the moment

of flashover is at 10 minutes on the x-axis. Additionally, after the peak heat release rate is reached, a moving average (of 5 datapoints) is plotted, which increased the visibility of the curves that are drawn behind other curves.

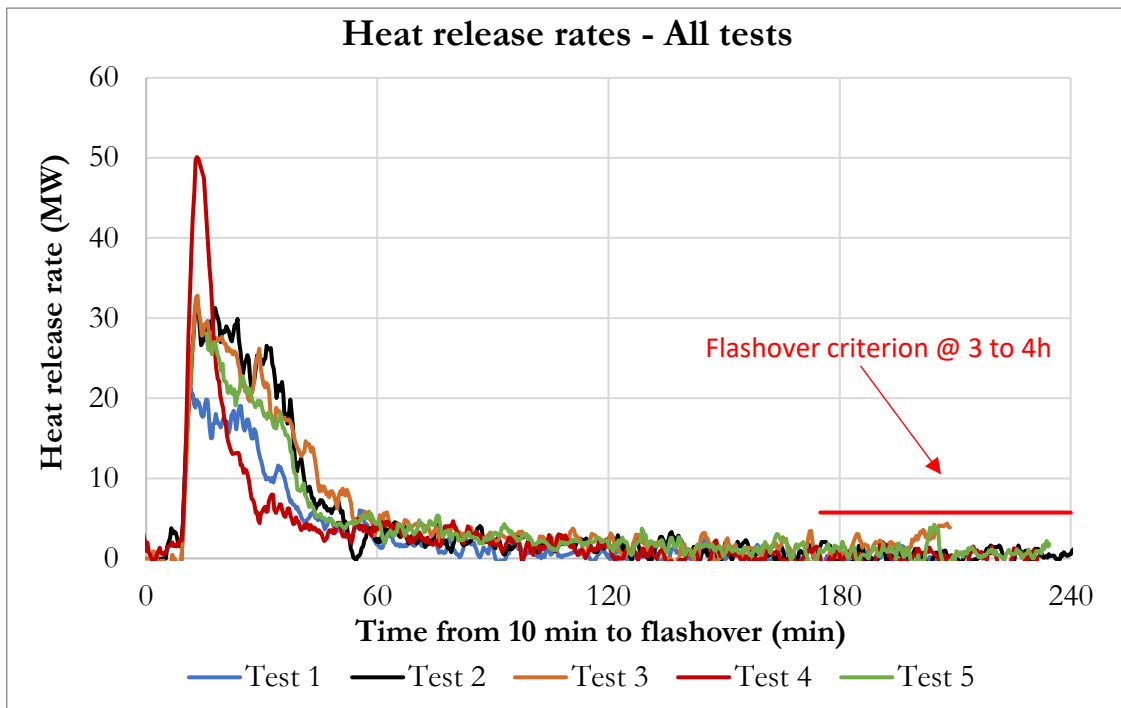


Figure 70: Heat release rates of all tests and the heat release rate flashover criterion of Chapter 5

6.12 Char depths

CLT char depths were measured after the test using a resistograph which is able to drill through the specimen while plotting the drill depth versus the torque resistance. The drilling is conducted from the unexposed side and the uncharred depth is identified as the depth at which the resistance drops significantly, as done previously by Brandon and Dagenais (2018) and Su et al. (2018b).

Figure 71 to Figure 75 show the depth of the char at the interior CLT surfaces of Test 1 to 5, respectively. The gypsum board protected surfaces are grey colored. After Test 1, the majority of the protected timber surface area was uncharred, but there were some locations with localized charring along CLT lap joints and gypsum board joints. There was no indication of any flaming as a result of this localized charring. Efforts were made to determine the deepest char depths at those locations as indicated in Figure 71. The protected surfaces of Tests 2 to 5 were mostly undamaged. Pictures of protected surfaces after removal of the gypsum boards, are shown in Section 6.8.

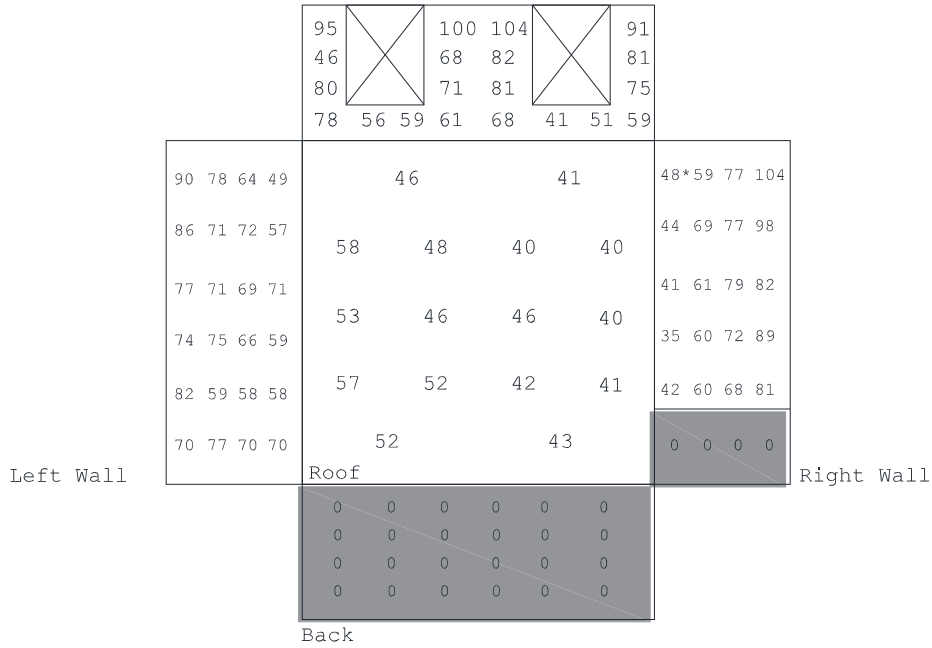


Figure 73: Char depths in mm measured after Test 3 (grey surfaces were protected)

Test 4

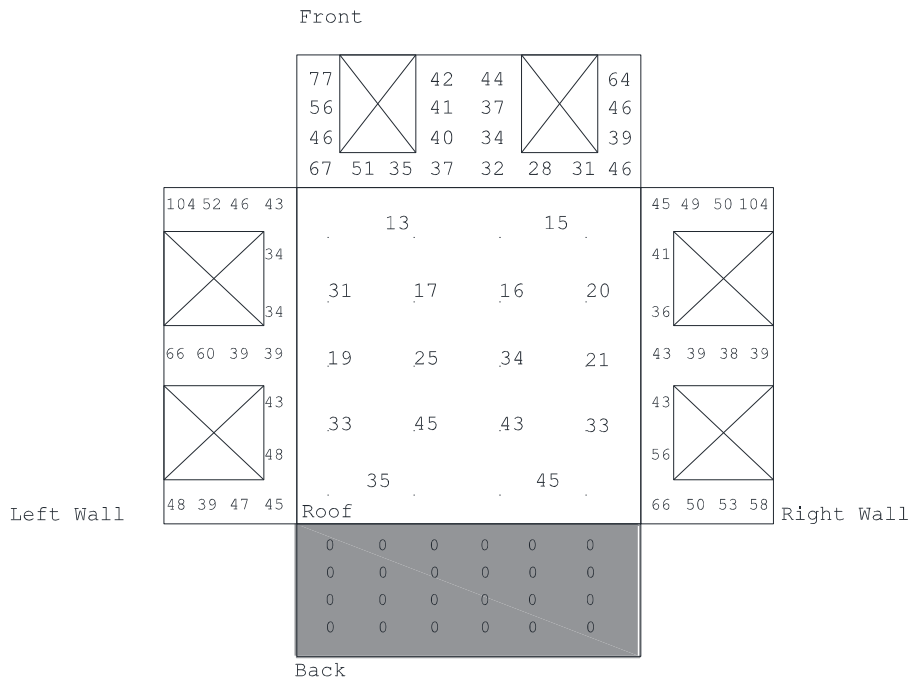


Figure 74: Char depths in mm measured after Test 4 (grey surfaces were protected)

Test 5

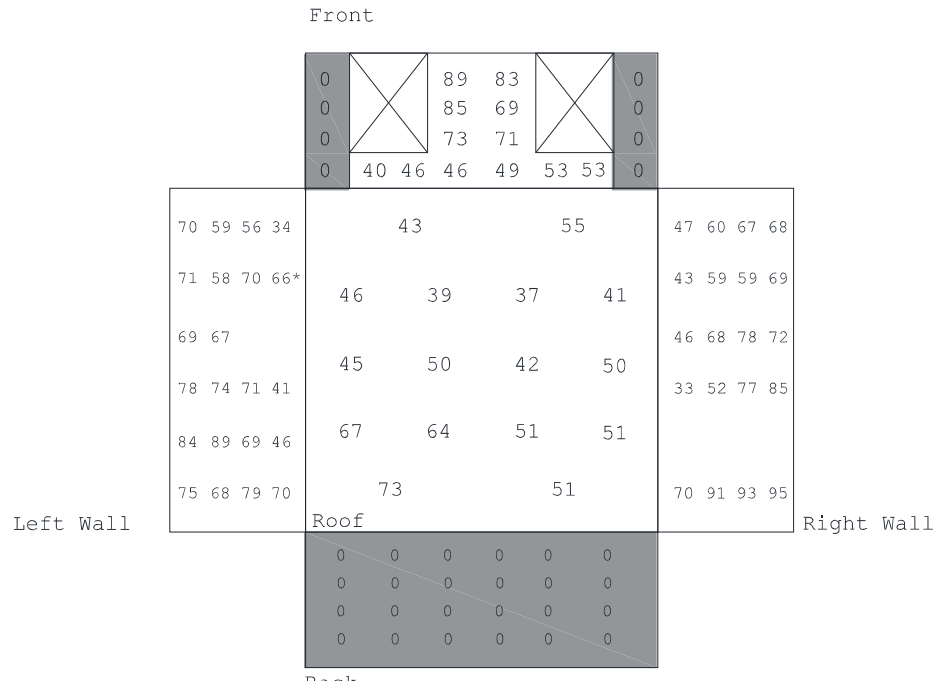


Figure 75: Char depths in mm measured after Test 5 (grey surfaces were protected)

The char depth during fire resistance tests (ASTM E119 and ISO 834) is generally used to calculate structural fire resistance of a load bearing wood member or assembly. Design standards, such as NDS (2018), use calculations of char depths to determine the load bearing capacity of mass timber elements to meet the fire resistance requirements.

These compartment tests are conducted to evaluate the safe limits of exposed mass timber surface areas, subject to a natural fire, which exhibits a growth phase, flashover, fully-developed phase, and decay phase. The time duration of 4 hours was chosen to assure that there is no reignition of mass timber elements after the natural fire has decayed. The comparisons of char depths after a 4-hour natural fire exposure to that of a 2-hour fire resistance test is not directly related to any U.S. code requirements. Nevertheless, this report provides a comparison for academic use. As such, this comparison is not intended for use in any regulatory requirements.

It should be noted that the NDS (2018) not only requires subtracting a char layer from the cross-section to calculate the load bearing capacity during fires, but also an additional 20% of the char layer thickness to account for strength reductions in the heated zone immediately adjacent to the char layer. An appropriate size of this damaged layer to determine the structural capacity of a member exposed to fire, is dependent on the fire exposure which, in most cases, differs between standard fire tests and real fires. However, for a wide range of non-standard fire exposures, Lange et al. (2015) found that this layer was up to 16 mm thick, which corresponds with the calculations of NDS (2018) for 2-hour fire resistance ratings. Therefore, the comparison of calculated char depth according to NDS and measured char depths is considered informative.

The CLT ceiling was exposed in all tests. Figure 76 shows box plots of the char depths measured after each test. It should be noted that Test 3 was stopped about 30 minutes earlier than all other tests⁹, which means that the values would have been higher if the test lasted 4 hours instead. Test 4, which has a larger opening factor, had the lowest char depth. The char depths in the other compartments seem to show some correlation with the surface area of exposed timber. This agrees with predictions that were sent out to the project steering group and stake holders before the tests were performed. The predictions and the corresponding calculation model will be discussed in a separate report. It can be noted that all char depths measured in the ceiling after the fire were lower than the char depth for a 2-hour fire resistance rating, according to NDS (2018).

From the measurements it can be concluded that the char depths were lowest in the ceiling and at the top of walls and gradually increased towards the bottom of walls. Figure 77 shows the average char depth at different heights within the compartment. For comparison, the char depth according to NDS (2018) is indicated. It can be seen that the char depths are lower than the char depth for 2-hour fire resistance by NDS (2018), with the exception of the bottom of walls in Test 3⁹.

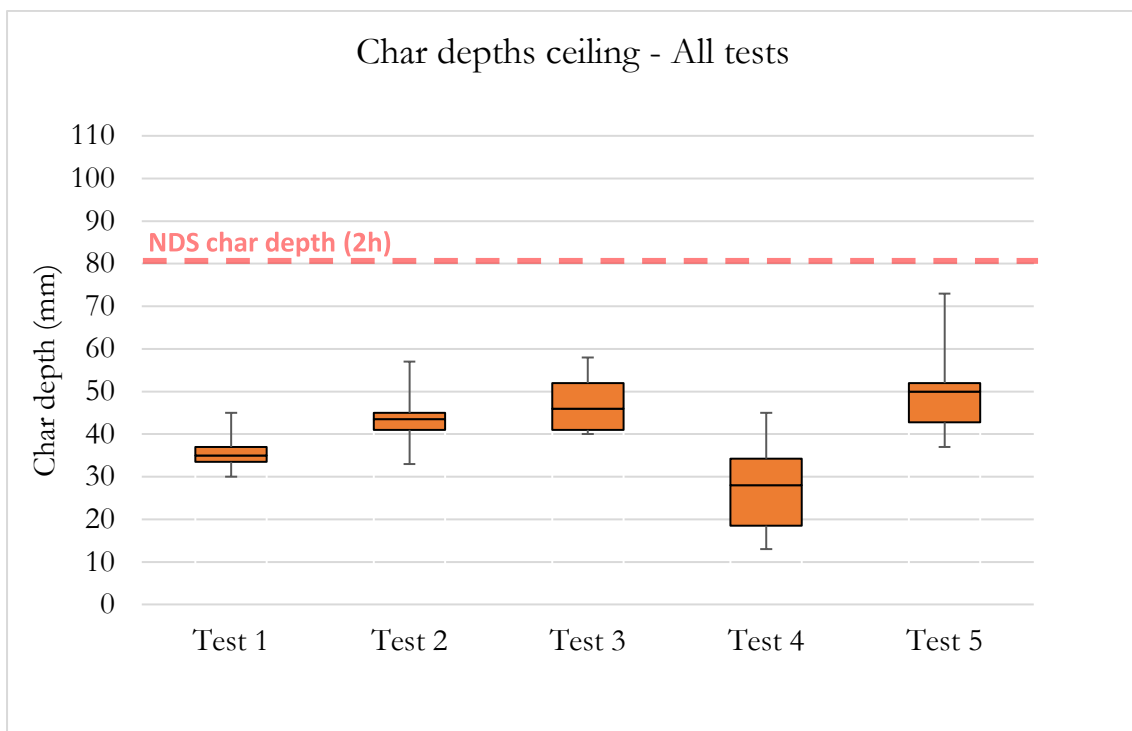


Figure 76: Box plots of char depths in the CLT surface of the ceiling

⁹ Test 3 was stopped at 3:30h as it did not pass the criterion set by the project steering group to have continuous decay until 4 hours after ignition, as such, this configuration of mass timber surface exposure (i.e., where two exposed surfaces meet at a corner) would not be recommended for high rise buildings, where there is possibility that an automatic sprinkler system could fail and that fire service intervention may not occur.

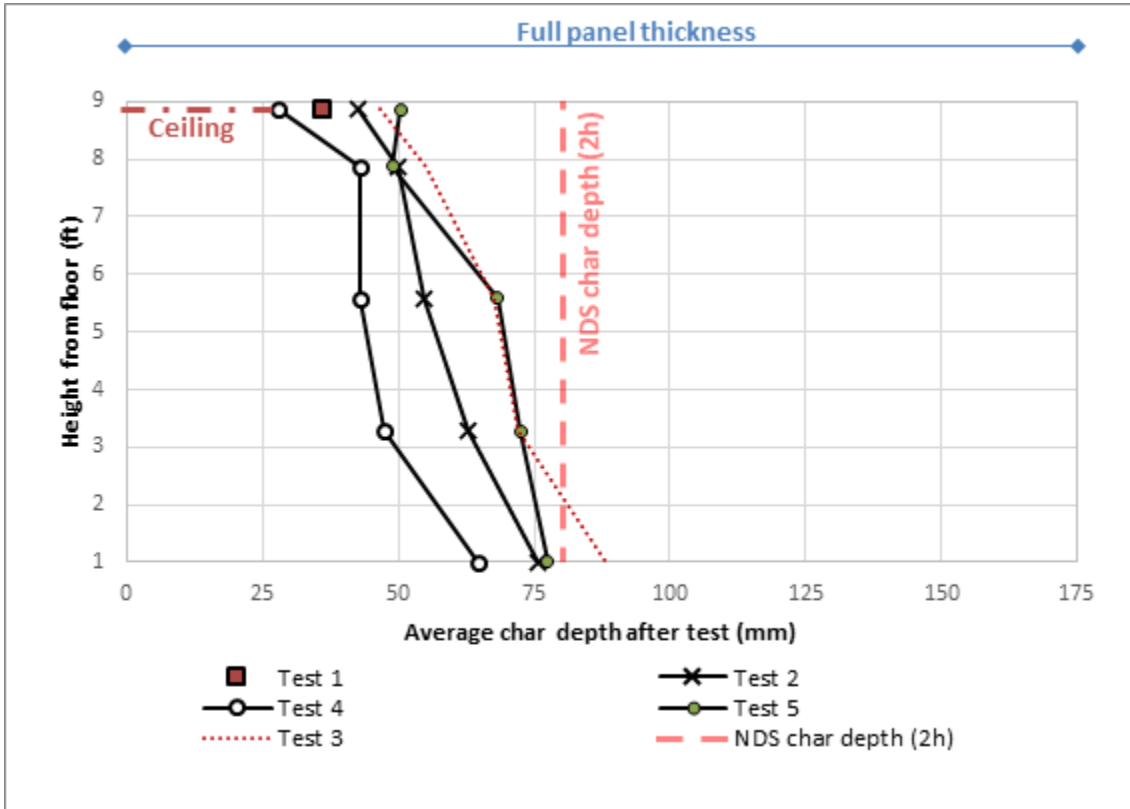


Figure 77: Average char depths in the walls and ceiling at different heights measured from the floor. In corners between two exposed timber members (CLT or glulam), the char depths were highest. Figure 78, shows box plots of the maximum measured char depth in corners of two exposed mass timber members and corners of one protected and one exposed member. As Test 4 had a different compartment design, its data is not included in the figure. The figure indicates a significantly higher char depth at the bottom of corners of two exposed members, indicating a significant influence of exchange of radiative heat between both combusting walls in the corner. At these locations the char depth exceeds the char depth of NDS (2018) for a fire rating of 2 hours. As Test 3 had a number of such corners, this significantly influenced the overall average char depth. In corners where only one member was exposed, the measured char depth was significantly lower and only outliers (indicated by the whisker of the box plot) exceeded the char depth of NDS (2018). In Test 4 a more significant difference was observed, as the maximum char depth at corners between two exposed walls was nearly twice as high as the maximum char depth in other wall corners.

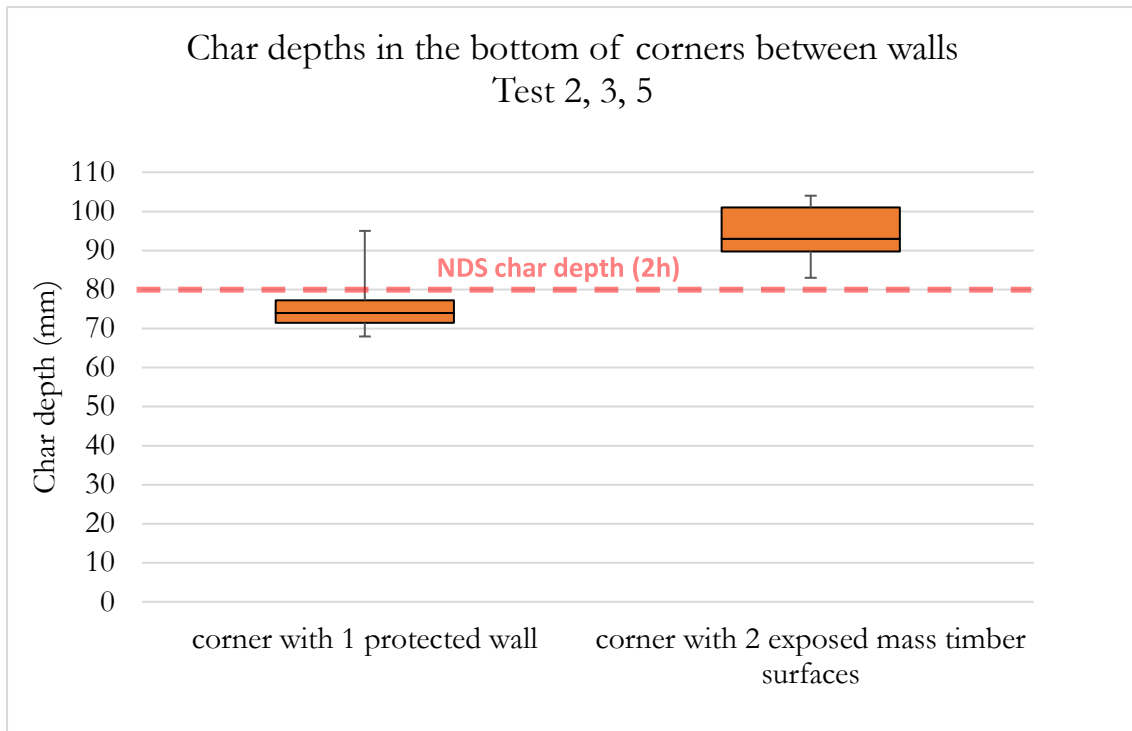


Figure 78: Box plots of measured char depths at the bottom of corners where two walls meet (generally the most damaged location)

Char depths for the glulam beam were estimated after the test from photographs of cross sections cut from the beam by tracing over the boundary between the char and un-charred wood, visible due to the change in color, as shown by the sketch in Figure 79. This has been done in CAD software to allow for easy measurements on the charred beam section.

Two methods of calculating an “average” char depth for the beam have then been utilized for each test. The traced cross sections can be seen in Figure 80, the calculated char depths in Table 7 and the methods are as follows:

- Method 1: The mean of 17 point measurements, every 50 mm from the top of the beam down either side, and on the centerline and 50 mm either side of it on the base.
- Method 2: The area of the post-test cross-section is calculated, the difference between this and the original cross-sectional area then giving the charred area. This is divided by the exposed perimeter of the original section to give an average char depth.



Figure 79: Example sketch of how the charred cross-sectional shape is established from a photo. Green line shows the char boundary and the white the original beam cross-section.

Table 7: Calculated beam char depths

	Test 1	Test 2	Test 3	Test 5
Point measurement average	32 mm	56 mm	56 mm	59 mm
Area based average	32 mm	52 mm	52 mm	54 mm

Note 1: As the method used for establishing the char depth are based on tracing over a photo there is relatively high levels of uncertainty in the measurements. The uncertainty is likely to be in the order of ± 5 mm. The relative charring levels between the tests is however likely to be sufficiently accurate to make qualitative comparisons.

Note 2: Due to logistical issues on site no beam cut was made for Test 4, and so no beam char depth estimations are available for this test.

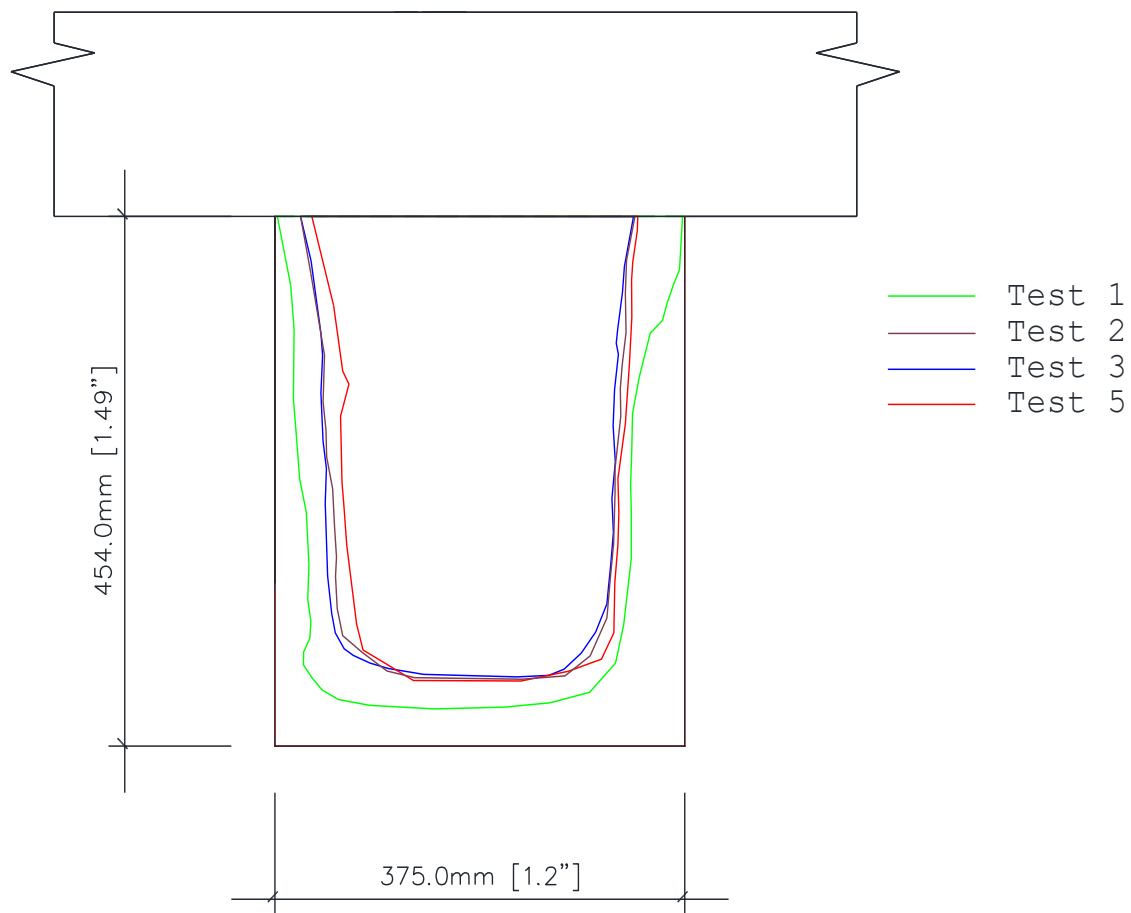


Figure 80: Post-test beam char shapes.

The photographs used for this depth estimation can be found in Annex G.

6.13 Façade exposure

The exposure to the façade was measured via a mix of Plate Thermometers flush with the façade wall (three at 1.25 m above the opening, and one at 2.1 m above the opening) and type k thermocouples at varying heights. A very short overview of the results from this instrumentation is provided below while full details on the measurements and comparisons against façade testing standards are given in *Exposure from mass timber compartment fires to facades* by Sjöström et. al (2021).

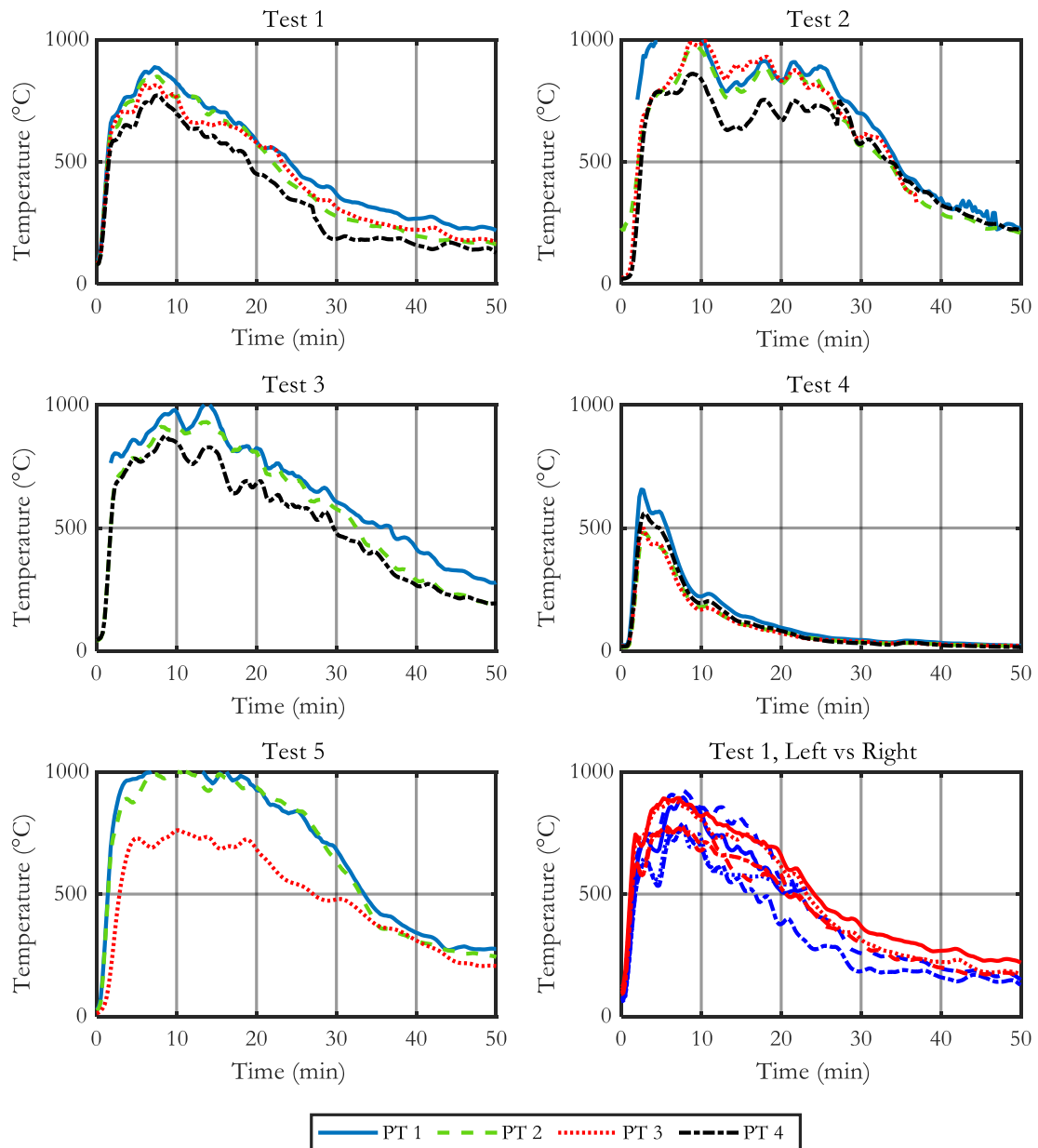


Figure 81: Temperature-time histories for facade PTs (all tests). PTs 1 to 3 are 1.25 m above the opening while PT 4 is 2.1 m above the opening.

The temperature-time histories for the four plate thermometers (averaged between the results for each opening) can be seen in Figure 81 below. While the variation of thermocouple temperatures with height has been plotted in Figure 82, for tests 1 to 4 (Test 5 only had a limited number of measurements on the façade). For this latter plot, rolling averages of 5 minutes (3 minutes for Test 4 due to the fully developed phase) were taken, with the maximum average plotted for each TC as representative of the peak flashover exposure.

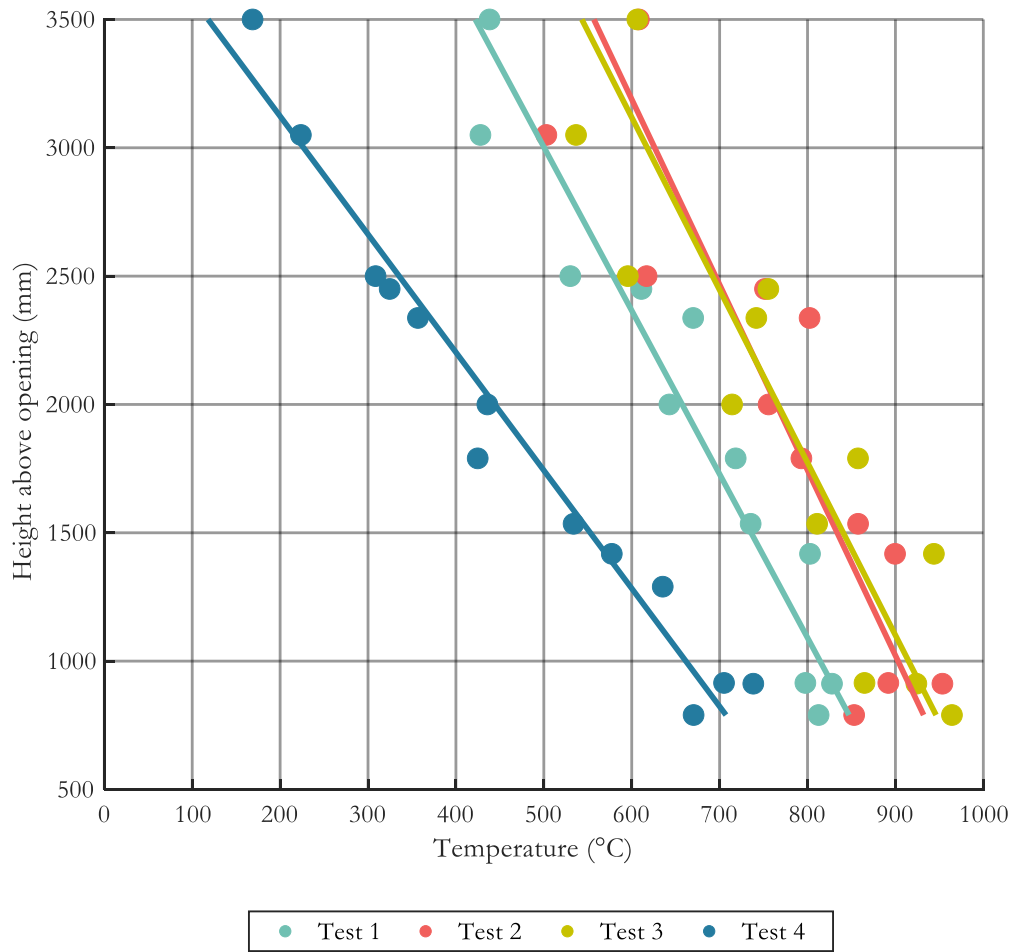


Figure 82: Variation in temperature recorded in façade TCs with height above the opening. Temperatures are the maximum 5-minute average for tests 1-3, and 3 minutes for test 4. Lines are linear fits to the data.

Additionally, external video recordings of the tests have allowed the measurement of the flame heights out of the opening. A detailed description of the methodology for calculating these can be found in the report by Sjöström et al. (2021) while the flame heights over the course of the tests can be seen in Figure 83.

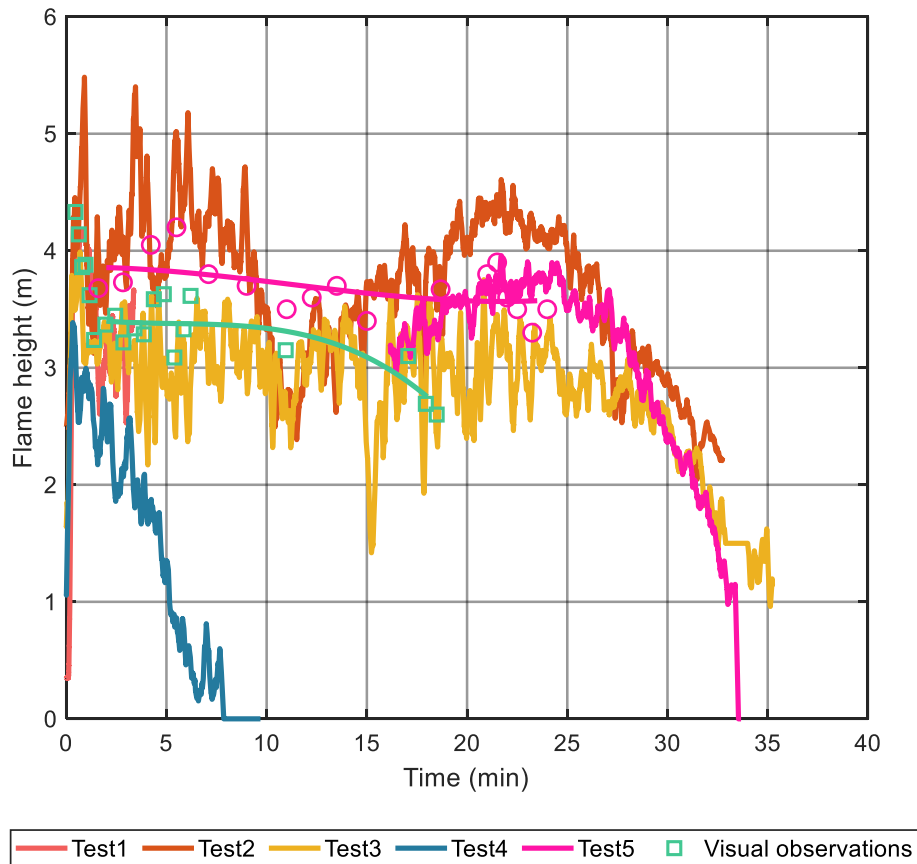


Figure 83: Flame height. Line are data obtained from image analysis on each frame. Dots are visually observed flame heights.

6.14 Potential exposure to other buildings

Irradiance exposure levels to other buildings was measured using plate thermometers (PT) placed opposite the front openings of the compartment. Opposite each opening a PT was placed at distances of 4.8 m and 8 m from the opening and at mid-height of the opening (1.3 m in Tests 1, 2, 3 and 5 and 1.1 m in Test 4 from the floor level). An additional plate thermometer was placed at 8 m distance and at a height of 4 m one additional standard PT was installed to exemplify differences in irradiance with height.

The use of plate thermometers (as used to control fire resistance furnaces) to measure irradiance (incident radiation heat flux) in ambient air has been demonstrated as an affordable, robust method which enables the implementation of more sensors compared to if water cooled heat flux gauges (such as Gardon or Schmidt-Boelter) were to be used (Ingason & Wikström, 2005). To increase accuracy and response of the probes, an updated version of the standard plate thermometer was constructed with calibrated and proven response (Sjöström et al, 2015). This plate has a thicker but lighter insulation and a thinner exposed metal sheet.

The irradiance to a plate in a known gas environment (known gas temperature and convective heat transfer coefficient) can be assessed as:

$$\dot{q}_{inc}'' = \varepsilon\sigma T_{PT}^4 + \frac{(h_c + K)(T_{PT} - T_g) + C \frac{\partial T_{PT}}{\partial t}}{\varepsilon} \quad \text{Eq. 3}$$

where ε is the plate surface emissivity, σ is Boltzmann's constant, h_c the convective heat transfer coefficient, T_g the surrounding gas temperature and K and C are correction parameters for thermal loss and storage, respectively. For these four plate thermometers the corrections parameters used matching those by Sjöström et al (2015) and Wickström et al (2019) of $K = 5 \text{ W/m}^2\text{K}$, $C = 2800 \text{ J/m}^2\text{K}$. Due to the low wind speeds, and therefore low relative velocity of air past the plates, during testing a h_c value of $12 \text{ W/m}^2\text{K}$ has been assumed. Resulting incident radiant heat fluxes are shown below for the two distances and the whole duration of the tests (Figure 84).

The elevated plate thermometer (4 m high) outside the left opening at a distance of 8 m was of traditional fire resistance design and the correction parameters for it are as defined in Häggkvist et al (2013), of $K = 8 \text{ W/m}^2\text{K}$, $C = 4200 \text{ J/m}^2\text{K}$. The maximum calculated heat fluxes (based on a moving mean over 1.5 minutes for each test) received at each location for each test are shown in Table 8.

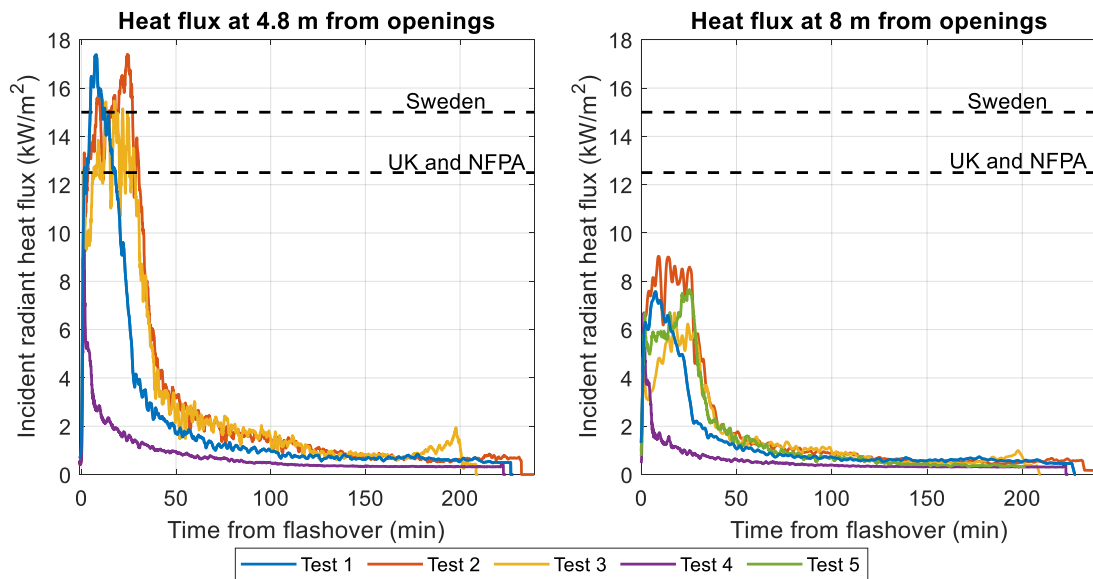


Figure 84: Incident radiant heat fluxes (irradiation) to vertical surfaces at 4.8 and 8 m from the openings calculated on a 1.5 minute moving mean of the PT temperatures.

Two thresholds for irradiance at the surface of other buildings from codes in Sweden, UK and the NFPA are shown in Figure 84 for comparison. These refer to expected levels of exposure to neighboring façades and windows for some specific occupancies and building types. At 8 m distance all tests show irradiation levels well below these thresholds whereas they would be surpassed for a hypothetical building distance of only 4.8 m.

Table 8: Maximum radiant heat fluxes opposite the openings.

Test	Maximum Incident HF (kW/m ²)		
	4.8 m from openings	8 m from openings	Elevated at 8 m from openings
1	17.1	7.5	-
2	17.1	9.0	11.0
3	14.8	6.6	7.7
4	6.7	4.9	5.7
5	-*	7.6	7.0

*Plates insulation wet and as such recordings ignored.

6.15 Intersections

With 2 exceptions, no flaming occurred on the exterior side of the compartment. At (1) an intersection between the glued laminated timber beam and the back wall of Test 1, and (2) an intersection between the left wall and the ceiling at the front of the wall of Test 3, there was some flaming on the exterior side. Table 9 shows an overview of smoldering/flame spread through intersections of mass timber members.

Table 9: observed flames through joints or details

	Location	Description	Images
Test 1	Beam-wall joint at back wall	<p>Minor flaming at one of the top corners of the beam at the location where the beam penetrated the back wall.</p> <p>Note: the rectangular hole in the CLT was made on site using a hand-held reciprocating (tiger) saw. The geometrical imperfections are not representative for factory made cuts.</p> <p>Some fire sealing adhesive, but no construction tape or expanding tape was used at this detail.</p>	
Test 2	None	-	-
Test 3	Wall-ceiling joint at the front side of the left wall	<p>Smoke exited the intersection at the top of the left wall on the front side directly after flashover, indicating the intersection was not sealed at this location. The smoke development took place at the location where several thermocouple wires were running (Note: these were moved before the photo was taken). To avoid loss of data, the stone wool was placed over the intersection (under the wires) to protect the wires. In extreme cases, small amounts of water on the external surface were used to minimize the exposure to the thermocouple wires.</p>	 <p>(Detail shown in Figure 6)</p>
Test 4	None	-	-
Test 5	None	-	-

As mentioned in 4.1, the sealing materials used in the different tests varied. Table 10 gives an overview of these sealant materials (as also indicated before in Figure 6 of Section 4.3). The green shaded cells of the table indicate that the connection details withstood the specific test without any occurrence of spread of smoldering or spread of flaming through the intersection. The orange shaded cell indicates local spread in one location, which was likely a result of compromised effective gas seal because of slight level differences between the top of connected wall members. Some of these locations

were identified before the start of Test 3 (Figure 85) and fire sealing adhesive was applied to close the void under and above the resilient profile in those locations only. During the test, however, smoke left the intersection at the top of the left wall at an early stage in the fire, indicating lack of effective gas seal at that location.

Figure 86 and Figure 87 show the top of the wall in Test 3. The photo of Figure 86 is taken at a lap joint where the top faces of the wall panels were on the same level and showed no damage near the exterior side of the joint. Figure 88 and Figure 89 show typical photos of walls with the alternative wall-ceiling joints that were tested in other tests. No damage was observed near the exterior side of the joint.

Table 10: Sealing materials at intersections between CLT members (**green** indicates fire spread to the external surface; **orange** indicates spread of flames to the external surface in one location)

	Ceiling-ceiling spline board joint (see Figure 6 A)	Wall-ceiling joint (see Figure 6 B)	Wall-wall lap joint (see Figure 6 C)	Wall-wall corner butt-joint (see Figure 6 D)
Test 1	2x Construction tape	Construction tape	Construction tape	Construction tape*
Test 2	2x Expanding tape close together	Construction tape & Resilient profile	2x Expanding tape	2x Expanding tape*
Test 3	2x Expanding tape apart	Resilient profile	Construction tape	Construction sealant
Test 4	Construction tape under spline board	Construction tape & Resilient profile	Construction tape	Construction tape
Test 5	Construction tape under spline board	Construction tape & Resilient profile	Construction tape	Construction tape*

* All wall-wall corner joints in Test 1, 2 and 5 had at least one gypsum protected surface which reduced the challenge of sealing the connection



Figure 85: Location of imperfect detail at wall-ceiling joint with a resilient profile identified before the test



Figure 86: Top of the wall lap joint after removal of the ceiling. Typical location without flame spread. Sealing method: resilient profile only (Test 3).



Figure 87: Top of the wall after removal of the ceiling and the resilient profile. Location of flame spread through intersection (front side of left wall) - Sealing method: resilient profile only (Test 3).



Figure 88: Top of the wall after removal of the ceiling. Typical location. Sealing method: construction tape only (Test 1).



Figure 89: Top of the wall after removal of the ceiling. Typical location. Sealing method: construction tape and resilient profile (Test 2).

Figure 90 to Figure 93 show the ceiling-ceiling spline board connection alternatives after the test. At most some discoloration of the CLT surface under the spline board was seen at some locations after Test 1 and Test 3. In the other tests, there was no sign of damage on the surface under the spline board.



Figure 90: Photo after removal of spline board. Sealing method: 2x construction tape on top of spline boards (Test 1)



Figure 91: Photo after removal of spline board. Sealing method: 2x expanding tape under spline board at CLT interface (Test 2)



Figure 92: Photo after removal of spline board. Sealing method: construction tape under spline boards at CLT interface (Test 4)



Figure 93: Photo after removal of spline board. Sealing method: 2x expanding tape at center of lap (Test 3). Note: the rain after the test cause additional discoloration

None of the corner joints between walls showed any sign of fire spread through the connection. Figure 94 shows the external side of typical wall-wall corner joints with construction sealant and Figure 95 shows the external side of typical wall-wall corner joints with construction tape (left) and expanding tape (right) after the test. Detail drawings of these connections are given in Figure 6 D.

The structure directly above the openings is highly exposed. It has therefore been reviewed separately, and details of this, including drawings and pictures of the area post fire can be seen in Section 6.16.



Figure 94: Typical wall-wall butt joint with construction sealing after the test.



Figure 95: Typical wall-wall butt joint with construction tape (left) and expanding tape (right) after the test.

6.16 Performance of different façade details

The detail above openings at the façade is a sensitive detail, which is subject to high gas velocities and thermal exposures. In order to identify an effective solution that results in minor damage, this study included different details for each test.

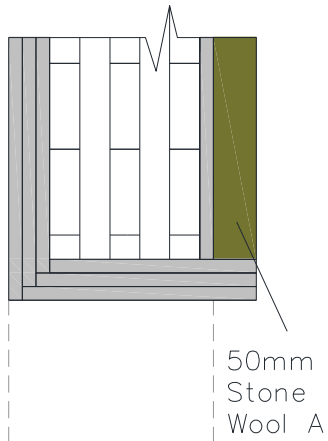
The highest damage was seen above the opening of Test 1 where significant smoldering occurred in the lap joints at the corners of the openings. In a part of the lap joint in the left corner of the right opening, the panel charred through. In the subsequent tests, the façade detail was changed to prevent direct inflow of hot gasses into the interface between the exterior gypsum board and the exterior CLT surface. The lap joints above the corners were also sealed with fire sealing adhesive or construction tape and 45 mm or 50 mm thick stone wool insulation was included.



Figure 96: Test 1 - Detail above opening (left) and front façade after removal of gypsum boards (right)

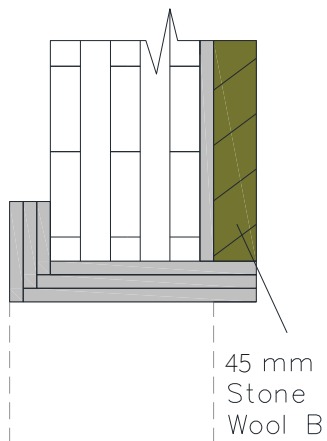
In Test 2, the top of the opening had 3 layers of gypsum boards, while the side of the opening had 2-layers of gypsum boards. The opening dimensions were the same as those of Test 1. After the test there was some minor charring on the sides under the inner corners. Note: the black fire sealing adhesive smeared out above the left corner of the left opening should not be confused with char.

Test 3 had thinner and smaller stone wool battens. A full batten above the right opening fell approximately 11 minutes after flashover. This resulted in some superficial charring of the CLT in that location. The other battens remained in place, for the whole period of external fire extension. Each batten was fastened with six screws and 2 inch diameter washers with an edge distance of about 2 inch. It is expected that improving the fastening method or the use of larger battens would have delayed this fall-off.



Test 2

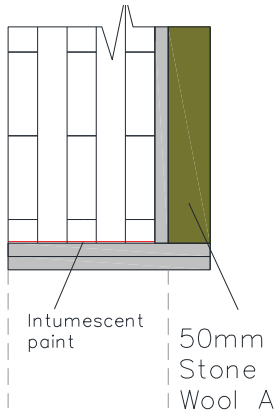
Figure 97: Test 2 - Detail above opening (left) and front façade after removal of gypsum boards. NOTE: the sides of the opening had 2 layers of gypsum boards.



Test 3

Figure 98: Test 3 - Detail above opening (left) and front façade after removal of gypsum boards. NOTE: Stone wool B (1200 x 555 x 45) was thinner and had smaller batt dimensions than stone wool A, which was used in other tests (1200 x 2700 x 50mm). The stone wool batt above the right opening fell at an early stage.

The façade of Test 4 was undamaged with the exception of a location where 5 thermocouples were positioned at the back opening of the left façade.



Test 4



Figure 99: Test 4 - Detail above opening (left) and front façade after removal of gypsum boards.

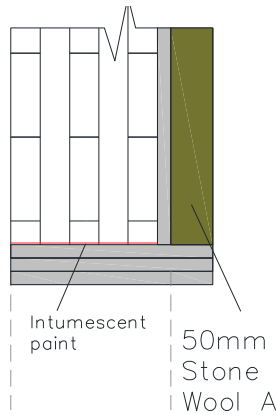


Figure 100: Test 4 - Left façade after removal of gypsum boards.



Figure 101: Test 4 - Right façade after removal of gypsum boards.

Test 5 included cavities in the front façade as it was originally planned to have larger openings. The damage in the façade of Test 5 is therefore, considered not representative for real buildings with a mass timber structure. Based on the damage it is expected that some combustion started in the right cavity. This led to charring above the right corner of the right opening.



Test 5



Figure 102: Test 5 - Detail above opening (left) and front façade after removal of gypsum boards. NOTE: Test 5 was originally planned to have larger openings. During the test series it was decided to perform a test with the same openings as Test 1, 2 and 3 and modify the opening width in the front façade. As a result a cavity existed between the external and internal gypsum boards at the outer side of both openings. It is expected that a smoldering fire entered the cavity on the right side of the right opening, which stayed behind the outer gypsum boards.

6.17 Smoldering inside the compartment at the end of the test

During much of the decay phase, the highest temperatures of exposed walls, as measured using thermal cameras, were located at the bottom of the exposed walls of Test 2, 3 and 5. For the duration of the decay phase, the wall temperatures continued to decrease in Test 2 and 5 but this decrease was slower at the back and the front corner of the walls. At the end of the test the temperatures in the back and the front corner were highest as can be seen in thermal camera photos of Figure 103. This is not visible without the thermal camera as the surface is mostly black (see Figure 104 and Figure 105).

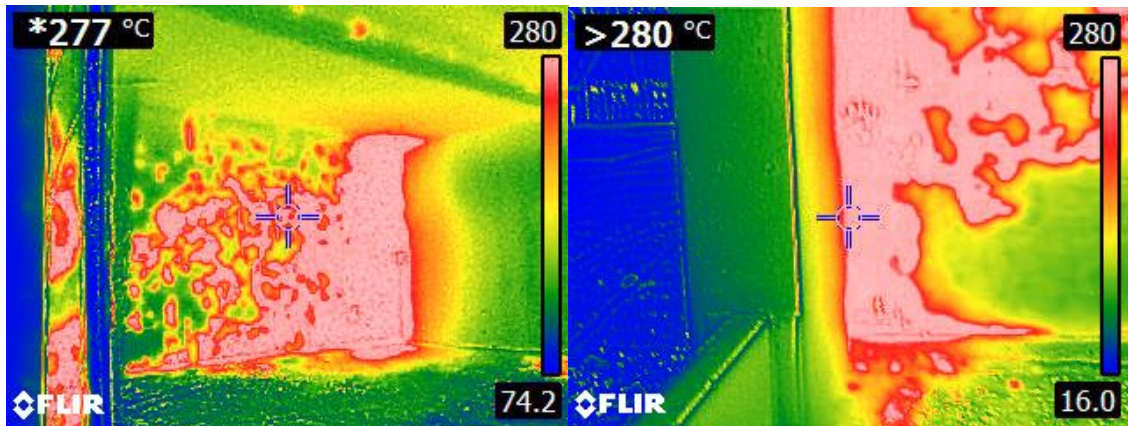


Figure 103: Thermal camera photo of hot spots in the back right and front left corner of exposed walls after the test. Multiple IR cameras have been used, colours used in the here have been altered to match those of the other thermal camera. The original output uses a purple to orange scale.



Figure 104: Left wall at the end of the test.

After Test 4, the locations of hot spots were limited but a few are shown in Figure 105.



Figure 105: A typical hot spot after Test 4 (left thermal camera, right regular camera)

The connection detail between the beam and the back wall which involved manual cutting of CLT with a tiger saw had local hot spots after every test (Figure 106). It should be noted that due to the used of hand-held saws, the gaps and geometrical imperfection are not representative for factory made cuts.

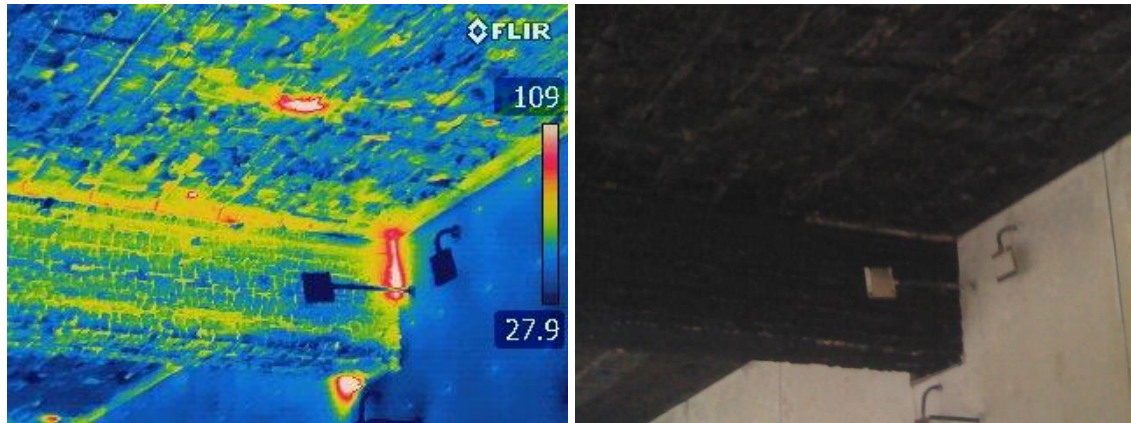


Figure 106: connection between beam and back wall after Test 4 (left thermal camera, right regular camera)

After the tests hot spots and smoldering were observed in various wall locations identified using a thermal camera but minor or not present in the ceiling.

After Test 1, no hot spots were seen in the ceiling but some were identified in the walls behind the two layers of gypsum boards. In the back wall these were seen at the end of the fire test and extinguished with water mist. Further hot spots appeared locally on the left, back and right wall and were identified approximately 2.5 hours after the test during a second check. After manual removal of the gypsum boards the smoldering stopped, and no water was needed. No other test showed sustained smoldering behind gypsum boards.

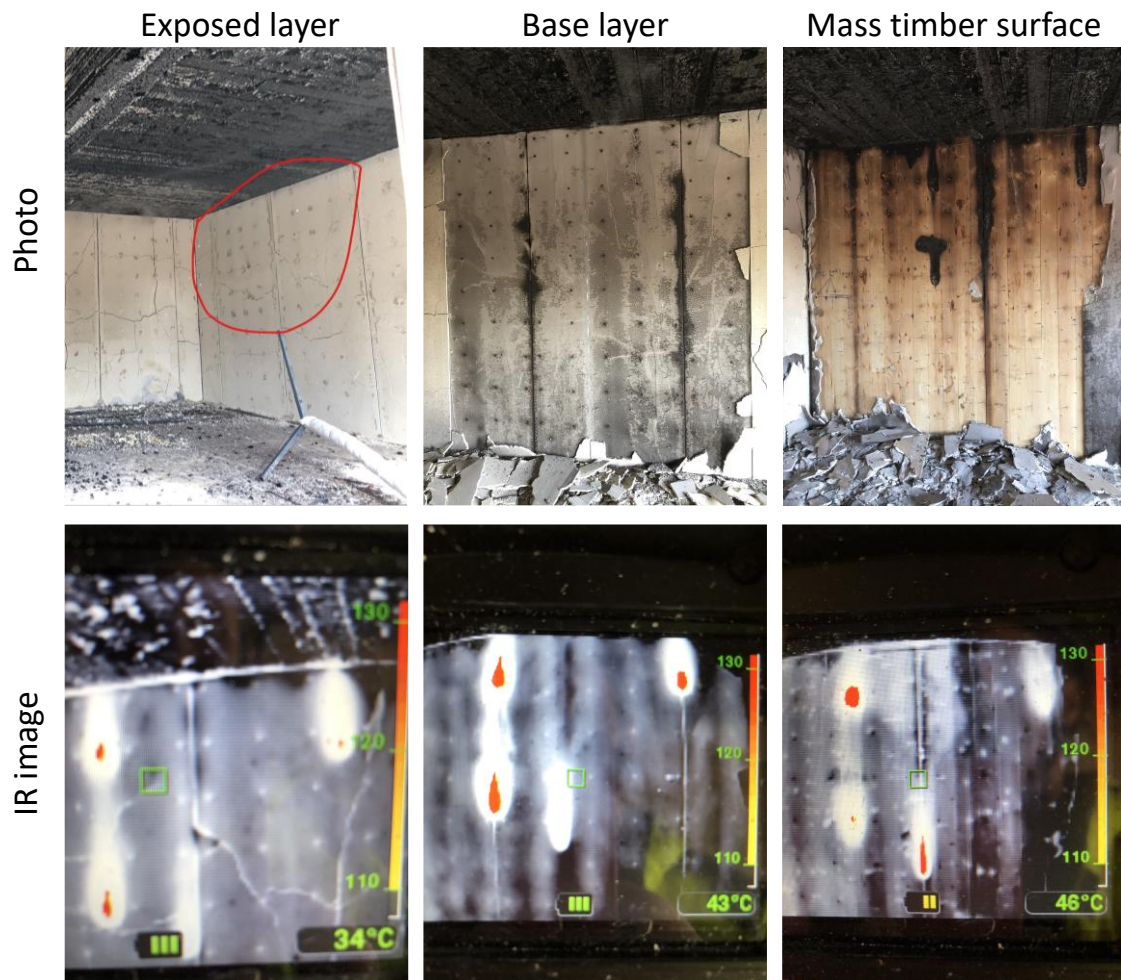


Figure 107: Thermal camera photo of hot spots in the left wall (at the joint between plaster boards and the back wall (at a lap joint, exactly where thermocouples are located in the CLT).

7 Discussion

7.1 Assessment against previous ICC performance criterion

For this project a quantifiable adaption of the performance criterion (where a compartment fire should exhibit continual decay without significant fire re-growth during the decay phase for 4 hours following fire initiation) was used by the International Code Council Ad Hoc Committee on Tall Wood Building (ICC-TWB) to develop code change proposals for the International Building Code 2021 (IBC 2021), which were accepted in 2019. The criterion was used for the assessment of the results by Zelinka et al. (2018) and a comparable criterion is being used in the required CLT compartment fire test of Annex B in the ANSI/APA PRG 320 (2018), where temperatures should be equal to or below 510 °C after 4 hours of compartment fire testing.

The performance criteria defined in Section 5 were met in all tests with the exception of Test 3. Table 11 gives an overview of these criteria.

Table 11: Performance criteria from test

	Maximum plate thermometer temperatures at the end of the test <300 °C	Maximum incident radiant heat flux at the end of the test <6 kW/m ²	No flaming out of the opening after start of decay	Average upper gas temperatures <600 °C	Heat release rate <0.12 MW/m ²
Test 1	Pass	Pass	Pass	Pass	Pass
Test 2	Pass	Pass	Pass	Pass	Pass
Test 3	Fail	Indefinite*	Indefinite*	Indefinite*	Indefinite*
Test 4	Pass	Pass	Pass	Pass	Pass
Test 5	Pass	Pass	Pass	Pass	Pass

* Test 3 was terminated at 3:31 h:mm as the plate thermometer criterion was not met. The other thresholds were not exceeded during the test time.

7.2 Compartment temperatures

Within the test the internal compartment temperatures were tracked via two means, Plate thermometers and thermocouple trees.

The plate thermometer temperatures were of a similar magnitude for all tests other than Test 4 (which had different ventilation conditions), as can be seen in Figure 108. Likewise the temperatures measured by type k thermocouples on thermocouple trees, which are used as surrogate for gas temperatures, were very similar across Test 2, 3 and 5. Test 1 temperatures started to reduce 8 to 10 minutes earlier (Figure 109), while Test 4 had a shorter duration and lower peak.

Within each test there is limited spatial variation for both the plate thermometers and the thermocouple trees, with the exception of thermocouple measurements at low level on tree 1, which are cooled by air from the openings. This confirms that the fires had well-mixed fire conditions, indicating under ventilated compartment fire conditions.

During the decay phase, Test 3 had higher temperatures plate thermometer than the other tests but only marginal higher TC temperatures. This is likely to be due to thermal feedback between adjacent exposed walls and the increased charring and oxidation this causes, as discussed further in Section 0.

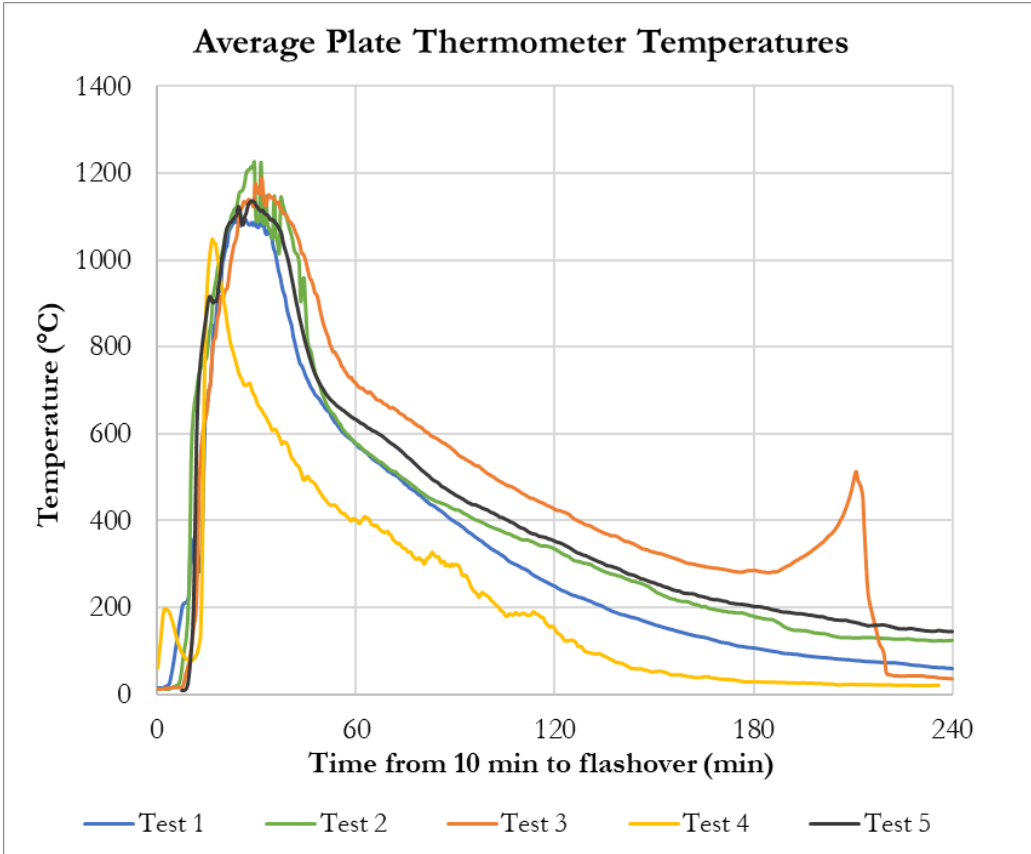


Figure 108: Average plate thermometer temperatures for each test.

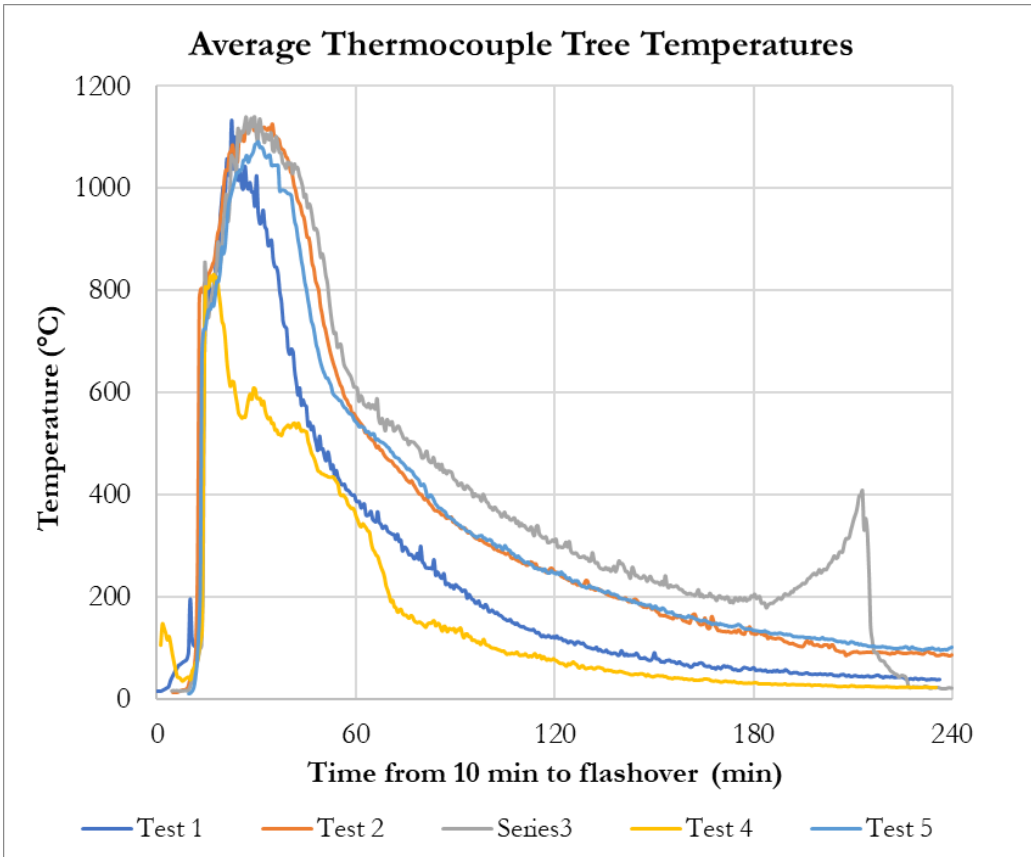


Figure 109: Average thermocouple tree temperatures.

7.3 Façade exposure and potential exposure to other buildings

Additional discussion of the façade exposure is undertaken within the report on façade exposure (Sjöström et al, 2021). The combination of a statistically severe compartment fire, see Annex C, and statistically slender openings (Sjöström et al, 2021) for Tests 1, 2, 3 and 4, means that the façade exposure should also be statistically severe.

An increase in exposed timber of 37 m² (test 1 to test 2) to 43 m² (test 1 to test 5) led to an increase of fire plume height (for Tests 2 and 5) and corresponding upwards shift of the temperature profile of 0.5 to 1.0 m as can be seen in Figure 83 in section 6.13.

The exposure to the façade in test 4 was significantly lower with the fire plume only briefly reaching a maximum height of ~3.5 m above the opening before quickly dropping away. This was also echoed in the temperature of the plumes with a temperature profile shifted approximately 0.75 m below Test 1 and a shorter duration. Comparisons with standard façade tests can be seen in the separate façade report by Sjöström et al. (2021).

As for the irradiation to neighboring buildings, at 8 m distance the irradiation levels are well below anything that could ignite common building materials and also well below the thresholds set out in codes for Sweden, UK and NFPA (Figure 84).

7.4 Progression of the thermal wave in CLT after the test

Temperatures deep inside fire-exposed materials can increase long after the fire, because of thermal diffusivity, i.e. the heat stored on the exposed side of a member takes time to spread through the member depending on its thermal properties. Because the strength of timber generally reduces with increasing temperature (Figure 110), the structural capacity of the structure reduces for a period after the highest fire exposure. As timber is a relatively good thermal insulator, there is a significant delay in the progression of the thermal wave through the thickness of the material and within the depth of the timber the maximum temperatures may be reached long after the peak of the fire.

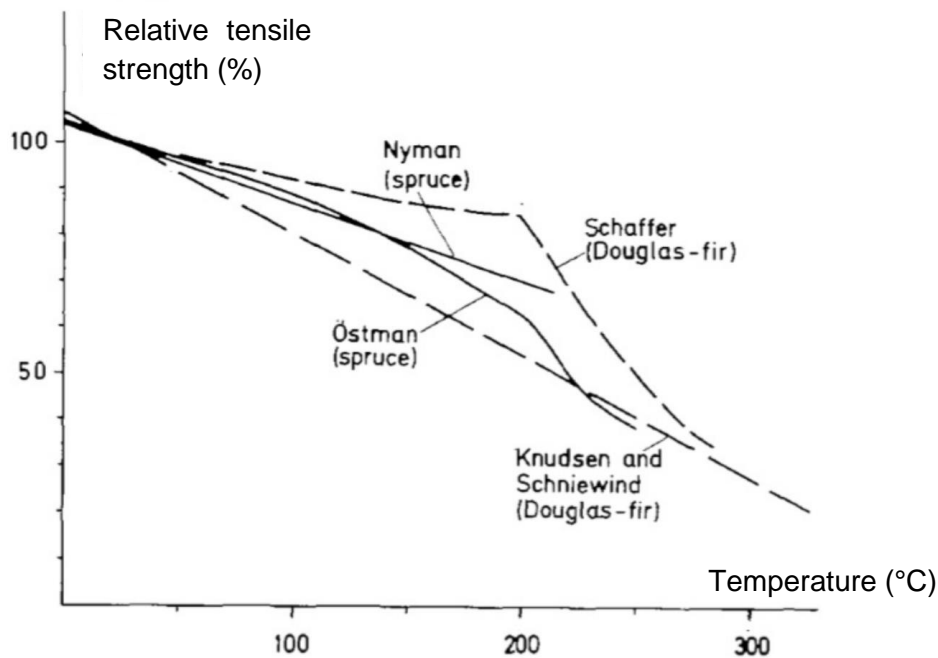


Figure 110: Reduction in tensile strength of timber with temperature, from Östman (1985).

Post-test measurements after Test 1 and Test 2 of temperatures inside the CLT members have been performed until the next day to assess the progression of the thermal wave after the 4-hour test. As can be seen section 6.9 and Annex J, the thermal wave had peaked for most locations prior to the completion of the test, and where it hadn't the remaining temperature increase is minor (e.g. from 53°C to 55°C at 70 mm depth and 29°C to 38°C 105 mm high on the back wall, see Figure 111). After Test 1, locally in one lap joint at the bottom of the back wall the temperatures initially increased because of smoldering, until the gypsum board was removed (see Figure 67 in section 6.9). Due to the very local nature of smoldering identified, the reduction of the overall loadbearing capacity is considered negligible. Therefore, it is concluded that the post-test thermal wave did not significantly reduce the structural capacity after the test.

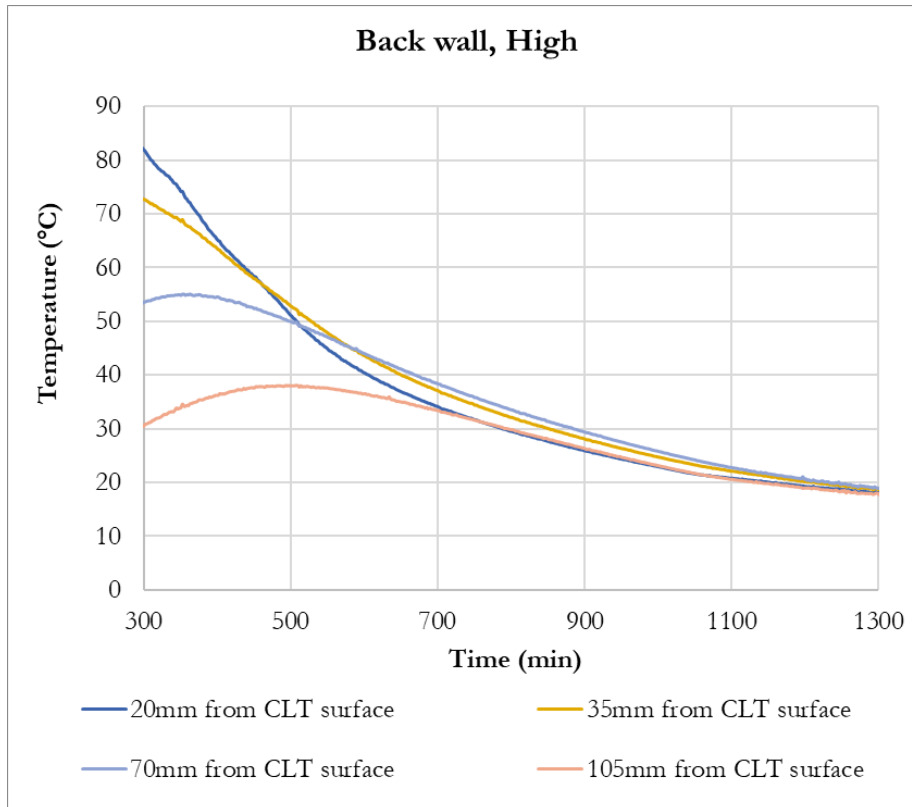


Figure 111: Through-depth temperatures in the CLT high on the back wall after Test 2 showing the delay to reach peak temperatures at 70 mm and 105 mm deep.

7.5 Intersections and detailing

Details of intersections between mass timber members have been designed with the aim to limit the flow of hot gasses through the intersection. The five compartment fire tests all had different details at intersections and used different sealing materials. Most of these sealants had a relatively low temperature resistance in comparison with the fire temperature. However, by implementing these materials in locations which were expected to stay relatively cool throughout the fire and preventing the flow of hot gasses, they could effectively prevent smoldering or flaming from spreading through the intersections.

In the two instances that flames reached through the intersection detail, there was visible smoke coming through the joint at an early stage of the fire, indicating a lack of effective gas seal. These locations, both, had relatively large geometrical imperfections, as the detail in one of these locations involved manual sawing on-site with a tiger saw and the other detail involved a geometrical jump of a few millimeters on the top of a wall. It is therefore, considered important that the sealant can ensure effective gas seal in scenarios that correspond with the allowed geometrical tolerances. Using two sealing methods or two barriers for gas flow, will naturally increase the robustness of the detail, which is in line with observations of these tests.

The column-beam connection had a maximum gap of 5 mm after installation to represent scenarios at the maximum allowable geometrical tolerances. In tests where the beam and column were both exposed, the beam end was painted using intumescent paint. This successfully kept temperatures of the aluminium connector well below the combustion temperature of wood (200°C) which indicates that the heating and conduction of the aluminum connector did not cause smoldering of any wood in the beam and column. No smoldering was seen in this connection after any of the tests.

In order to limit smoldering above the opening in the façade, it is recommended to design the detail above the opening robustly. Improved performance was found by placing the gypsum board in a manner that the joints between gypsum boards are not directly exposed to the expected flow of hot gasses. It is also recommended to extend the gypsum boards that are protecting the opening edges to partly lead the fire plume away from the façade, as shown in Figure 112. Although the detail has not been tested as such, implementing a line of fire sealing adhesive between the CLT at the top of the opening and the base layer of gypsum board instead of intumescent paint (used in Test 4 and 5) is expected to improve the performance of this detail.

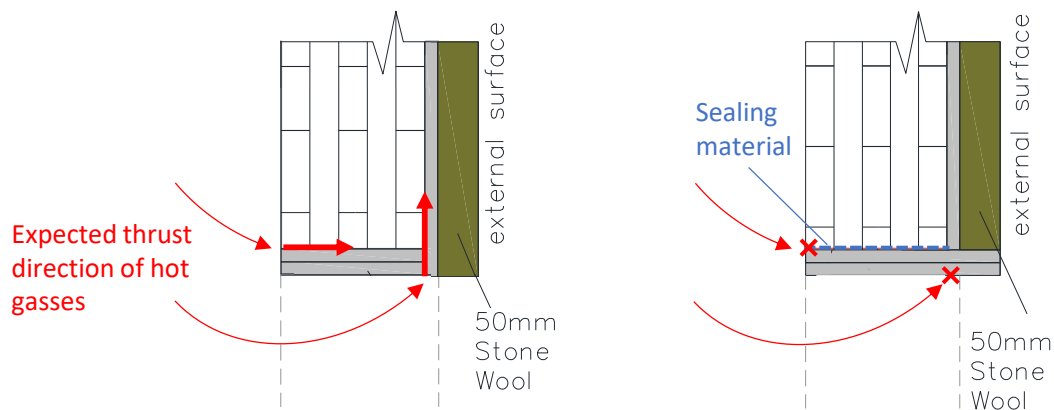


Figure 112: Example of a sensitive detail (left) and a variant with improved fire performance (right)

7.6 Radiative interaction at bottom of wall corners

The highest char depth was seen at the bottom of corners where two exposed walls intersect. The presence of significantly lower char depths in corners where only one wall is exposed and the other wall is protected, indicated that two exposed walls meeting in one corner influence each other's charring behavior. Since the main mode of heat transfer for the majority of the fire is radiation and walls intersecting in a corner have a relatively high view factor to each other, it can be expected that radiative interaction caused this effect in the corner. The increased charring was, however, only observed in the bottom part of wall corners, despite similar or lower thermocouple temperatures and plate thermometer temperatures (Figure 40 to Figure 44) at the bottom of the compartment. The discussion of this section links the low location of the highest char depths to char oxidation.

Charred surface material can oxidize at elevated temperatures if sufficient oxygen is available (Weng et al. 2006). This is supported by the difference between the thermogravimetric analyses results at 20% and 0% oxygen concentration environments (see Section 4.1, Figure 4), i.e. an increase of oxygen concentration for charred material with high temperatures would lead to an additional mass loss and potential release of heat. This mass loss does not occur for material of colder temperatures (approx. ≤ 500 °C). As cold oxygen-rich air flows into the bottom of the compartment a switch from oxygen poor to oxygen rich environment occurs first in the bottom of the compartment. At the bottom of the walls this switch can occur before the fuel on the floor starts to burn out, which is in agreement with the results of Annex K. Therefore, char oxidation is an explanation for higher surface temperatures at the bottom of the walls during the decay phase. This is supported by the increased surface temperatures of the timber remained generally in the bottom of the compartment (Figure 113) despite the irradiation to the wall being very similar along the height of the walls (or even slightly higher at the top, Section 6.6).

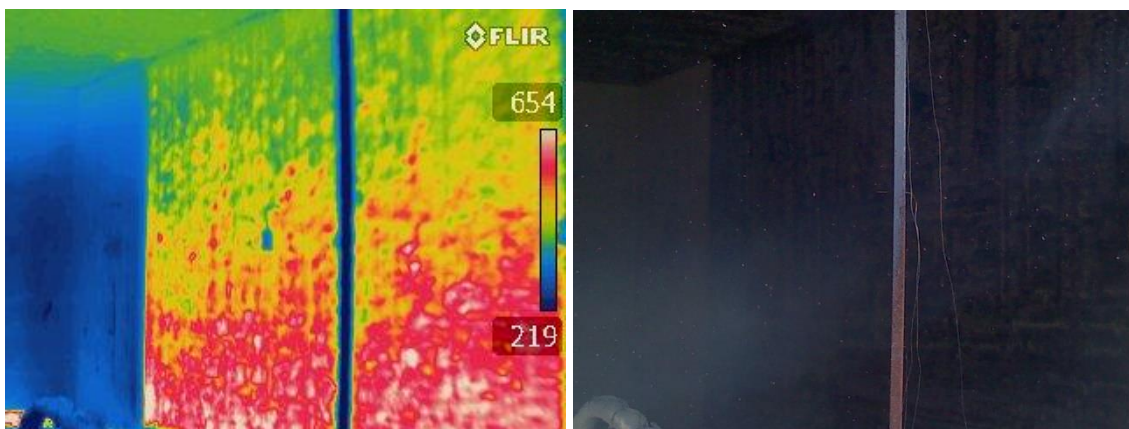


Figure 113: Infrared camera picture and corresponding photo of right wall at 2 hours after ignition in Test 3.

As surfaces radiate heat, they interact with one another. This interaction is more significant if the surfaces have a high view factor relative to each other, such as in corners.

As the surface temperatures are higher in the bottom part of the walls due to oxidation, this interaction is more significant in the bottom of a corner between two exposed walls. The increased charring is a consequence of both an additional heat flux and a reduced protective char layer. The photo of Figure 114 shows a corner where two exposed walls intersect at a late stage of decay of Test 4. At the time of this photo, smoldering combustion in most other surfaces started to extinguish as concluded using an infrared camera. However, the bottom corners where two exposed walls intersected were visibly smoldering more severely and significantly longer than other surfaces.



Figure 114: Photo at the final stage of Test 4

Tests 3, and 5 had approximately the same surface area of exposed wood and Test 2 had roughly 5 % less surface area of exposed wood (Table 12). Between Test 3 and 5 only one test parameter was changed, which is the location of the gypsum board protection. As indicated in Table 12 the gypsum boards of Test 5 were positioned such that one wall surface at each corner was protected, which was not the case for Test 3. Figure 115 shows that the average temperature of measurements by thermocouple trees is the same for Test 3 and 5. As the measurements of thin thermocouples are mostly sensitive to convection, these measurements approximate the gas temperature. Despite the indicated similarity between gas temperatures of the tests, the average plate thermometer temperature is significantly higher in Test 3 than in Test 5 during the decay phase. At these temperatures, plate thermometers are dominated by thermal radiation, and in

most of the decay phase the walls radiate to each other after thick flames disappear. The temperature measurements of Figure 115 therefore indicate an increased radiative interaction between compartment boundary surfaces in Test 3, while the internal gas temperatures are the same as in Test 5.

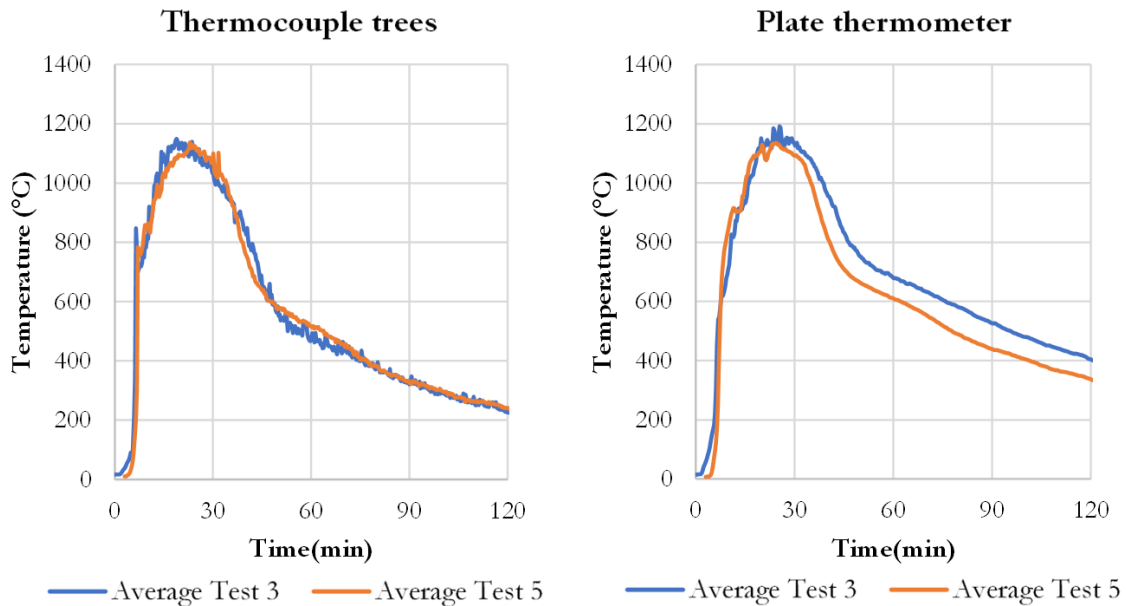


Figure 115: Thermocouple tree temperatures (left), plate thermometer temperature (right)

As indicated in Table 12, Test 3 did not pass the ICC criterion, in which a continual decay without significant fire re-growth during the decay phase for 4 hours after fire initiation is required (Chapter 5), while Test 5 (and all other tests) did. As there was only one test variable between Test 3 and Test 5 and because there are indications that radiative feedback between two exposed walls at the bottom of a corner is significant, the data indicates that the contrast between the outcome of Test 3 and Test 5 (and probably Test 2) is a result of the presence of wall corners with two exposed CLT surfaces.

Based on the fact that Test 3 did not pass the ICC criterion, it is not recommended to implement two exposed CLT wall surfaces that intersect in one corner. However, the data from Tests 2 and 5 do not indicate a similar phenomenon at the intersection between an exposed wall and an exposed ceiling. Further research is recommended to study the radiative interaction between the lower part of exposed CLT walls of high relative view factors in compartment fires.

Table 12: Overview of tests with an opening factor of 0.062 m^{1/2}

Test	Opening factor m ^{1/2}	Protection (interior). Number of 5/8 inch thick (15.9 mm) type X gypsum boards	Surface area of timber exposed			Presence of corner intersection between exposed walls	Pass criteria at 4 h
			m ²	ft ²	%*		
Test 1	0.062	2GB	53.8	579	44.2	No	Fulfilled
Test 2	0.062	3GB	91.2	981	75.0	No	Fulfilled
Test 3	0.062	3GB	96.2	1035	79.2	Yes	Not fulfilled
Test 5	0.062	3GB	97.2	1046	80.0	No	Fulfilled

* Percentage of all surface areas except the floor

Test 4 fulfilled the ICC criterion, despite the presence of corners between two exposed walls. It can, however, be stated that the char damage to the mass timber structure corresponding to the full fire duration becomes less with increasing opening factor (Su et al 2018a, Su et al 2018b, Brandon and Anderson, 2018). Thus, the large openings of Test 4, representing a building with business occupancy (Annex C), lost significantly more heat through openings (by radiation and convection). Despite the significantly higher HRR at flashover, the fire rapidly decayed to just a small number of local hot-spots.

Table 13: Information of Test 4 with an opening factor of 0.25 m^{1/2}

Test	Opening factor m ^{1/2}	Protection (interior)	Surface area of timber exposed			Presence of corner intersection between exposed walls	Pass criteria at 4h
			m ²	ft ²	%*		
Test 4	0.25	2GB type X 15.9 mm	77.9	838	80.2	Yes	Fulfilled

* Percentage of all surface areas except the floor

7.7 Difference with previous test series

Most previous test series involving compartment fire tests with exposed CLT involved fire delamination of CLT, which was identified as a reason for fire regrowth or the complete absence of a decay phase (McGregor 2014, Medina Hevia, 2015, Hadden et al. 2017, Emberley, 2017, Su et al. 2018, Brandon et al. 2018). Additional causes of fire regrowth or lack of decay is the fall-off of the base layer of gypsum board protection (Su et al. 2018a). In addition, significant charring behind gypsum boards as a consequence of too few/thin gypsum board layers has been identified as a reason for fire temperatures to drop slower, or plateau at relatively high temperatures (Su et al.

2018b). Using a CLT adhesive (HB X) and lay-up that complies with the compartment fire test requirements of the 2018 version of ANSI/APA PRG 320, has led to significantly improved compartment fire performance in this study. In addition, the implementation of sufficient gypsum boards has shown to limit damage of protected mass timber and avoid significant contribution of the protected mass timber to the fire as fuel. There have been some fire tests that have led to continuously decaying fires, without the implementation of ANSI/APA PRG 320 (2018) compliant CLT (e.g. Medina Hevia, 2015; Zelinka et al. 2018). However, those compartments had significantly smaller exposed CLT surface areas implemented.

7.8 Variables

This study focused on the fire conditions in compartments with exposed mass timber areas and varying gypsum board protection (surface area and number of layers). These variables were chosen for this study because of their significance as identified by previous research (e.g. Brandon and Östman 2016). Other significant parameters, such as the fuel load density and the compartment opening factor have been chosen using a probabilistic approach (Annex C).

Besides these parameters, there are material parameters that can influence the combustion rate of timber, such as density, moisture content, gaps between lamellas and species. As indicated by previous studies (e.g. Mikkola 1991, Hietaniemi, 2005, Leikanger Friquin 2010) density and moisture content could be expected to have the most significant influence of these factors, which can change the charring rate (and combustion rate) by a few percent¹⁰. Using modeling predictions (e.g. by using the method of the predictive modeling report of this project) these variables could be accounted for by adjusting material properties of wood and/or fall-off criteria of gypsum boards. Alternatively, for implementing of the findings of this study in real design, it is recommended that a safety factor is implemented to lower the exposed surface area of timber, reducing the contribution of mass timber more than these variables are expected to increase this contribution.

¹⁰ A drop of moisture content to 6 % (corresponding to a constant relative humidity of approximately 30%) can be expected to increase the charring rate by 8 %, based on the median increase of charring rate per percentage of moisture content of 1.2 % from 32 tests (16 test couples of a dry and wetter test) summarized by Leikanger (2010). This is roughly in line with relationships by Mikkola (1991) and Hietaniemi (2005). A drop of wood density from 470 kg/m³ to 420 kg/m³ would correspond to an increase of char rate of approximately 5 % according to a modelling study by Brandon (2020) which corresponded with 45 fire tests of timber of varying densities by Njankouo et al. (2005) and Yang et al. (2008). The same study also indicated that the change of mass loss rate (and potential heat release rate) will be smaller than this percentage, because less mass is lost per millimetre of charring as a consequence of lower density.

8 Full list of project reports

Besides this final report, the project results/resulted in other reports. A full overview of project reports is given in Table 14.

Table 14: Overview of published and expected project reports

Reference	Description	Due
Brandon, Sjöström, Temple, Hallberg, Kahl (2021) <i>Fire Safe implementation of visible mass timber in tall buildings – compartment fire testing – Final Project Report</i> . RISE Report 2021:40, ISBN: 978-91-89385-26-9, Research Institutes of Sweden, Borås, Sweden.	This report	Published 2021
Brandon, Sjöström, Temple, Hallberg, Kahl (2021) <i>Fire Safe implementation of visible mass timber in tall buildings – compartment fire testing – Summary Report</i> . RISE Report 2021:40, ISBN: 978-91-89385-26-9, Research Institutes of Sweden, Borås, Sweden.	Summary of main compartment test results	Published 2020
Sjöström, Brandon, Temple, Hallberg, Kahl (2021) Exposure from mass timber compartment fires to facades. RISE Report 2021:39, ISBN: 978-91-89385-24-5, Research Institutes of Sweden, Borås, Sweden.	façade exposure and comparison to standard full-scale façade tests	Published 2021
Brandon, Temple, Sjöström (2021) Predictive method for fires in CLT and glulam structures – Disseminated predictions versus real scale compartment fire tests & an improved method. RISE report 2021:44, ISBN 978-91-89385-34-4, Research Institutes of Sweden, Borås, Sweden.	Modeling predictions of fire scenarios	May 2021
Brandon, Kahl, Sjöström, Hallberg, (2021) Rehabilitation of fire exposed CLT - a case study. RISE report 2021:45, ISBN 978-91-89385-35-1. Research Institutes of Sweden, Borås, Sweden.	Case study of repairing fire exposed CLT	May 2021

9 Conclusions

Five compartment fire tests, designed to represent statistically severe and realistic fire scenarios, were performed. The tests were performed outside and, therefore, there were no laboratory limitations regarding the heat release rates of the fires and the surface area of mass timber that could be exposed.

The conclusions of this study are only applicable for mass timber materials that have been demonstrated to withstand long duration compartment fires without the occurrence of delamination, such as CLT qualified in accordance with ANSI/APA PRG 320 (2018).

The fire scenarios tested in this study correspond to the improbable event that (NFPA 13 compliant) sprinklers are not functioning, combined with the absence of fire service interference for the first 4 hours. Under those conditions various configurations of exposed mass timber were tested under a statistically severe fire scenario (with a statistically high fuel load density and low opening factor), in order to make the conclusions more generally applicable. More information on the statistical analysis can be found in Annex C.

From the compartments tested against the selected severe fire scenario, it can be concluded that:

(A) A flashover fire in a compartment with:

- (1) 100 % exposed (PRG 320, 2018 compliant) CLT ceiling and
- (2) 100 % exposed glulam beam under the ceiling and
- (3) two layers of 5/8 inch thick Type X gypsum board protection on all other mass timber surfaces,

decayed continuously until 4 hours after ignition and reached radiation temperatures that were significantly below 300 °C within two hours.

(B) Flashover fires in compartments with:

- (1) 100 % exposed (PRG 320, 2018 compliant) CLT ceiling and
- (2) 100 % exposed beam under the ceiling and
- (3) additional exposed surface areas of column and walls equal to 78 % or 90 % of the floor area, extending to the exposed ceiling and
- (4) 3 layers of 5/8 inch thick Type X gypsum board protection on all other mass timber surfaces,

decayed continuously until 4 hours after ignition and reached radiation temperatures that were significantly below 300 °C.

(C) A third test with similar surface areas of exposed mass timber walls, where exposed CLT wall surfaces intersected in corners, decayed continuously for more than 3 hours but was followed by surface flaming on walls and increased temperatures. Analysis showed higher damage in the corners of two exposed walls and higher radiation temperature throughout the compartment in this test.

(D) A post flashover fire in a similar compartment with a larger opening factor was conducted and decayed relatively quickly and reached ambient temperature within 4

hours. The design corresponds to the range of opening factors of office buildings and only the back wall was protected with two layers of 5/8 inch thick Type X gypsum board.

(E) In all tested compartments with walls and the ceiling surfaces exposed, the char depth in the ceiling and the top part of the wall was lower than the char depth at the bottom part of walls. Also, spots of smoldering and hot-spots were more present in the walls than in the ceiling at the end of all fire tests. Thus, the intersection between exposed wall and exposed ceiling did not exhibit the surface flaming and increased temperatures noticed for exposed walls intersecting in corners.

(F) For these tests, an increase of roughly 40 m² exposed surface area (from ~54 to ~94 m² or from 113 % to 196 % of the floor area) resulted both an increased flame height and shifted flame temperature profile of zero to one meter along the façade. The same increase in exposed mass timber increased the duration of the fully developed fire from 22 to ~30 minutes.

(G) After manually extinguishing smoldering and cooling of hot spots with water mist after the 4-hour mark, the exposed and protected walls and ceiling cooled down throughout the thickness, indicating no further loss of structural capacity.

The work upon which this publication is based was funded in whole or in part through a Wood Innovation grant by the Southern Region, State & Private Forestry, Forest Service, U.S. Department of Agriculture.

In accordance with Federal law and U.S. Department of Agriculture policy, this institution is prohibited from discriminating on the basis of race, color, national origin, sex, age, or disability. To file a complaint of discrimination, write USDA Director, Office of Civil Rights, Room 326-W, Whitten Building, 1400 Independence Avenue, SW, Washington, DC 20250-9410 or call (202) 720-5964 (voice and TDD). USDA is an equal opportunity employer.

References

- APA—The Engineered Wood Association. (2017). ANSI A190.1-2017: Standard for Wood Products-Structural Glued Laminated Timber.
- APA—The Engineered Wood Association. (2018). ANSI/APA PRG 320: 2018: Standard for performance-rated cross-laminated timber. American National Standard. Tacoma, WA: APA-The Engineered Wood Association, 246.
- ANSI (2018) National Design Specification (NDS) for Wood Construction.
- Brandon D, Just A, Andersson P, Östman B (2018) Mitigation of fire spread in multi-storey timber buildings – statistical analysis and guidelines for design. RISE Report 2018:43.
- Brandon, D. (2018). Fire Safety Challenges of Tall Wood Buildings—Phase 2: Task 4-Engineering methods. National Fire Protection Association. NFPA report: FPRF-2018-04.
- Brandon, D., & Anderson, J. (2018). Wind effect on internal and external compartment fire exposure. RISE Report 2018:72. Research Institutes of Sweden.
- Brandon, D., & Dagenais, C. (2018). Fire Safety Challenges of Tall Wood Buildings—Phase 2: Task 5—Experimental Study of Delamination of Cross Laminated Timber (CLT) in Fire. National Fire Protection Association. NFPA report: FPRF-2018-05.
- Brandon, D., Temple, A., & Sjöström, J. (2021a). Predictive method for fires in CLT and glulam structures – Disseminated predictions versus real scale compartment fire tests, RISE Report 2021:63, RISE Research institutes of Sweden, ISBN: 978-97-89385-53-5.
- Brandon, D., Sjöström, J., & Kahl, F., (2021b). Rehabilitation of fire exposed CLT, RISE Report 2021:67, RISE Research institutes of Sweden, ISBN: 978-91-89385-57-3.
- Breneman, S., Timmers, M., & Richardson, D. (2019). Tall Wood Buildings in the 2021 IBC. Up to 18 Stories of Mass Timber. Wood Products Council.
- Buchanan, A. H., & Abu, A. K. (2017). Structural design for fire safety. John Wiley & Sons.
- Bwayla A.C., Loughheed G.D., Kashef A., Saber H.H. (2010) Survey results of combustible contents and floor areas in Canadian multi-family dwellings. Fire Technology, 46-1, pp. 1-20.
- Crielaard, R., van de Kuilen, J. W., Terwel, K., Ravenshorst, G., & Steenbakkens, P. (2019). Self-extinguishment of cross-laminated timber. Fire Safety Journal, 105, 244-260.
- EN 1991-1-2 (2009). Eurocode 1: Actions on structures – Part 1-2: General actions – Actions on structures exposed to fire, *Swedish Standards Institute*
- Emberley R., Gorska Putynska C., Bolanos A., Lucherini A., Solarte A. , Soriguer D., Gutierrez Gonzalez M., Humphreys K., Hidalgo JP., Maluk C., Law A., and Torero JL. (2017) Description of Small and Large-Scale CLT Fire Tests, Fire Safety Journal, doi:10.1016/j.firesaf.2017.03.024

Fahrni, R., Schmid, J., Klippel, M., & Frangi, A. (2018). Investigation of different temperature measurement designs and installations in timber members as low conductive material. In *Structures in Fire SiF'2018: 10th International Conference on Structures in Fire, Belfast, United Kingdom, 6-8 June 2018* (pp. 257-264). Ulster University.

Frangi, A., & Fontana, M. (2005). Fire Performance of Timber Structures under Natural Fire Conditions. Fire Safety Science Symposium 8: 279-290. IAFSS, Beijing, China.

Hadden RM., Bartlett AI., Hidalgo JP., Santamaria S., Wiesner F., Bisby LA., Deeny S., Lane B. (2017) Effects of exposed cross laminated timber on compartment fire dynamics. *Fire Safety Journal* (91): 480-489.

Hox K. (2015) Branntest av massivtre. SPFR-rapport SPFR A15101. SP Fire Research, Trondheim, Norway (unpublished). (in Norwegian)

Janssens, M. (2017). Development of a Fire Performance Test Method for Evaluating CLT Adhesives. Southwest Research Institute.

Lange, D., Boström, L., Schmid, J., & Albrektsson, J. (2015). The reduced cross section method applied to glulam timber exposed to non-standard fire curves. *Fire technology*, 51(6), 1311-1340.

McGregor, C.J. (2013) Contribution of cross-laminated timber panels to room fires. Master thesis. Department of Civil and Environmental Engineering Carleton University. Ottawa-Carleton Institute of Civil and Environmental Engineering, Ottawa, Ontario, Canada.

Medina Hevia A.R. (2014). Fire resistance of partially protected cross-laminated timber rooms. Master thesis. Department of Civil and Environmental Engineering Carleton University. Ottawa-Carleton Institute of Civil and Environmental Engineering, Ottawa, Ontario, Canada.

Mikkola 1991, <https://www.iafss.org/publications/fss/3/547/view>

Sjöström, J., Amon, F., Appel, G. & Persson, H. (2015), Thermal exposure from large scale ethanol fuel pool fires, *Fire safety Journal* **78**, 229-237.

Sjöström, J. Brandon, D. Temple, A. Hallberg, E. Kahl, F. (2021) Exposure from mass timber compartment fires to facades. *Brandforsk Report 2021:3/RISE Report 2021:39*, ISBN: 978-91-89385-24-5.

Su J.Z. and Loughheed G.D. (2014) Report to research consortium for wood and wood hybrid mid-rise buildings – Fire safety summary – Fire research conducted for the project on mid-rise wood construction. National Research Council Canada, Client report: A1-004377.1, Ottawa, Ontario, Canada

Su, J., Lafrance, P. S., Hoehler, M. S., & Bundy, M. F. (2018a). Fire Safety Challenges of Tall Wood Buildings—Phase 2: Task 3-Cross Laminated Timber Compartment Fire Tests (No. Fire Protection Research Foundation).

Su, J., Leroux, P., Lafrance, P. S., Berzins, R., Gratton, K., Gibbs, E., & Weinfurter, M. (2018b). Fire testing of rooms with exposed wood surfaces in encapsulated mass timber construction. National Research Council of Canada, Ottawa.

Weng, W.G., Hasemi, Y., & Fan, W.C. (2006) Predicting the pyrolysis of wood considering char oxidation under different ambient oxygen concentrations, combustion and Flame 145(4), 723-729.

Zelinka, S. L., Hasburgh, L. E., Bourne, K. J., Tucholski, D. R., Ouellette, J. P., Kochkin, V., & Lebow, S. T. (2018). Compartment fire testing of a two-story mass timber building. United States Department of Agriculture, Forest Service, Forest Products Laboratory.

Annex A – Instrumentation locations

The tables contained within this annex provide a full list of the instrumentation used, within these tests. They provide a description of the instrument, a short device name, the type of instrument, and its location. For the location, 3 main co-ordinate systems are used (see also Figure A.1):

- Interior (INT): Devices within the compartment, the origin of this system is at floor level in the front left corner of the compartment. The X direction is from the left to the right of the compartment, the Y from the front to the back and the Z the height above the floor. All distances are given in mm.
- Opening: Plate thermometers in front of the opening, all are placed on the centerline of the opening at a distance on X and a Z coordinate, the height above floor level. All distances are given in mm.
- Façade: Devices on the façade, the origin for this system is the center of the top of the opening above which each device is positioned. The X direction is from the left to the right of the compartment, the Y the offset from the wall's surface and the Z the height above the opening. All distances are given in mm.

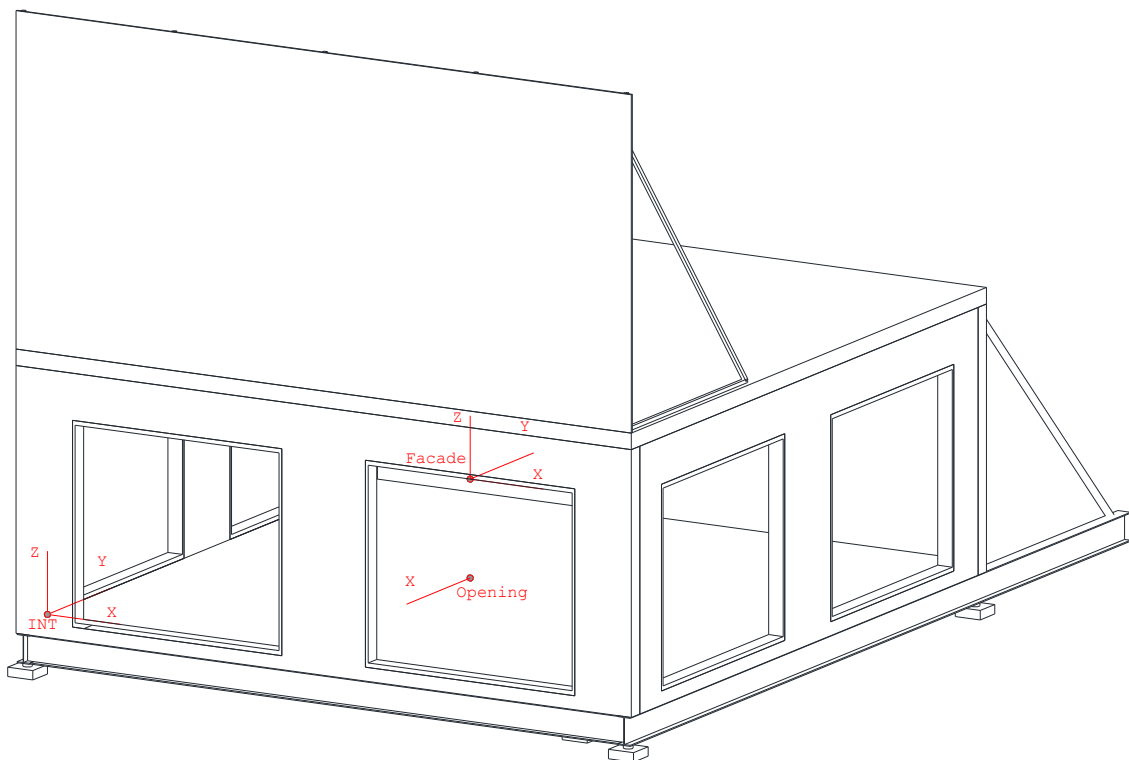


Figure A.1: Coordinate systems used to indicate locations

Table A.1: Primary instrumentation details

Description	Device Name	X	Y	Z	Type	Co-ordinate system
Thermocouple tree 1	TCT1-1	1500	1500	200	Sheathed type K long	INT
	TCT1-2	1500	1500	800	Sheathed type K long	INT
	TCT1-3	1500	1500	1200	Sheathed type K long	INT
	TCT1-4	1500	1500	1800	Sheathed type K long	INT
	TCT1-5	1500	1500	2400	Sheathed type K long	INT
Thermocouple tree 2	TCT2-1	5500	3425	200	Sheathed type K long	INT
	TCT2-2	5500	3425	800	Sheathed type K long	INT
	TCT2-3	5500	3425	1200	Sheathed type K long	INT
	TCT2-4	5500	3425	1800	Sheathed type K long	INT
	TCT2-5	5500	3425	2400	Sheathed type K long	INT
Thermocouple tree 3	TCT3-1	3500	5350	200	Sheathed type K long	INT
	TCT3-2	3500	5350	800	Sheathed type K long	INT
	TCT3-3	3500	5350	1200	Sheathed type K long	INT
	TCT3-4	3500	5350	1800	Sheathed type K long	INT
Plate thermometer left wall HIGH	PTLW-Hi	100	3500	2000	Plate thermometer	INT
Thermocouple PT left wall HIGH	TCPTLW-Hi	100	3500	2000	Sheathed type K	INT
Plate thermometer left wall LOW	PTLW-Lo	100	3500	700	Plate thermometer	INT
Thermocouple PT left wall LOW	TCPTLW-Lo	100	3500	700	Sheathed type K	INT
Plate thermometer back wall HIGH	PTBW-Hi	4570	6900	2000	Plate thermometer	INT
Thermocouple PT back wall HIGH	TCPTBW-Hi	4570	6900	2000	Sheathed type K	INT
Plate thermometer back wall LOW	PTBW-Lo	4570	6900	700	Plate thermometer	INT
Thermocouple PT back wall LOW	TCPTBW-Lo	4570	6900	700	Sheathed type K	INT
Plate thermometer right wall Centre	PTRW-Hi	6900	3500	1350	Plate thermometer	INT

Description	Device Name	X	Y	Z	Type	Co-ordinate system
Thermocouple PT right wall Centre	TCPTRW-Hi	6900	3500	1350	Sheathed type K	INT
Plate thermometer ceiling Front	PTC-Fr	4500	1500	2600	Plate thermometer	INT
Thermocouple PT ceiling Front	TCPTC-Fr	4500	1500	2600	Sheathed type K	INT
Plate thermometer ceiling Back	PTC-Ba	4500	5500	2600	Plate thermometer	INT
Thermocouple PT ceiling Back	TCPTC-Ba	4500	5500	2600	Sheathed type K long	INT
Thermocouple CLT left wall 1 HIGH*	TCCLT-Le1-Hi			2000	Glass fiber insulated type K	INT
Thermocouple CLT left wall 2 HIGH*	TCCLT-Le2-Hi			2000	Glass fiber insulated type K	INT
Thermocouple CLT left wall 3 HIGH*	TCCLT-Le3-Hi			2000	Glass fiber insulated type K	INT
Thermocouple CLT left wall 4 HIGH*	TCCLT-Le4-Hi			2000	Glass fiber insulated type K	INT
Thermocouple CLT left wall 5 HIGH*	TCCLT-Le5-Hi			2000	Glass fiber insulated type K	INT
Thermocouple CLT left wall 1 LOW*	TCCLT-Le1-Lo			700	Glass fiber insulated type K	INT
Thermocouple CLT left wall 2 LOW*	TCCLT-Le2-Lo			700	Glass fiber insulated type K	INT
Thermocouple CLT left wall 3 LOW*	TCCLT-Le3-Lo			700	Glass fiber insulated type K	INT
Thermocouple CLT left wall 4 LOW*	TCCLT-Le4-Lo			700	Glass fiber insulated type K	INT
Thermocouple CLT left wall 5 LOW*	TCCLT-Le5-Lo			700	Glass fiber insulated type K	INT
Thermocouple CLT Back wall 1 LOW*	TCCLT-Ba1-Lo			700	Glass fiber insulated type K	INT
Thermocouple CLT Back wall 2 LOW*	TCCLT-Ba2-Lo			700	Glass fiber insulated type K	INT

Description	Device Name	X	Y	Z	Type	Co-ordinate system
Thermocouple CLT Back wall 3 LOW*	TCCLT-Ba3-Lo			700	Glass fiber insulated type K	INT
Thermocouple CLT Back wall 4 LOW*	TCCLT-Ba4-Lo			700	Glass fiber insulated type K	INT
Thermocouple CLT Back wall 5 LOW*	TCCLT-Ba5-Lo			700	Glass fiber insulated type K	INT
Thermocouple CLT Back wall 1 HIGH*	TCCLT-Ba1-Hi			2000	Glass fiber insulated type K	INT
Thermocouple CLT Back wall 2 HIGH*	TCCLT-Ba1-Hi			2000	Glass fiber insulated type K	INT
Thermocouple CLT Back wall 3 HIGH*	TCCLT-Ba1-Hi			2000	Glass fiber insulated type K	INT
Thermocouple CLT Back wall 4 HIGH*	TCCLT-Ba1-Hi			2000	Glass fiber insulated type K	INT
Thermocouple CLT Back wall 5 HIGH*	TCCLT-Ba1-Hi			2000	Glass fiber insulated type K	INT
Thermocouple CLT right wall 1 LOW*	TCCLT-Ri1-Lo			700	Glass fiber insulated type K	INT
Thermocouple CLT right wall 2 LOW*	TCCLT-Ri2-Lo			700	Glass fiber insulated type K	INT
Thermocouple CLT right wall 3 LOW*	TCCLT-Ri3-Lo			700	Glass fiber insulated type K	INT
Thermocouple CLT right wall 4 LOW*	TCCLT-Ri4-Lo			700	Glass fiber insulated type K	INT
Thermocouple CLT right wall 5 LOW*	TCCLT-Ri5-Lo			700	Glass fiber insulated type K	INT
Thermocouple CLT ceiling front 1	TCCLT-Ce1-Fr	4500	1500		Glass fiber insulated type K	INT
Thermocouple CLT ceiling front 2	TCCLT-Ce2-Fr	4500	1500		Glass fiber insulated type K	INT
Thermocouple CLT ceiling front 3	TCCLT-Ce3-Fr	4500	1500		Glass fiber insulated type K	INT

Description	Device Name	X	Y	Z	Type	Co-ordinate system
Thermocouple CLT ceiling front 4	TCCLT-Ce4-Fr	4500	1500		Glass fiber insulated type K	INT
Thermocouple CLT ceiling front 5	TCCLT-Ce5-Fr	4500	1500		Glass fiber insulated type K	INT
Thermocouple CLT ceiling back 1	TCCLT-Ce1-Ba	4500	5500		Glass fiber insulated type K	INT
Thermocouple CLT ceiling back 2	TCCLT-Ce2-Ba	4500	5500		Glass fiber insulated type K	INT
Thermocouple CLT ceiling back 3	TCCLT-Ce3-Ba	4500	5500		Glass fiber insulated type K	INT
Thermocouple CLT ceiling back 4	TCCLT-Ce4-Ba	4500	5500		Glass fiber insulated type K	INT
Thermocouple CLT ceiling back 5	TCCLT-Ce5-Ba	4500	5500		Glass fiber insulated type K	INT
Thermocouple tree Opening 1	TCT-O1-1	1850		600	Sheathed type K	INT
	TCT-O1-2	1850		1000	Sheathed type K	INT
	TCT-O1-3	1850		1400	Sheathed type K	INT
	TCT-O1-4	1850		1800	Sheathed type K	INT
	TCT-O1-5	1850		2200	Sheathed type K	INT
Thermocouple tree Opening 2	TCT-O2-1	5250		600	Sheathed type K	INT
	TCT-O2-2	5250		1000	Sheathed type K	INT
	TCT-O2-3	5250		1400	Sheathed type K	INT
	TCT-O2-4	5250		1800	Sheathed type K	INT
	TCT-O2-5	5250		2200	Sheathed type K	INT
Plate thermometer opening 1 close	PT-O1-cl	4800		1050	Plate thermometer	Opening
Plate thermometer opening 1 far	PT-O1-fa	8000		1050	Plate thermometer	Opening
Updated PT opening 1 far	PT-O1-Fa-Elev	8000		4000	Glass fiber insulated type K	Opening

Description	Device Name	X	Y	Z	Type	Co-ordinate system
Plate thermometer opening 2 closes	PT-O2-cl	4800		1050	Plate thermometer	Opening
Plate thermometer opening 2 far	PT-O2-fa	8000		1050	Plate thermometer	Opening
Thermocouple Gypsum left 1 HIGH†	TCGyp-Le1-Hi			2000	Sheathed type K long	INT
Thermocouple Gypsum left 2 HIGH†	TCGyp-Le2-Hi			2000	Sheathed type K long	INT
Thermocouple Gypsum left 1 LOW†	TCGyp-Le1-Lo			700	Sheathed type K long	INT
Thermocouple Gypsum left 2 LOW†	TCGyp-Le2-Lo			700	Sheathed type K long	INT
Thermocouple Gypsum Back 1 LOW†	TCGyp-Ba1-Lo			700	Sheathed type K long	INT
Thermocouple Gypsum Back 2 LOW†	TCGyp-Ba2-Lo			700	Sheathed type K long	INT
Thermocouple Gypsum right 1 LOW†	TCGyp-Ri1-Lo			700	Sheathed type K long	INT
Thermocouple Gypsum right 2 LOW†	TCGyp-Ri2-Lo			700	Sheathed type K long	INT
<p>* CLT through depth temperatures were measured within joints between CLT panels. For each wall, they were installed within the joint closest to the center. Where this wasn't at the center the first gap was to the right (facing the wall in question).</p> <p>† Thermocouples were provided between each gypsum layer at the same location as the through depth CLT measurements (see note above) where the wall was protected. These are numbered so that the boundary between the CLT and the Gypsum is layer 1, increasing in number each layer towards the inside of the compartment.</p>						

Table A.2 below includes instrumentation which was not used in all tests. See usage column for details.

Table A.2: Instrumentation only used in some tests.

Description	Device Name	X	Y	Z	Type	Co-ordinate system	Usage
Thermocouple Gypsum right 3 LOW	TCGyp-Ri3-Lo			700	Sheathed type K long	INT	Only: if gypsum protected & if 3 GB layers
Thermocouple Gypsum right 3 LOW	TCGyp-Ri3-Lo			700	Sheathed type K long	INT	Only: if gypsum protected & if 3 GB layers
Thermocouple Gypsum left 3 HIGH	TCGyp-Le3-Hi			2000	Sheathed type K long	INT	Only: if gypsum protected & if 3 GB layers

Description	Device Name	X	Y	Z	Type	Co-ordinate system	Usage
Thermocouple Gypsum left 3 LOW	TCGyp-Le3-Lo			700	Sheathed type K long	INT	Only: if gypsum protected & if 3 GB layers
Thermocouple Gypsum Back 3 LOW	TCGyp-Ba3-Lo			700	Sheathed type K long	INT	Only: if gypsum protected & if 3 GB layers
O ₂ Back Low*	Lambda 1 Lo B	-	5350	720	Lambda sensor	INT	Test 2, 3 and 5
O ₂ Back High*	Lambda 1 Hi B	-	5350	2000	Lambda sensor	INT	Test 2, 3 and 5
O ₂ Front Low*	Lambda 1 Lo F	-	1500	720	Lambda sensor	INT	Test 2, 3 and 5
O ₂ Front High*	Lambda 1 Hi F	-	1500	2000	Lambda sensor	INT	Test 2, 3 and 5
O ₂ Middle Low*	Lambda 1 Lo M	-	3425	720	Lambda sensor	INT	Test 5 only
O ₂ Middle Middle*	Lambda 1 Mi M	-	3425	1360	Lambda sensor	INT	Test 5 only
O ₂ Middle High*	Lambda 1 Hi M	-	3425	2000	Lambda sensor	INT	Test 5 only
O ₂ Front Low Left	Lambda 1 Lo F	0	1500	300	Lambda sensor	INT	Test 5 only
PT Left Front Low	PT LW Fr Lo (30cm)	100	1500	300	Plate thermometer	INT	Test 5 Only, facing wall.
PT Right Centre High	PT RW Cent Hi (70)	6900	3425	2000	Plate thermometer	INT	Test 5 only
PT Right Front Low	PT RW Fr Lo (30cm)	6900	1500	300	Plate thermometer	INT	Test 5 Only, facing wall.
PT Right Front High	PT RW Front Hi	6900	1500	2000	Plate thermometer	INT	Test 5 only
PT Surface Left Wall Low	PT LW Lo 180†	100	3500	700	Plate thermometer	INT	Test 2 only
PT Surface Back Wall Low	PT BW Lo 180†	4750	6750	700	Plate thermometer	INT	Test 2 only
PT Surface Right Wall Rear	PT RW 180†	6900	6100	1000	Plate thermometer	INT	Test 3 only
PT Surface Left Wall Rear	PT LW 180†	100	6100	1000	Plate thermometer	INT	Test 3 only
PT Right Wall Rear	PT RW 1m 0	6900	6100	1350	Plate thermometer	INT	Test 3 only
PT Left Wall Rear	PT LW 1m 0	100	6100	1350	Plate thermometer	INT	Test 3 only
PT Surface Back Wall High	PT BW Hi 180†	3890	6750	2500	Plate thermometer	INT	Test 4 only
PT Surface Beam	PT BW Beam	3760	6450	2500	Plate thermometer	INT	Test 4 only

Description	Device Name	X	Y	Z	Type	Co-ordinate system	Usage
PT Surface Left Wall Front Low	PT LW Front Lo (30) 180†	100	1500	300	Plate thermometer	INT	Test 5 only
PT Surface Right Wall Front Low	PT RW Front Lo (30) 180†	6900	1500	300	Plate thermometer	INT	Test 5 only
* Lambda sensors are placed on the left wall for Tests 2 and 3 (X = 0 mm) and on the right wall for Test 5 (X = 6850)							
† 180 indicates plate thermometers that were directed towards a wall or ceiling surface 100 mm from this surface							

Table A.3 below contains the full list of façade instrumentation, these use the façade coordinate system.

Table A.3: Façade instrumentation

Description	Device Name	X	Y	Z	Type
External Façade Left TC1	TCEXL1		100	2337	Thick sheathed type K
External Façade Left TC2	TCEXL2	0	100	1418	Thick sheathed type K
External Façade Left TC3	TCEXL3	0	100	912	Thick sheathed type K
External Façade Left TC4	TCEXL4	0	25	915	Sheathed type K
External Façade Left TC5	TCEXL5	0	25	1535	Sheathed type K
External Façade Left TC6	TCEXL6	-500	50	2000	Sheathed type K
External Façade Left TC7	TCEXL7	0	50	2000	Sheathed type K
External Façade Left TC8	TCEXL8	500	50	2000	Sheathed type K
External Façade Left TC9	TCEXL9	0	25	2450	Sheathed type K
External Façade Left TC10	TCEXL10	-1000	50	2500	Sheathed type K
External Façade Left TC11	TCEXL11	-500	50	2500	Sheathed type K
External Façade Left TC12	TCEXL12	0	50	2500	Sheathed type K
External Façade Left TC13	TCEXL13	500	50	2500	Sheathed type K
External Façade Left TC14	TCEXL14	1000	50	2500	Sheathed type K
External Façade Left TC15	TCEXL15	-610	25	3050	Sheathed type K
External Façade Left TC16	TCEXL16	0	25	3050	Sheathed type K
External Façade Left TC17	TCEXL17	610	25	3050	Sheathed type K
External Façade Left TC18	TCEXL18	-1220	25	3050	Sheathed type K
External Façade Left TC19	TCEXL19	1220	25	3050	Sheathed type K
External Façade Left TC20	TCEXL20	-500	50	3500	Sheathed type K
External Façade Left TC21	TCEXL21	0	50	3500	Sheathed type K
External Façade Left TC22	TCEXL22	500	50	3500	Sheathed type K
External Façade Left TC23	TCEXL23	0	100	790	Sheathed type K
External Façade Left TC24	TCEXL24	1000	100	1290	Sheathed type K
External Façade Left TC25	TCEXL25	0	100	1790	Sheathed type K
External Façade Left PT 1 (flush)	PTEXL1	0	0	1250	PT
External Façade Left PT 2 (flush)	PTEXL2	500	0	1250	PT
External Façade Left PT 3 (flush)	PTEXL3	-500	0	1250	PT
External Façade Left PT 4 (flush)	PTEXL4	0	0	2100	PT

Description	Device Name	X	Y	Z	Type
External Façade Right TC1	TCEXR1		100	2337	Thick sheathed type K
External Façade Right TC2	TCEXR2	0	100	1418	Thick sheathed type K
External Façade Right TC3	TCEXR3	0	100	912	Thick sheathed type K
External Façade Right TC4	TCEXR4	0	25	915	Sheathed type K
External Façade Right TC5	TCEXR5	0	25	1535	Sheathed type K
External Façade Right TC6	TCEXR6	-500	50	2000	Sheathed type K
External Façade Right TC7	TCEXR7	0	50	2000	Sheathed type K
External Façade Right TC8	TCEXR8	500	50	2000	Sheathed type K
External Façade Right TC9	TCEXR9	0	25	2450	Sheathed type K
External Façade Right TC10	TCEXR10	-1000	50	2500	Sheathed type K
External Façade Right TC11	TCEXR11	-500	50	2500	Sheathed type K
External Façade Right TC12	TCEXR12	0	50	2500	Sheathed type K
External Façade Right TC13	TCEXR13	500	50	2500	Sheathed type K
External Façade Right TC14	TCEXR14	1000	50	2500	Sheathed type K
External Façade Right TC15	TCEXR15	-610	25	3050	Sheathed type K
External Façade Right TC16	TCEXR16	0	25	3050	Sheathed type K
External Façade Right TC17	TCEXR17	610	25	3050	Sheathed type K
External Façade Right TC18	TCEXR18	-1220	25	3050	Sheathed type K
External Façade Right TC19	TCEXR19	1220	25	3050	Sheathed type K
External Façade Right TC20	TCEXR20	-500	50	3500	Sheathed type K
External Façade Right TC21	TCEXR21	0	50	3500	Sheathed type K
External Façade Right TC22	TCEXR22	500	50	3500	Sheathed type K
External Façade Right TC23	TCEXR23	0	100	790	Sheathed type K
External Façade Right TC24	TCEXR24	1000	100	1290	Sheathed type K
External Façade Right TC25	TCEXR25	0	100	1790	Sheathed type K
External Façade Right PT 1 (flush)	PTEXR1	0	0	1250	PT
External Façade Right PT 2 (flush)	PTEXR2	500	0	1250	PT
External Façade Right PT 3 (flush)	PTEXR3	-500	0	1250	PT
External Façade Right PT 4 (flush)	PTEXR4	0	0	2100	PT

Annex B – Façade drawings

This Annex includes drawings of the facades with openings. All tests, including Test 4 had a symmetrical structure. Therefore, only one of the side elevations of Test 4 is included.

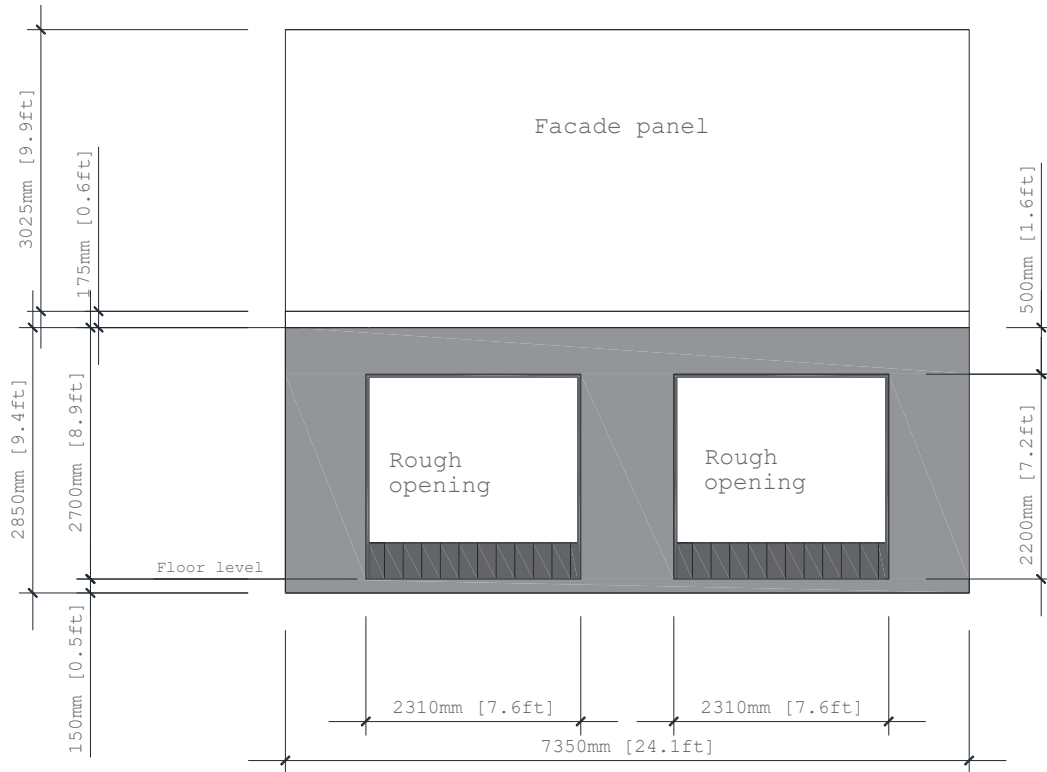


Figure B.1: Front view of the compartments of Test 1, 2, 3 and 5. After gypsum board installation, the rough openings were 2246 x 1780 mm.

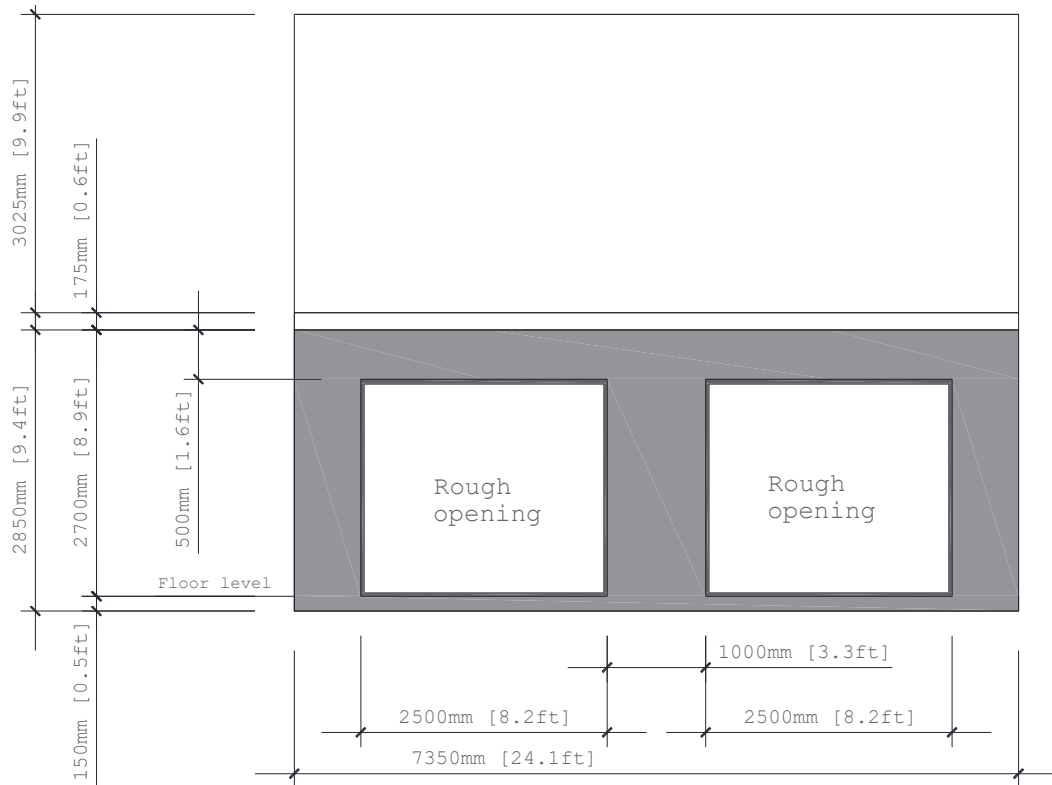


Figure B.2: Front view of the compartment of Test 4. After gypsum board installation, the rough openings were 2436 x 2104 mm.

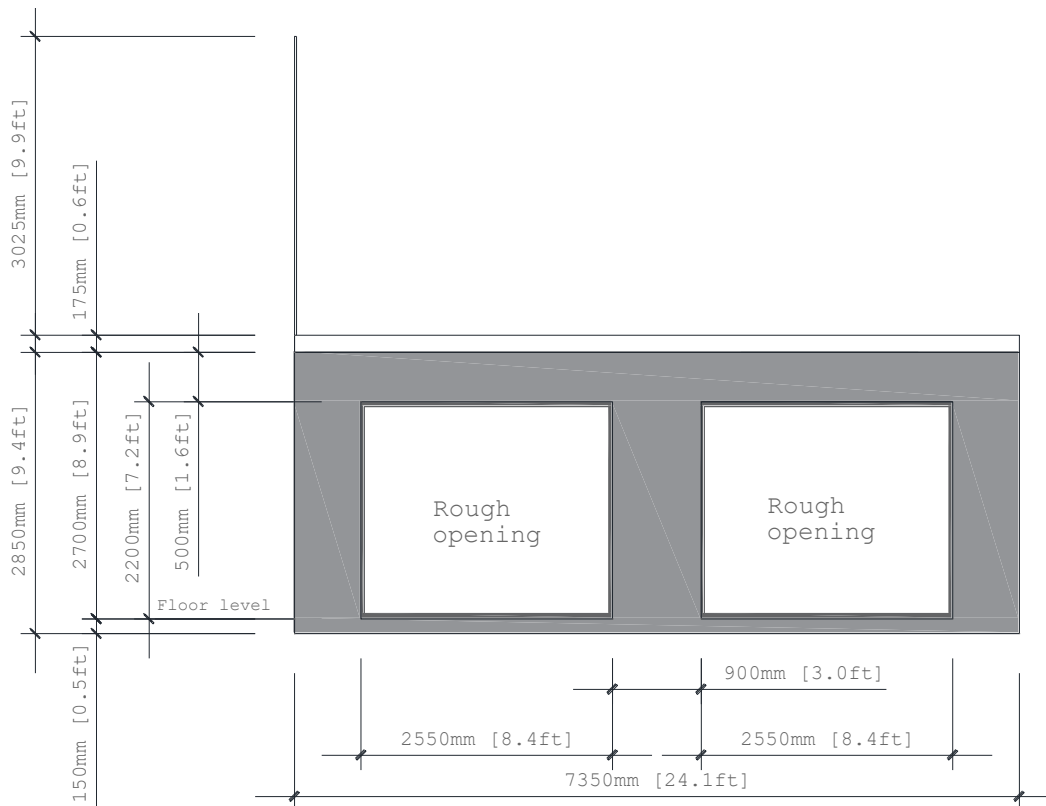


Figure B.3: Side view of the compartment of Test 4. After gypsum board installation, the rough openings were 2486 x 2104 mm.

Annex C – Statistical compartment design

A statistical approach has been utilized in the design of the test compartments, to ensure relevance for real scenarios. A review of the publicly available general arrangement, sections, elevation and façade drawings, of 513 compartments in residential buildings of at least four stories high, constructed within the past decade in the UK, has been conducted to provide a statistical overview of modern apartment design, and specifically:

- The distribution of floor areas, and
- The distribution of opening factors (O)¹¹.

It has been indicated previously, for example by Zelinka et al. (2018) or Su and Lougheed (2014), that typical non-fire-rated walls within enclosures provide limited impediment to the spread of fire. Therefore, when considering the floor area and perimeter of the apartments, the internal walls have been ignored.

In order to confirm that buildings utilizing mass timber are not being designed in any significantly different manner, a review of 185 compartments in large residential mass timber buildings¹², has also been conducted. The distributions established for the compartment area and opening factors can be found in Figure C.1 and Figure C.2, respectively. Based on multiple studies (e.g. Hox, 2015 and Frangi and Fontana, 2005), it is presumed that regular windows will break before the post-flashover phase of the fire, if the fire has enough oxygen supply to develop to flashover. Therefore, windows and glass doors are counted as openings during flashover fires.

Lastly, drawings from 31 compartments in mass timber office buildings were collected and the distribution of corresponding opening factors are displayed alongside the ones for residential compartments in Figure C.2. The opening factors of compartments in office buildings are in a range that is clearly higher than that of residential compartments.

¹¹ Definition of opening factor: $O = A_0\sqrt{H_0}/A_t$, where $A_0 = \sum A_i$ is the sum of all opening areas, A_t is the total enclosing area (incl openings), $H_0 = \sum (A_i h_i)/A_0$, and h_i is the height of each opening

¹² The Cube, Dalston Lane and Stadthaus buildings, all of which are in London

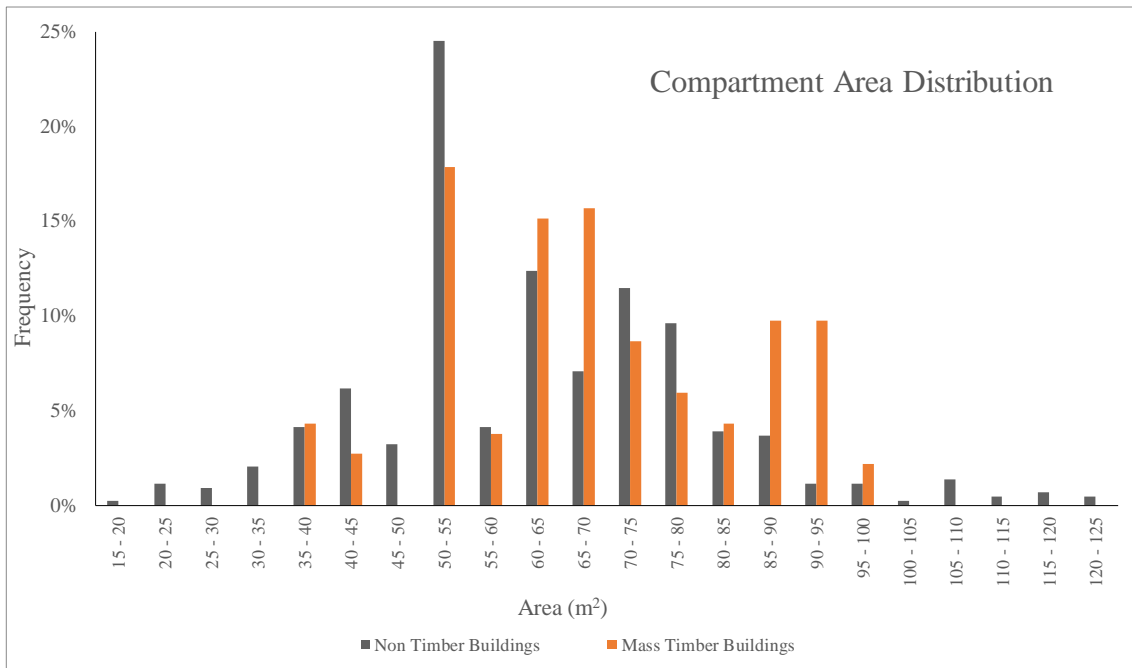


Figure C.1: Compartment area frequencies from residential buildings ($n=513$ for non-timber buildings and $n=185$ for mass timber buildings)

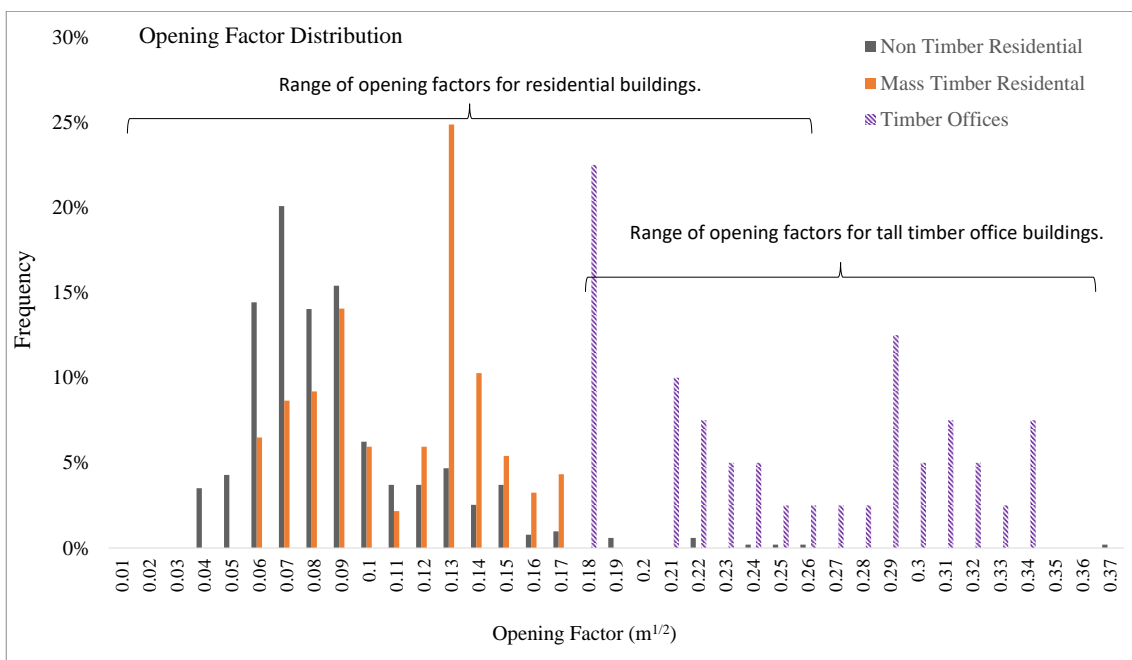


Figure C.2: Opening factor frequencies for residential and office buildings. Note that the statistical basis for the office buildings is only 31 compartments. The results are, therefore, used as an indication of a range rather than a distribution

In addition to these distributions, results from a survey of combustible contents and floor areas in Canadian multi-family dwellings (Bwalya et al. 2010) were utilized. By

combining the results and standard deviations, which are presented for different room types individually, the distribution of fuel load densities (FLD) of the total compartments are derived. These are normally distributed with an average FLD of 502 MJ/m² and a standard deviation of 92 MJ/m².

With the distributions of floor areas, opening factors and fuel loads in residential compartments we can estimate the damage, characterized by the final charring depth, from fires in timber buildings. The damage is assessed using the method specified by Brandon (2018) which is a conservative method to determine the char depth at the end of a decay phase, evaluated against most of the previously performed real compartment fire tests. The final charring depth after the cooling phase is modelled based on four characteristics of the compartment.

1. The opening factor
2. The moveable fuel load density
3. The area of exposed timber
4. The overall dimensions of the compartment

The model assumes that no charring occurs on the walls with unexposed timber. Thus, either they are incombustible or sufficiently protected by gypsum plaster boards or alike.

For the case shown here, we use the distribution of opening factors of all 698 residential compartments in Figure C.2 (bearing in mind that, generally, residential buildings of mass timber structures had larger openings than non-timber buildings, which in turn would generally result in less structural fire damage). The floor area and FLD distributions are taken from the results of (Bwalya et al. 2010). The analysis corresponds to a compartment structure of mass timber and a ceiling that is 100 % exposed and walls that are sufficiently protected from charring by gypsum boards. 200 000 simulations have been run, randomly choosing the floor area, FLD and Opening factor according to the probability distributions described above and calculating the total damages described by the final char depth of the exposed timber, Figure C.3.

The tests performed in this report were chosen to have the floor area of 49 m² which is the mean of floor areas of the 698 residential compartments reviewed here, and therefore realistic. The FLD should represent a high density of live fuel and is chosen to be 560 MJ/m² corresponding to the 74th percentile of the values reported by Bwalya et al. Both of these design values are indicated in Figure C.3.

Two different opening factors are decided to be used, one smaller opening factor characteristic for residential buildings and one larger opening factor representative for office buildings. The value for the residential buildings is chosen based on the estimated damage from the 200 000 simulations and represent the 85th percentile of damage to the exposed surfaces. This opening factor, 0.062 m^{1/2}, its corresponding final char depth and how it relates to the distributions from the simulations are shown in Table C.1. The design value is conservative for the residential buildings in general and in particular for the residential timber buildings in the survey above.

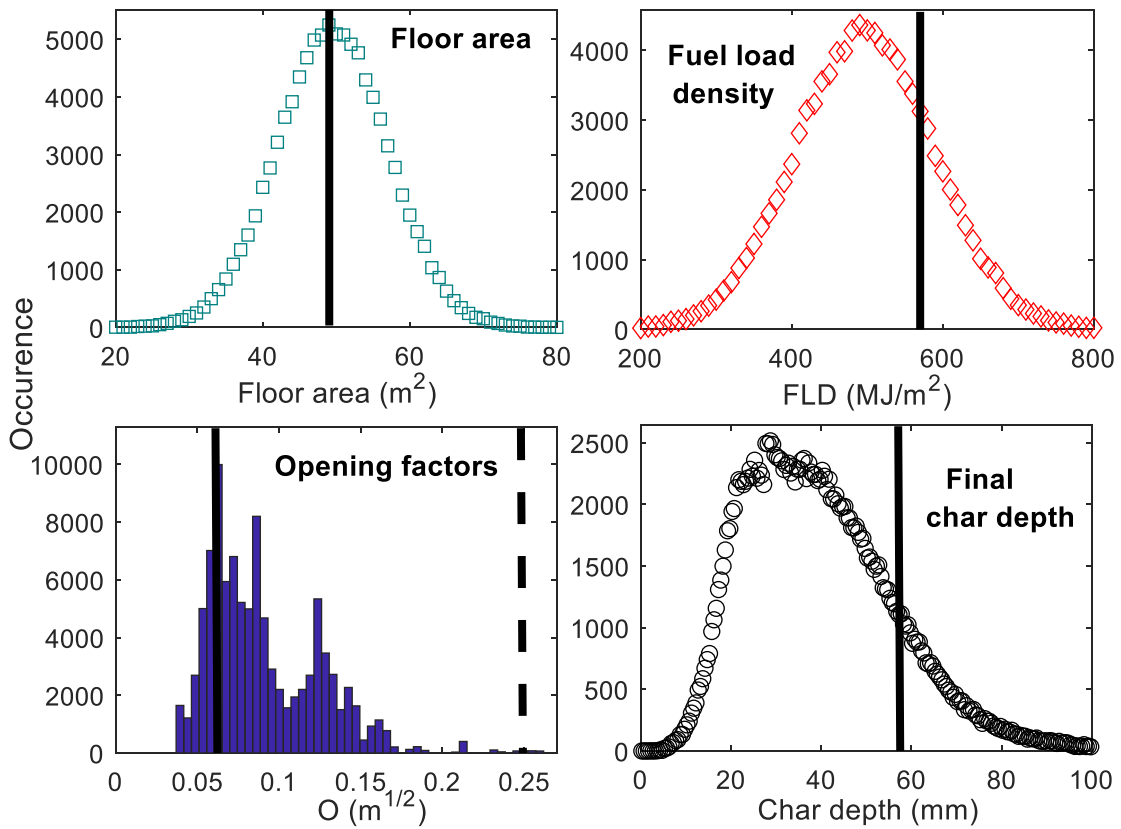


Figure C.3: Results of the probabilistic study using the distributions for floor area and FLD according to Bwalya et al. (2010) and Opening factor from the 698 residential compartments in the survey described above. The simulations are done assuming that the ceiling is 100 % exposed timber and all other surfaces protected. The solid lines represent the design values chosen for the residential buildings and the dashed line that of the office building.

Table C.1: The opening factor highlighted in Figure , corresponding final char depth predicted percentile of the damage (char depth) after the fire.

Opening factor (m ^{1/2})	Percentile of all residential buildings	Percentile of timber residential buildings	Final char depth (mm)*	Percentile of damages for all residential buildings
0.062	25	7	57.4	85

* Assuming 49 m², full ceiling exposed and 560 MJ/m².

All previous experience show that larger openings will result in less damage. The design for the tests with a larger opening includes $O = 0.250 \text{ m}^{1/2}$, which is right in the range of mass timber offices shown in Figure C.2 and where the damage is expected to be less than for the small opening tests.

Annex D – Fuel load

Annex C discusses a probabilistic approach, concluding that a fuel load density of 560 MJ/m² would result in statistically severe scenarios, which was based on a statistical survey by NRC Canada (Bwayla et al 2010). To limit uncertainties introduced by using the NRC Canada survey based on one set of calorific values and using another set of calorific values to determine the fuel load density, this study also uses calorific values published by the same Unit at NRC Canada, partly involving the same researchers. Table D.1 shows the calorific values of the NRC Canada study that are also used for this research.

Table D.1: Calorific values from Su et al. (2018a)

Material	Calorific Value
Hardboard	19.9 MJ/kg
White pine	19.2 MJ/kg
Douglas Fir	21.0 MJ/kg
Polyurethane foam	29.0 MJ/kg
Cotton	20.3 MJ/kg
Paper	17.0 MJ/kg

In the compartments of this study several objects contained wood cribs of Norway Spruce for which a calorific value of 17.8 MJ/kg is calculated. The floor and several objects consist of particle board for which for which a calorific value of 21.2 MJ/kg is calculated based on data from *Phyllis 2*, a database of material properties performed according to relevant international test standards for the physico-chemical composition of lignocellulosic biomass, micro- and macroalgae, various feedstocks for biogas production and biochar, made available by TNO (the Netherlands). Some small amount of polypropylene (polyester) was used in the compartment, for which 47.3 MJ/kg is calculated based on the *Phyllis 2* database. The weights of the object were individually determined and the total weight of the fuel on the floor was checked using load cell measurements before and after installation of the fuel. Table D.2 shows the calculated calorific value per object. This excludes the energy of the exposed gypsum board paper, which is estimated to be between 2 and 5 MJ/m² depending on the area of gypsum board protection in each test.

Table D.2: Calculated moveable fuel load density per test

	Brand	QTY	Material 1	(kg)	Material 2	(kg)	Material 3	(kg)	Total cal. value
Hemnes sofa bed	Ikea	2	Particle board	85	Spruce	9.8	Hardboard	8.2	4281
Friheten sofa bed	Ikea	1	Particle board	63	PU foam	40	Cotton	3	2557
Kleppstad wardrobe	Ikea	2	Particle board	74.1	Hardboard	4.8	none		3333
Göran table	Ikea	2	Particle board	8	Hardboard	2.5	none		439
Lack coffee table	Ikea	1	Particle board	18	none		none		382
Stefan chair	Ikea	8	White pine	4	none		none		614
Gersby bookshelves	Ikea	6	Particle board	8	Hardboard	2.5	none		1316
Sköldbädd cushions	Ikea	12	PU foam	0.37	none		none		129
Pärkla storage bags	Ikea	2	Polypropylene	0.14	none		none		13
Hemnes mattress	Ikea	4	PU foam	6.7	none		none		777
Fullkomlig Table cloth	Ikea	2	Polypropylene	0.57	none		none		54
Particle board floor		1	Particle board	289	none		none		6127
Wood cribs in total	Södra	1	Spruce	380	none		none		6802
Paper in bin		1	Paper	1	none		none		17
Total fuel load (MJ)									26840
Fuel load density (MJ/m²)									560

The wood cribs were positioned in storage spaces to correspond to a realistic distribution of fuel throughout the compartment. In addition, a wood crib was installed under the dinner table to more closely resemble a heavier table and set of chairs. Table D.3 indicates mass of the wood cribs at the locations indicated with the letters A to J in Figure 2 and Figure 3 of the main text.

Table D.3: Mass of spruce wood crib at locations indicated in Figure 2 and Figure 3

Location	Type	Mass of wood crib (kg)
A	Hemnes sofa bed	19.4
B	Lack coffee table	23.3
C	Gersby bookshelves (4x)	103.6
E1	Kleppstad wardrobe at back wall	36.3
E2	Kleppstad wardrobe towards center	41.5
F	Hemnes sofa bed	20.7
G	Göran dinner tables	66.1
H	Gersby bookshelf	25.9
I	Gersby bookshelf	25.9
J	Pärkla storage bags	17.3
Total mass of wood cribs		380.0

Annex E – Mass loss measurements and heat release rate calculations

Mass loss rates of the floor and the mass loss of the structure were determined using load cells that were positioned under a steel frame that bared the floor or a steel frame that bared the remaining structure (walls, ceiling and external façade). The initial mass of the bare floor was determined before every test using load cell measurements. The mass of the movable fuel load was determined from load cell measurements before and after installation of the fuel. After each fire test, the material left on the floor was limited to some metallic parts of the furniture and some equipment, weighing 36 kg (79 lb) in total. The combustible material left on the floor is considered negligible and the mass of the floor after the test was determined from load cell measurements at the end of the test.

As the bare mass of the floor was determined before and after the test, the total mass loss, due to drying of the floor (175 mm (20.7 inch) CLT, 20 mm (2.4 inch) Stone Wool and 100 mm (11.8 inch) light weight concrete on top) could be determined. As the mass loss of the floor was relatively small, for the calculations of the mass loss rate, it was considered reasonable to assume that the ratio between mass loss rate of water in the floor and mass loss rate of the movable fuel was constant. By subtracting the mass loss rate of the floor structure from the total mass loss rate, the mass loss rate of the fuel load on the floor was determined.

The structure (walls, ceiling and glulam members) was weighed during the tests using load cells under a separate frame. The mass loss of the CLT and glulam of the structure is determined by subtracting an estimated mass loss of gypsum and the mass loss of the facade extension from the measured mass loss. The total mass loss of the lightweight concrete façade extension was determined by weighing the total structure before the façade extension was installed on top of the compartment before the test and after removing it. The mass loss of the façade extension was relatively small in comparison with the total mass loss (approximately 3%). Given the small overall influence on the total mass loss, for calculations of the mass loss rates of the combustible structure, it was considered reasonable to assume that the ratio between mass loss rate of the total structure and mass loss rate of the façade extension was constant. The mass loss rate of gypsum board protection was determined using temperature measurements and a heat transfer model described previously by Brandon and Andersson (2018, Annex A & B). The heat transfer model was used to estimate the temperatures in a large amount of locations in the gypsum board cross section. The calculation included the following steps:

1. Finite element calculation of the temperatures throughout the gypsum boards, using the average plate thermometer temperature curve measured during the test as boundary conditions for both radiation temperature and gas temperature. The gypsum thermal properties, convection coefficient and emissivity used are given by Brandon and Andersson (2018).
2. Comparison with measured temperature to assess the accuracy of the calculation.
3. Use Thermo Gravimetric Analysis (Figure 5) of the tested gypsum board to determine the mass loss throughout the gypsum board.

Step 2 mentioned above is a crucial step to assess the accuracy of the method. In order to have an indication of the accuracy, the total density loss corresponding to the predicted and measured temperatures of Figure E.1 was calculated using the thermogravimetric analysis results of the gypsum shown in Figure 5. The difference between the total mass loss determined from measurements and from predictions is ranging between 0 % and 11 % percent. This error translates in an error of approximately 0 to 1.3 % for the calculation of the mass loss of the combustible structure in Test 2 to 5.

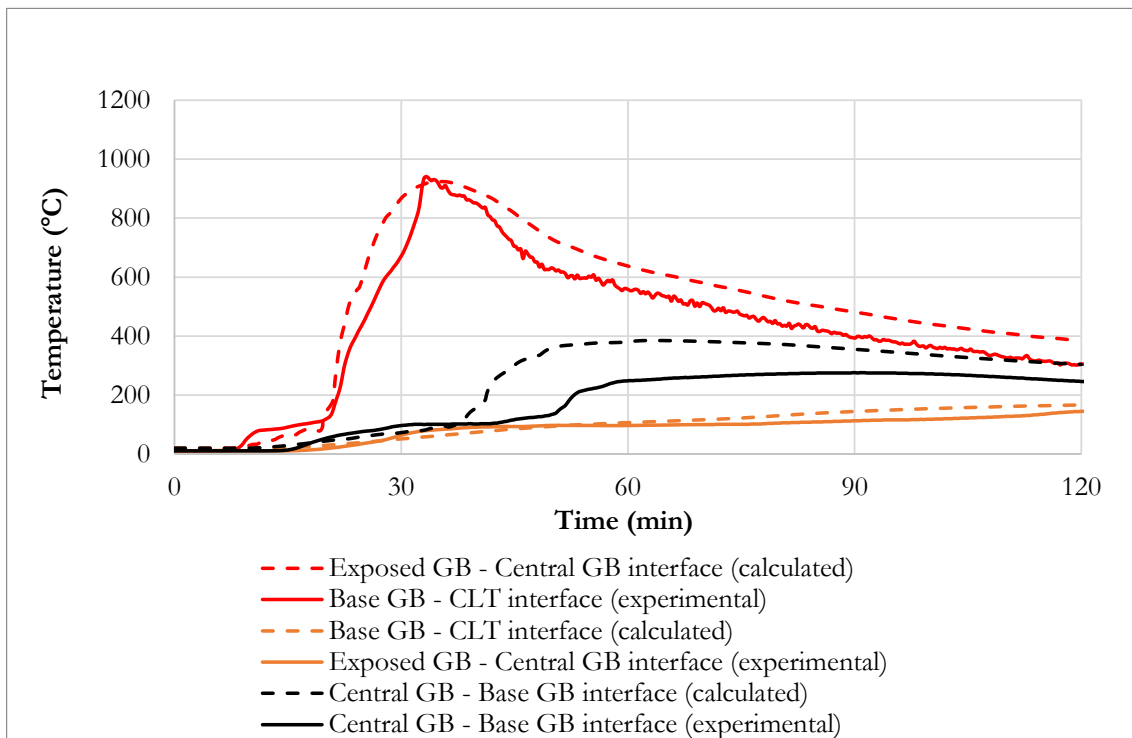


Figure E.1: Measured and calculated temperatures at interfaces between gypsum boards (Example for Test 3).

Figure E.2 shows the mass loss rate of the floor and the mass loss rate of the movable fuel of Test 2. The small difference between the two curves is explained by the relatively small mass loss due to drying of the floor during Test 2, as most water presumably evaporated during Test 1. In the figure, three instances are indicated in which a fire fighter left the compartment. This happened at the beginning of every test and during Test 2 several times at around 145 and 160 minutes after ignition to fix a test-setup related problem¹³. For the calculation of the heat release rate the mass loss rate jumps caused by persons leaving the floor are disregarded.

Figure E.3 shows the mass loss rate of the structure excluding the floor and the fuel load on the floor together with the mass loss of the façade and the estimated mass loss of gypsum boards. The mass loss of the structural timber is determined by subtracting the mass loss of the gypsum boards and façade from the measured mass loss.

¹³ During Test 2, the fire fighter responsible for safety during the test added wet stone wool insulation in a gap between the floor and the right wall to avoid downward fire spread. It should be noted, that the floor and the walls were not mechanically connected to allow separate measurements of the mass of the floor and the mass of the rest of the structure. The detail is therefore not representative for the design of real buildings.

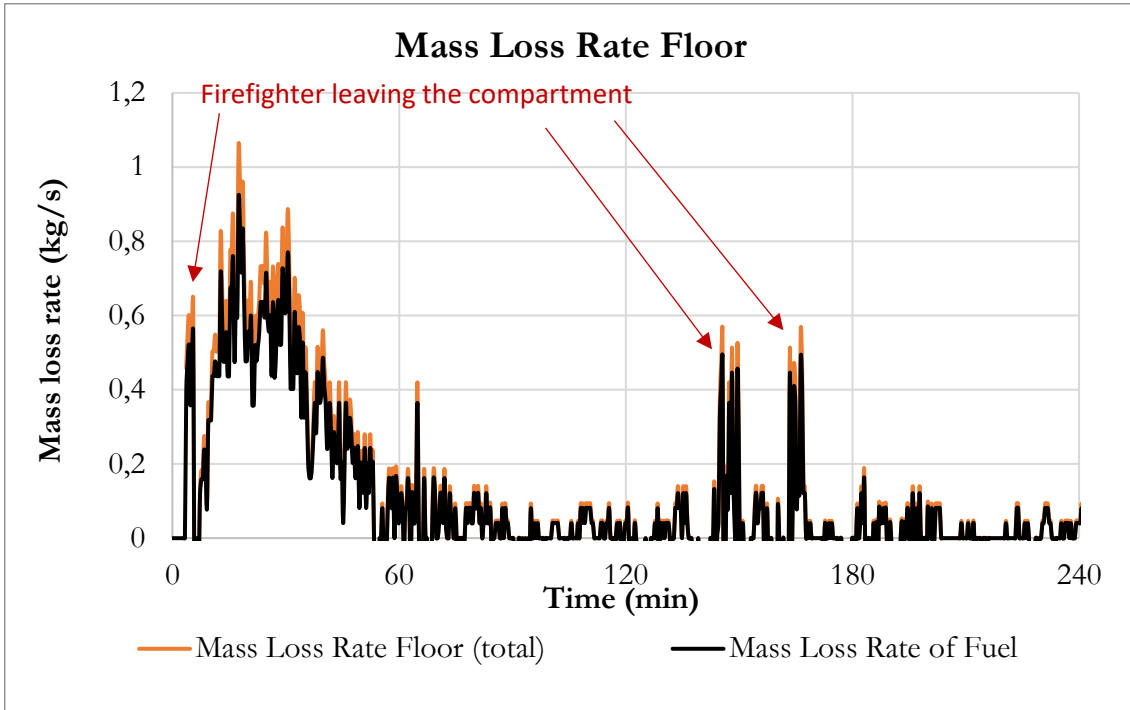


Figure E.2: Mass loss rate of floor and mass loss rate of fuel of Test 2

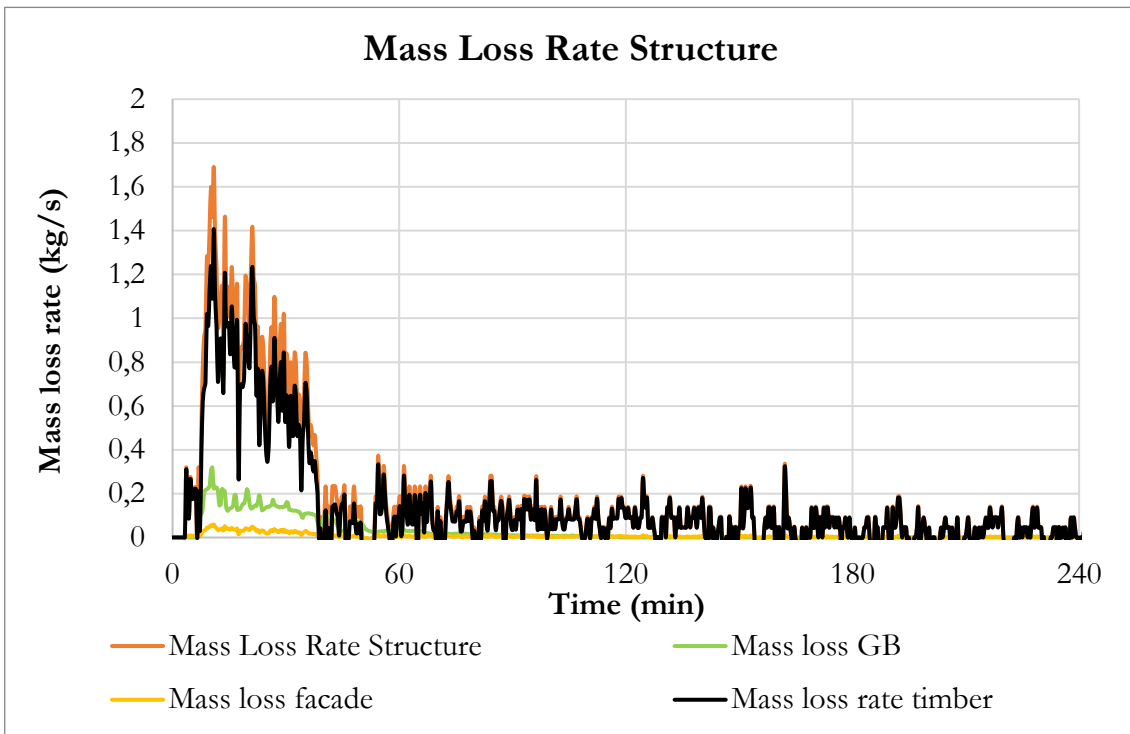


Figure E.3: Mass loss rate of the structure (excluding floor), façade, gypsum boards and timber surfaces for Test 2.

From the mass loss rates the heat release rates are estimated using the calorific values summarized in Annex D – Fuel load (17.8 MJ/kg for the structural timber and 20.5 MJ/kg for the moveable fuel load). The heat release calculation assumes that all combustible volatiles that are released in the fire will combust. Figure E.4 shows the heat release rates of Test 2. It was found that the floor and the structure clearly interacted in

multiple tests, which is evidenced by simultaneous extreme values of the mass loss/mass gain rate in opposite direction. The total mass of both is however not affected by the pressure interaction between the floor and the ceiling. Therefore, only the total heat release rate is plotted in the in the main text of the report.

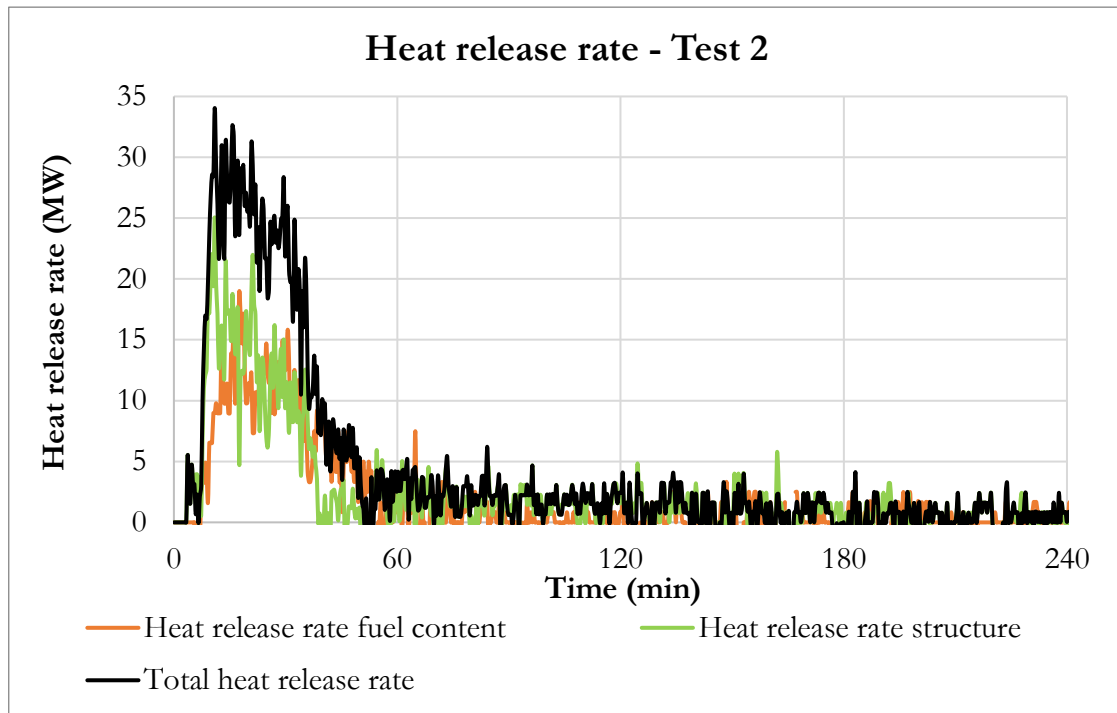


Figure E.4: Heat release rate Test 2

Annex F – Maximum Flame Extensions

This section contains still from videos illustrating the magnitude of the flame extensions for each test.

F.1 Test 1



Figure F.1 Test 1 15min 28s after ignition



Figure F.2 Test 1 16 min 52s after ignition

F.2 Test 2



Figure F.3 Test 2 15 min 39s after ignition



Figure F.4 Test 2 23 min 39s after ignition

F.3 Test 3



Figure F.5 Test 3 17min 45s after ignition



Figure F.6 Test 3 19min 22s after ignition

F.4 Test 4



Figure F.7 Test 4 17 min after ignition

F.5 Test 5



Figure F.8 Test 5 19min 34s after ignition



Figure F.9 Test 5 23min 30s

Annex G – Beam Post-test Cross Sections



Figure G.1: Post-test beam cross section, **Test 1.**

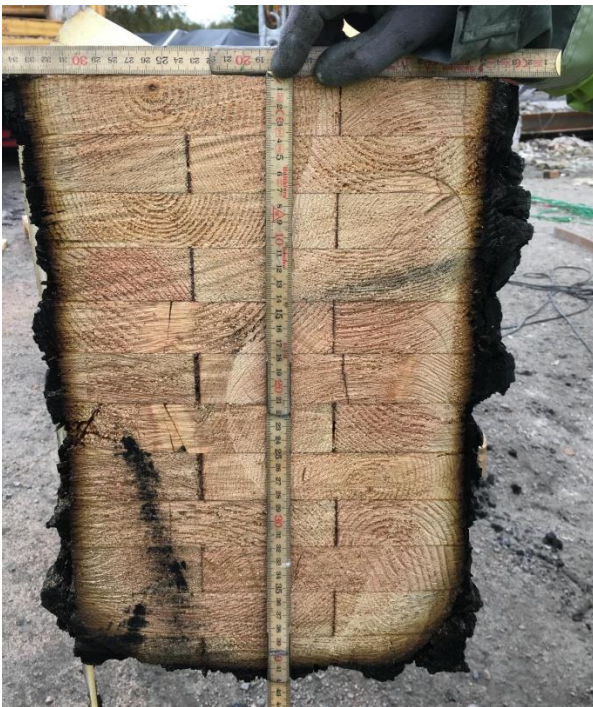


Figure G.2: Post-test beam cross section, **Test 2.**



Figure G.3: Post-test beam cross section, Test 3.



Figure G.4: Post-test beam cross section, Test 5.

Annex H – Interior thermocouple trees

H.1 Test 1

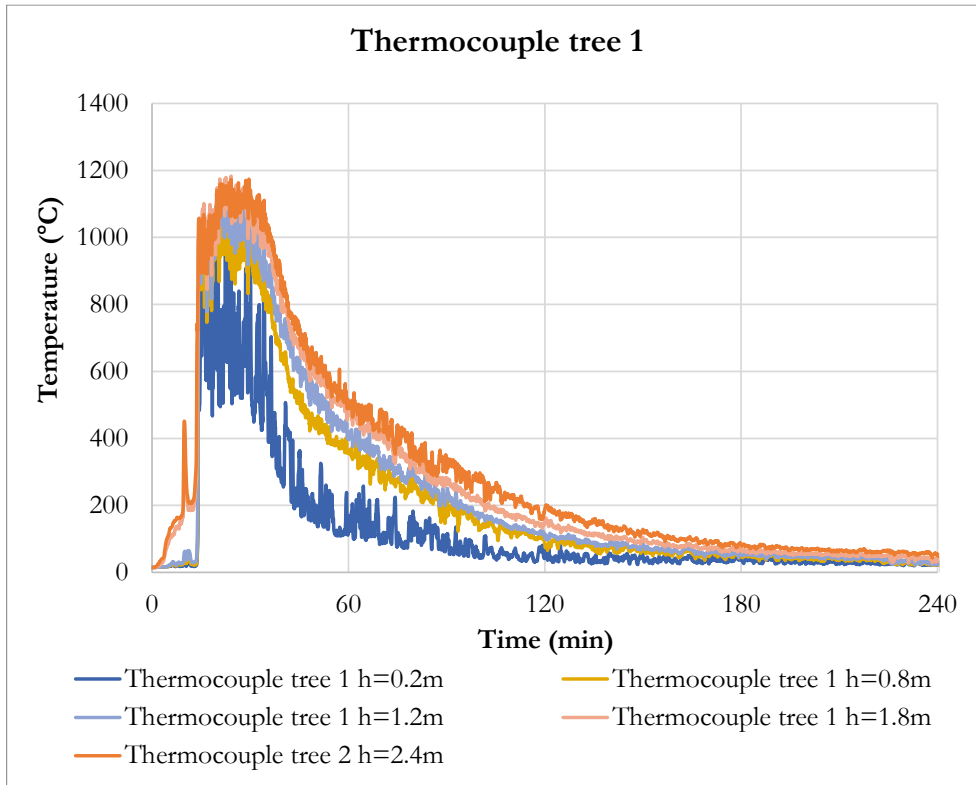


Figure H.1: Test 1 Thermocouple tree 1

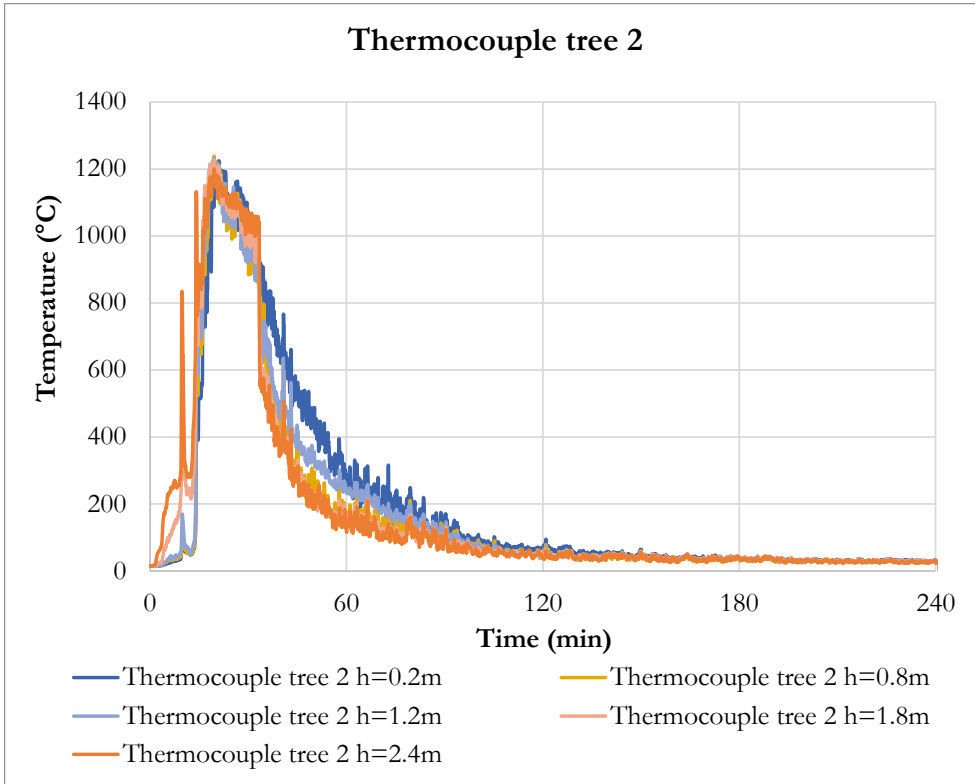


Figure H.2: Test 1 Thermocouple tree 2 (fell at 33 min)

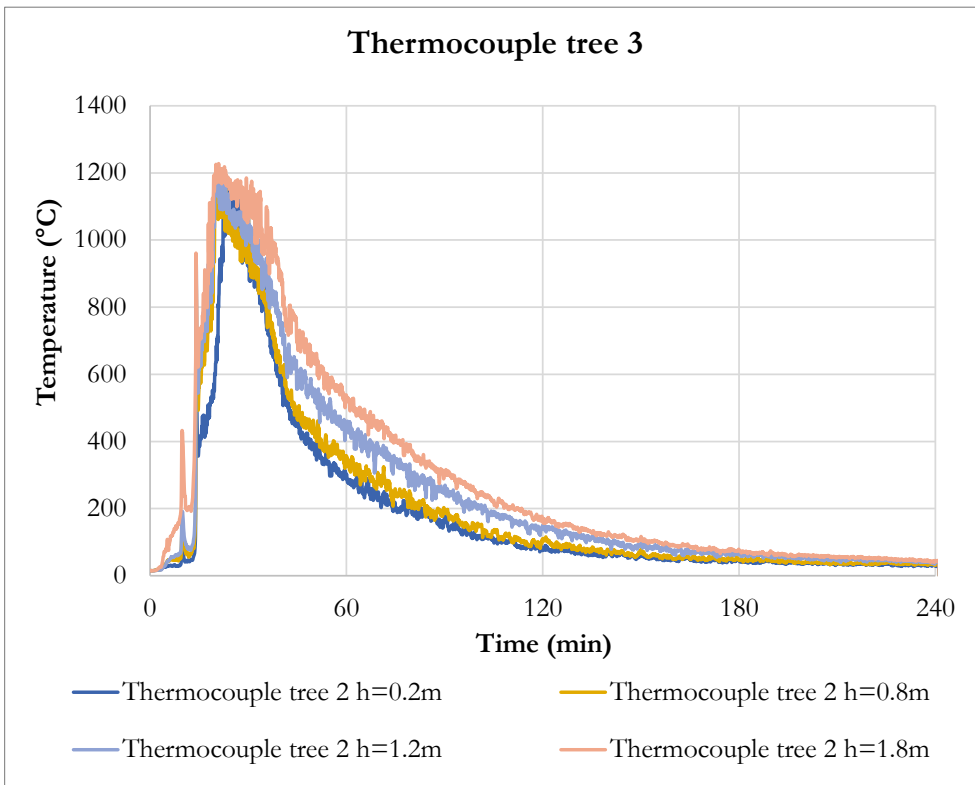


Figure H.3: Test 1 Thermocouple tree 3

H.2 Test 2

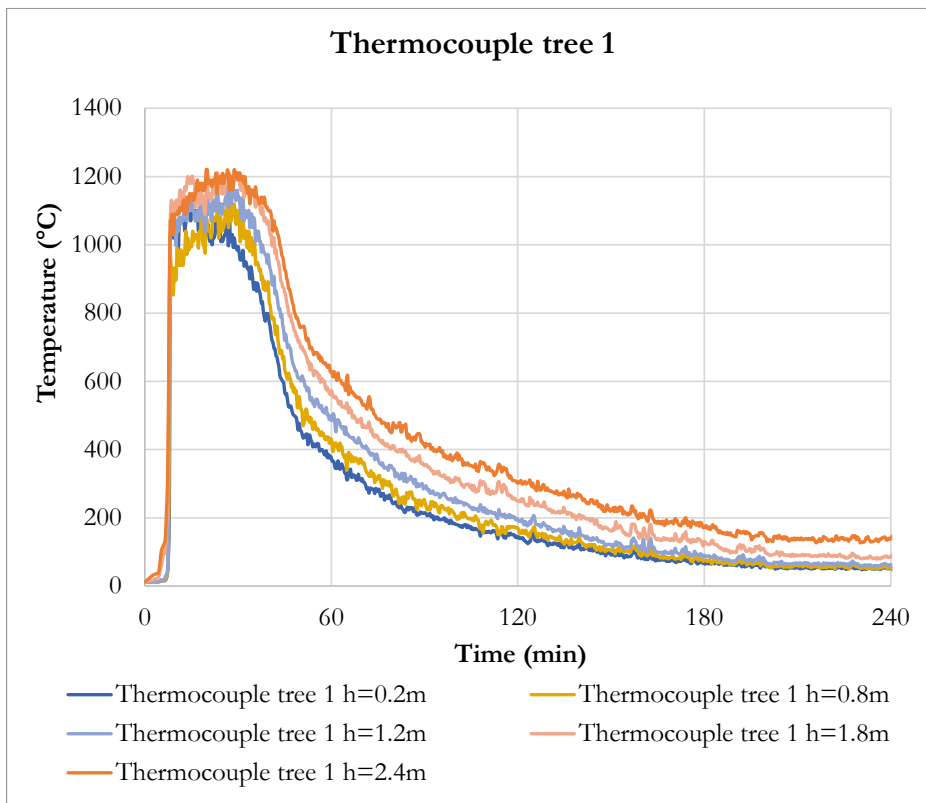


Figure H.4: Test 2 Thermocouple tree 1

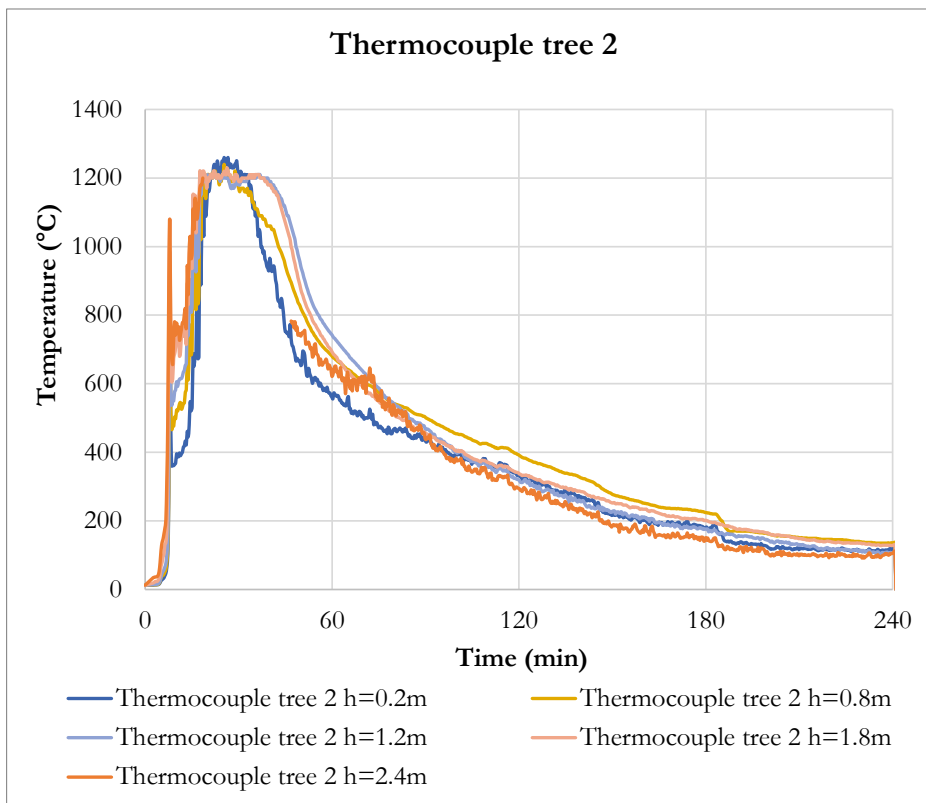


Figure H.5: Test 2 Thermocouple tree 2 (fell at 40 min)

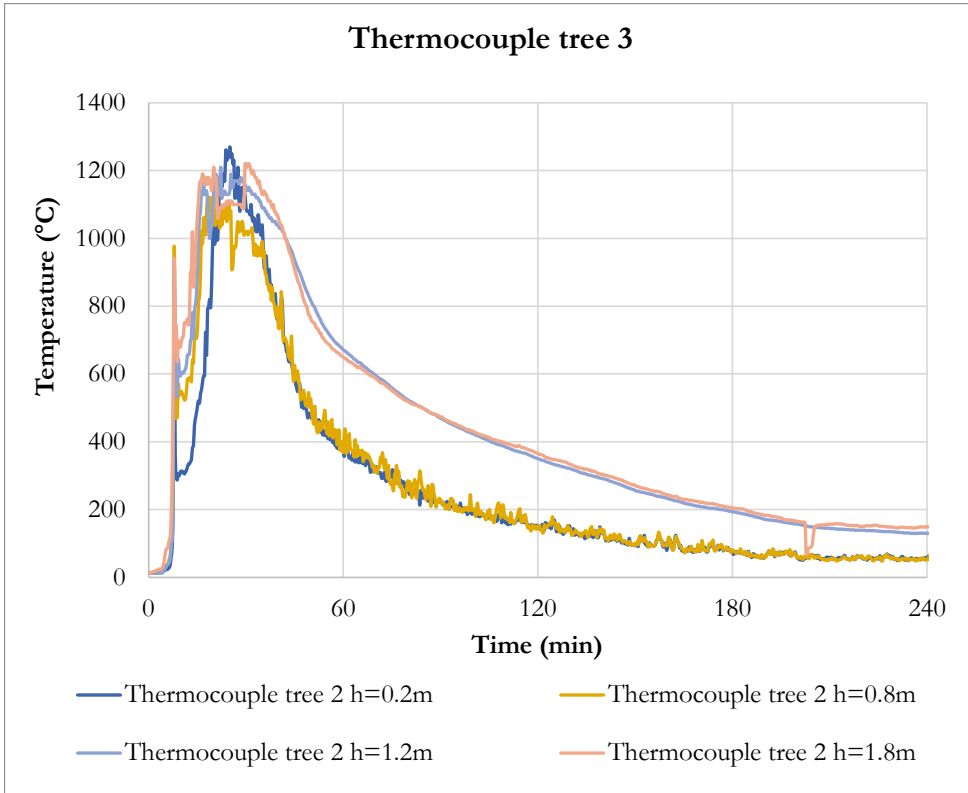


Figure H.6: Test 2 Thermocouple tree 3

H.3 Test 3

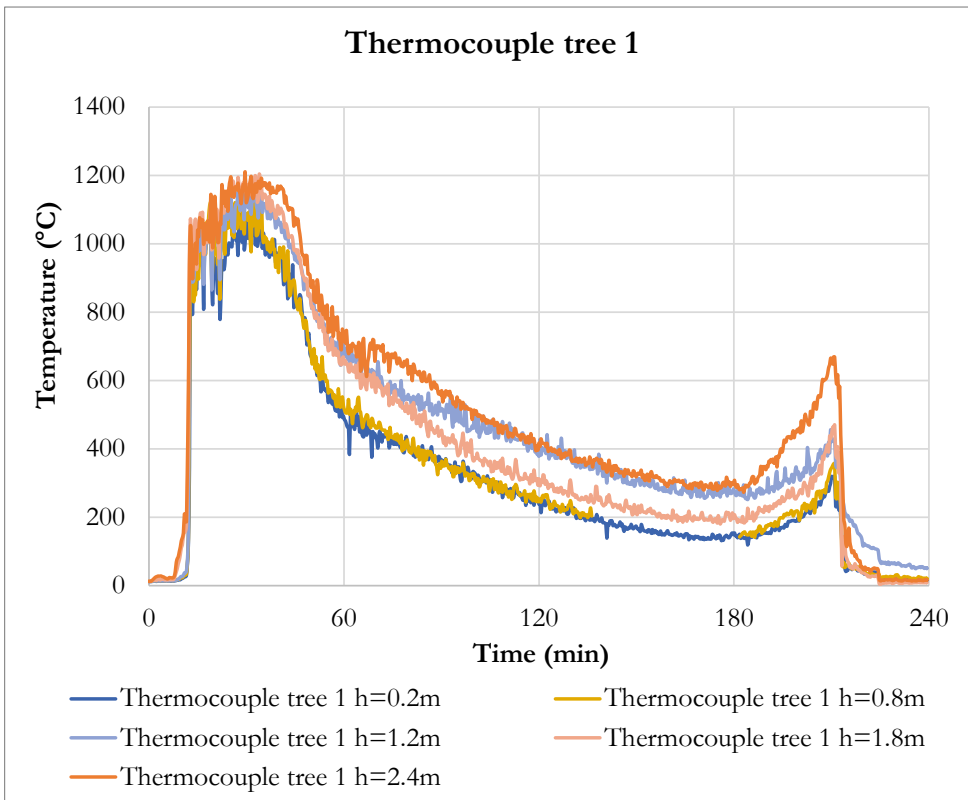


Figure H.7: Test 3 Thermocouple tree 1

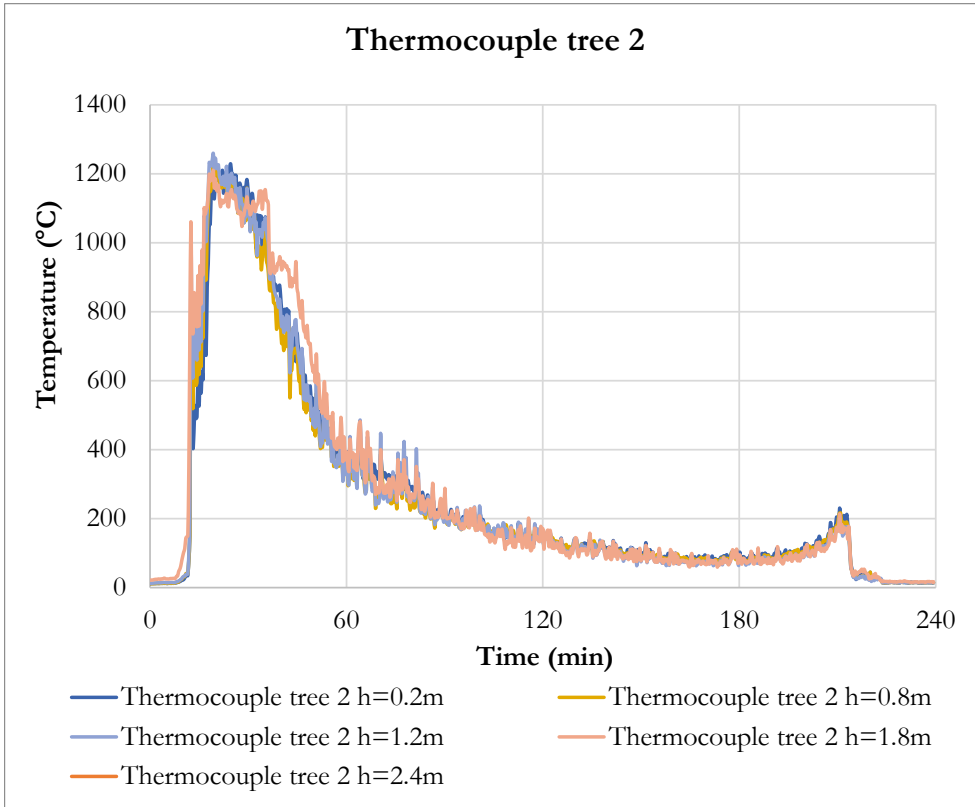


Figure H.8: Test 3 Thermocouple tree 2 (malfunctioning at h=2.4m, fell at 30 min)

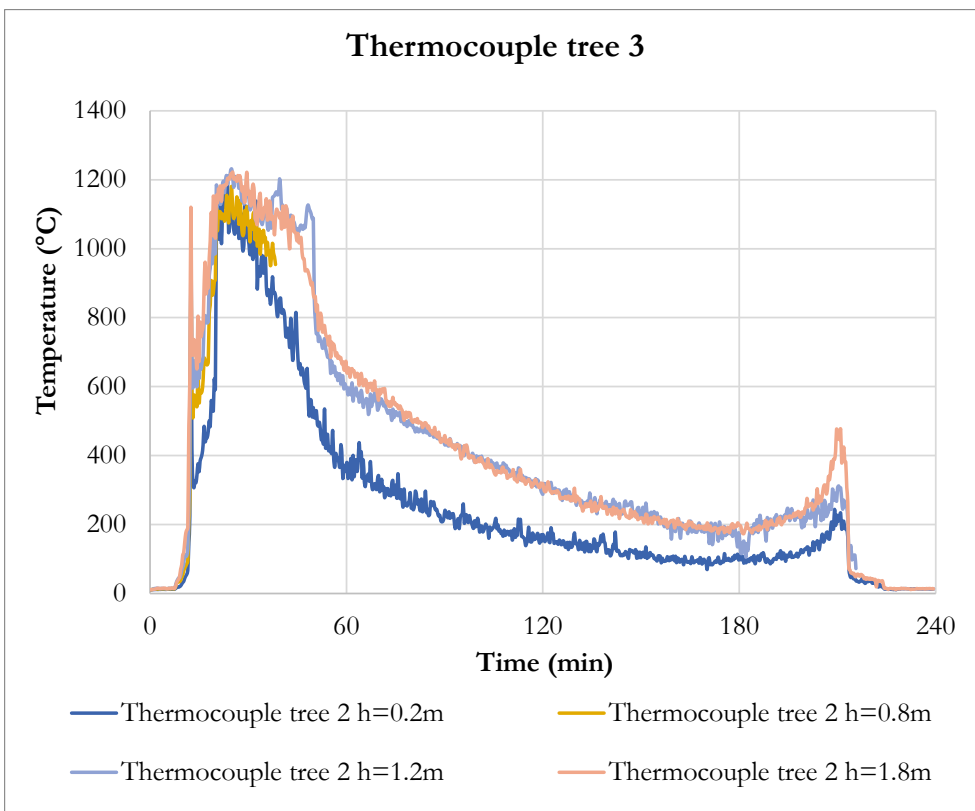


Figure H.9: Test 3 Thermocouple tree 3

H.4 Test 4

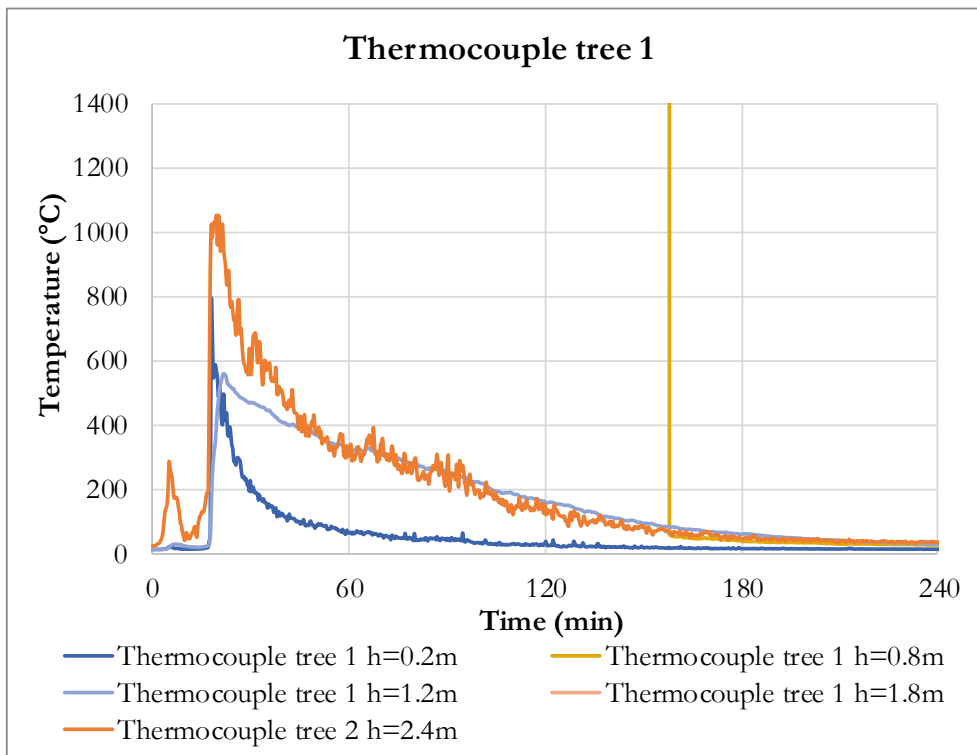


Figure H.10: Test 4 Thermocouple tree 1 (malfunctioning at h=0.8m)

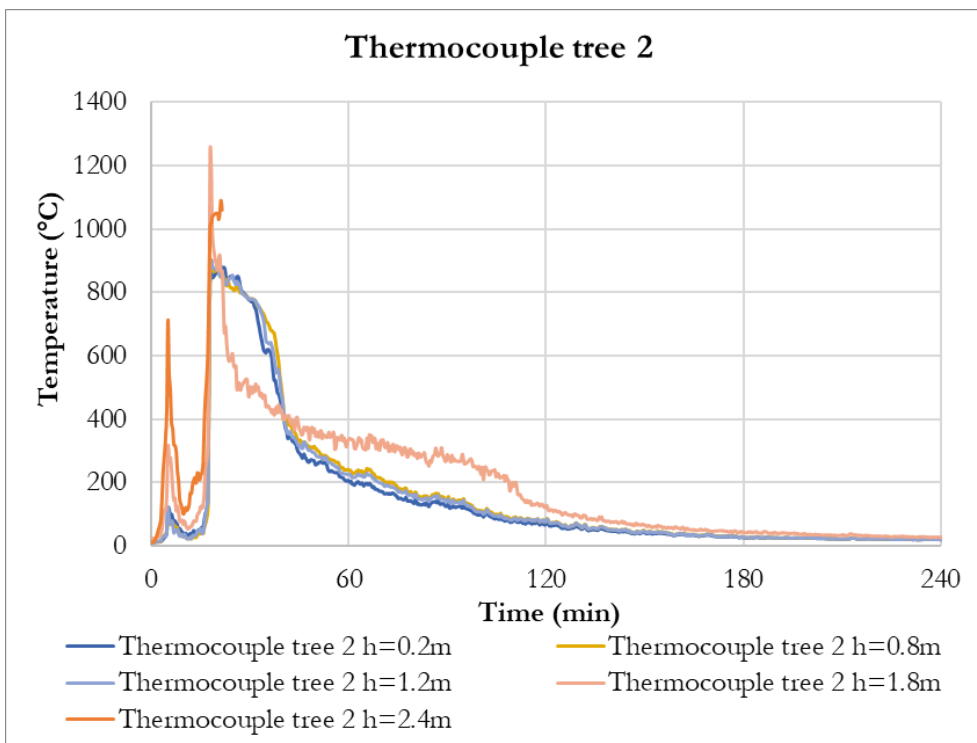


Figure H.11: Test 4 Thermocouple tree 2

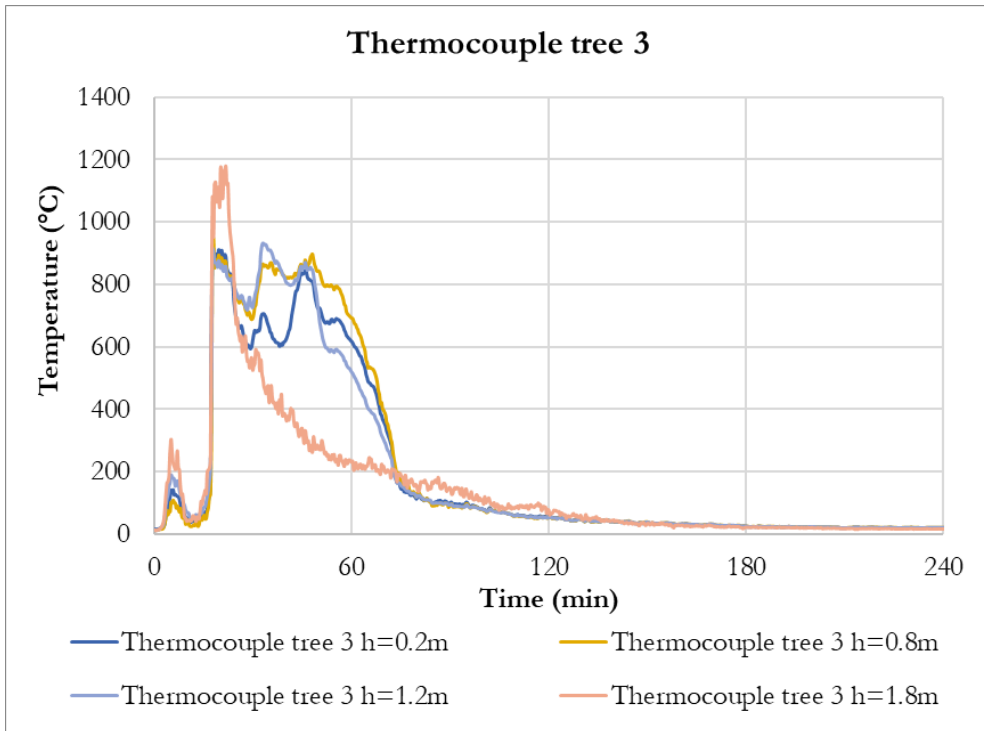


Figure H.12: Test 4 Thermocouple tree 3

H.5 Test 5

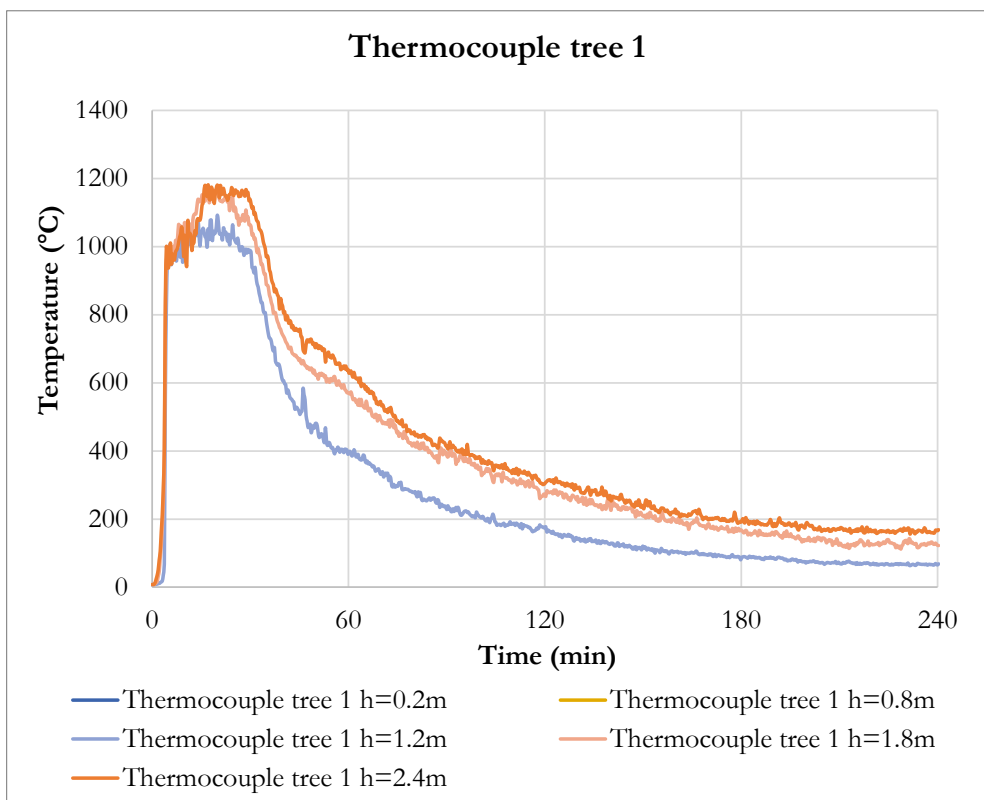


Figure H.13: Test 5 Thermocouple tree 1 (malfunctioning at h=0.2, 0.8m)

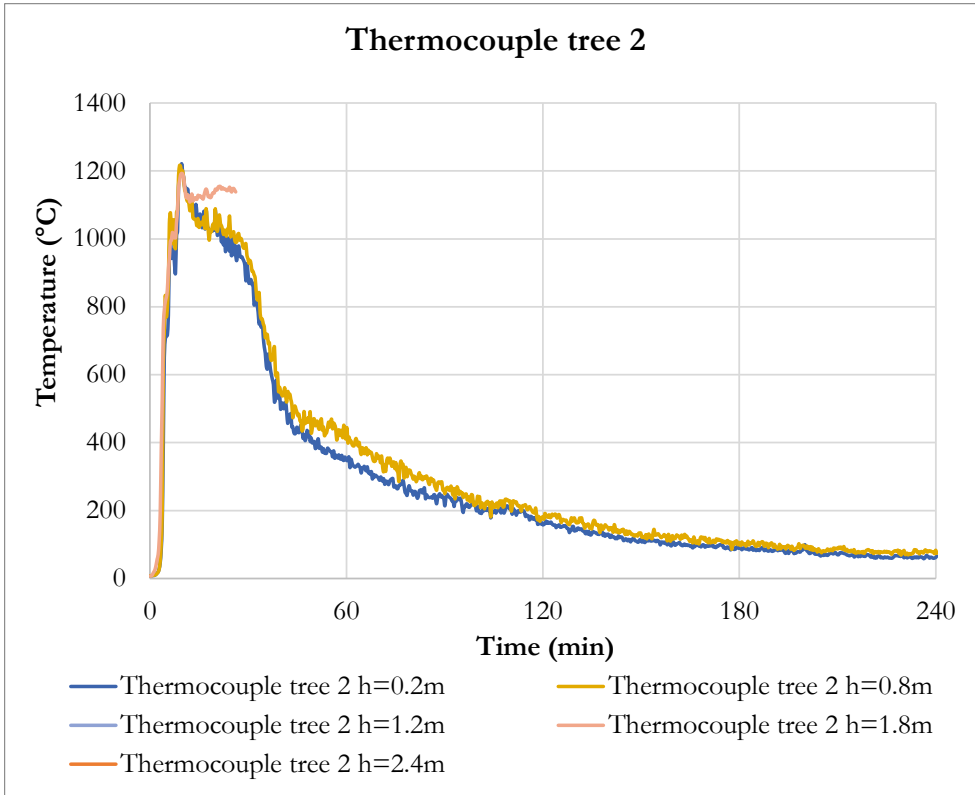


Figure H.14: Test 5 Thermocouple tree 2 (malfunctioning at h=1.2, 1.8 & 2.4m)

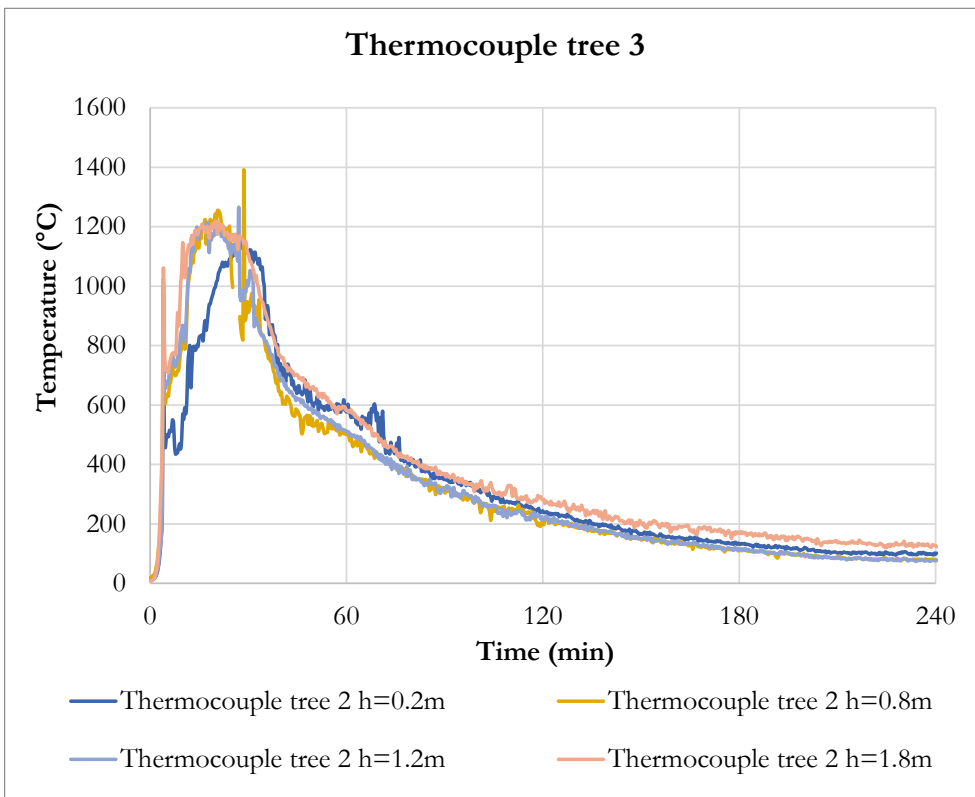


Figure H.15: Test 5 Thermocouple tree 3

Annex I – Thermocouples at opening

This annex contains the temperature-time histories for the thermocouple trees placed in the front openings for each test. The legend for each graph shows the height of the thermocouple above the floor level in mm.

I.1 Test 1

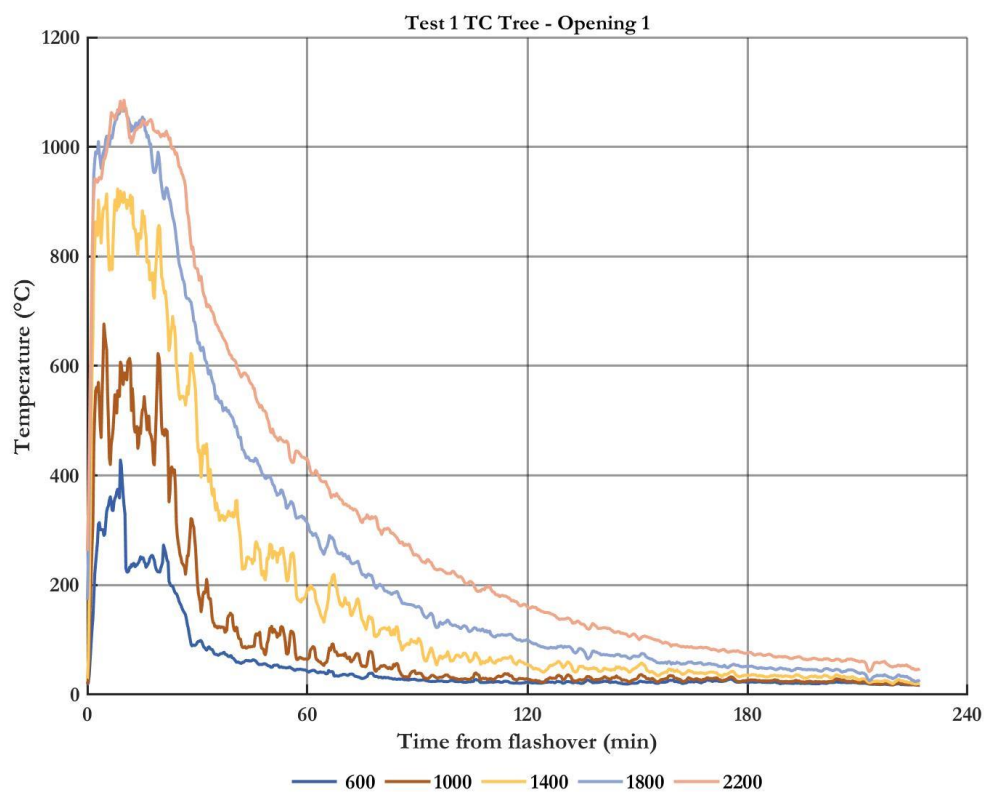


Figure I.1: Test 1 Thermocouple tree in opening 1 (left opening). Legend shows thermocouple height above floor level in mm.

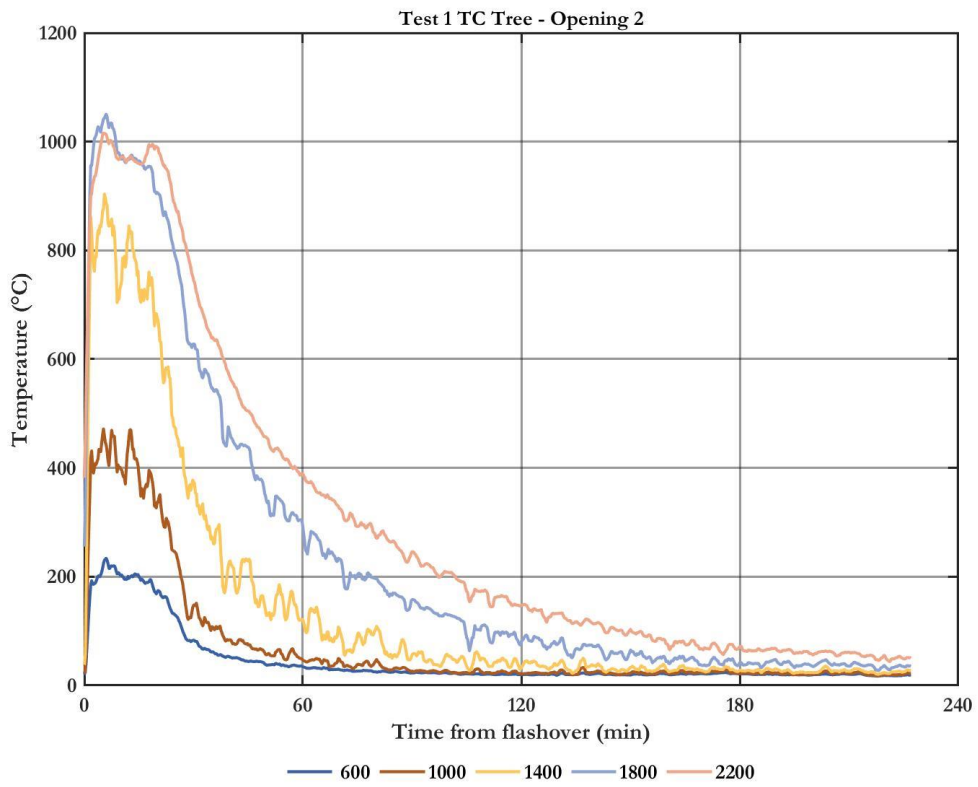


Figure I.2: Test 1 Thermocouple tree in opening 2 (right opening). Legend shows thermocouple height above floor level in mm.

I.2 Test 2

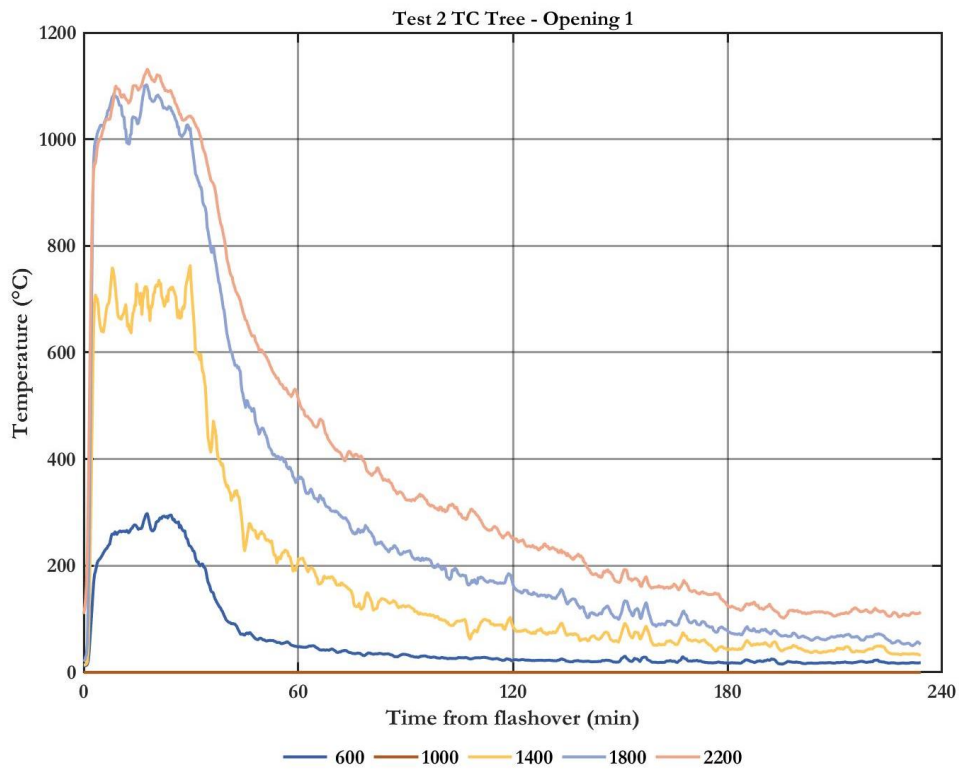


Figure I.3: Test 2 Thermocouple tree in opening 1 (left opening). Legend shows thermocouple height above floor level in mm.

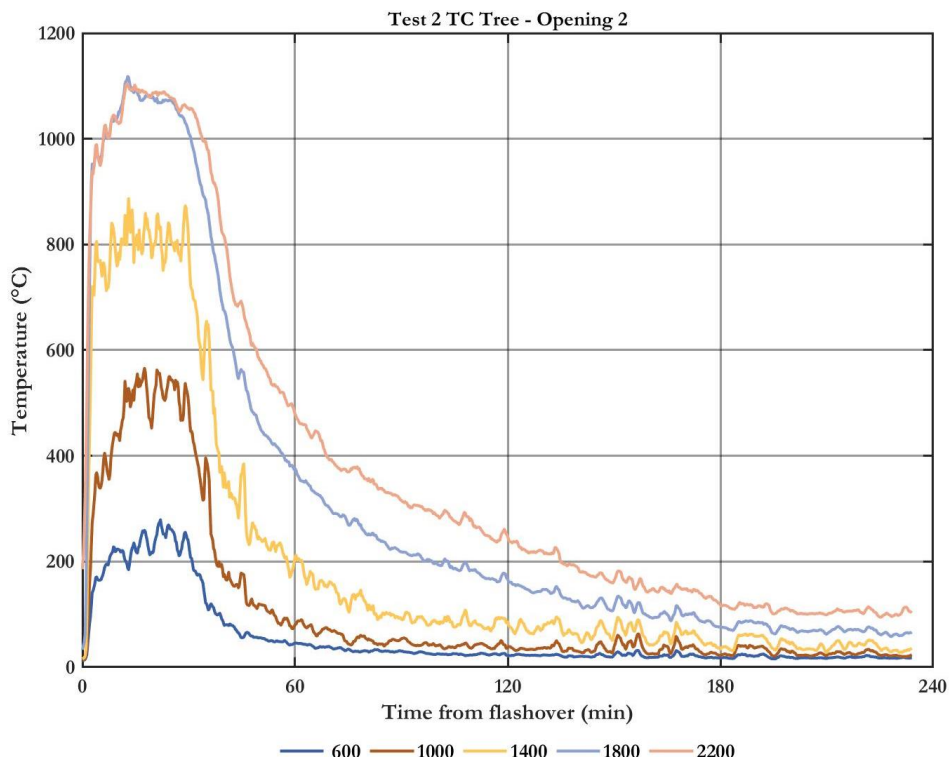


Figure I.4: Test 2 Thermocouple tree in opening 2 (right opening). Legend shows thermocouple height above floor level in mm.

I.3 Test 3

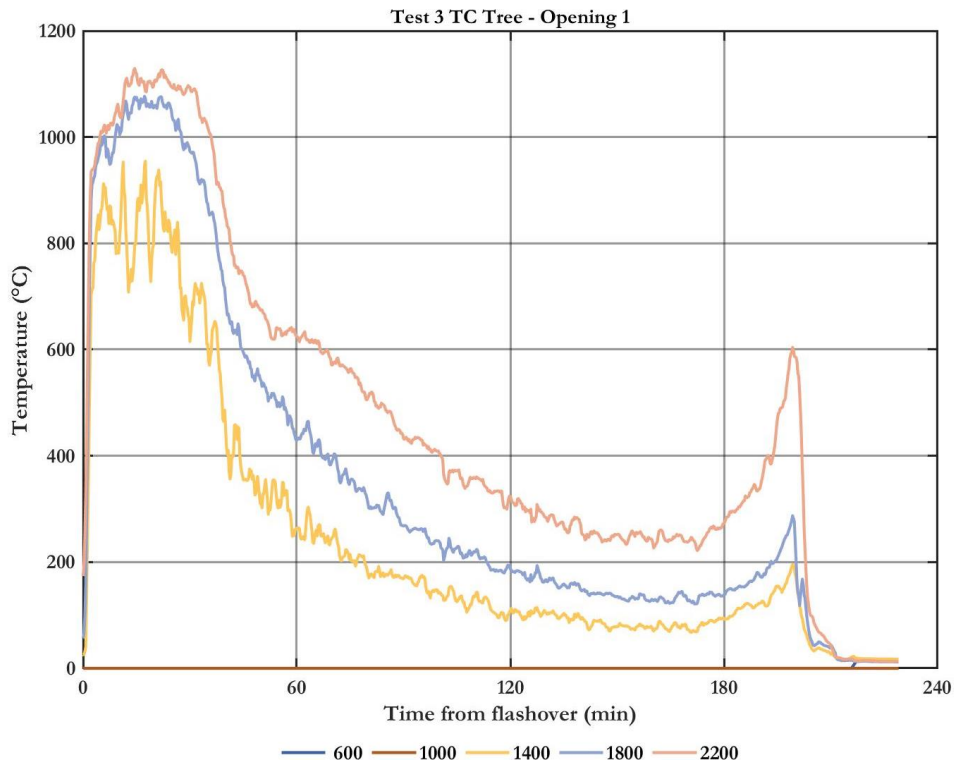


Figure I.5: Test 3 Thermocouple tree in opening 1 (left opening). Legend shows thermocouple height above floor level in mm.

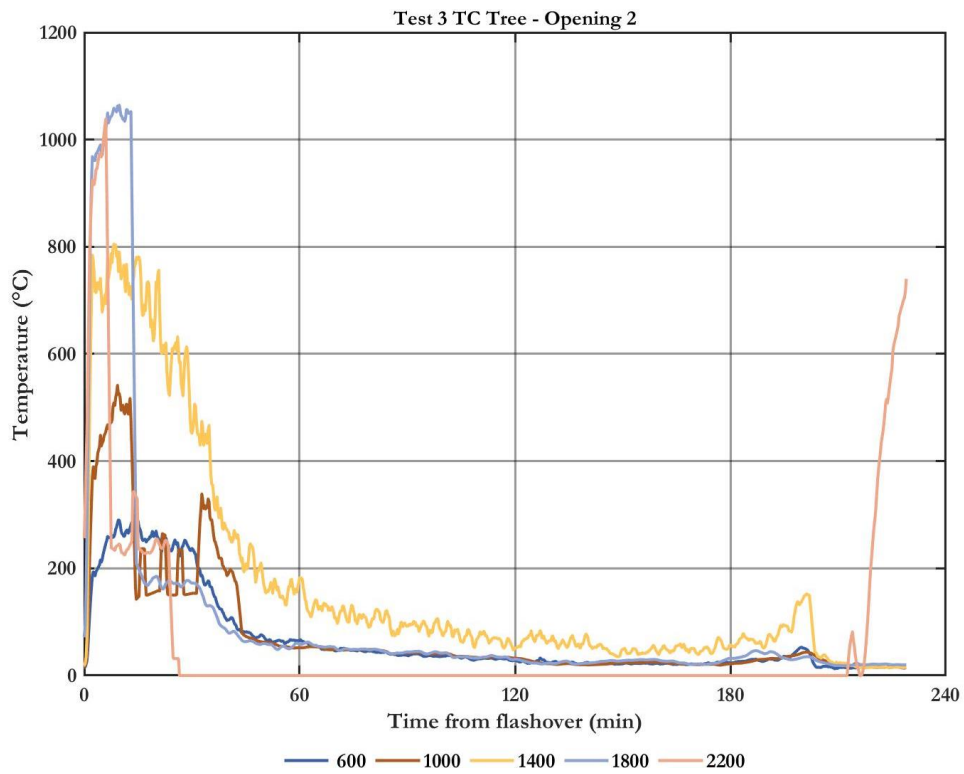


Figure I.6: Test 3 Thermocouple tree in opening 2 (right opening). Legend shows thermocouple height above floor level in mm.

I.4 Test 4

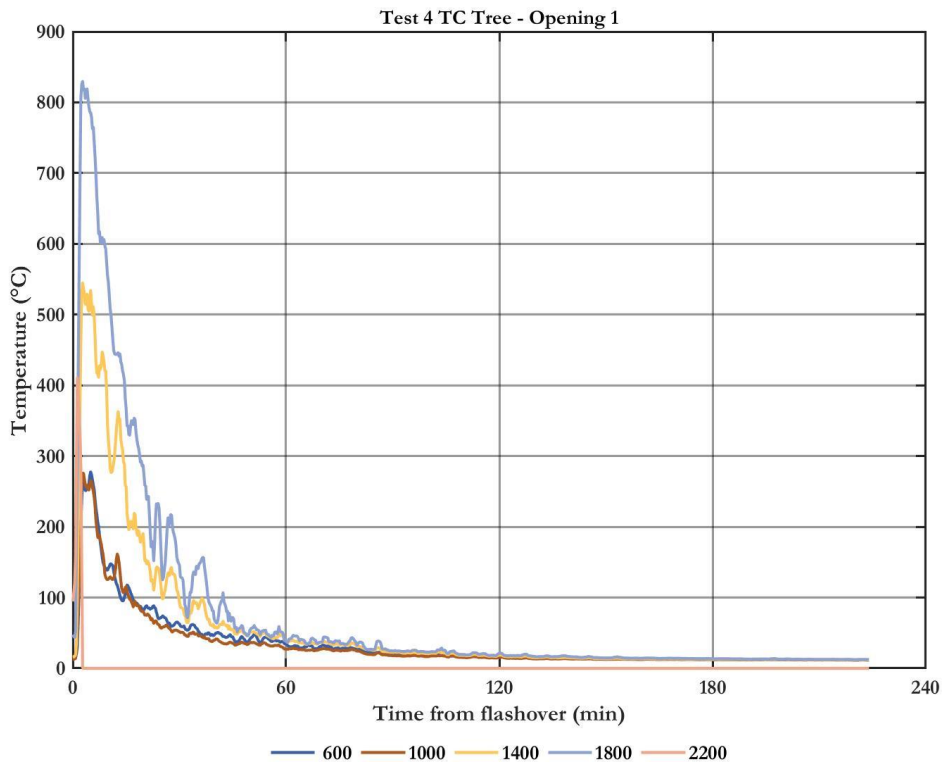


Figure I.7: Test 4 Thermocouple tree in opening 1 (left opening). Legend shows thermocouple height above floor level in mm.

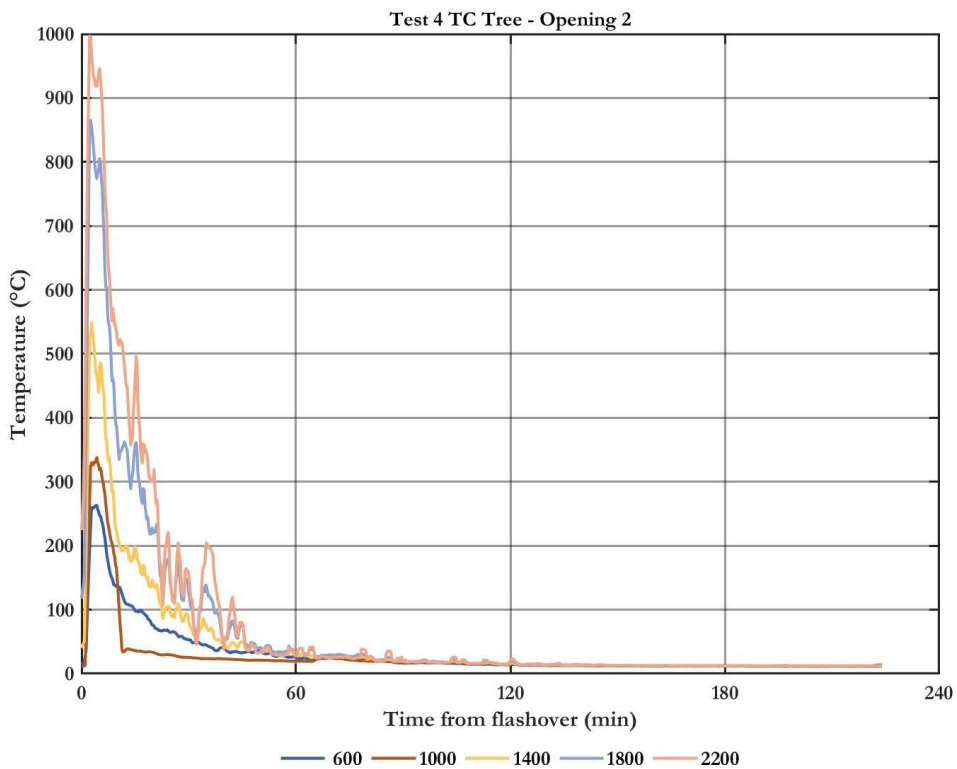


Figure I.8: Test 4 Thermocouple tree in opening 2 (right opening). Legend shows thermocouple height above floor level in mm.

I.5 Test 5

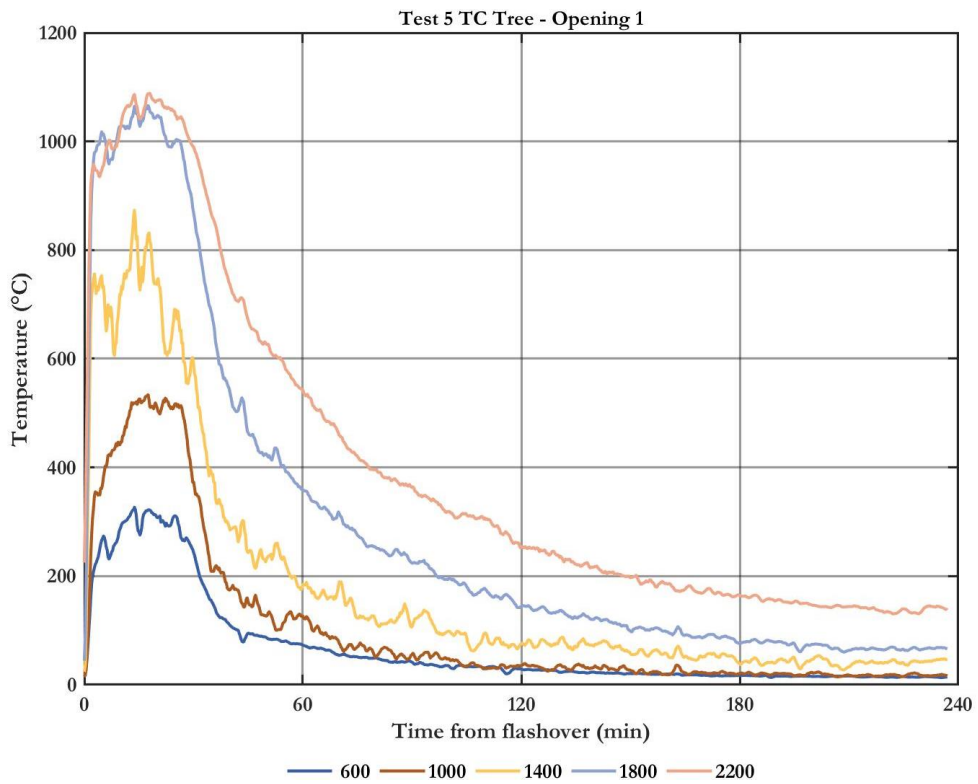


Figure I.9: Test 5 Thermocouple tree in opening 1 (left opening). Legend shows thermocouple height above floor level in mm.

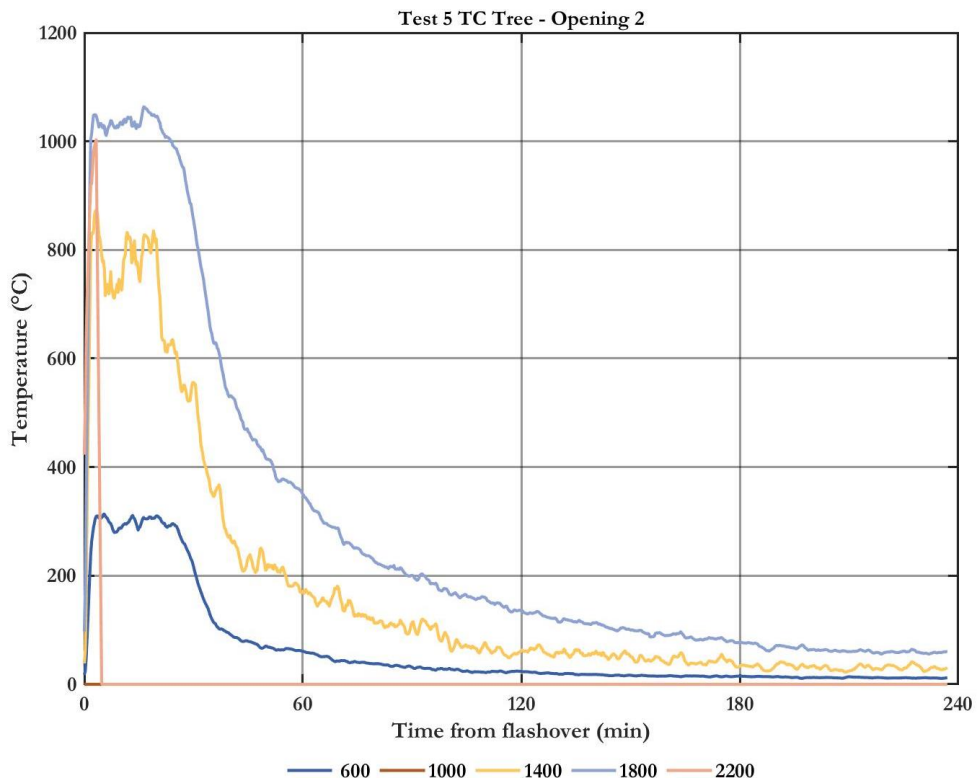


Figure I.10: Test 5 Thermocouple tree in opening 2 (right opening). Legend shows thermocouple height above floor level in mm.

Annex J – Internal CLT and gypsum interface temperatures

Details of the locations for each measurement can be found in Annex A.

J.1 Test 1

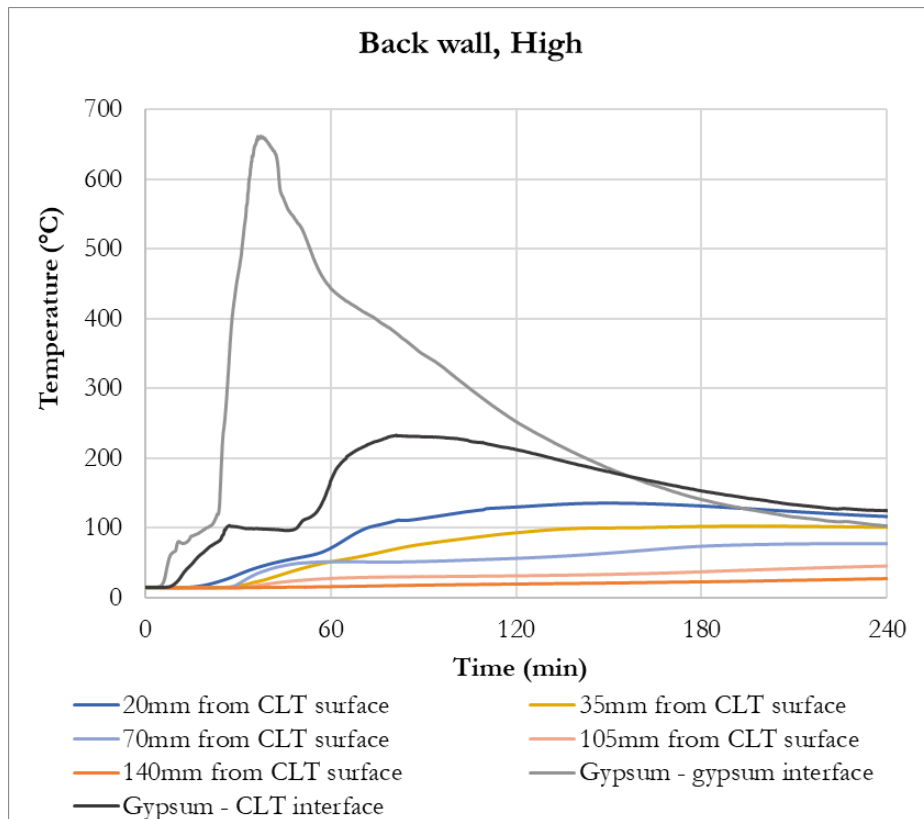


Figure J.1: Test 1 CLT temperature measurements, back wall, high

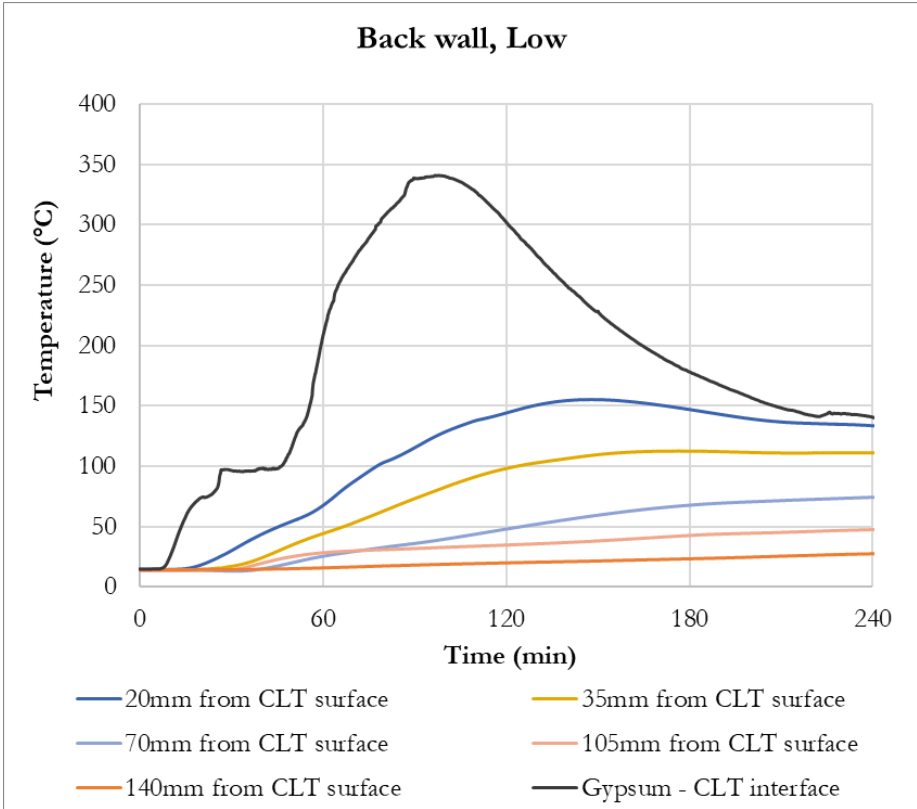


Figure J.2: Test 1 CLT temperature measurements, back wall, low

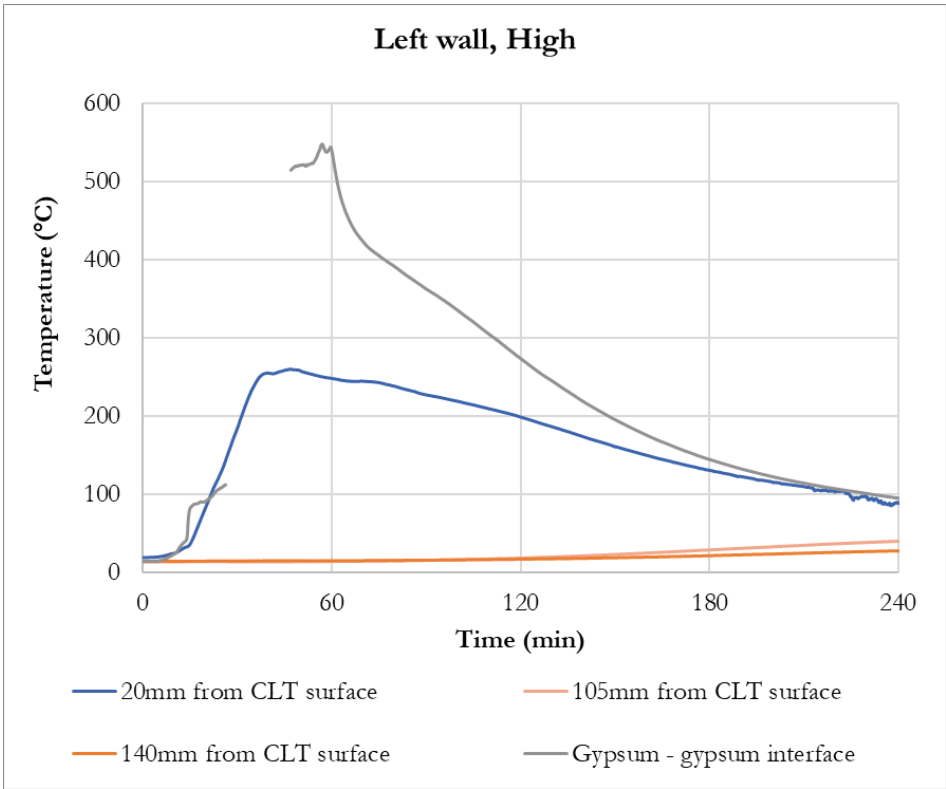


Figure J.3: Test 1 CLT temperature measurements, left wall, high

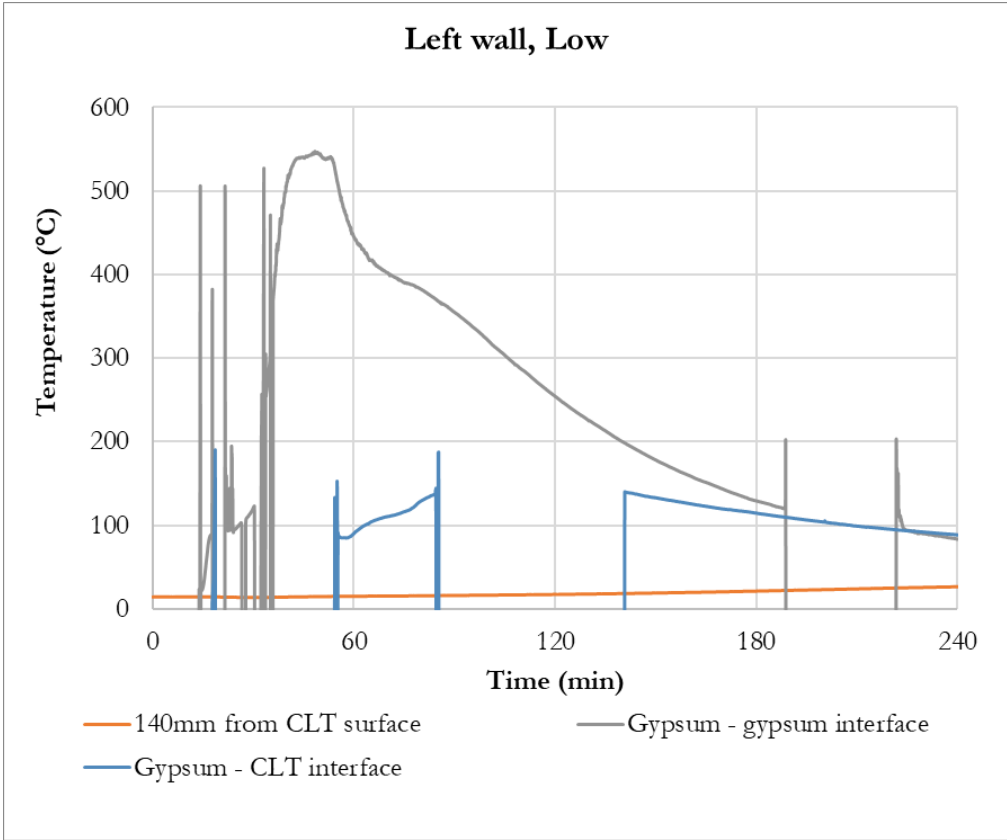


Figure J.4: Test 1 CLT temperature measurements, left wall, low

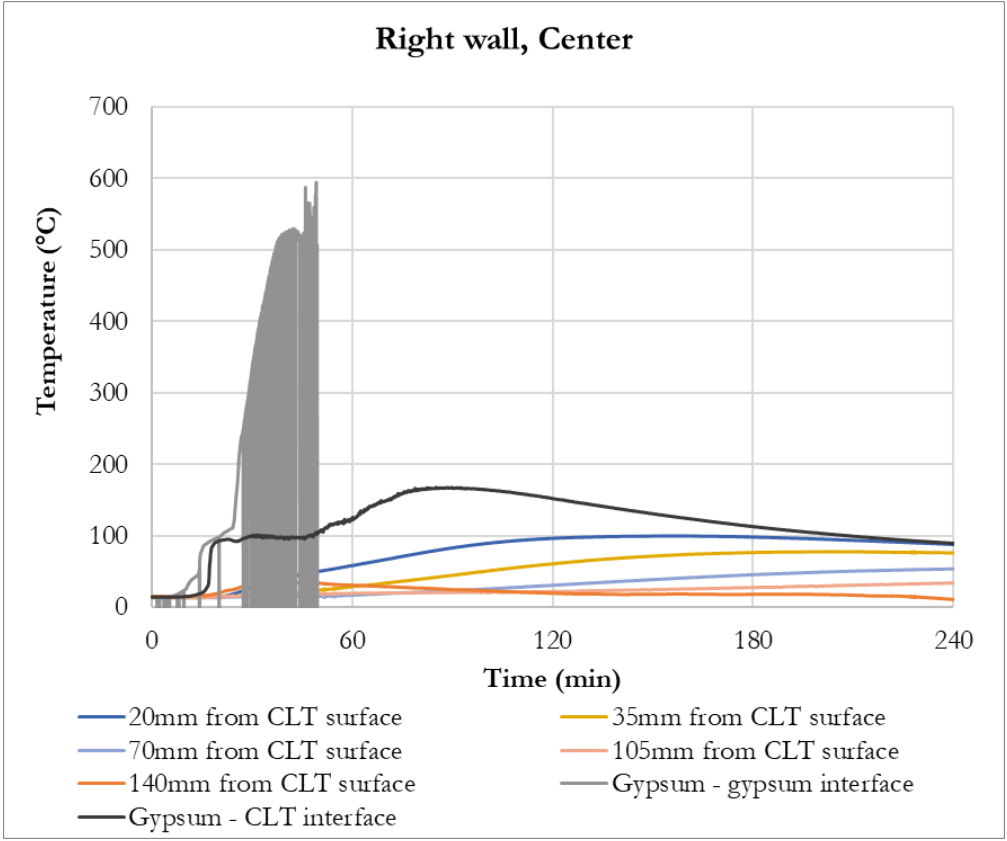


Figure J.5: Test 1 CLT temperature measurements, right wall, center

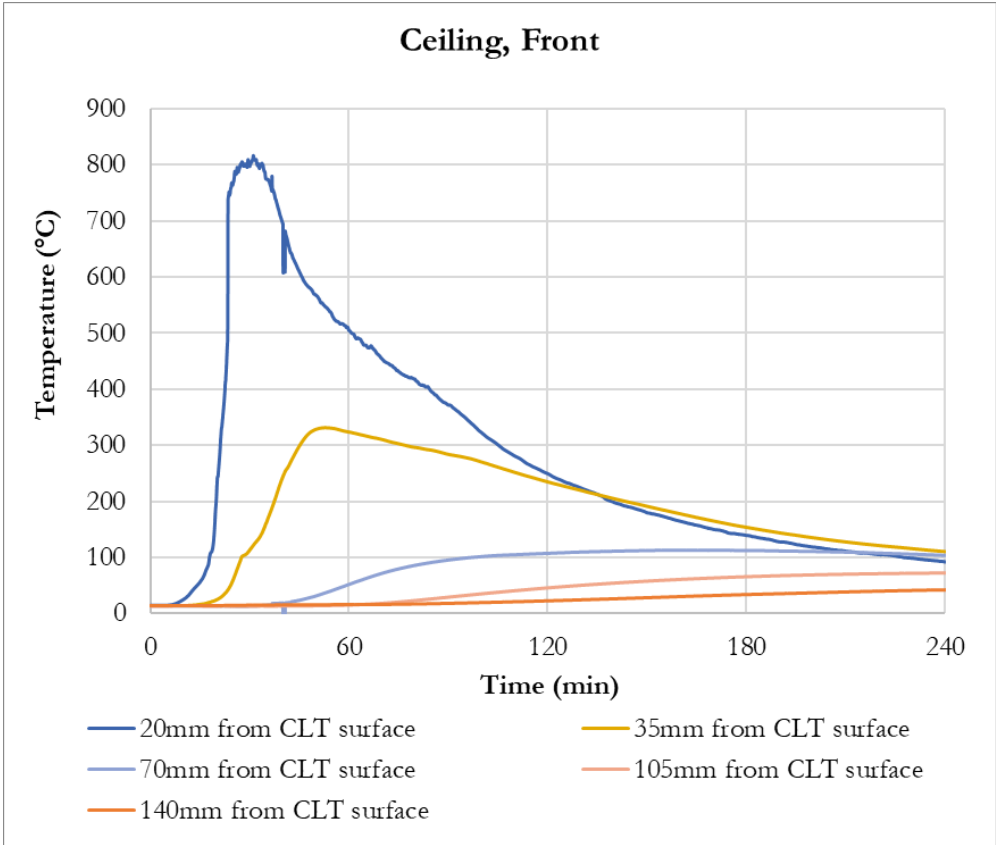


Figure J.6: Test 1 CLT temperature measurements, ceiling, front

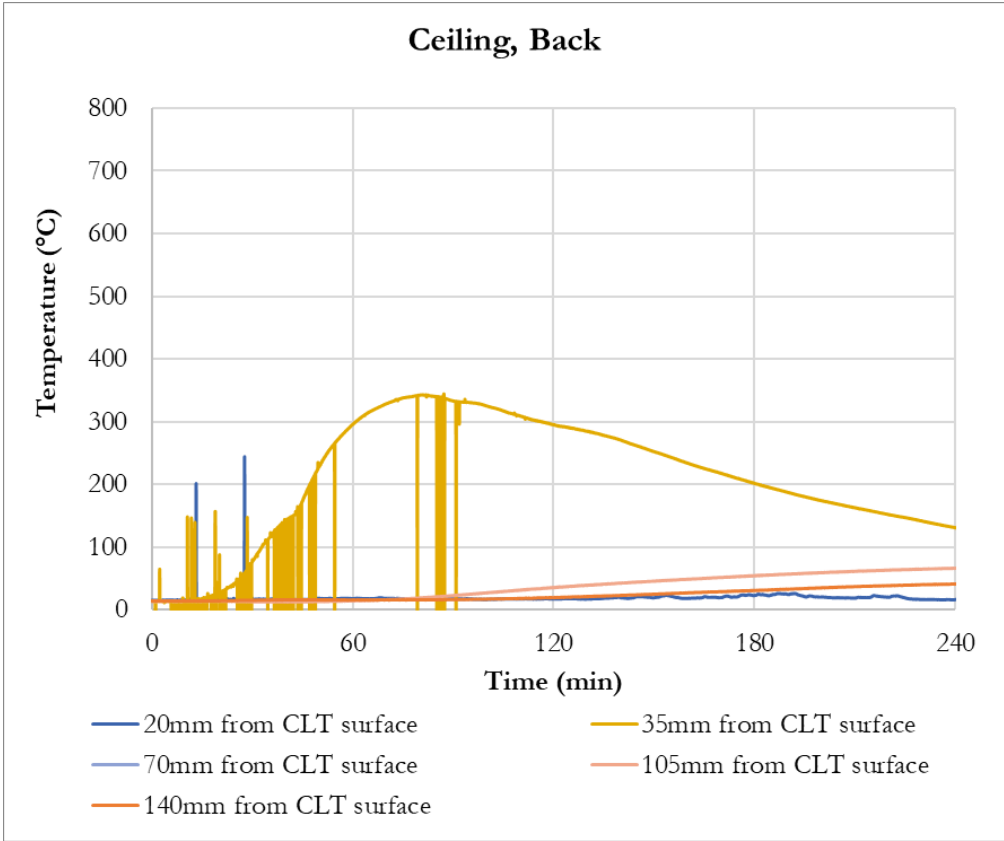


Figure J.7: Test 1 CLT temperature measurements, ceiling, back

The following graphs show data recorded overnight after the fire.

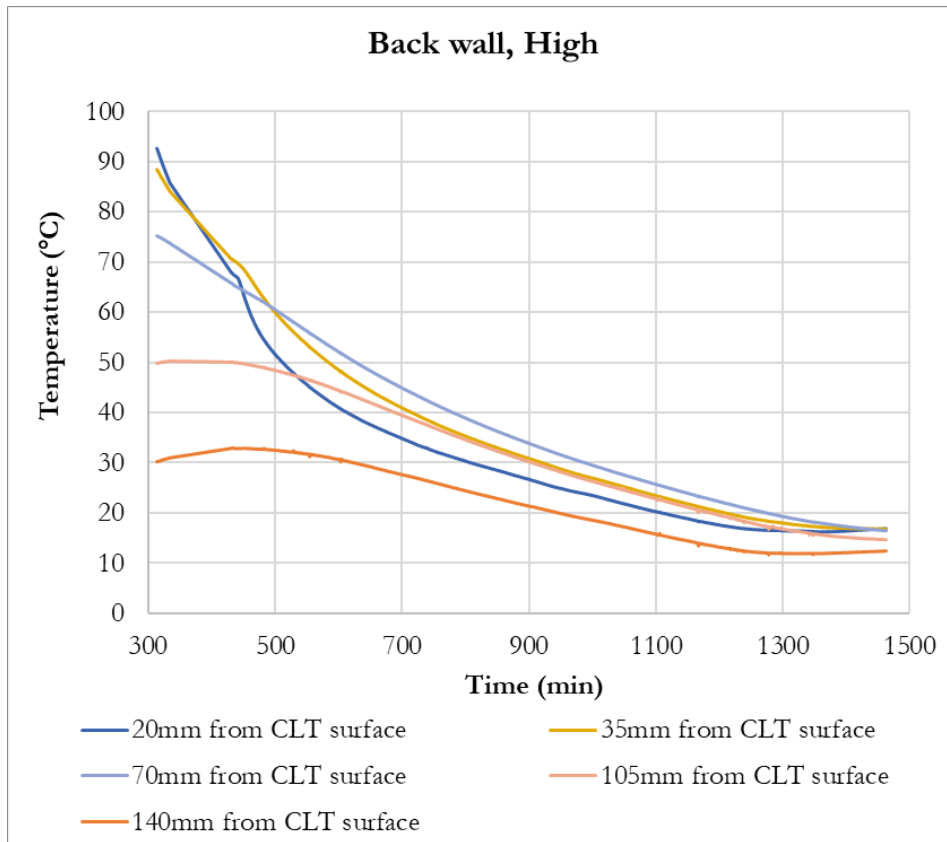


Figure J.8: Test 1 post fire CLT temperature measurements, back wall, high

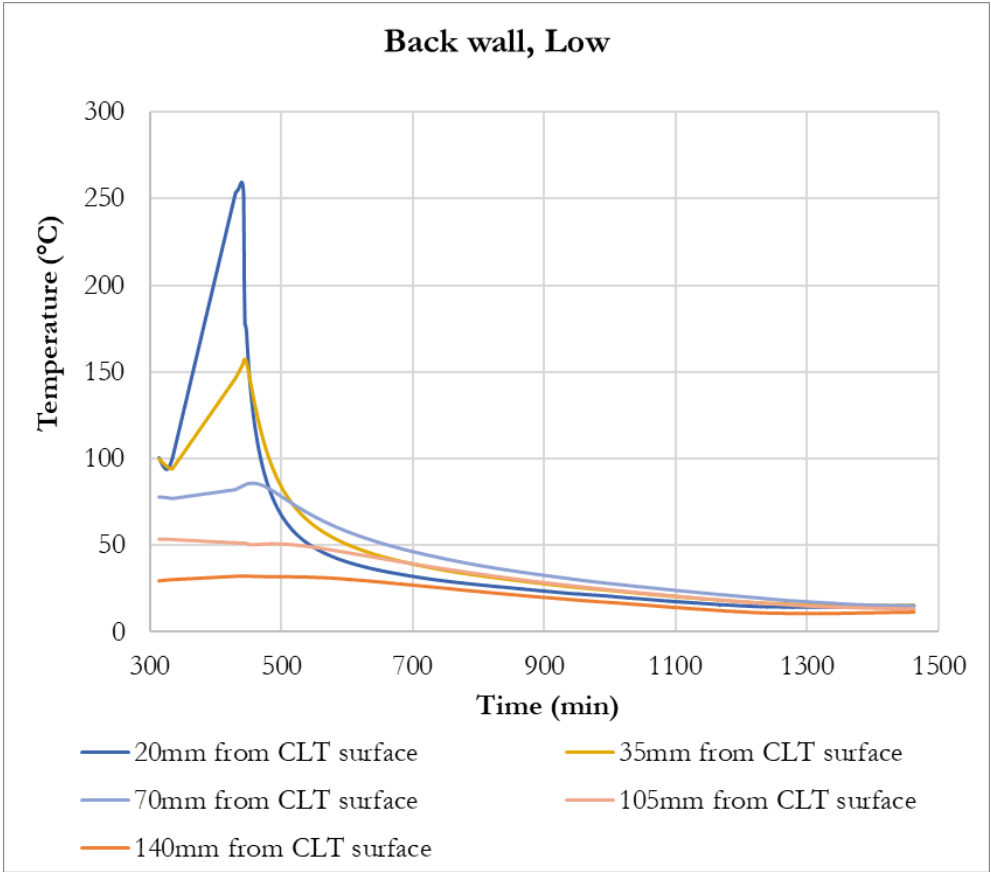


Figure J.9: Test 1 post fire CLT temperature measurements, back wall, low

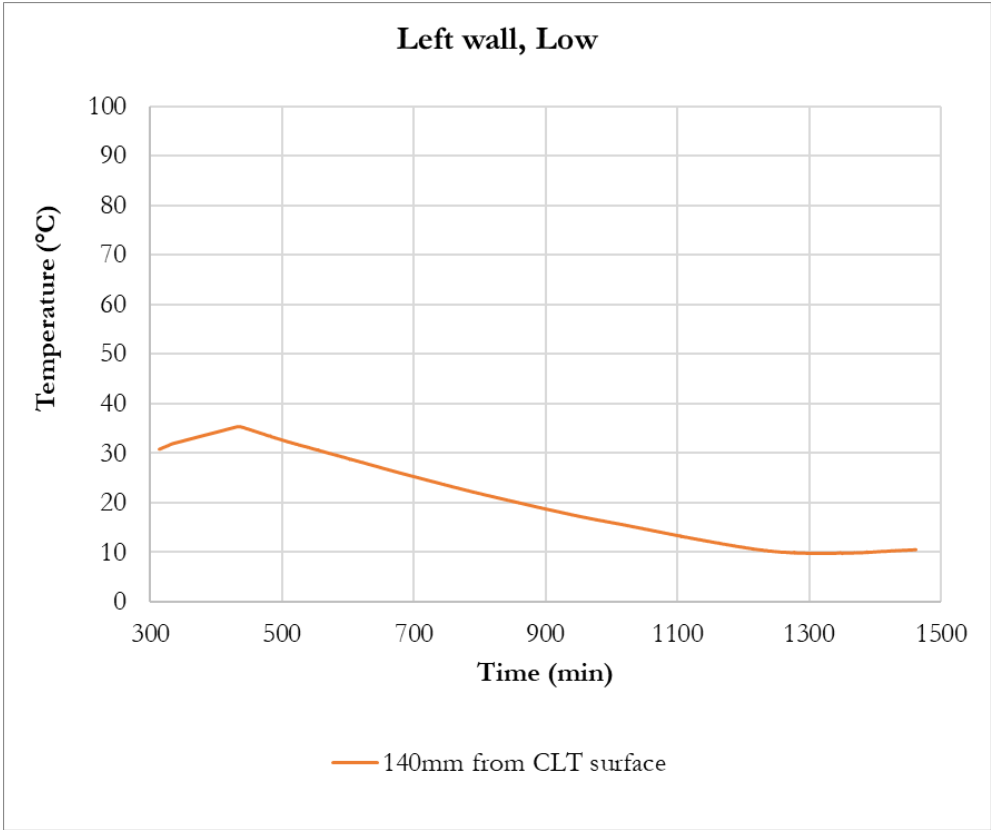


Figure J.10: Test 1 post fire CLT temperature measurements, left wall, low

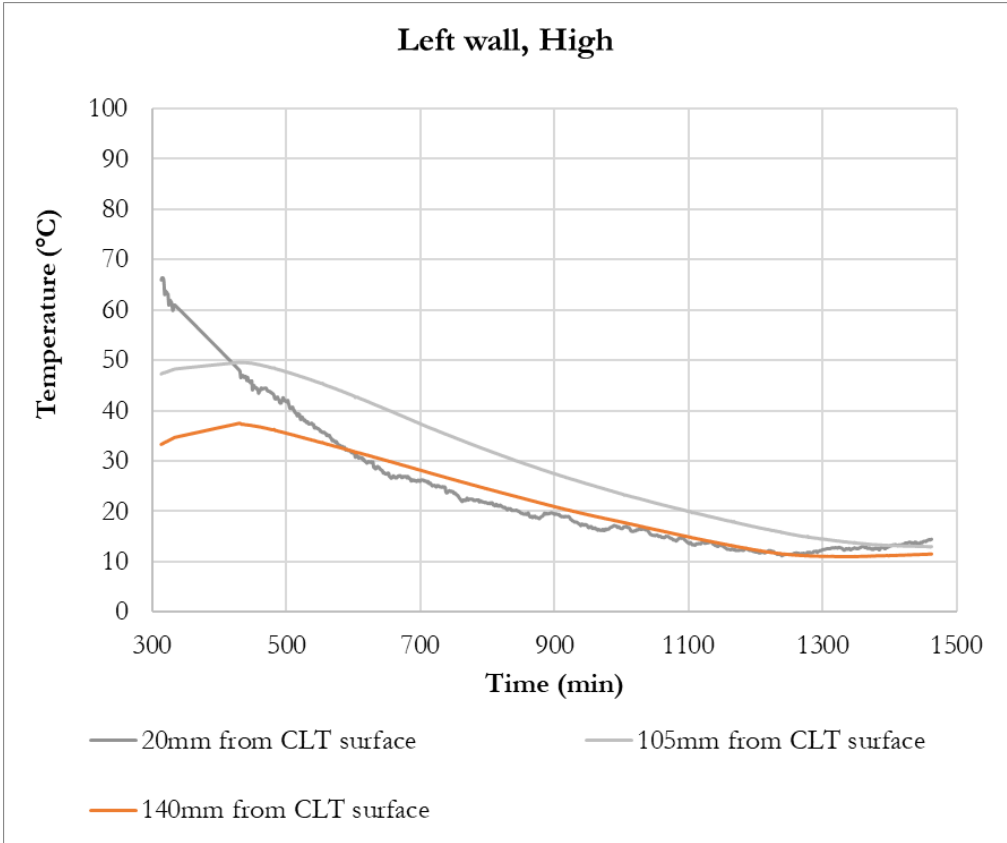


Figure J.11: Test 1 post fire CLT temperature measurements, left wall, high

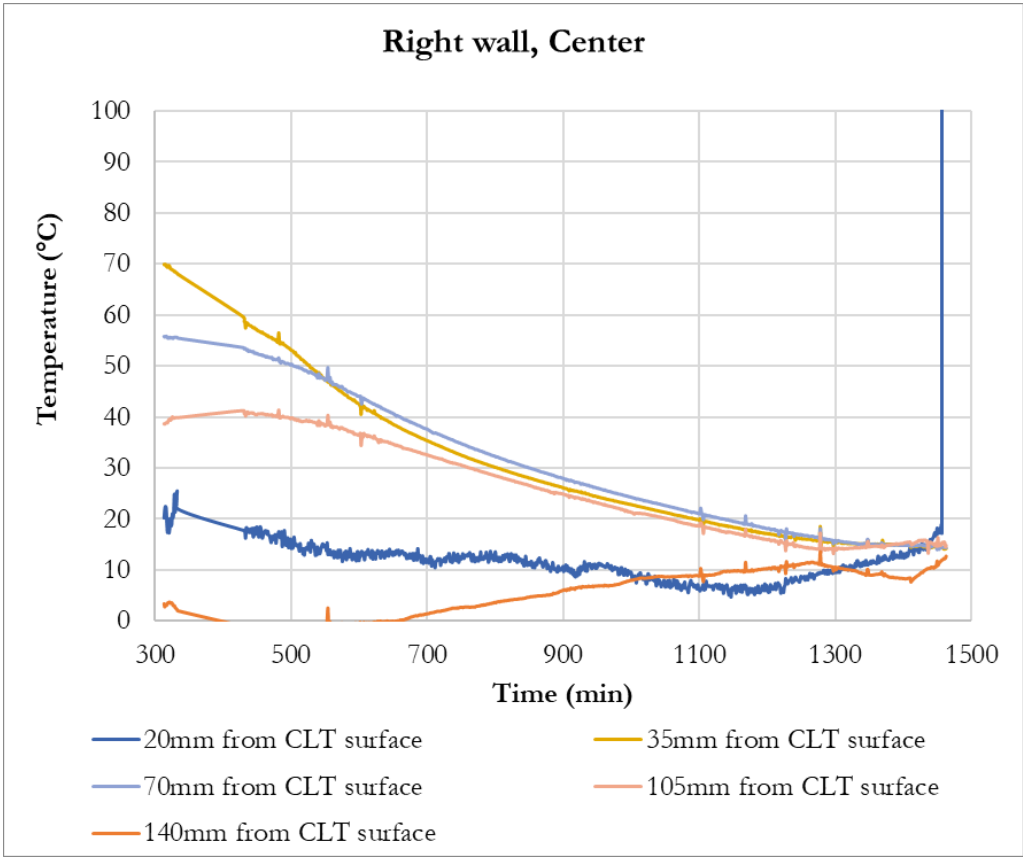


Figure J.12: Test 1 post fire CLT temperature measurements, right wall, center

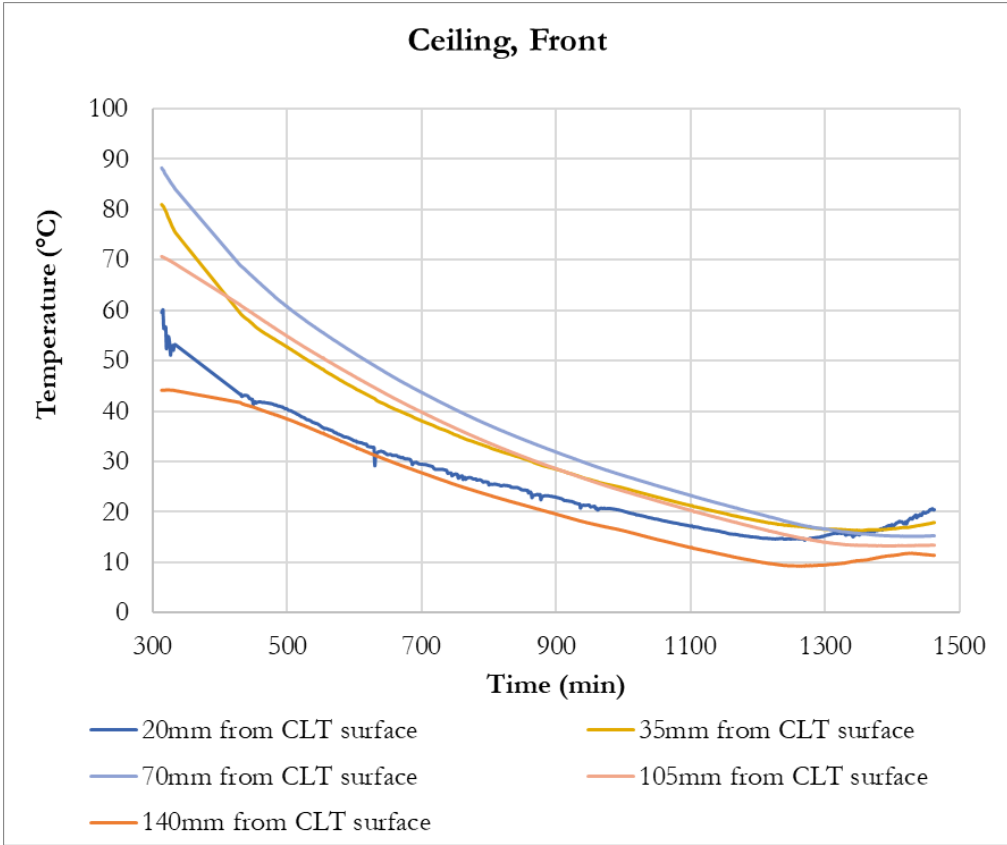


Figure J.13: Test 1 post fire CLT temperature measurements, ceiling, front

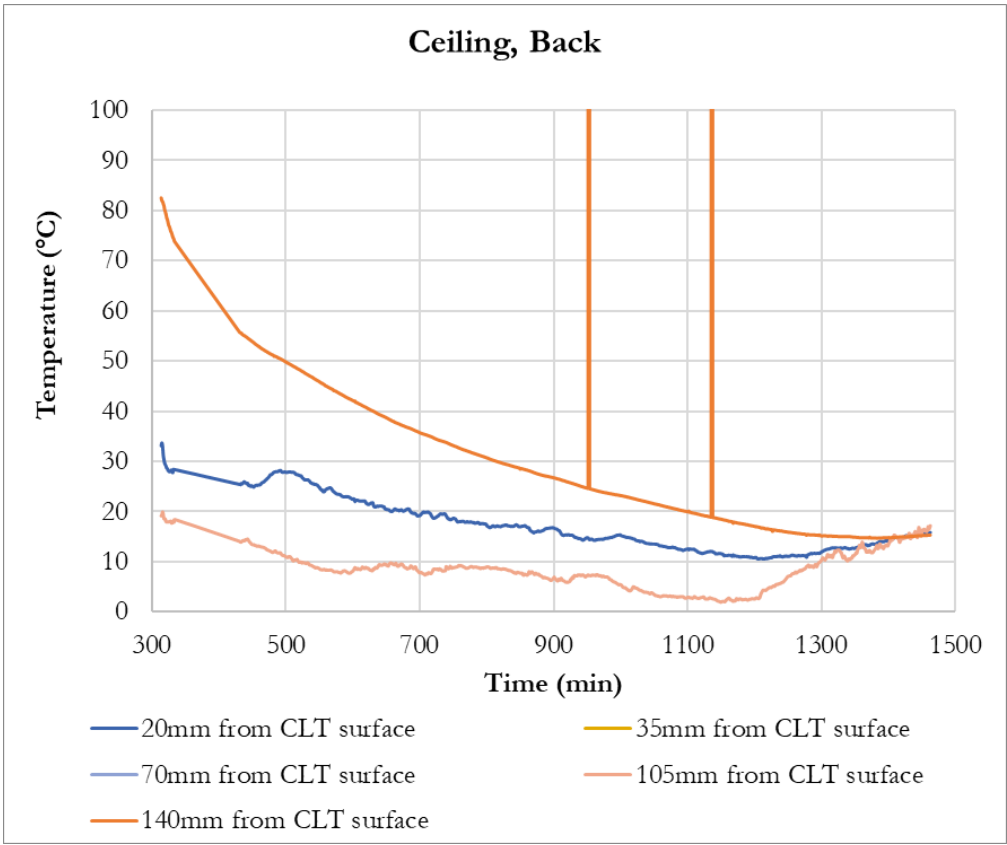


Figure J.14: Test 1 post fire CLT temperature measurements, ceiling, back

J.2 Test 2

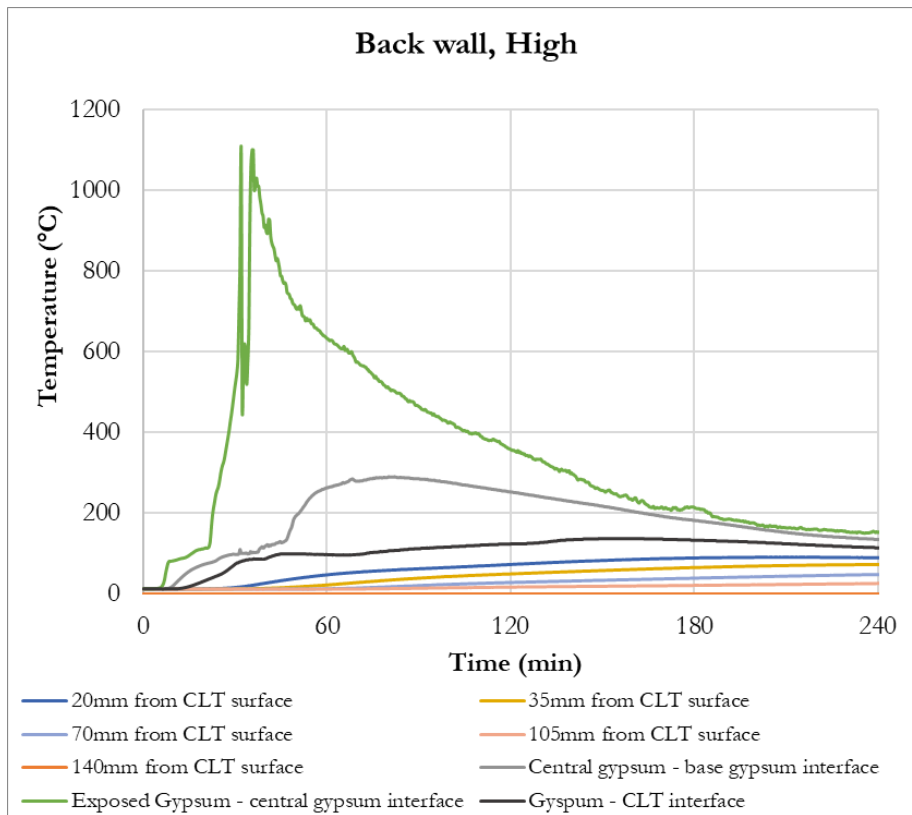


Figure J.15: Test 2 CLT temperature measurements, back wall, high

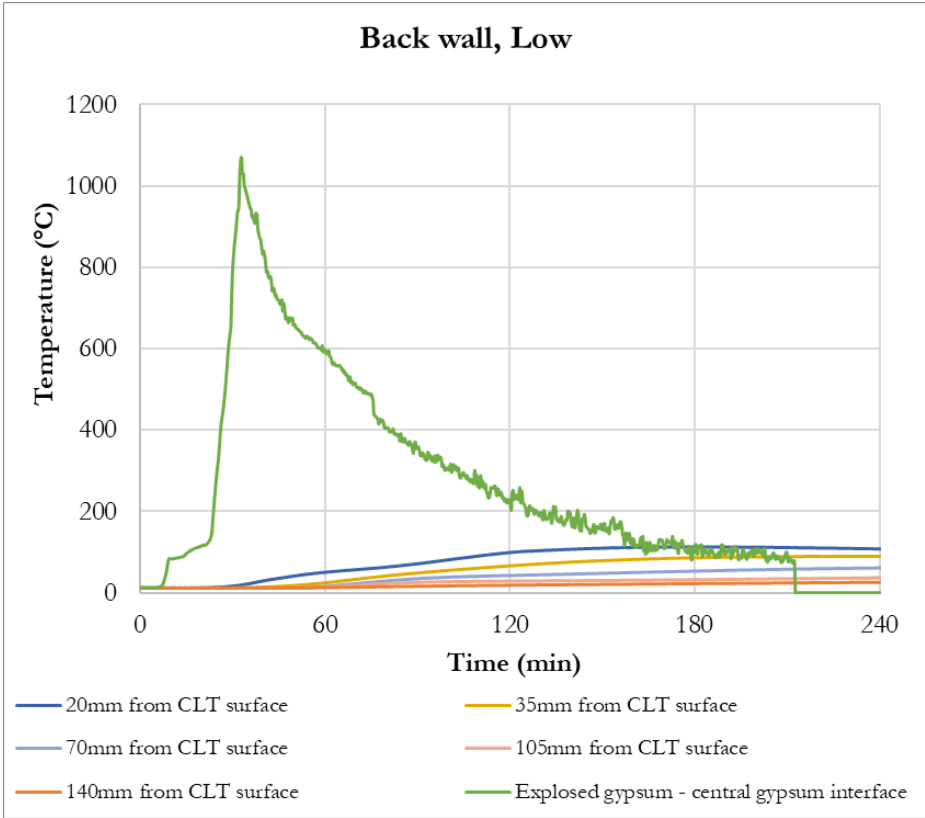


Figure J.16: Test 2 CLT temperature measurements, back wall, low

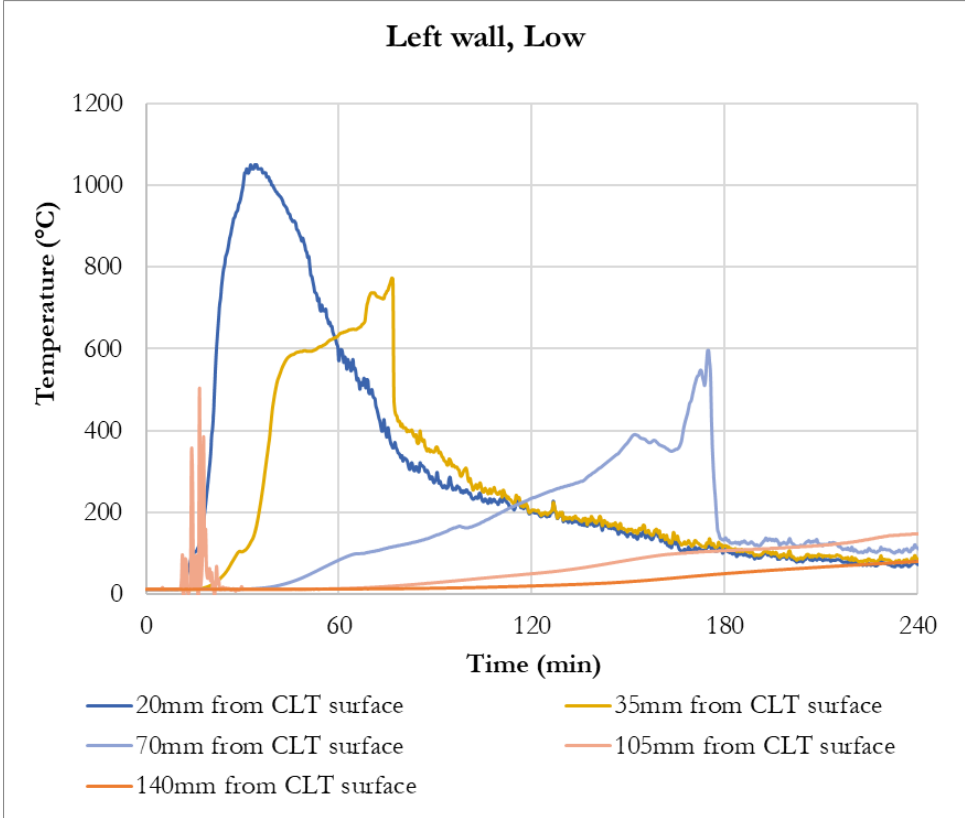


Figure J.17: Test 2 CLT temperature measurements, left wall, low

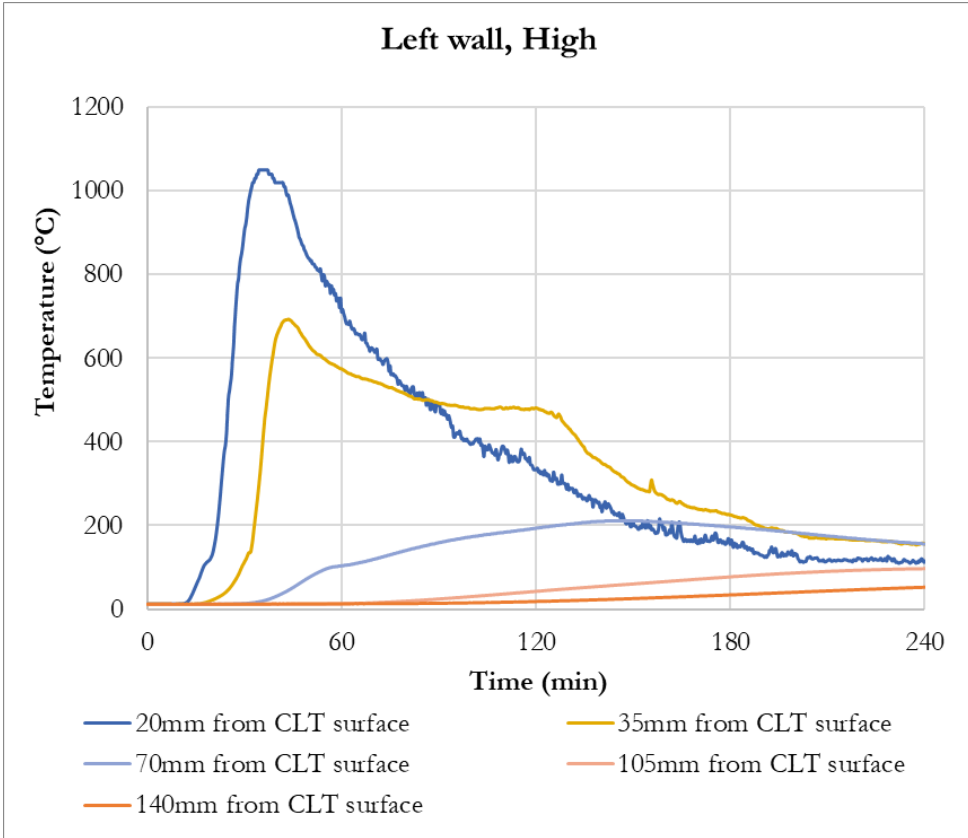


Figure J.18: Test 2 CLT temperature measurements, left wall, high

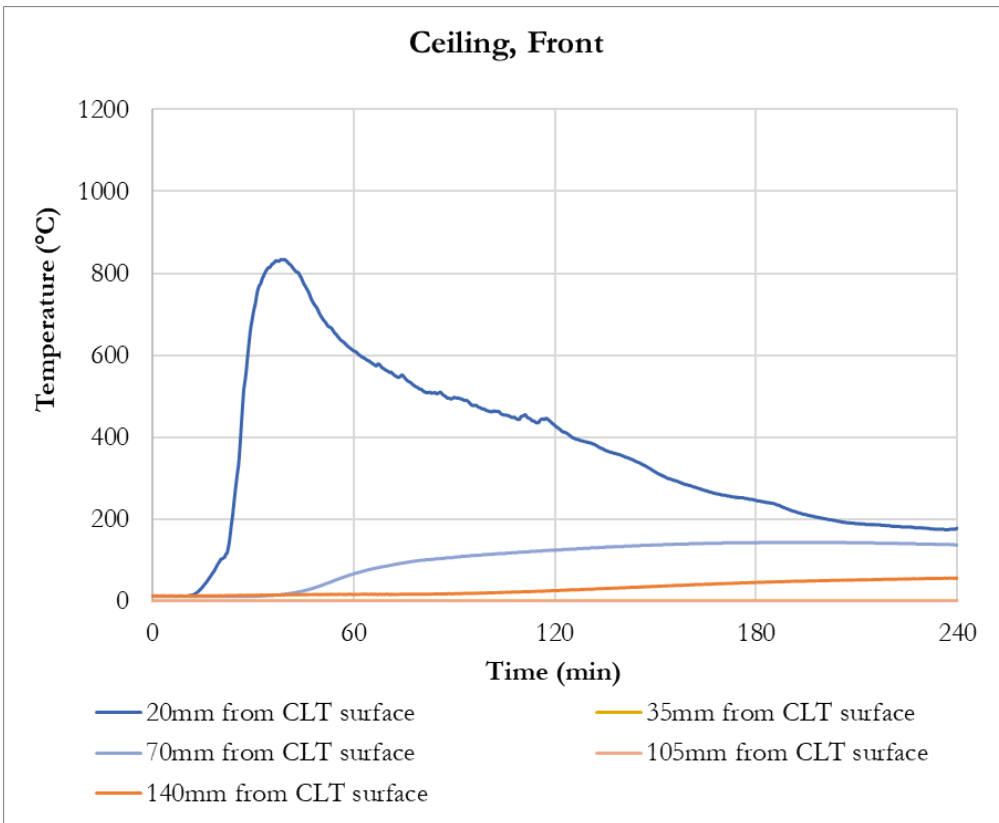


Figure J.19: Test 2 CLT temperature measurements, ceiling, front

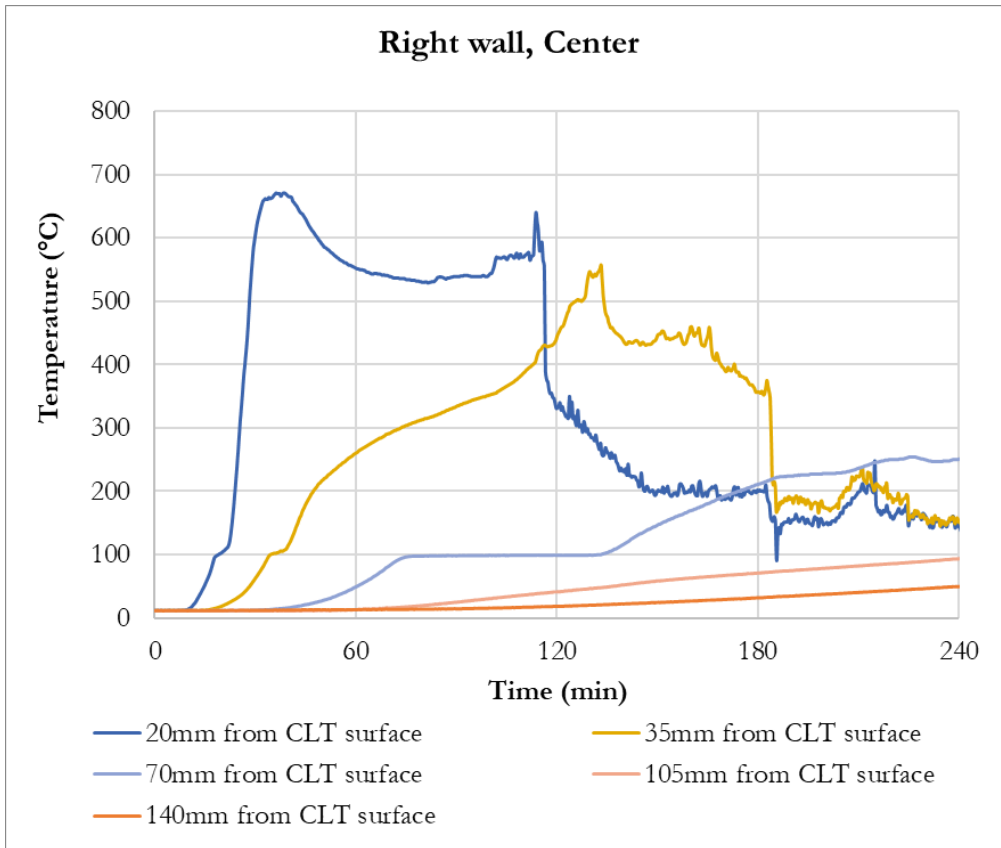


Figure J.20: Test 2 CLT temperature measurements, right wall, center

The following graphs show data recorded overnight after the fire.

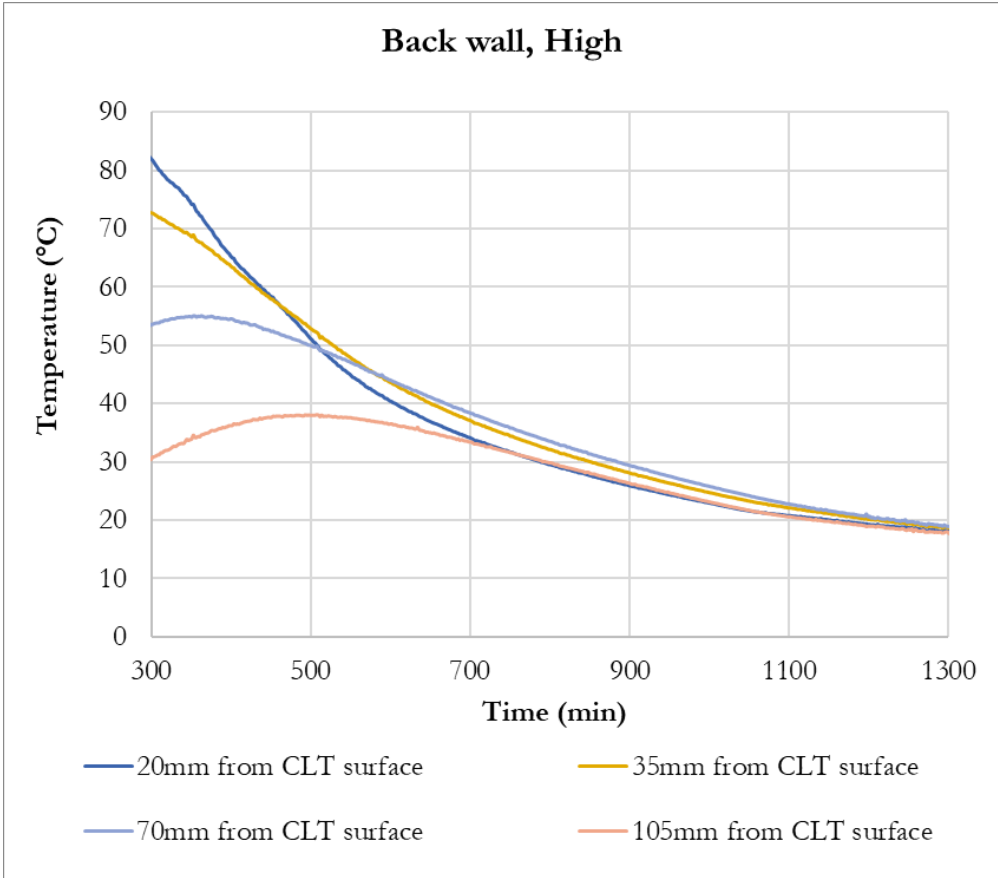


Figure J.21: Test 2 post fire CLT temperature measurements, back wall, high

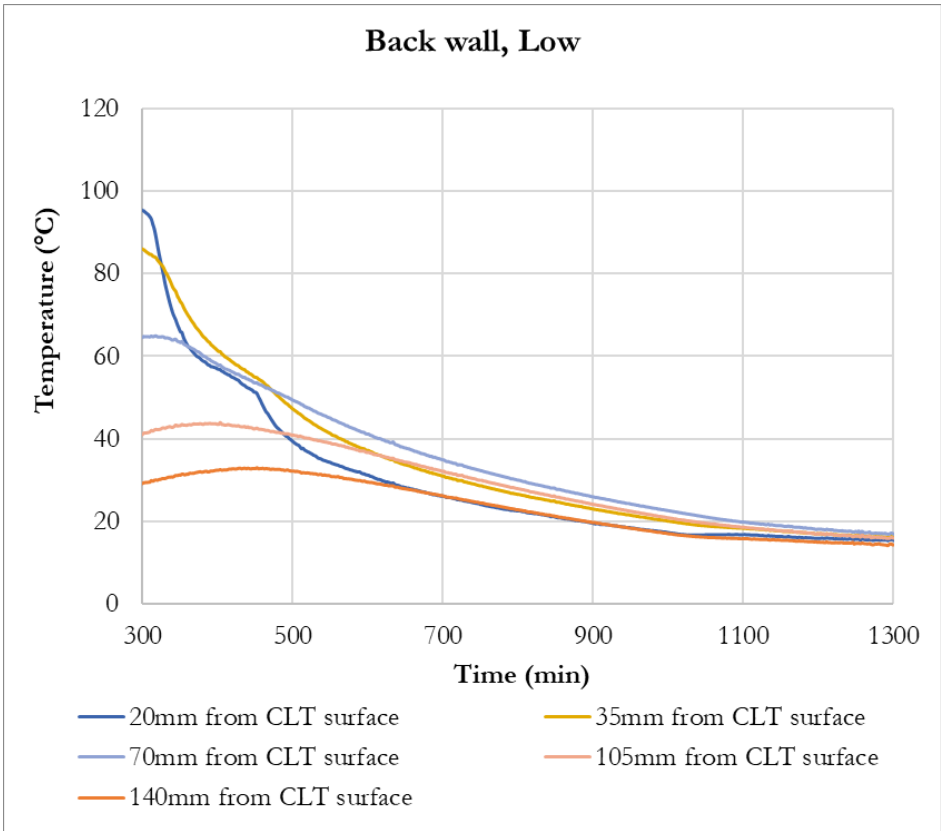


Figure J.22: Test 2 post fire CLT temperature measurements, back wall, low

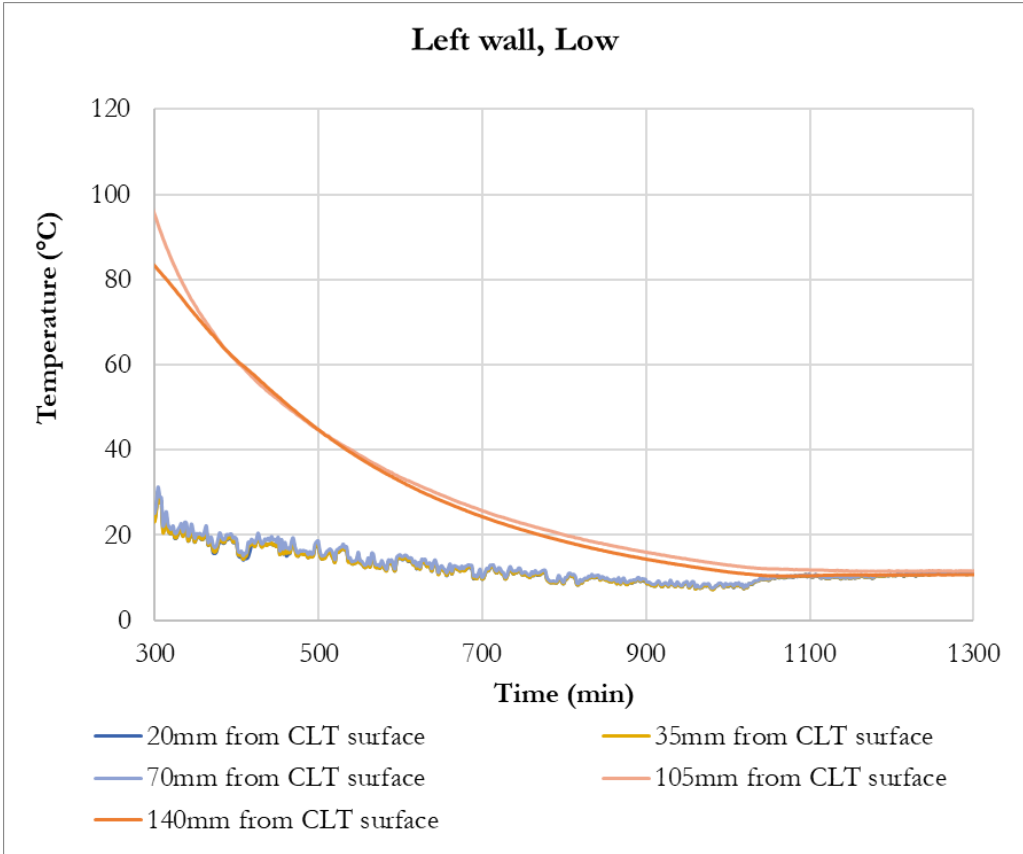


Figure J.23: Test 2 post fire CLT temperature measurements, left wall, low

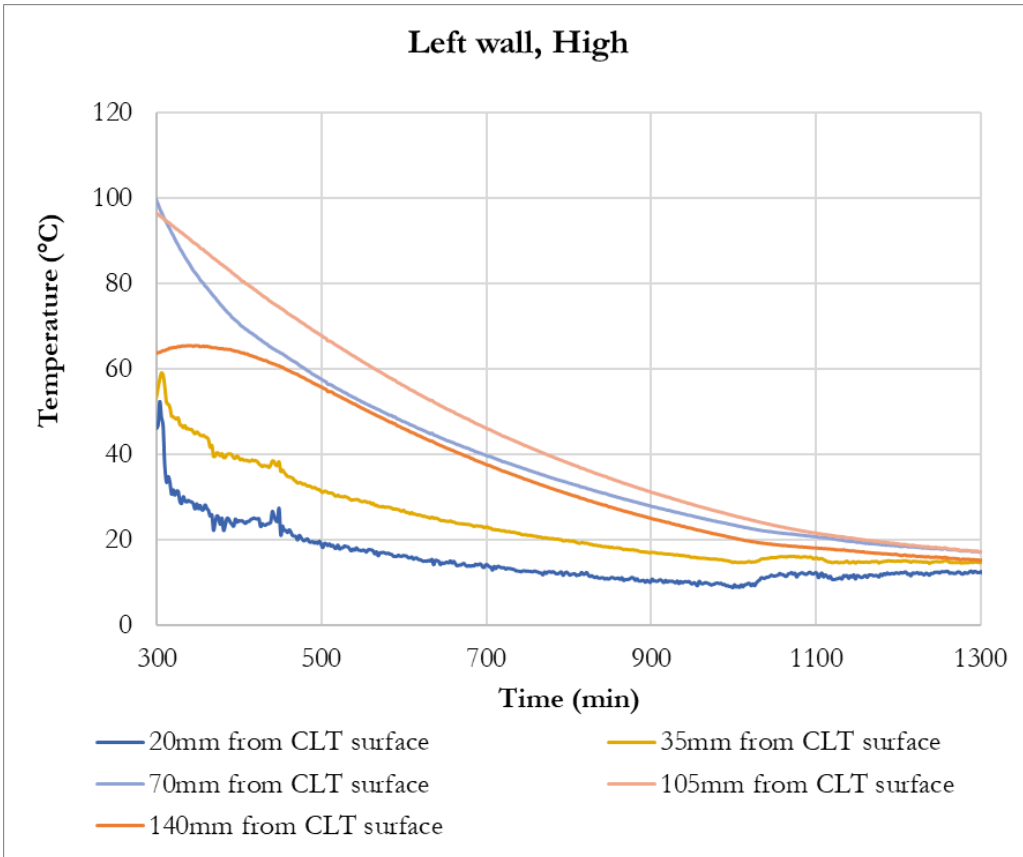


Figure J.24: Test 2 post fire CLT temperature measurements, left wall, high

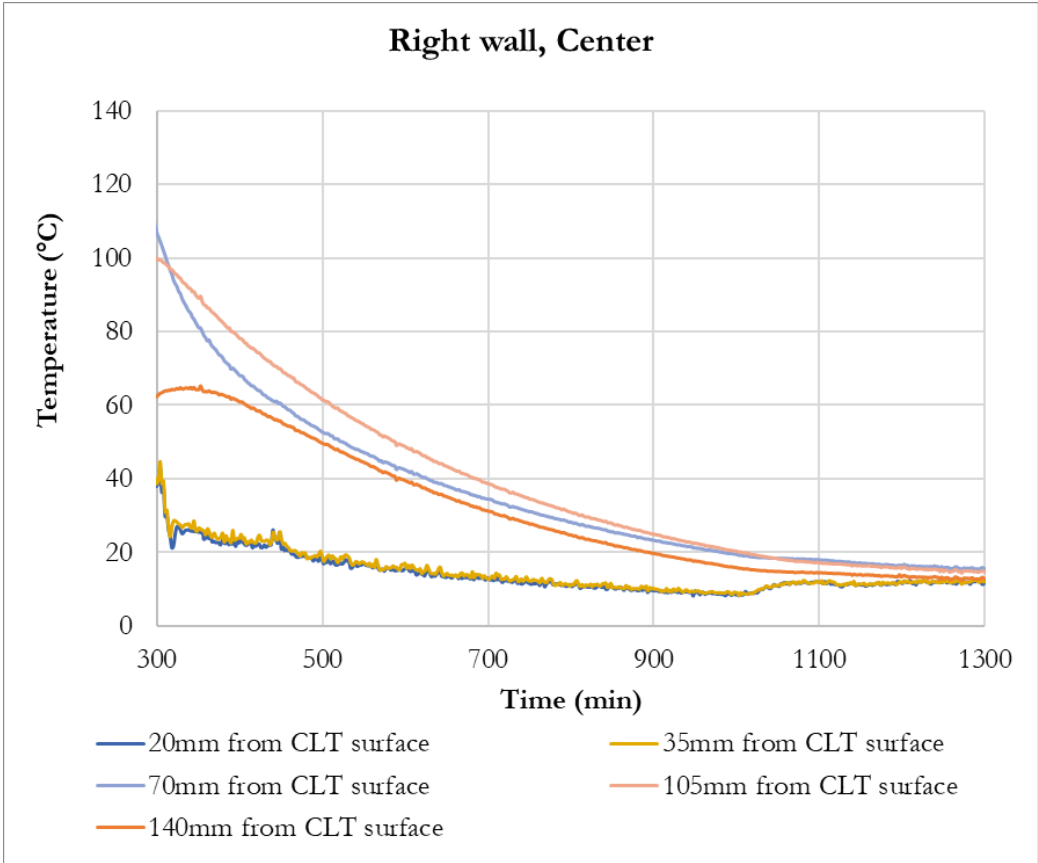


Figure J.25: Test 2 post fire CLT temperature measurements, right wall, center

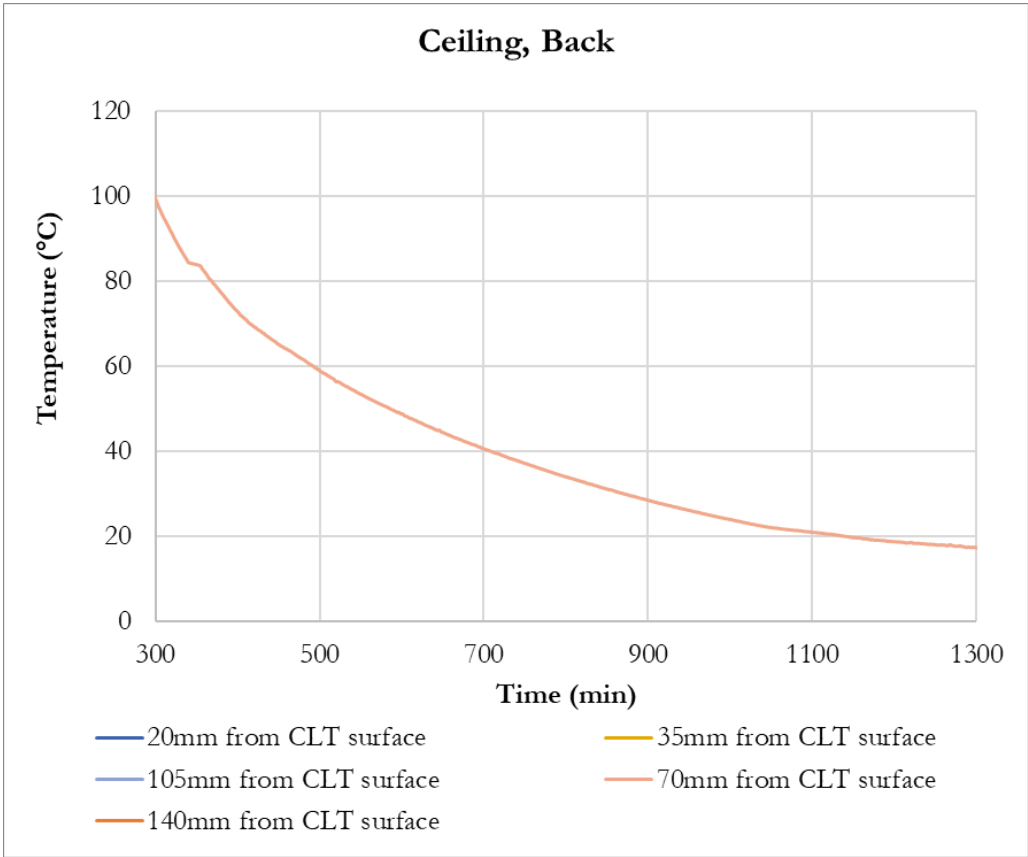


Figure J.26: Test 2 post fire CLT temperature measurements, ceiling, back

J.3 Test 3

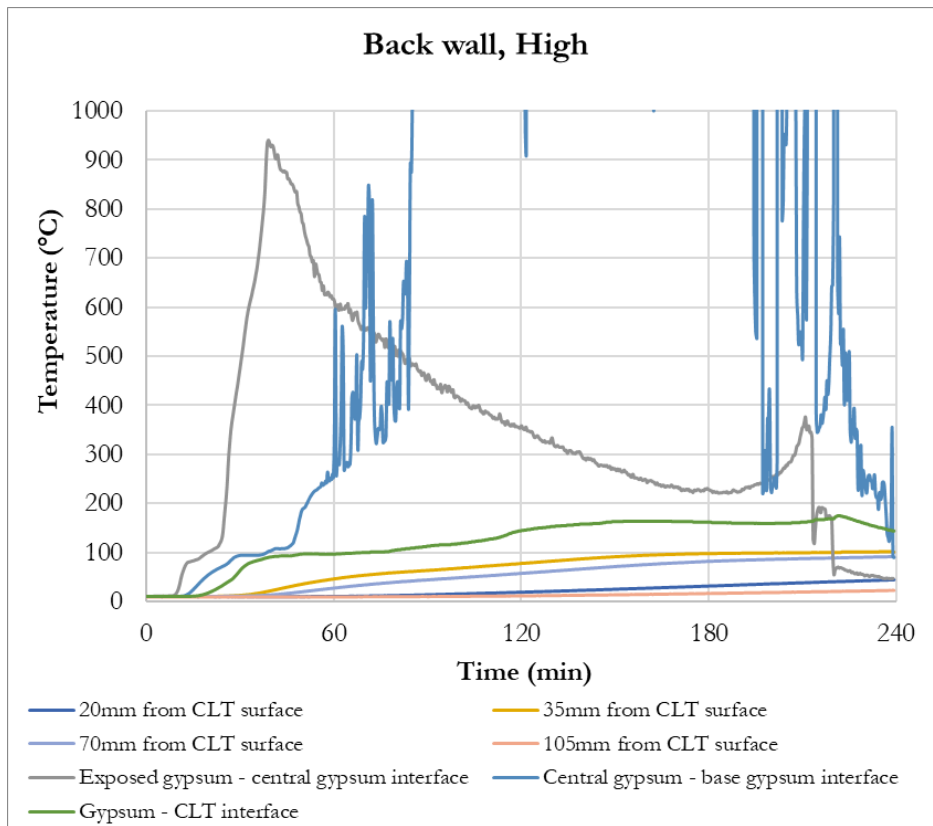


Figure J.27: Test 3 CLT temperature measurements, back wall, high

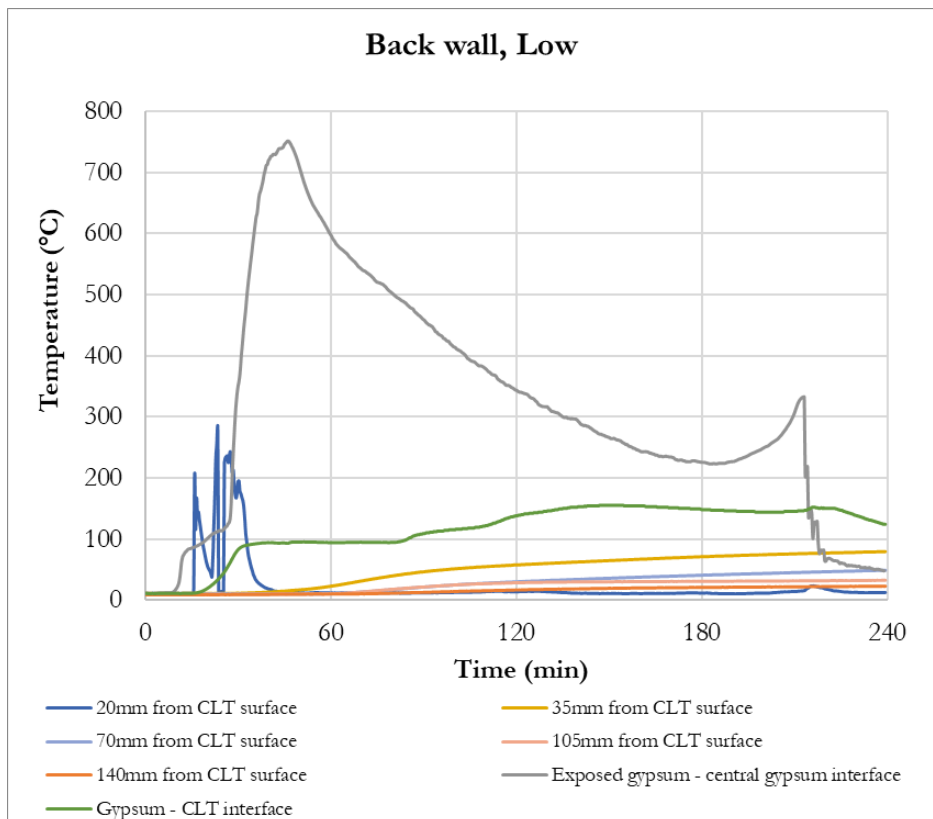


Figure J.28: Test 3 CLT temperature measurements, back wall, low

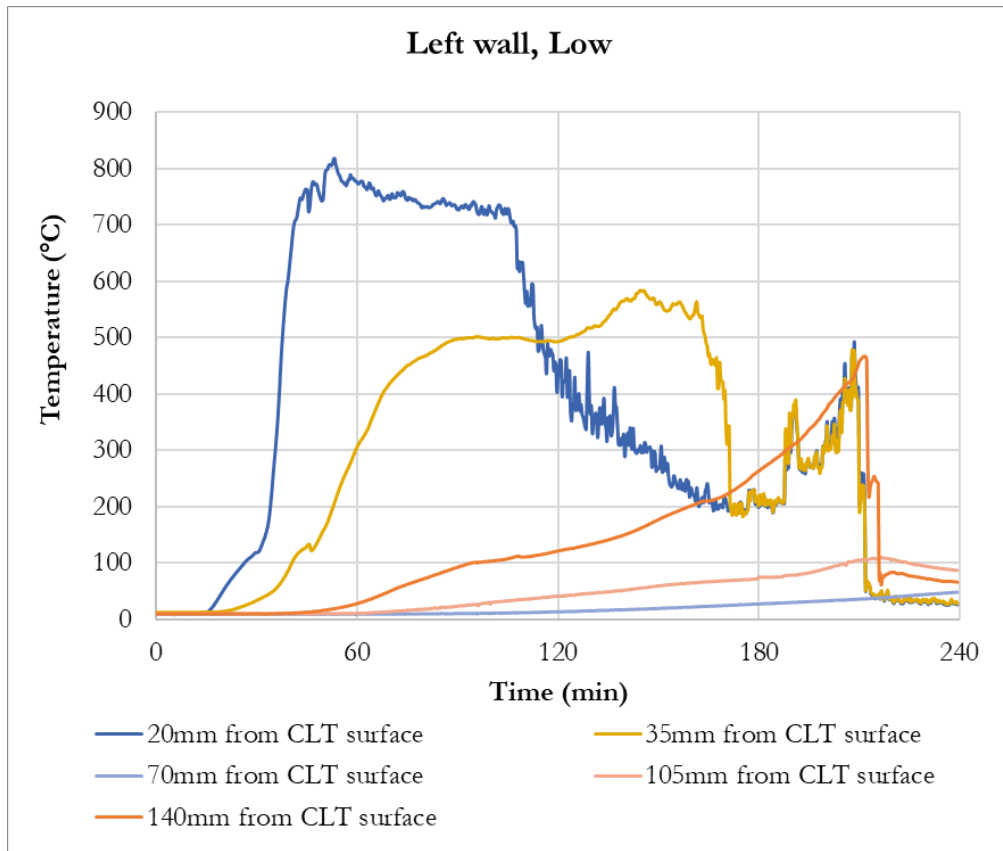


Figure J.29: Test 3 CLT temperature measurements, left wall, low

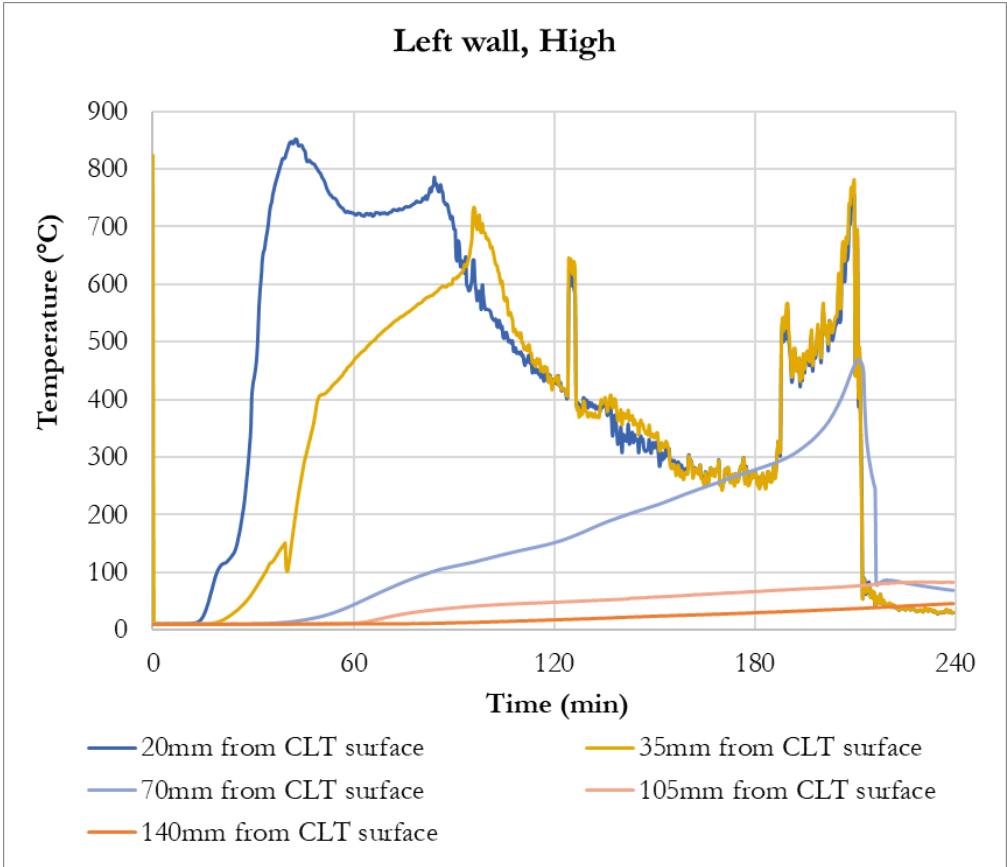


Figure J.30: Test 3 CLT temperature measurements, left wall, high

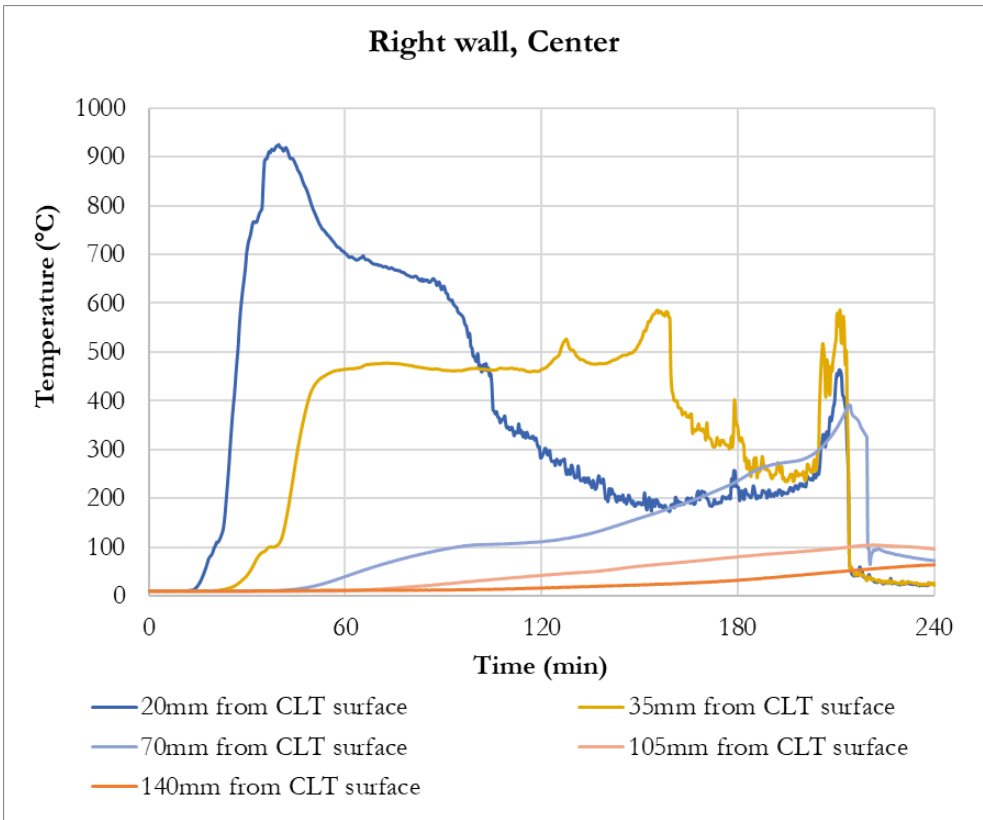


Figure J.31: Test 3 CLT temperature measurements, right wall, center

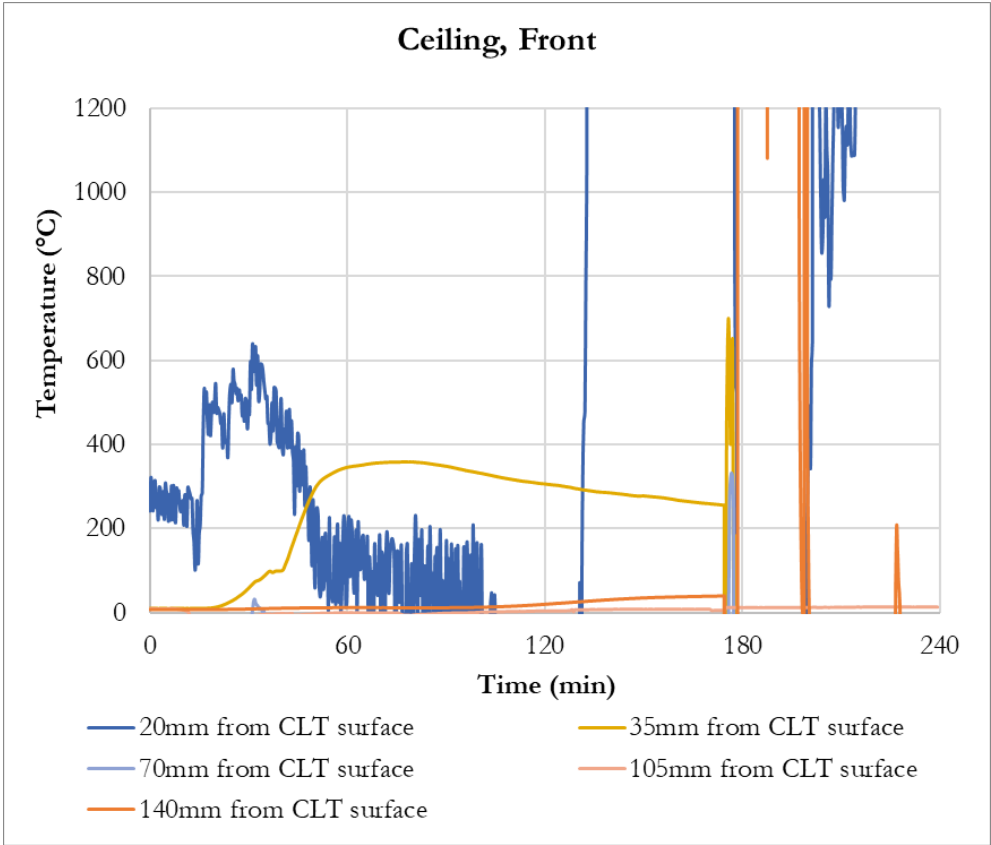


Figure J.32: Test 3 CLT temperature measurements, ceiling, front

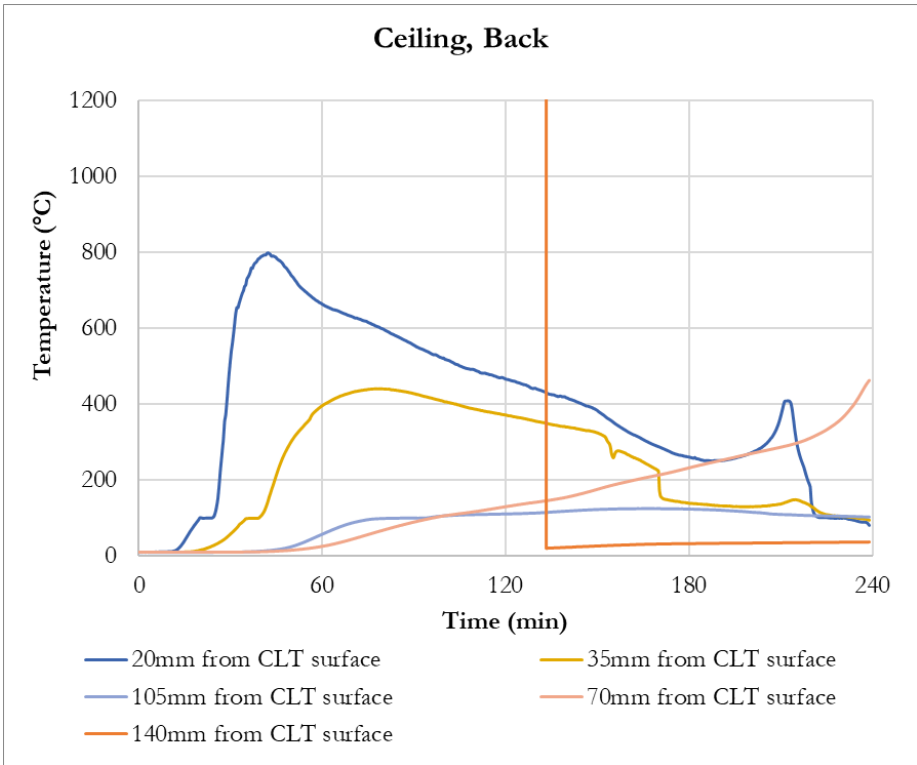


Figure J.33: Test 3 CLT temperature measurements, ceiling, back

J.4 Test 4

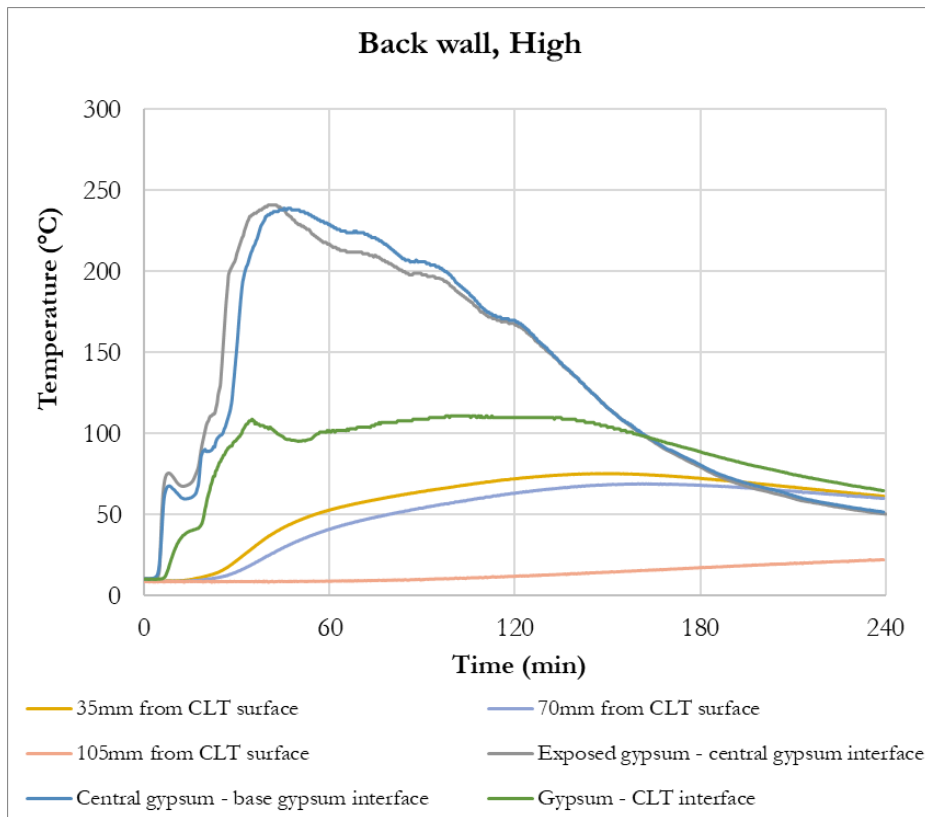


Figure J.34: Test 4 CLT temperature measurements, back wall, high

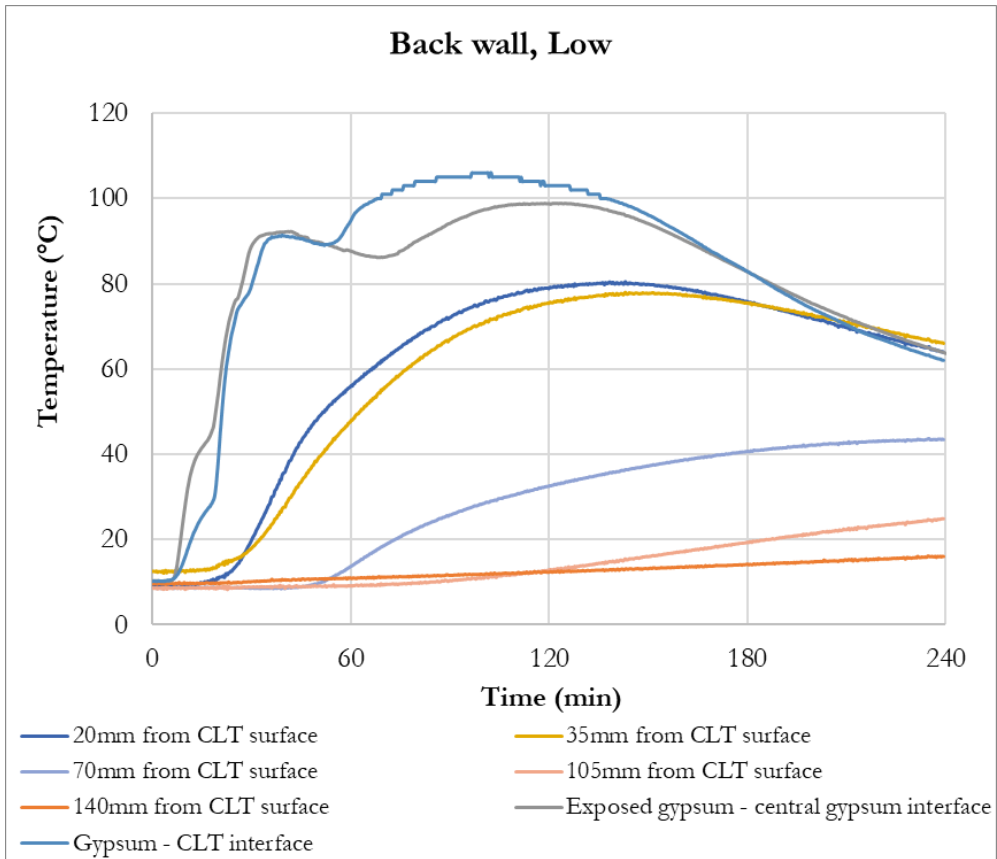


Figure J.35: Test 4 CLT temperature measurements, back wall, low

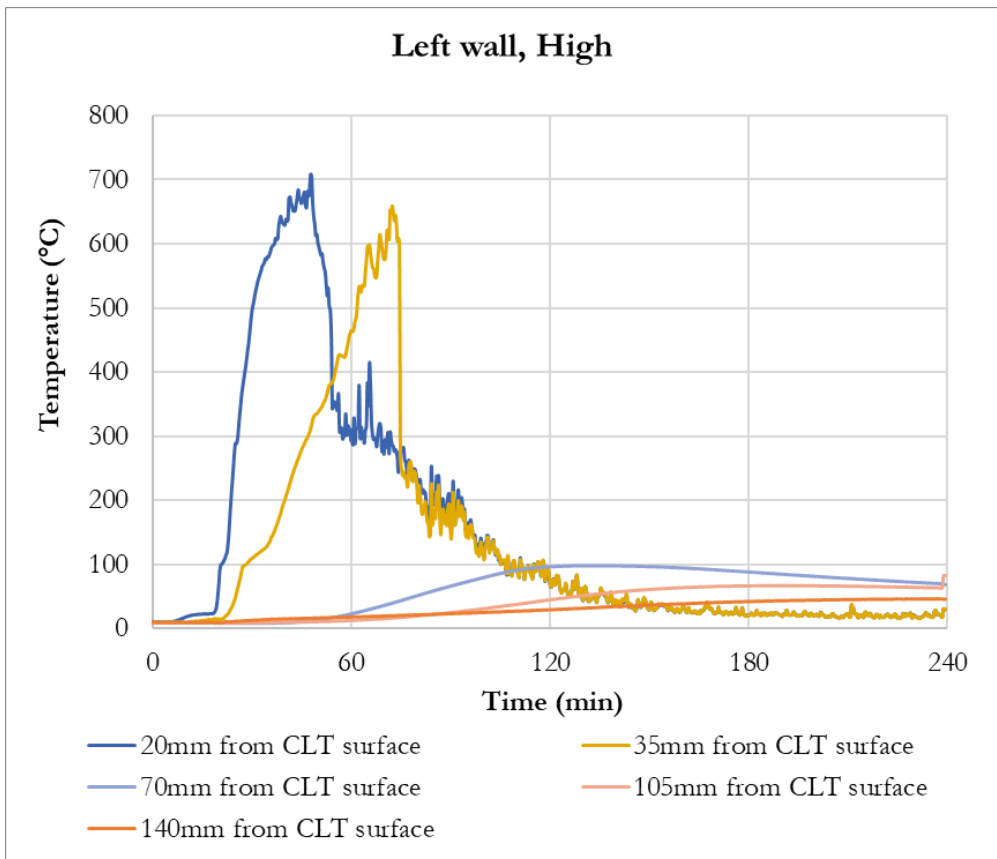


Figure J.36: Test 4 CLT temperature measurements, left wall, high

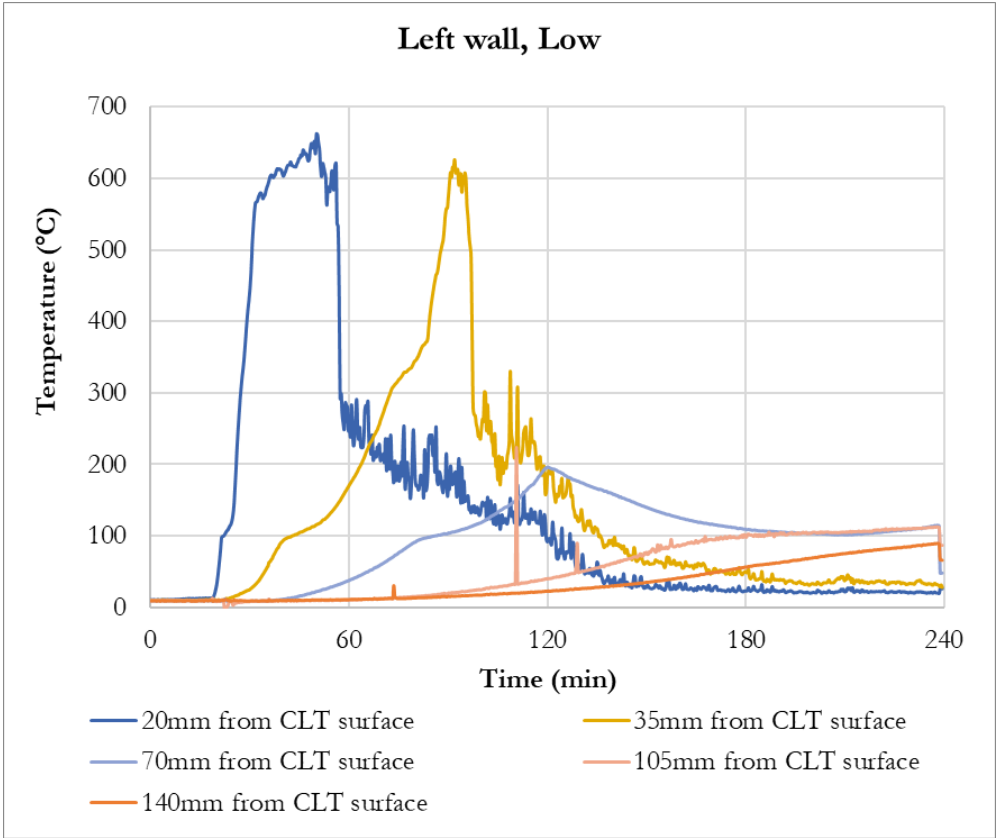


Figure J.37: Test 4 CLT temperature measurements, left wall, low

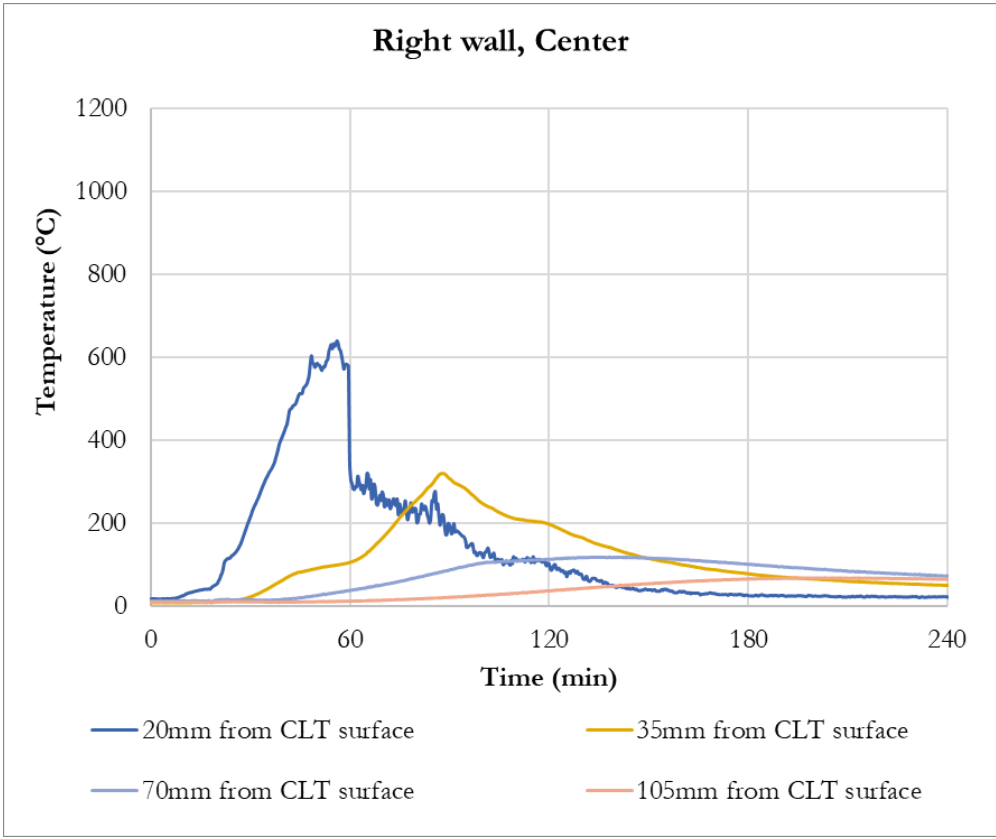


Figure J.38: Test 4 CLT temperature measurements, right wall, center

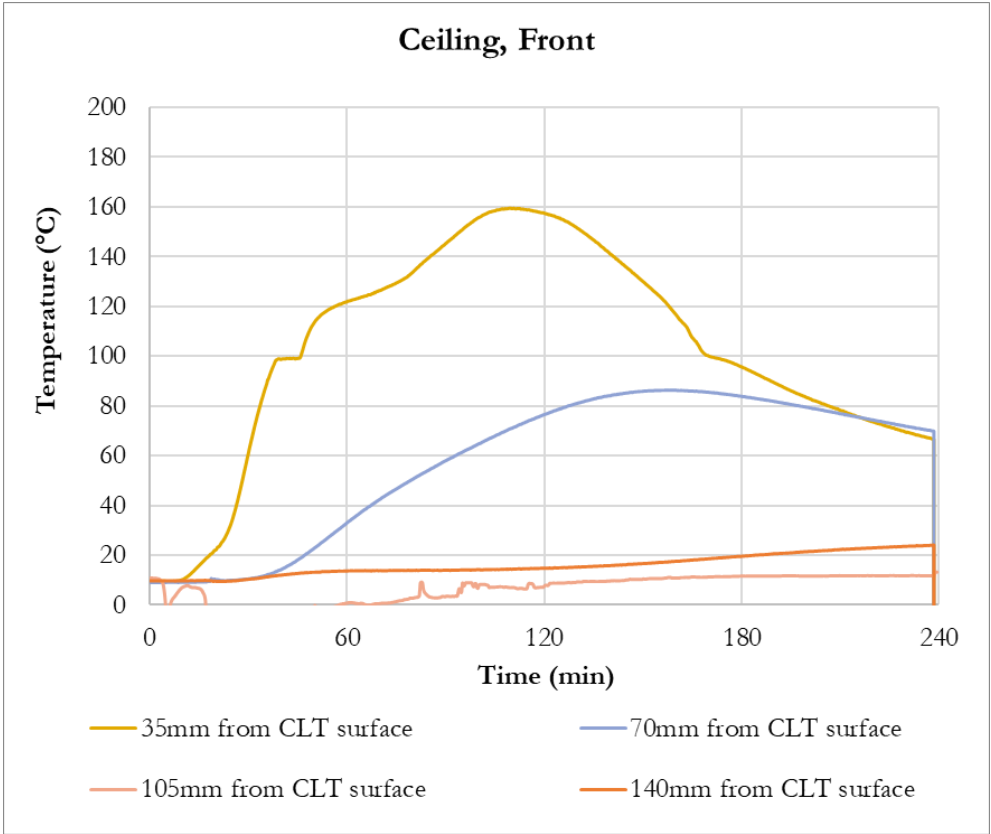


Figure J.39: Test 4 CLT temperature measurements, ceiling, front

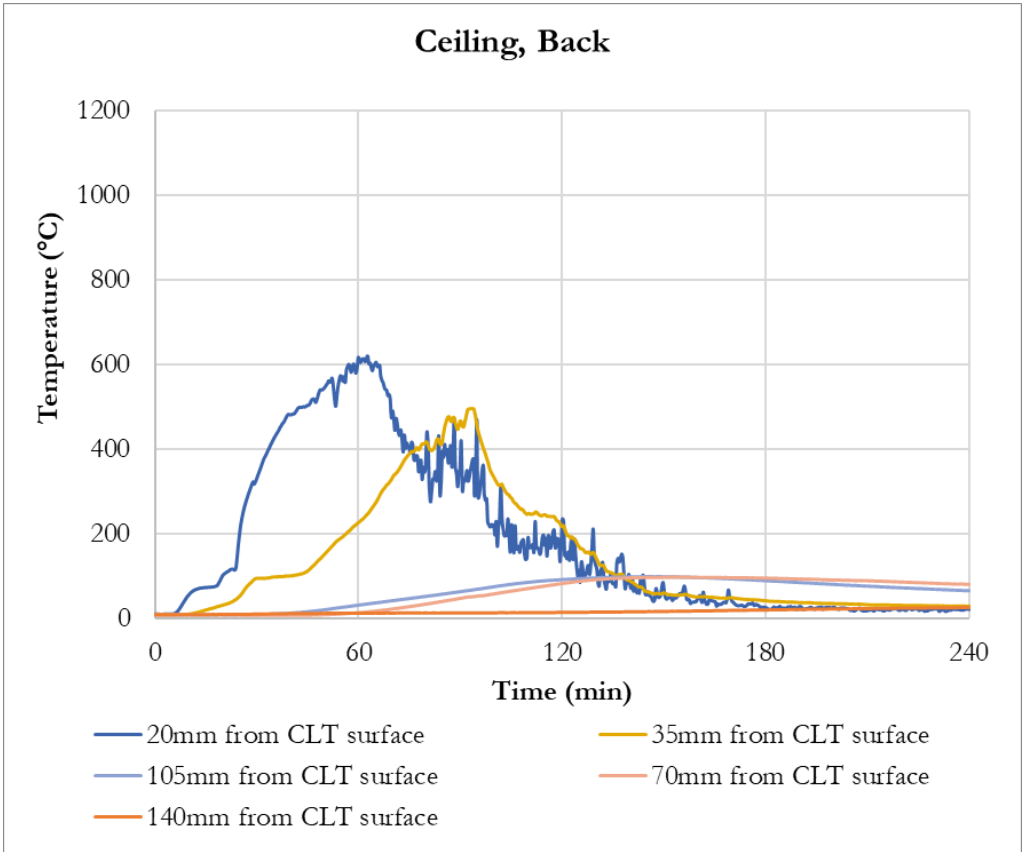


Figure J.40: Test 4 CLT temperature measurements, ceiling, back

J.5 Test 5

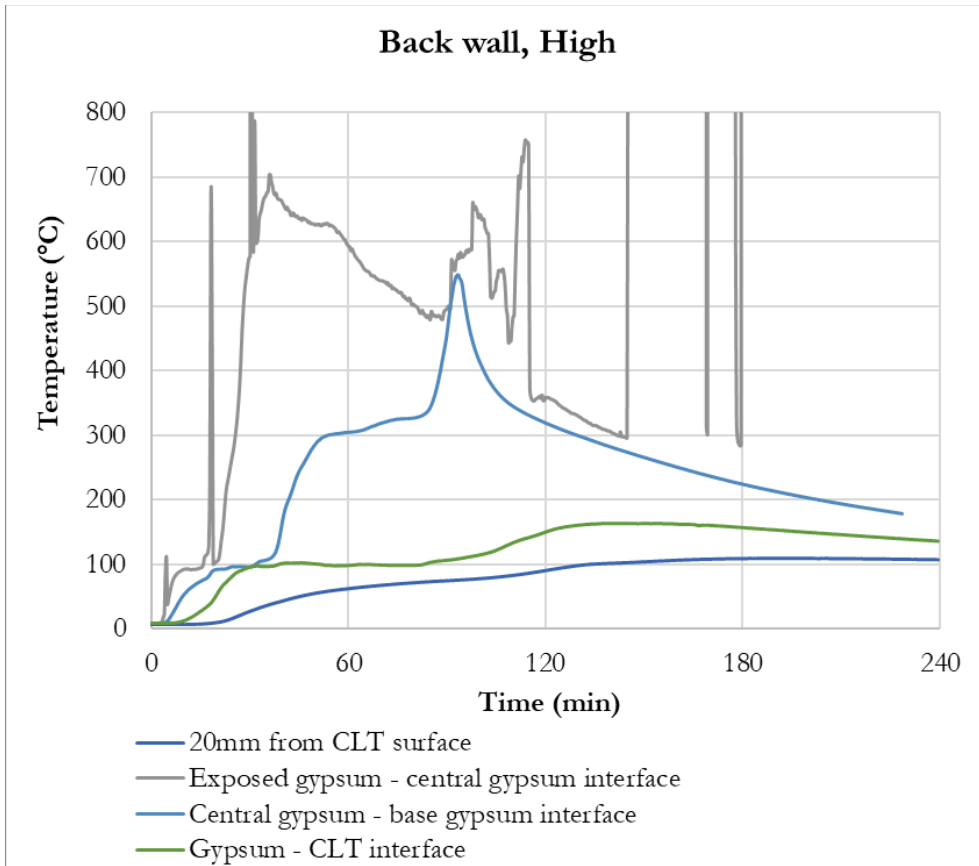


Figure J.41: Test 5 CLT temperature measurements, back wall, high

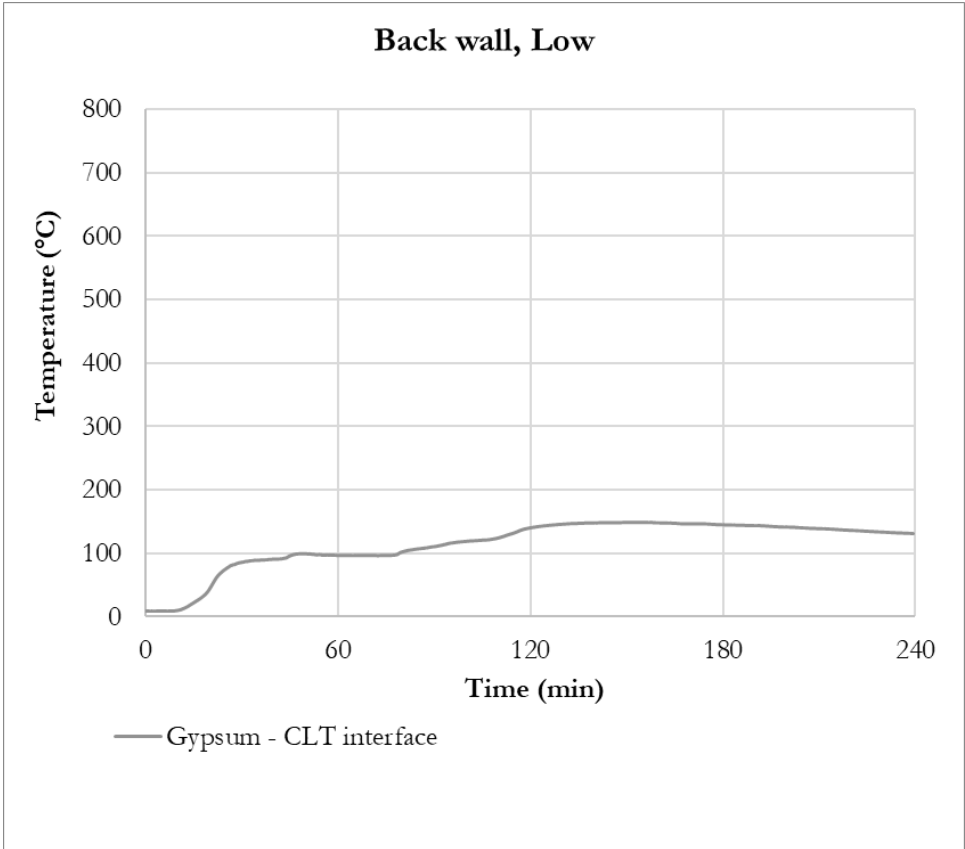


Figure J.42: Test 5 CLT temperature measurements, back wall, low

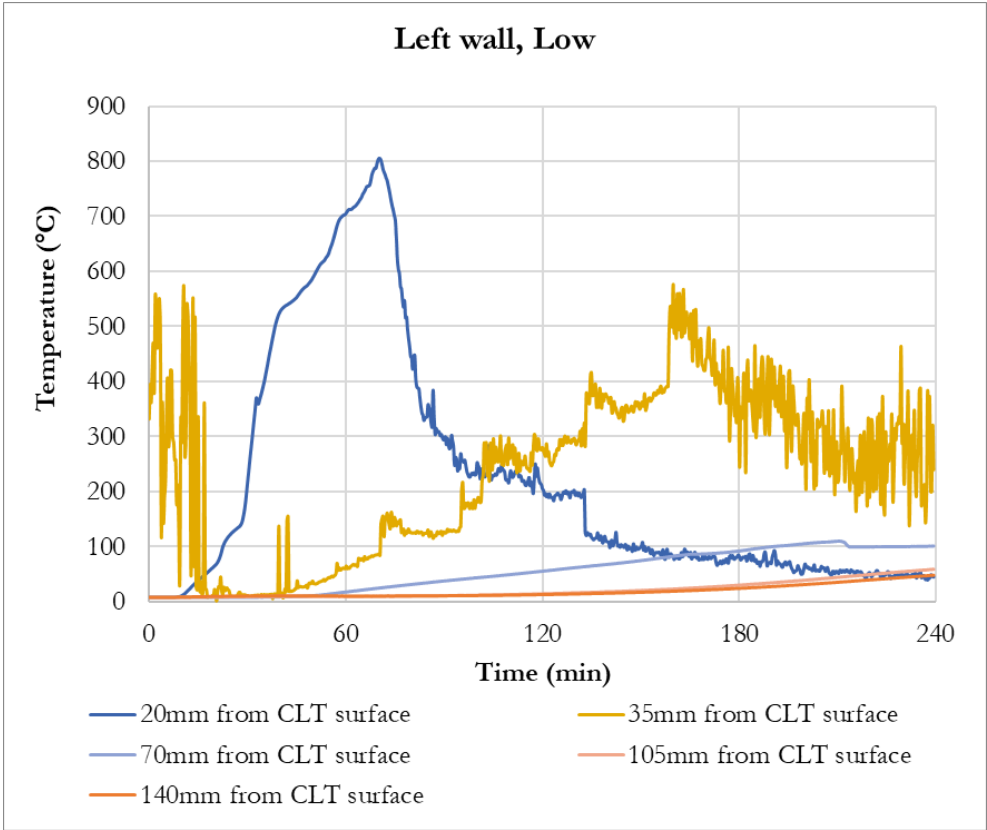


Figure J.43: Test 5 CLT temperature measurements, left wall, low

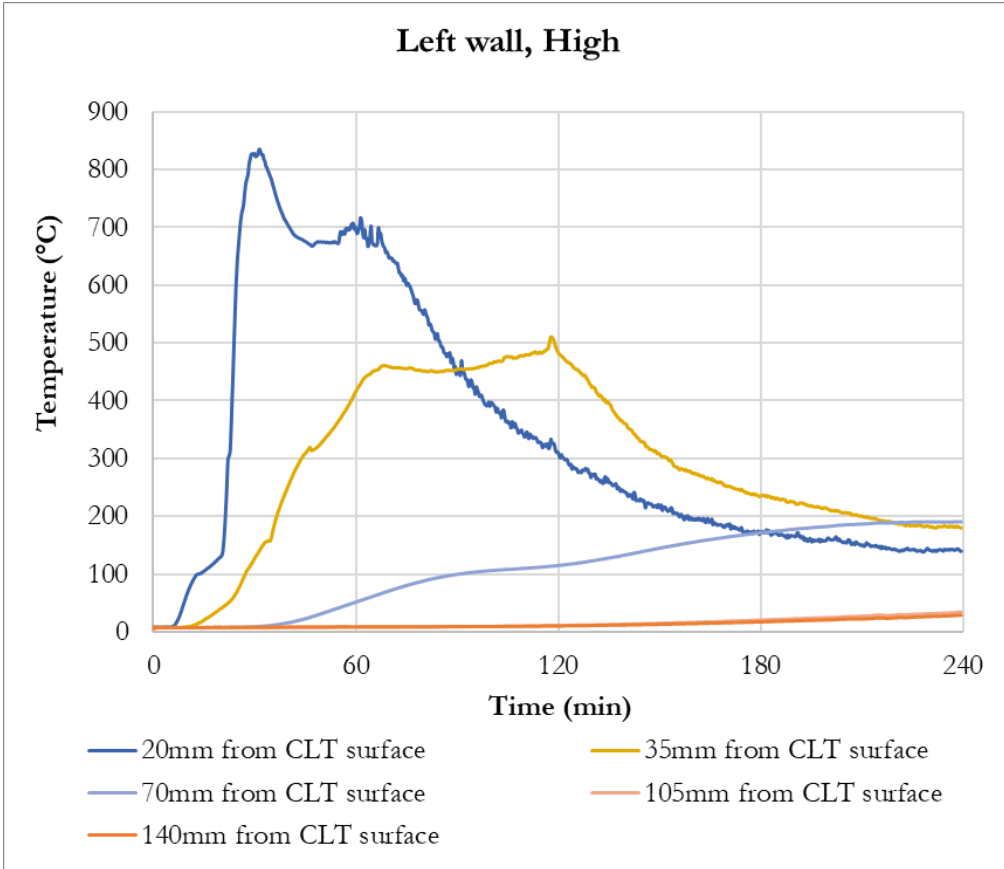


Figure J.44: Test 5 CLT temperature measurements, left wall, high

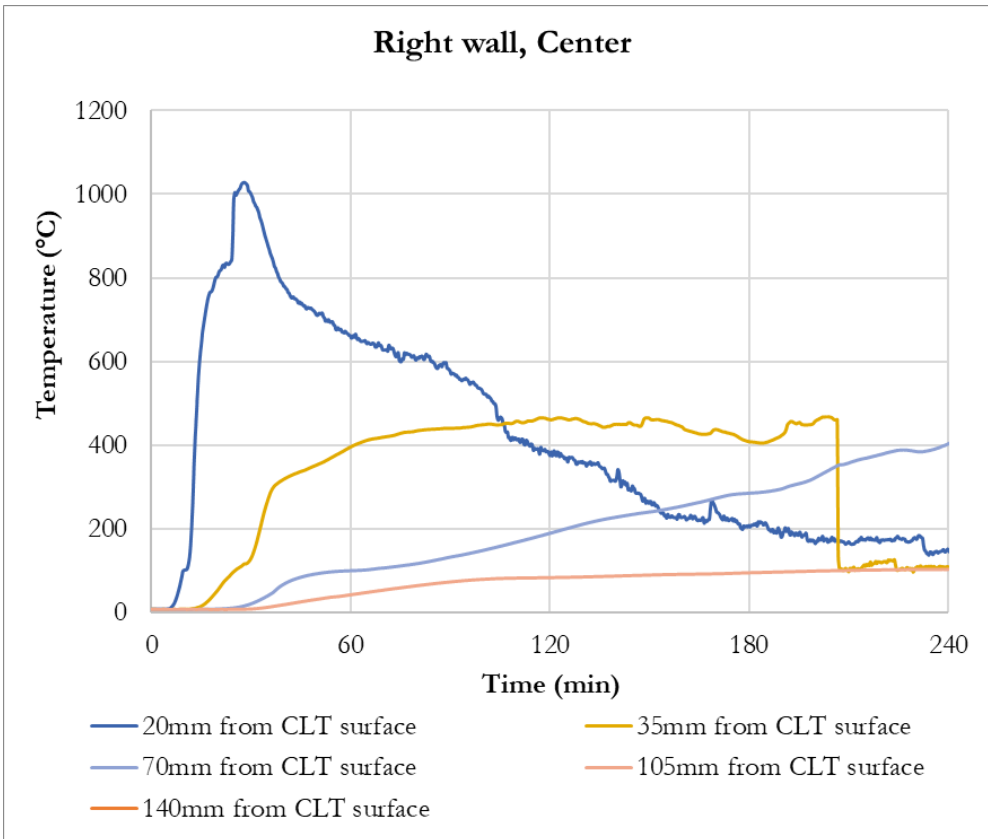


Figure J.45: Test 5 CLT temperature measurements, right wall, center

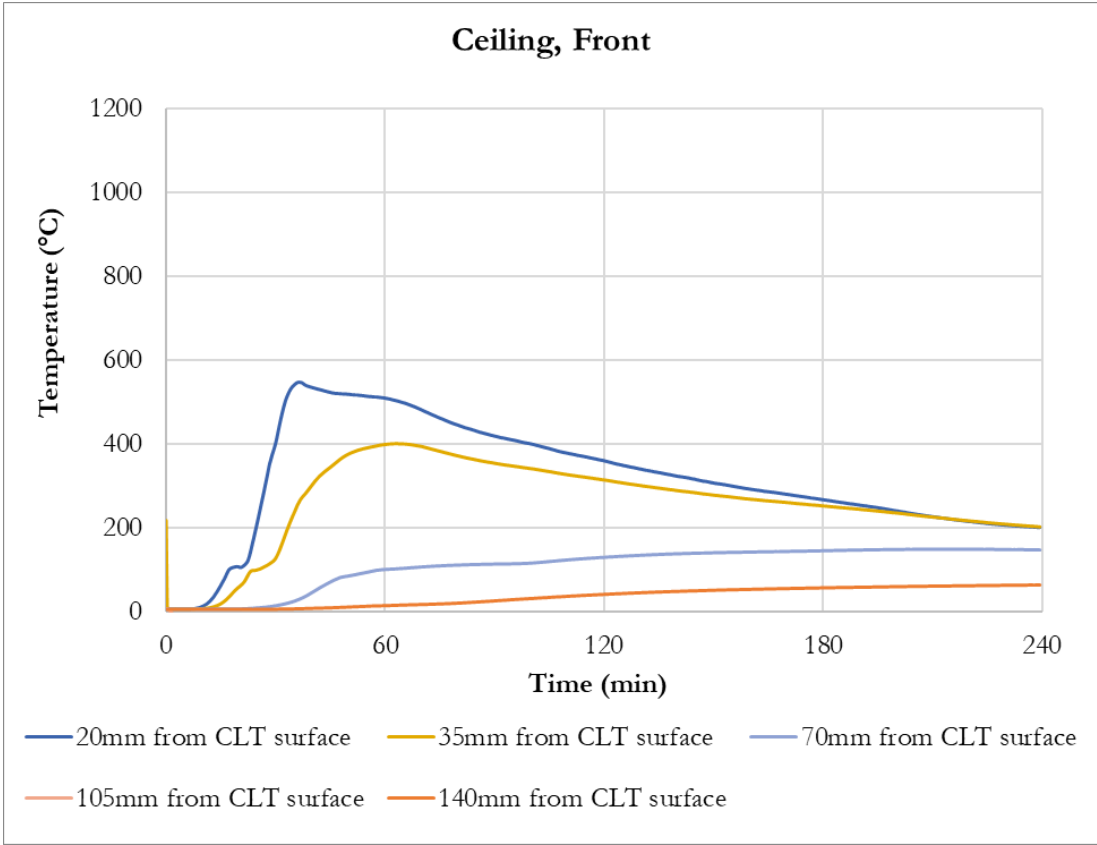


Figure J.46: Test 5 CLT temperature measurements, ceiling, front

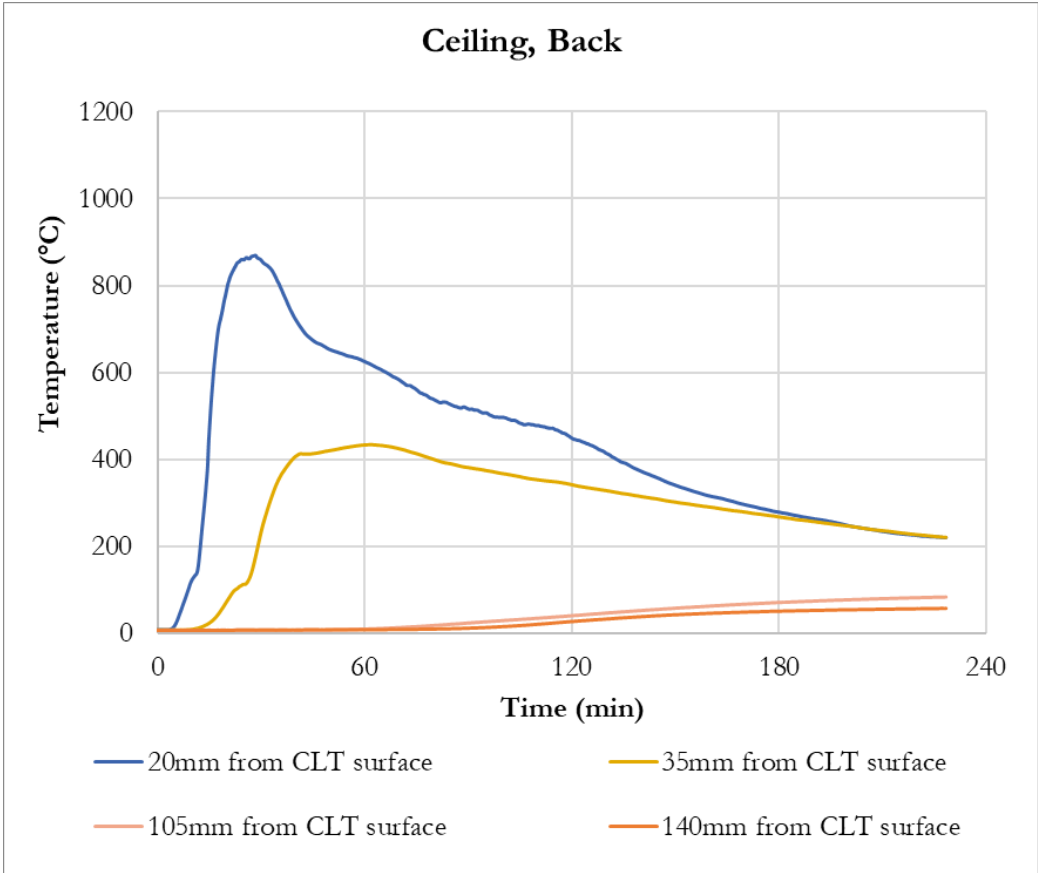


Figure J.47: Test 5 CLT temperature measurements, ceiling, back

Annex K – Oxygen concentration

Due to the use of novel measurement systems, as discussed in Section 4.3.5, oxygen measurements were varied in the different tests. Based on the difference of results of thermogravimetric analysis of timber in nitrogen environment and in ambient air environment, the highest damage is expected at periods of high thermal exposure and high oxygen concentration. In an environment with no or little oxygen, the temperature of char can be close to the fire temperature, which peaked at approximately 1200°C in Test 1, 2, 3 and 5. If the oxygen concentration locally around the timber would increase while the char temperature is still relatively high, char oxidation will take place and the thickness of the char layer will reduce. In high oxygen concentration environment char cannot exceed certain temperatures (<600 °C, for an oxygen concentration of 20.9 % (Figure 4)). If the gas and radiation temperatures are still significantly higher than the surface temperature of the char layer, a significant heat flux into the char can be expected. Therefore, when assessing the oxygen concentration, it is considered important to know the fire exposure as well. Since radiation is by far the most dominant mode of heat transfer under these conditions and the radiation was relatively similar throughout the whole compartment, it is chosen to plot the average plate thermometer temperature along with the oxygen data.

Figure K. 1, Figure K. 2 and Figure K. 3 show the data of Tests 2, 3 and 5 respectively together with the average internal plate thermometer temperatures for each test. The locations of these sensors were on the side walls as shown in Figure 22. In the graphs: “front” indicates a distance of 1.5 m from the front wall; “back” indicates a distance of 1.5 m from the back wall; and “middle” indicates the middle of the side wall in horizontal direction. “High” indicates a distance of 2.0 m from the floor and “low” indicates either 0.7 or 0.3 m from the floor as indicated in Figure 22.

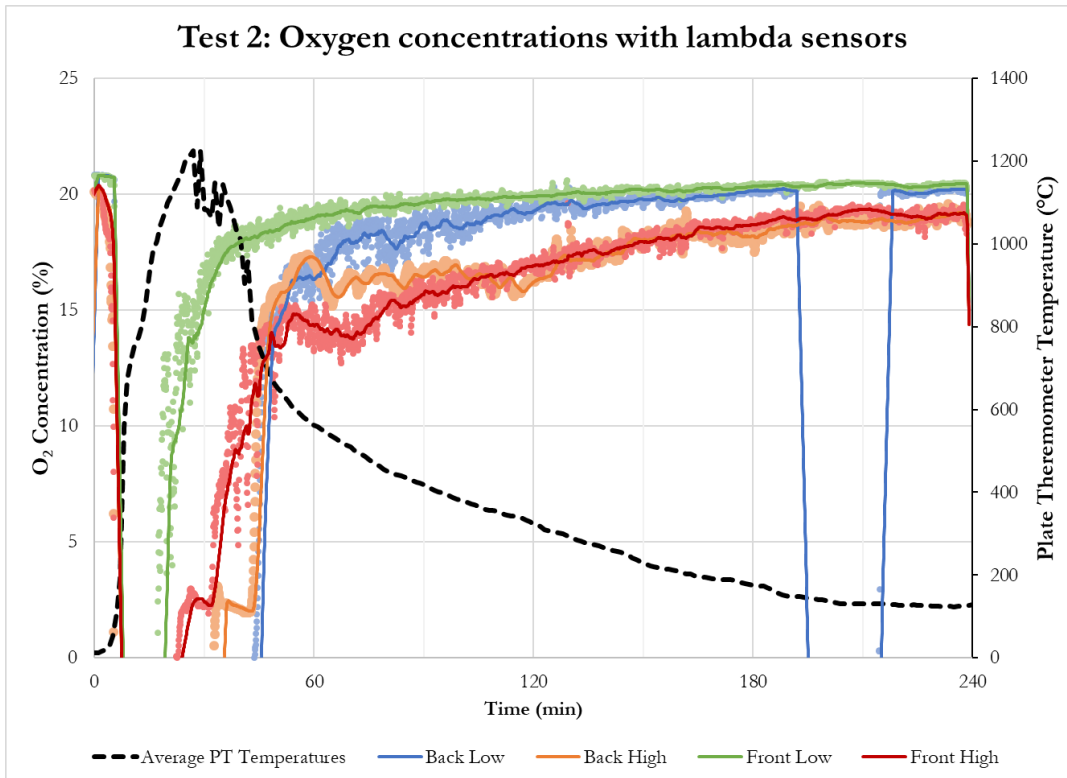


Figure K. 1: Oxygen concentrations at 4 locations measured in Test 2 with lambda sensors. Plots show raw data as points and a rolling average as a solid line. Average plate thermometer temperatures from within the compartment plotted on a secondary y-axis.

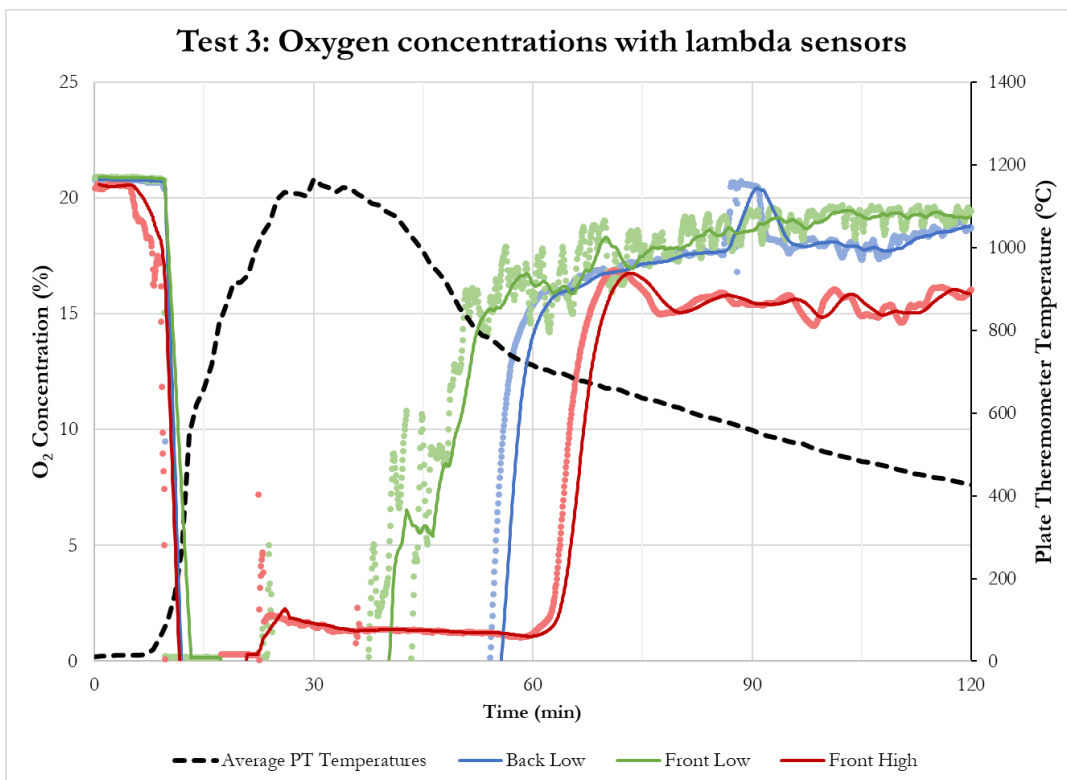


Figure K. 2: Oxygen concentrations at 4 locations measured in Test 3 with lambda sensors. Plots show raw data as points and a rolling average as a solid line. Average plate thermometer temperatures from within the compartment plotted on a secondary y-axis. Due to malfunction, the

measurement for the position “Back High” is not included in the figure. Just after 120 minutes technical difficulties led to a complete stop of lambda sensor measurements.

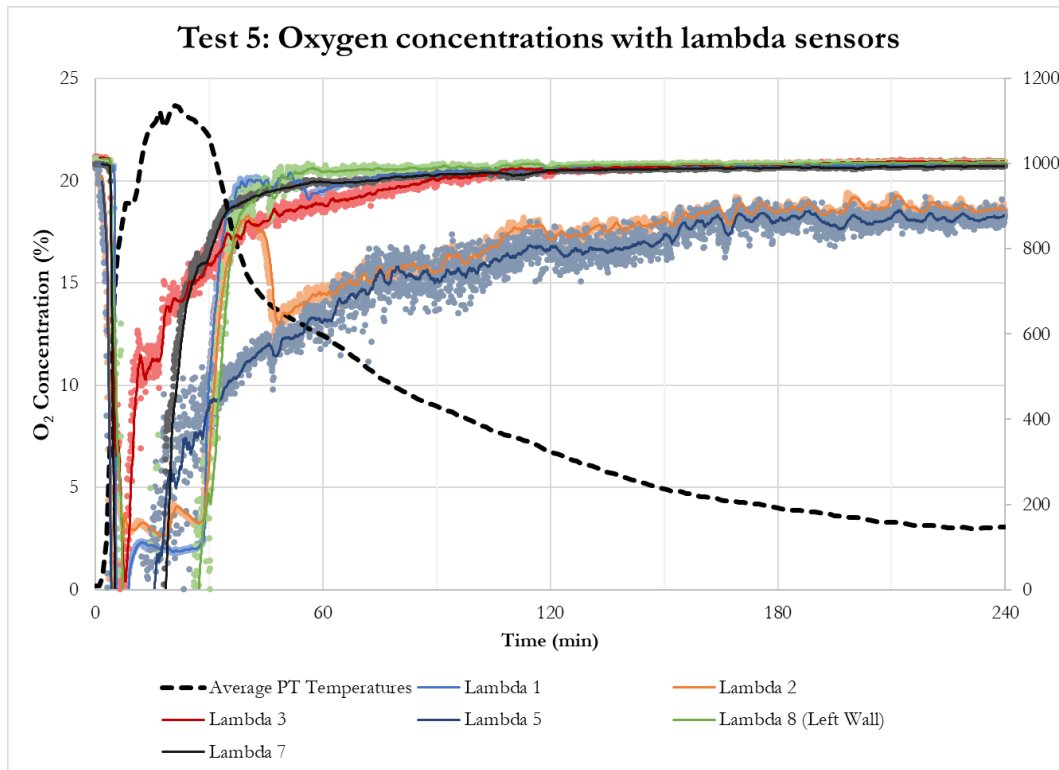


Figure K. 3: Oxygen concentrations at 4 locations measured in Test 5 with lambda sensors. Plots show raw data as points and a rolling average as a solid line. Average plate thermometer temperatures from within the compartment plotted on a secondary y-axis. The position “Front low” was taken, both, on the right and the left wall. See Figure 22 for sensor locations.

Annex L – Extinguishing smoldering timber with small quantities of water

It is recognized that smoldering timber can be extinguished with regular extinguishment methods, as has been done after most previous compartment fire tests (e.g. Brandon et al. 2018). This test series presented the opportunity to trial a method for extinguish smoldering after the test using a water mist extinguishing system. This system uses only small quantities of water thereby potentially reducing the risk of water damage to the structure. As the equipment used is not standard in many countries, these case studies are considered informative for countries that have such equipment.

Besides regular fire protective clothing, the main equipment used for this study is:

1. A water mist extinguisher (Fire Stop Cristiani)
2. Infra-red thermal camera

Test 1 and Test 3 were used to develop extinguishment method strategies while in Test 2, 4 and 5 were used as case studies where the water consumption was measured. These case studies had the following aims:

- Assess the ability to locate smoldering combustion with thermal cameras
- Find effective ways to extinguish smoldering combustion in combusting of exposed wood with less water, than used with regular fire hoses.
- Develop effective extinguishing methods for smoldering of gypsum protected wood.
- Record the amount of water needed for extinguishment in tests if possible.

L.1 Locating smoldering combustion

Smoldering combustion is often not visible. In these case studies a thermal camera was used to locate areas of smoldering combustion. With respect to locating areas of smoldering the following experience was gained:

- In exposed timber surfaces smoldering is generally easy recognized with an infrared camera. Extinguishing/cooling down spots that are over 50-60°C with a water mist extinguisher for at most a few seconds seemed to be effective in stopping smoldering in most locations. However, a check with an infrared camera after 15 to 30 minutes is needed as some locations can start smoldering again.
- Smoldering behind gypsum board can require more time to locate with infrared cameras. Sustained smoldering was observed for test 1 Only and not for the other tests. It was immediately identified behind the gypsum at the left side of the back wall, using a thermal camera at the end of the test. A second check with an infrared camera approximately 2.5 h after Test 1 identified all remaining local spots of smoldering combustion that were not seen directly after the test. These spots were more clearly visible after removing the exposed layer of gypsum board (which was brittle and easy to remove). Removing the base layer of gypsum board, led to automatic extinction of the smoldering, and no water was needed. A technique described in K.3 uses the water mist extinguisher to remove the gypsum boards.

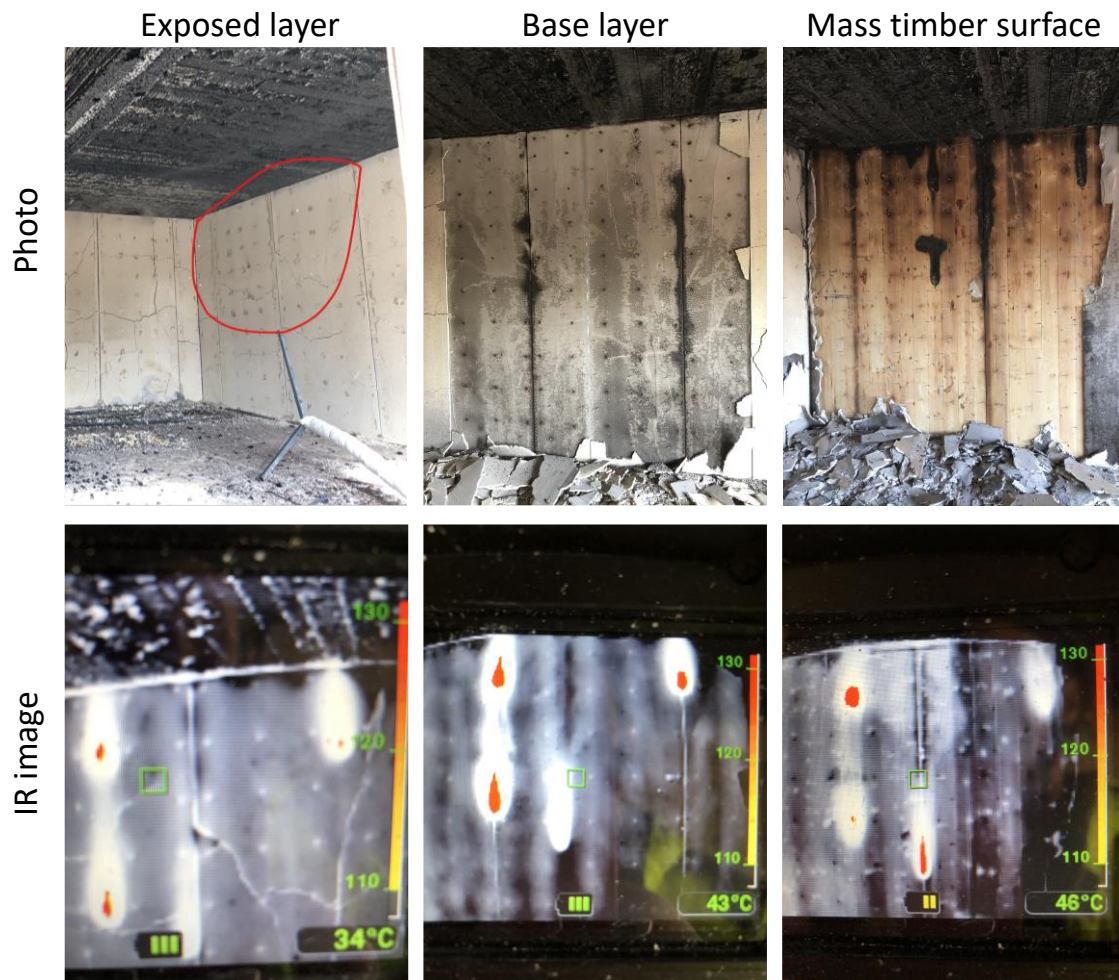


Figure L.4: Three identified spots of smoldering behind gypsum in the left wall of Test 1. Upper panels show visual images and the lower panels show IR images of the exposed layer (left), base layer (middle) and CLT surface (right)

L.2 Extinguishing smoldering in exposed timber

After all tests, extinguishment of smoldering and cooling down of hot spots in exposed surfaces was done using a 200 bar water mist extinguisher of the model *Fire Stop Cristiani*, which uses 8 gallons (30 liters) of water per minute. Due to the pressure, the water mist easily penetrates through the char layer, which is beneficial for the extinguishment of local smoldering timber.

If the hot spots were only identified in a number of specific locations, the water mist extinguisher was used at these identified spots only (Figure L.5). This approach was taken for the extinguishment after Test 4. It required 16 gallons of water to extinguish any interior smoldering combustion. It took approximately 15 minutes to identify and cool down or extinguish all hot spots. A second check with a thermal camera 15 minutes later, confirmed that all smoldering had stopped.

Where larger surface areas had temperatures over 60 °C, the surface was first cooled down by systematically going past all exposed surfaces with the water mist extinguisher first (Figure L.6). Remaining hot spots were thereafter identified. This was used for tests Test 2 and 5, which had post fire smoldering, mostly in exposed wall surfaces. 90 gallons (340 liters) and 110 gallons (415 liters) were used to extinguish the interior with water mist for Test 2 and 5, respectively. For extinguishment of any remaining combustion in the façade of Test 5 a regular hose was used from the outside. The water from this hose is not included in this quoted volume (Note: Test 5 had cavities in the front wall, which increased the challenge for fire protection).



Figure L.5: Cooling down/extinguishing local identified hot spots, directly after Test 4

To get a rough idea of the percentage of water mist absorbed, the total mass of the structure before and after extinguishment was determined using the load cells under the structure. This only provides a limited level of accuracy as the resolution of the load cell resolution (1 kg per load cell) is relatively coarse for this measurement. After Test 2 no equipment was removed from the compartment until the end of extinguishment. The mass gained during extinguishment after Test 2 is 41 kg, while the amount of water mist used was 340 kg. During the time of extinguishment, the extension wires for roof and façade measurements were decoupled, which would reduce the mass by a few kg. The measurement suggests that only a small portion of the water mist is actually absorbed by the structure is relatively small (roughly 10 to 20%). This indicates that a very significant amount of water mist left the compartment through the openings, which was in line with visual observations.



Figure L.6: Systematically cooling all exposed surfaces after directly after Test 2

Table K.1: Extinguishment overview of smoldering inside the compartment (façade smoldering if present is excluded)

	Water used	Time from start of extinguishment of smoldering until declaring the fire to be extinguished	Description of extinguishment strategy
Test 2	90 gallons (340 liter)	40 min (last water used at 40 min)	<ol style="list-style-type: none"> 1. Water mist to cool down most of the surface, by systematically passing all exposed surfaces 2. Check for remaining hot spots with the IR camera and extinguish these hot spots
Test 4	16 gallons (60 liter)	30 min (last water was used at 15 min)	Check for remaining hot spots with the IR camera and extinguish these hot spots
Test 5	110 gallons (415 liter)	75 min (last water was used at 72 min)	<ol style="list-style-type: none"> 1. Water mist to cool down most of the surface, by systematically passing all exposed surfaces 2. Check for remaining hot spots with the IR camera and extinguish these hot spots

L.3 Extinguishing smoldering combustion behind gypsum boards

In Tests 2 to 5 no sustained smoldering was observed behind gypsum boards. In Test 1, which had two layers of boards on protected surfaces, such smoldering was present. Some locations of hot spots behind gypsum boards could be identified directly after the test using infrared cameras. Those locations were extinguished by using the water mist extinguisher, which cut through the gypsum boards and simultaneously cooled down these hot spots. Other locations of smoldering, self-extinguished after the gypsum boards were removed. Although there was no smoldering identified behind interior gypsum boards in Test 3 the test was used to find a method to remove the gypsum boards effectively.

Based on the exercise of removing gypsum boards with water mist after Test 3, the following steps are recommended:

- Remove any brittle layers of gypsum board by hand. This should be possible to do with relatively limited effort.
- Layers that are less damaged, be cut in rectangular parts using a water mist extinguisher Figure L.7. To remain visibility, it is advised to perform all actions with the water mist extinguisher in a way that the deflected water misses the firefighter.
- After applying water mist behind the gypsum board layer for a few seconds, the gypsum board can be peeled off relatively easily (Figure L.8)

A board of 1.2 x 1.7 m took about 1.5 minutes to remove and took around 22 liters of water to remove, indicating a water usage of around 11 l/m² (it should be noted that this water usage is determined from a relatively small sample). A part of this water is absorbed by the gypsum boards, the mass timber and a share of the water mist escaped as water mist through the compartment openings. However, because of the relatively low change of mass of the structure and the available resolution of the load cells, it was not possible to get a reliable quantification of these shares.



Figure L.7: Cutting the gypsum boards in rectangular parts



Figure L.8: Applying water mist behind the boards for a few seconds, separating the board from the wall (left), removing the board by hand (right).

L.4 Summary of findings

Smoldering, which was generally invisible could be identified using an infrared thermal camera. In some locations behind gypsum boards this required some time before these could be identified. In case hot spots were larger than a few square feet in more locations, all exposed surfaces were systematically cooled down using a water mist extinguisher first. If this was not the case, this step was skipped. The next step was to cool down / extinguish remaining local spots of temperatures over 60°C, after identifying the exact locations with a thermal camera first. In case smoldering occurred behind gypsum boards the pressure of the water mist extinguisher could be used to penetrate the gypsum boards and simultaneously cool/down and extinguish the timber surface behind it. This method may require waiting until the hot spots show up. Alternatively, the gypsum

boards can be removed using a method with the water mist extinguisher (Annex L.3) or another method of removal. No signs of continued smoldering or increased damage after this process was finished.

The approach taken used a relatively small amount of water (up to 110 gallon). For reference, this corresponds to roughly one minute (dependent on the hose properties and pressure) of water usage by a regular water hose. The mass measurements also indicate that only a relatively small share of the water used is absorbed by the structure. The case studies of this annex, therefore, show a potential to limit water damage to a structure.

Annex M - Photos

M.1 Photos of the fuel setup

Photos of the fuel setup can be seen below; it was consistent for all tests.



Figure F. 10 Photos of the furniture in Test 1 (replicated for all tests)

M.2 Construction, testing and post-test photos

Test 1



1 - Test 1. Back wall before gypsum board installation



2 - Test 1. 2 mm jump between top of wall members



3 - Test 1. Geometrical jump of milled surface



4 - Test 1. Left back corner



5 - Test 1. Spline board connection additionally sealed at thermocouple locations



6 - Test 1. Construction tape at external surfaces



7 - Test 1. Exposed ceiling



8 - Test 1. Back wall after gypsum board installation



9 - Test 1. Lap joint above corners of openings, without sealant in Test 1



10 - Test 1. Implementation of 50 ml of charcoal lighter fluid



11 - Test 1. Developing phase



12 - Test 1. Flashover from side view



13 - Test 1. Near end of fully developed phase



14 - Test 1. Some smoke on the external surface



15 - Test 1. Final stage of decay



16 - Test 1. Decay phase



17 - Test 1. Column to beam connection post fire.



18 - Test 1. Post fire, beam penetrating through rear wall. Charring visible on the left where gap wasn't sufficiently sealed (see Section, 6.15), none visible on the right.



19 - Test 1. Interior post fire (gypsum still attached)



20 - Test 1. Exterior post fire (protection still attached)



21 - Test 1. Exposed roof and beam post fire.



22 - Test 1. Roof joint post fire, no visible charring on unexposed surface at joint.



23 - Test 1. Penetration for instrumentation in wall, no visible charring within the hole.



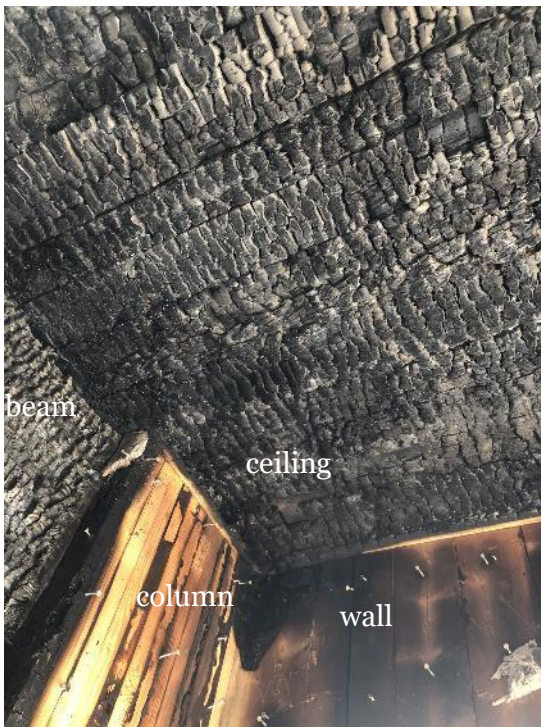
24 - Test 1. Gypsum post fire after using a water mist extinguisher to extinguish local smoldering.



25 Test 1. Damage above the openings after Test 1. Highest damage occurred above the left corner of the right opening. The lap joints above the corners were not sealed in Test 1.



26 - Test 1. Exposed ceiling and unexposed walls (after gypsum removal). Right back corner visible.



27 Test 1. Glued laminated column and front wall after removal of gypsum boards. (glued laminated beam and CLT ceiling were exposed during the fire)



28 - Test 1. Front of the compartment posttest. Some charring directly above the openings. Especially, in the lap-joints which had no sealant applied.

Test 2



29 - Test 2. Expanding tape to seal where the beam penetrates the back wall.



30 - Test 2. Fire sealing on the beam end by column connection.



31 - Test 2. Resilient profile between wall and ceiling.



32 - Test 2. Sealant over TCs installed in CLT.



33 - Test 2. Installing expanding foam tape on the ceiling joint.



34 - Test 2. Expanding foam tape on the ceiling joint.



35 - Test 2. Wall-ceiling joint from outside before tape installation.



36 - Test 2. Wall-ceiling joint from outside before tape installation.



37 - Test 2. Detail around opening (outside)



38 - Test 2. Resilient profile between beam and ceiling.



39- Test 2. Bin shortly after ignition



40 - Test 2. Early stages of fire.



41 - Test 2. Fully developed phase.



42 - Test 2. Fully developed phase.



43 - Test 2. Fully developed phase.



44 - Test 2. Fully developed phase.



45 - Test 2. End of fully developed phase.



46 - Test 2. During decay



47 - Test 2. Decay phase.



48 - Test 2. Decay phase.



49 - Test 2. Decay phase.



50 - Test 2. Small smoldering areas at end of fire.



51 - Test 2. Small smoldering areas at end of fire.



52 - Test 2. Outside of compartment post fire.



53 – Test 2. Post fire wall-ceiling interface.



54 – Test 2. Post fire gypsum board condition.



55 – Test 2. Façade after gypsum removal.



56 – Test 2. Back wall after gypsum removal



57 - Test 2. Column - beam (on column) connection post fire.



58 - Test 2. Right wall post fire.



59 - Test 2. Ceiling spline board joint post fire.



60 - Test 2. Protected wall post fire and gypsum removal.



61 - Test 2. Ceiling spline board joint post fire.



62 - Test 2. Ceiling underside post fire



63 - Test 2. Back wall after gypsum removal.

Test 3



64 - Test 3. External face of the CLT by front opening.



65 - Test 3. Interior of compartment after gypsum applied.



66 - Test 3. Back wall.



67 - Test 3. Exposed CLT wall in a corner.



68 – Test 3. Early stages of the fire



69 – Test 3. Fully developed fire.



70 – Test 3. Fully developed fire.



71 – Test 3. Fully developed fire.



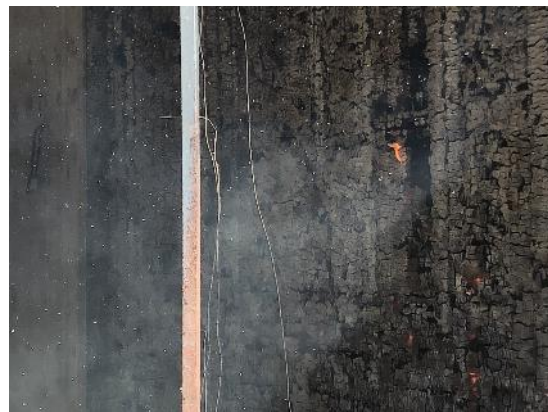
72 - Test 3. Decay phase



73 - Test 3. Decay phase



74 - Test 3. Flaming on the left wall late in the decay



75 - Test 3. Small area of smoldering on an exposed wall



76 - Test 3. Small amount of discoloration visible on the unexposed side of the back wall around pipe penetration (for oxygen measurements)



77 - Test 3. Small flame showing from behind gypsum board around opening.



78 - Test 3. Post fire gypsum removal from rear wall.



79 - Test 3. gaps visible at wall - ceiling interface post fire.



80 - Test 3. example of char depth post fire



81 - Test 3. exposed wall post test.



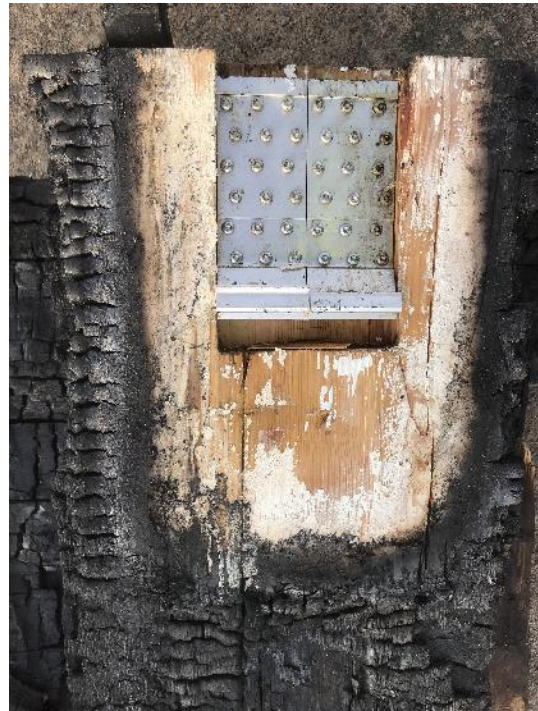
82 - Test 3. Charring of external CLT face above opening visible after protection removed.



83 - Test 3. Rear wall condition after protection removed.



84 - Test 3. Area of charring visible from outside post test.



85 - Test 3. Condition of column to beam connection after fire.



86 - Test 3. Demonstration of resilient profile providing protection at the wall-ceiling interface.



87 - Test 3. Area where resilient profile failed (likely due to lack of airtight seal) to provide protection at wall top.

Test 4



88 - Test 4. Installation of thermocouple wires for through depth CLT measurements.



89 - Test 4. Beam end protected with intumescent paint.



90 - Test 4. Light plastic sheeting covering openings to prevent wind for blowing out fire in very early stages.



91 - Test 4. Fire shortly after ignition.



92 - Test 4. Early stages of the fire.



93 - Test 4. Fire shortly before flashover, flames visible along ceiling and small flame extension out of front opening.



94 - Test 4. Fully developed fire.



95 - Test 4. Fully developed fire.



96 - Test 4. Smoldering in front left corner of compartment.



97 - Test 4. Fire late in decay phase.



98 - Test 4. Smoldering ongoing in corner after fire stopped elsewhere.



99 - Test 4. Unprotected surfaces after test.



100 - Test 4. Unprotected surfaces after test



101 - Test 4. Beam wall connection post fire.



102 - Test 4. Column post fire.



103 - Test 4. Lifting the back wall panel. The uncharred part is the position of the beam and the charring depth in the first lamella is clear.



104 - Test 4. Wall section from outside. (same as photo 100 but from the outside and after removal of GB and char due to a local smoldering fire at the position of inserted thermocouples)



105 - Test 4. Front wall from outside post fire.



106 - Test 4. Front wall from outside post fire.



107 - Test 4. Beam from above after the removal of the roof.



108- Test 4. Rear wall after removal of gypsum.



109 - Test 4. Beam after partial removal of the roof showing the resilient profile.

110 - Test 4. Wall section at opening post test.

Test 5



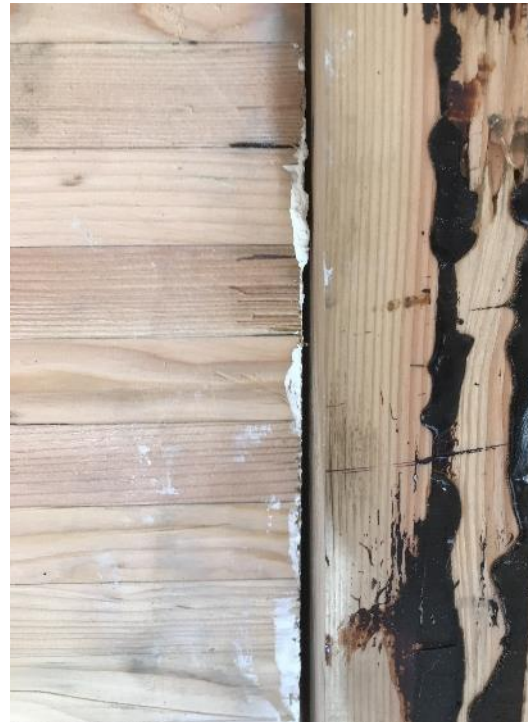
107 - Test 5. Beam end protected with intumescent paint.



108 - Test 5. Installation of plate thermometers low on the left wall



109 - Test 5. exposed right wall and protected front wall.



110 - Test 5. Gap behind column as it meets the wall.



111 - Test 5. Fully developed fire.



112 - Test 5. Fully developed fire.



113 - Test 5. Fully developed fire from the side showing flame extension.



114 - Test 5. Fully developed fire from the side showing flame extension



115 - Test 5. Late in the fully developed phase



116 - Test 5. Late in the fully developed phase



117 - Test 5. Late in the fully developed phase



118 - Fire fighter removing gypsum around opening showing penetration of fire into the cavity behind the protection. This cavity was only present in Test 5.



119 - Test 5. Right wall. 50 minutes after ignition.



120 - Test 5. Right wall at 2 hours, 47 min after ignition



121 - Back wall after gypsum removal



122 - Front of the compartment after protection removed. Areas where fire penetrated the void behind the gypsum boards clearly visible.



123 - Test 5. Post fire photo of the artificial cavity in the opening of Test 5 to correct the opening size.



124 - Test 5. Left wall post fire.



125 - Beam post fire after ceiling removal. Resilient profiles still in place.

The work upon which this publication is based was funded in part through a Wood Innovation grant by the Southern Region, State & Private Forestry, Forest Service, U.S. Department of Agriculture.

In accordance with Federal law and U.S. Department of Agriculture policy, this institution is prohibited from discriminating on the basis of race, color, national origin, sex, age, or disability. To file a complaint of discrimination, write USDA Director, Office of Civil Rights, Room 326-W, Whitten Building, 1400 Independence Avenue, SW, Washington, DC 20250-9410 or call (202) 720-5964 (voice and TDD). USDA is an equal opportunity employer.

Through our international collaboration programs with academia, industry, and the public sector, we ensure the competitiveness of the Swedish business community on an international level and contribute to a sustainable society. Our 2,800 employees support and promote all manner of innovative processes, and our roughly 100 testbeds and demonstration facilities are instrumental in developing the future-proofing of products, technologies, and services. RISE Research Institutes of Sweden is fully owned by the Swedish state.



RISE Research Institutes of Sweden AB
Box 857, 501 15 BORÅS, SWEDEN
Telephone: +46 10-516 50 00
E-mail: info@ri.se, Internet: www.ri.se

Fire Research
RISE Report 2021:40
ISBN: 978-91-89167-79-7